

The Silicon Isotopic Composition of Inner Solar System Materials



Rosalind M. G. Armytage

Wolfson College

University of Oxford

A thesis submitted for the degree of

Doctor of Philosophy

Trinity Term 2011

To see a world in a grain of sand,
And a heaven in a wild flower,
Hold infinity in the palm of your hand,
And eternity in an hour.

Auguries of Innocence, William Blake

“De hoc lapide multi multa, omnes aliquid, nemo satis”
*Concerning this stone many have said much, all have said something,
none have said enough.*

Inscription on plaque in church next to the displayed Ensisheim meteorite
(Marvin, 1992)

CMP Well, do the rocks - do the rocks all look same? They're different - good,
great; I'm glad to hear it.

LMP Little sparkly stuff; quite a bit of it all over

.....

CMP That's great; fantastic! That'll keep those geologists jumping for years.

Apollo 11 onboard voice transcription, recorded on the command module

July 21, 1969

(CMP = Command module pilot - Michael Collins)

(LMP = Lunar module pilot - "Buzz" Aldrin)

Abstract

The Silicon Isotopic Composition of Inner Solar System Materials

A thesis submitted for the degree of Doctor of Philosophy

Trinity Term 2011

Rosalind M. G. Armytage

Wolfson College

This study uses high precision silicon isotopic measurements to understand events that occurred during the earliest stages of formation of the terrestrial planets. The isotopic compositions of diverse materials such as chondrites, lunar rocks and asteroidal basalts can shed light on the homogeneity of the solar nebula, metal-silicate differentiation on planetary bodies, and terrestrial moon formation.

Limited variation in the Si isotopic composition of meteorites is evidence for a relatively homogeneous inner solar system with respect to silicon isotopes. The Si isotopic composition of bulk silicate Earth (BSE) is, however, heavier than meteorites. This points to an event unique to Earth that fractionated Si isotopes, such as core formation at terrestrial conditions. The $\Delta^{30}\text{Si}_{\text{BSE-meteorite}}$ value from this study indicates that the Earth's core contains $8.7^{+8.1}_{-6.2}$ wt% Si.

No systematic $\delta^{30}\text{Si}$ differences were found between any of the lunar lithologies analysed, implying a Si isotopic homogeneity of the sampled lunar source regions. The lunar average, $\delta^{30}\text{Si} = -0.29 \pm 0.08\text{‰}$ ($2\sigma_{SD}$), is identical to the recent value of Savage et al. (2010) for BSE of $\delta^{30}\text{Si} = -0.29 \pm 0.08\text{‰}$ ($2\sigma_{SD}$). The best explanation of the data is that Si isotopes must have homogenised in the aftermath of the Moon-forming impact with no subsequent fractionation in the proto-lunar disk.

The Si isotopic composition of olivine within lunar basalts was found to be the same or heavier than $\delta^{30}\text{Si}_{\text{pyroxene}}$. This is not consistent with terrestrial data where $\delta^{30}\text{Si}_{\text{pyroxene}}$ is always lighter than $\delta^{30}\text{Si}_{\text{olivine}}$. Crystallisation history cannot explain the data, and the slow diffusion rates of Si rule out cooling rates as a cause. Therefore, it appears that inter-mineral fractionation of Si isotopes occurs differently on the Moon.

The $\delta^{30}\text{Si}$ of chondrules picked from Allende spanned a range of $\sim 0.6\text{‰}$, a factor of two greater than the bulk meteorite range. There is no evidence for the variable $\delta^{30}\text{Si}$ of the chondrules being the result of post-formation alteration and there is no convincing evidence for precursor heterogeneity being the primary cause. It is likely that Si isotopic composition of chondrules is the result of evaporation and re-equilibration with the evaporated phase.

Extended abstract

The Silicon Isotopic Composition of Inner Solar System Materials

A thesis submitted for the degree of Doctor of Philosophy

Trinity Term 2011

Rosalind M. G. Armytage

Wolfson College

The formation of a terrestrial planet is the culmination of a series of processes that began even before the formation of the proto-planetary disk. The Earth's tectonic activity has erased the first few hundred million years of its history from the rock record. Therefore, in order to understand processes in the solar nebula or early differentiation events on planetary bodies, it is necessary to study a wide variety of inner solar system materials. The isotopic compositions of diverse materials such as chondrites, lunar rocks and asteroidal basalts can shed light on formation of solids in the nebula, metal-silicate differentiation on planets and planetesimals, and terrestrial moon formation. This study uses high precision silicon isotopic measurements to understand events that occurred during the earliest history of the Earth. Silicon is a major element in the majority of rock-forming phases, and recent development of high precision multi-collector inductively-coupled-plasma mass spectrometry (MC-ICPMS) techniques make Si isotopes an attractive tool to apply to high temperature systems.

The initial investigation was to assess the reliability of the high precision method, recently developed for analysing Si isotopes in silicates (Georg et al., 2006a), for meteorite samples. Previous studies of bulk meteorite and terrestrial samples were at odds over the mean values for meteorites and the bulk silicate Earth (BSE), and whether any offset existed and could be resolved between them (Georg et al., 2007a; Fitoussi et al., 2009; Chakrabarti and Jacobsen, 2010b; Ziegler et al., 2010). In this study a number of putative explanations were ruled out such as sample compositional control and pH during chemical separation. To test the effects of sample heterogeneity, the nature of the solvent (HCl or HNO₃) and solution filtration, eight aliquots of the well-studied CV3 chondrite Allende were analysed. Three different powders from three different initial cuts of Allende were used, and the reproducibility across the eight aliquots was $\pm 0.07\%$, $2\sigma_{SD}$. Standard addition tests were carried out by doping

Allende with the pure Si standard IRMM-018, but no clear matrix effects were apparent. No systematic offsets related to mass spectrometry on different instruments could be detected either.

The Si isotopic composition of 36 meteorites and 6 terrestrial mantle samples were measured using multi-collector inductively-coupled mass spectrometry (MC-ICPMS). Achondrites from Mars and Vesta were shown to have the same Si isotopic composition as the undifferentiated chondrites ($\delta^{30}\text{Si}_{\text{Chondrite}} = -0.49 \pm 0.15\text{‰}$, $2\sigma_{SD}$; $\delta^{30}\text{Si}_{\text{Achondrite}} = -0.47 \pm 0.11\text{‰}$, $2\sigma_{SD}$). Enstatite chondrites were the only meteorite group that showed any systematic difference, with their lighter composition of $\delta^{30}\text{Si} = -0.63 \pm 0.07\text{‰}$ ($2\sigma_{SD}$). The Si isotopic composition of BSE however, was heavier than the meteorites ($\delta^{30}\text{Si} = -0.32 \pm 0.09\text{‰}$, $2\sigma_{SD}$), which pointed to some event or sequence of events unique to Earth that fractionated Si isotopes. The obvious interpretation of $\Delta^{30}\text{Si}_{\text{BSE-meteorite}} > 0$ is silicon entering the core during metal-silicate differentiation, which would be consistent with the superchondritic Mg/Si ratio of the bulk silicate Earth. The conditions at which Si partitions into metal would not have existed on the other measured differentiated bodies of Mars or Vesta, hence their chondritic $\delta^{30}\text{Si}$ compositions. Also it has been shown that the Si isotopic composition of corresponding metal phase (i.e. the core) would be light as the stiffer Si bonds, preferred by the heavy isotopes, would exist in the silicate phase (Schauble, 2004).

The uncertainties on $\Delta^{30}\text{Si}_{\text{BSE-meteorite}}$ (~ 0.1) are such that Si isotopic data has only limited use in constraining conditions of terrestrial core formation such as temperature. It is of more value to use $\Delta^{30}\text{Si}_{\text{BSE-meteorite}}$ to calculate the wt% of Si in the core. Fixing the temperature of core formation to the peridotite liquidus and using an appropriate literature metal-silicate fractionation factor ($\epsilon = 0.89$), the $\Delta^{30}\text{Si}_{\text{BSE-meteorite}}$ value from this study indicates that the Earth's core contains at least 2.5 and possibly up to 17wt% Si. Therefore, on the basis of the isotopic evidence, there is strong case of Si being one of the light elements (if not the only one) necessary to explain the low density of the Earth's outer core inferred from seismic studies.

The initial Si isotopic evidence from lunar samples suggested little or no offset between the bulk Moon and the BSE (bulk silicate Earth) in Si isotopic composition (Georg et al., 2007a; Fitoussi et al., 2010). However, models of rainout in the protolunar disk in the aftermath of the Moon-forming Giant Impact predicted Si isotopic fractionations between the Moon and the BSE on the order of 0.14‰ (Pahlevan et al., 2011). To investigate this, 24 lunar samples from high and low-Ti basalts to

crustal anorthosites and lunar glasses were analysed, covering all the Apollo sampling missions. No systematic $\delta^{30}\text{Si}$ differences were found between any of the bulk sample lithologies ($\pm 2\sigma_{SD}$) ($\delta^{30}\text{Si}_{\text{Low-Ti basalt}} = -0.29 \pm 0.06\text{‰}$; $\delta^{30}\text{Si}_{\text{High-Ti basalt}} = -0.32 \pm 0.09\text{‰}$; $\delta^{30}\text{Si}_{\text{Lunar glass}} = -0.29 \pm 0.05\text{‰}$; $\delta^{30}\text{Si}_{\text{Highland Rocks}} = -0.27 \pm 0.10\text{‰}$). This implies a Si isotopic homogeneity of the source regions for all these different lunar rocks. The lunar average is $\delta^{30}\text{Si} = -0.29 \pm 0.08\text{‰}$ ($2\sigma_{SD}$), which is identical to the recent value of Savage et al. (2010) for bulk silicate Earth of $\delta^{30}\text{Si} = -0.29 \pm 0.08\text{‰}$ ($2\sigma_{SD}$). The BSE Si isotope composition is thought to be the result of Si partitioning between metal and silicate and consequent isotopic fractionation during core formation. The Moon-forming impactor would not be expected to share that composition, because it is thought to have been relatively small (0.1 Earth masses) like Mars and formed under relatively low temperatures and pressures that are insufficient for Si to partition into the core. Smooth particle hydrodynamic simulations of the Giant Impact show that the majority of material in the proto-lunar disk originated from the impactor rather than the Earth. If these models are correct, the identical lunar and BSE Si isotope data imply that Si isotopes, like those of oxygen, must have homogenised in the aftermath of the Moon-forming impact.

The $\sim 0.14\text{‰}$ offset predicted by Pahlevan et al. (2011) corresponded to the bulk Moon having an Fe/(Fe+Mg) ratio twice that of BSE. The current resolution and sample population size of the Si data for the Moon and Earth would allow such an offset to be detected. The fact that it is not observed, constrains the Fe/(Fe+Mg) ratio of the Moon to be only $1.0 - 1.3\times$ bulk silicate Earth as modelled by Pahlevan et al. (2011).

The Si isotopic composition of mineral separates (olivine, pyroxene and plagioclase) from five lunar basalts were analysed in order to further probe differentiation processes on the Moon. The Si isotopic composition of plagioclase was the heaviest and the most uniform of all the mineral phases with $\delta^{30}\text{Si} = -0.27 \pm 0.04\text{‰}$ ($2\sigma_{SD}$). The mafic minerals, by contrast, were lighter and more variable in their Si isotopic composition with $\delta^{30}\text{Si}_{\text{pyroxene}} = -0.43 \pm 0.14\text{‰}$ ($2\sigma_{SD}$) and $\delta^{30}\text{Si}_{\text{olivine}} = -0.37 \pm 0.09\text{‰}$ ($2\sigma_{SD}$). These averages however, mask the fact that within individual basalts the olivines were the same or heavier than pyroxene in their Si isotopic composition. This is in direct contrast to terrestrial data from the Skaergaard intrusion or spinel lherzolites where pyroxene was always lighter than the olivine in $\delta^{30}\text{Si}$ composition by up to $\sim 0.11\text{‰}$. The olivine normative lunar basalt 15555 was shown to be anomalous with a very restricted range of Si isotopic compositions of its mineral phases (0.06‰). However, both cooling history and crystal accumulation were ruled

out as explanations for the $\delta^{30}\text{Si}$ measurements from 15555. Investigations of the closure temperatures for Si in olivine, diopside and plagioclase indicate that cooling rates on the order of 1-100K/Myr are necessary for there to be significant diffusion of silicon. As these rates are much too slow even for the intrusive Skaergaard minerals, the difference in direction of offset between olivine and pyroxene in lunar and terrestrial settings cannot be attributed to crystallisation history. Therefore it appears that inter-mineral fractionation of Si isotope occurs differently on the Moon.

The lack of offset observed between bulk anorthosites and bulk mare basalt in $\delta^{30}\text{Si}$, despite the early differentiation of the lunar magma ocean, was shown to be consistent with the fraction of plagioclase crystallising and the plagioclase-melt fractionation factors.

The Si isotope composition of a number of chondrules and other components picked from the CV3 chondrite Allende was determined. Corresponding petrographic and bulk major element data were collected for the chondrules. The $\delta^{30}\text{Si}$ compositions of the chondrules spanned a range of $\sim 0.6\%$ in contrast to the bulk meteorite range of $\sim 0.3\%$. The Si isotopic compositions of a matrix sample and chondrules from Allende are consistent with a complementary relationship where chondrules and matrix formed from the same chemical reservoir.

The range in Si isotopic composition of the chondrules is limited however, in the context of evaporation into a free vacuum. The variation in $\delta^{30}\text{Si}$ did not correlate with petrology or with any indicators of evaporation with limited isotopic fractionation, such as size or Si/Al ratio. The one CAI (calcium aluminium inclusion) analysed from Allende had a Si isotopic composition of $\delta^{30}\text{Si} = 2.81 \pm 0.03$, $2\sigma_{SEM}$, consistent with an evaporative origin at nebular pressures. The variable $\delta^{30}\text{Si}$ of the chondrules is unlikely to have resulted from post-formation alteration, whether nebular or planetary, due to the slow diffusion rates of Si. There is also no strong evidence for precursor heterogeneity being the primary cause of the Si isotopic composition variability; but equally it cannot be ruled out completely. The most likely cause of the limited variation in $\delta^{30}\text{Si}$ of chondrules is evaporation overprinted by re-equilibration with the evaporated phase.

Acknowledgments

This thesis would not have happened without the support and encouragement from numerous individuals over the past four years.

First, and foremost, I would like to thank my three supervisors, Alex Halliday, Bastian Georg and Helen Williams for all the help and support they have given me throughout my time as a postgraduate. I am deeply indebted to them all for the scientific discussions, numerous corrections and guidance I have enjoyed over the years. I am grateful to Alex for providing me with the opportunity of working on such an exciting and entrancing subject. His constant energy and enthusiasm whenever I presented him with some new data was always cheering. His abilities with presenting science whether in spoken or written form provided an excellent example to follow. I will forever be beholden to Bastian for teaching me all I know of Si isotope measurements (despite his professed antipathy towards high-temperature systems). I am very grateful for all the hours he spent teaching me column chemistry and the ways of mass spectrometry. I am deeply appreciative for Helen for all those times of being able to bounce around ideas with her, from “What is the best way to plot this?” to “Diffusion calculations, help!”. I have also benefited greatly from her skills at making sure I was properly introduced to people at conferences. Much appreciation also goes to the Science and Technologies Facilities Council (and the British taxpayer) for funding my research. Don Porcelli and Tim Elliott are both deserving of many thanks for examining this thesis.

There are numerous other individuals who supplied key assistance during my time as a DPhil student in Oxford. Kevin Burton helped and supported me tremendously with scientific chats, and advice and equipment to work on lunar and meteoritic samples. He also gave me the wonderful opportunity to visit Iceland despite never having analysed a sample from there. Julie Prytulak has also been an important presence during my years as postgrad. She has been a constant source of wisdom and always unstinting in her opinions, whether it be on clean lab etiquette, the low-down on other scientists or the abilities of certain football teams. Jon Wade has been very helpful, particularly in the last year or so, for all the discussions about element partitioning and enstatite chondrites. In addition, I am very grateful to him for all his help in preparing the polished chondrule samples. Paul Savage, my fellow Si comrade in arms also deserves many thanks. From shared analytical tribulations, to PT nights, to road(and train)trips to conferences, I am grateful for all the support and friendship I have received from him over the course of our DPhils. Steve Wyatt

(and the ubiquitous ClassicFM) merits immense appreciation for all the provision of clean acid and furnace capabilities over the years. Many thanks go to Phil Holdship for all the help with the elemental analyses. I am grateful to Norman Charnley for teaching me (again) how to use the department SEM.

Caroline Smith, Dominik Hezel and Sara Russell at the NHM deserve many thanks, not least for providing me with meteorite samples. They also helped me tremendously with understanding these fascinating rocks. I am indebted to CAPTEM for providing me with the lunar samples.

Many other members (past and present) of the Oxford isotope laboratory (for) Earth tracers deserve boundless gratitude for all the science, support and occasional cider: Dave Cook for the MFL3 and cosmochem chat; Chris Siebert for P3 troubleshooting and often letting me run into the morning of his mass spec days; Sophie Opfergelt who made clays seem interesting for the first time; Nick Belshaw and Theo Krastev for all the help when the mass spec gremlins decided to go to work; Louise Gall for the coffee breaks (well tea in my case) and non-geological discussions; Emily Stevenson for being continually enthusiastic about everything and being a great officemate during the writing-up period.

There are many other Earth Scientists who have been integral to my sanity during the past four years and deserve profound appreciation and thanks. My co-years: Aisha (occasional officemate and good source of book recommendations); Jodi (always good for a chat); Marcus (ideal ranting partner); Alex and David who have been there from our first days in Oxford, from maths tutes to mapping in Skye and finally DPhilling. I am also grateful to Lara, for the walks and the chats about life, the universe and everything; Andrew for all the Seismolab entertainment; and officemates Al and Xinyuan who put up with me during the final months of writing-up.

The Wolfson Crew have also been a key part of keeping me going for past four years. For all the times outside Wolfson bar or in the bunker: Matt, Rae, Iana, Vanina, Mike, Laurie and Dale. Also Hannah, for the chats, squash and cryptic crosswords. Other Oxford people deserving of thanks include Abi, Flick, Kathryn, Lisa and Méabh.

Finally I would like to thank Mum and Dad, without whom none of this would have happened.

Contents

Abstract	ii
Extended abstract	iii
Acknowledgments	vii
1 Introduction	1
1.1 Solar System evolution and planetary formation	1
1.2 Meteorites	3
1.2.1 Chondrites	4
1.2.2 Achondrites	7
1.2.2.1 Primitive achondrites	8
1.2.2.2 Differentiated achondrites	9
1.3 Stable isotopes in meteorites	10
1.3.1 Mass independent variation	11
1.3.2 Mass dependent fractionation	15
1.4 Silicon isotopes	17
1.5 Previous Si isotope data	18
1.6 Motivation for this study	21
2 Method	23
2.1 Introduction to Si isotope methods	23
2.2 Analytical Method	26
2.2.1 Chemical preparation	26
2.2.1.1 Alkaline fusion	26
2.2.1.2 Column chemistry	28
2.2.2 Mass spectrometry	30
2.2.2.1 Principles of MC-ICPMS	30
2.2.2.2 Pseudo high resolution analysis	37
2.2.2.3 Data collections protocols	41

3	Assessing potential sources of inter-laboratory variation in $\delta^{30}\text{Si}$	46
3.1	Introduction	46
3.2	Compositional effects	48
3.3	Re-analysis of samples	51
3.3.1	Sample powders	51
3.3.2	Sample solutions	54
3.4	Sample heterogeneity and sample preparation	56
3.5	Sample solution pH	59
3.6	Standard Addition	61
3.7	Conclusions	66
4	Silicon isotopes in meteorites and planetary core formation	67
4.1	Introduction	67
4.2	Samples and analytical methods	69
4.2.1	Sample preparation	69
4.3	Results and Discussion	76
4.3.1	Introduction	76
4.3.1.1	Chondrites	76
4.3.1.2	Achondrites	81
4.3.1.3	Terrestrial rocks	83
4.3.1.4	Comparison with previous studies	83
4.3.2	Assessment of recent of Si isotope data	84
4.3.2.1	Meteorite and terrestrial mean values	84
4.3.2.2	Sample by sample comparison	86
4.3.3	$\Delta^{30}\text{Si}_{\text{BSE-meteorite}}$	88
4.3.4	Evidence for silicon in the Earth's core	92
5	Silicon isotopes in lunar rocks: implications for the Moon's formation and the early history of the Earth	99
5.1	Introduction	99
5.2	Method	102
5.2.1	Samples	102
5.2.2	Analytical methods	102
5.3	Results	106
5.4	Discussion	110
5.4.1	Lunar mantle composition	110
5.4.2	Highland rocks	114

5.4.3	Moon formation	115
5.4.4	Core formation post lunar formation?	118
5.5	Conclusions	120
6	Silicon isotopic composition of lunar basalt mineral separates	122
6.1	Introduction	122
6.2	Method	124
6.3	Results	124
6.4	Discussion	128
6.4.1	Variations in fractionation factors in lunar basalts	128
6.4.1.1	Thermal effects	131
6.4.2	Variation between terrestrial and lunar mineral-melt fractionation factors	133
6.4.2.1	Crystallisation of the lunar basalts	136
6.4.2.2	Different lunar fractionation factors	138
6.4.3	Lunar magma ocean and source variation in $\delta^{30}\text{Si}$?	139
6.5	Conclusions	141
7	Silicon isotopic variation in chondrules: evidence of nebular formation	143
7.1	Introduction	143
7.2	Method	146
7.2.1	Sample preparation	147
7.2.2	Petrological examination	148
7.2.3	Isotopic and elemental analysis	148
7.3	Results	149
7.3.1	Petrological examination	151
7.3.2	Chondrules	154
7.3.3	Refractory inclusions	164
7.3.3.1	Calcium aluminium inclusions	164
7.3.4	Other components	167
7.4	Discussion	168
7.4.1	Si isotopic composition of CAIs	168
7.4.2	Cause of variation in $\delta^{30}\text{Si}$ of chondrules	169
7.4.2.1	Heterogeneity in $\delta^{30}\text{Si}$ of source reservoirs	169
7.4.2.2	Formation mechanisms of chondrules as cause of $\delta^{30}\text{Si}$ variations	173

CONTENTS

7.4.2.3	Alteration of chondrules post formation	175
7.4.3	Relationship between chondrules and bulk chondrite	176
7.5	Conclusion	178
	Summary and Outlook	179
	References	184

List of Figures

1.1	Beta Pictoris	2
1.2	Meteorite classification	5
1.3	Oxygen isotopes in chondrites	11
1.4	Oxygen isotopes in achondrites	12
1.5	Si isotope composition of pre-solar grains	14
1.6	$\delta^{30}\text{Si}$ of a selection of terrestrial (and extra terrestrial) reservoirs	20
2.1	Elution curves	28
2.2	Mass spectrometer schematic	31
2.3	Pseudo high resolution	38
2.4	Peak scans	39
2.5	Diatomite	42
2.6	IRMM-018 and BHVO-1, -2	44
3.1	Comparison of the previous high resolution Si datasets	47
3.2	$\delta^{30}\text{Si}$ versus Fe and S	49
3.3	Georg et al. (2007) versus this study	52
3.4	Re-analysing Georg et al. (2007) solutions	53
3.5	Re-analysis of sample solutions	57
3.6	Allende aliquots	58
3.7	$\delta^{30}\text{Si}$ versus pH	60
3.8	Standard addition tests	62
4.1	$\delta^{29}\text{Si}$ versus $\delta^{30}\text{Si}$	70
4.2	Meteorite $\delta^{30}\text{Si}$ data	75
4.3	$\delta^{30}\text{Si}$ vs Mg/Si	78
4.4	$\delta^{30}\text{Si}$ of enstatite chondrites	80
4.5	Histograms of meteorite and terrestrial populations	85
4.6	Sample by sample inter-lab comparison	87

LIST OF FIGURES

4.7	High-resolution $\delta^{30}\text{Si}$ data compared to earlier studies	88
4.8	Parameter space for Si in the core	94
4.9	Temperature of core formation calculated from $\Delta^{30}\text{Si}_{\text{BSE-meteorite}^*}$	96
5.1	$\delta^{30}\text{Si}$ versus $\delta^{29}\text{Si}$ for lunar samples	104
5.2	$\delta^{30}\text{Si}$ of bulk lunar samples	111
5.3	$\delta^{30}\text{Si}$ lunar data histograms	112
6.1	$\delta^{30}\text{Si}$ of lunar basalt mineral separates	127
6.2	$\Delta^{30}\text{Si}_{\text{fractionation factors}}$	129
6.3	Calculated bulk $\delta^{30}\text{Si}$ lunar basalt separates	130
6.4	Closure temperature calculations	134
6.5	$\delta^{30}\text{Si}$ of melts in equilibrium with the minerals	135
6.6	Rayleigh fractionation curves for olivine and pyroxene	137
6.7	Plagioclase fractionation in the LMO	140
7.1	$\delta^{30}\text{Si}$ of CV3 chondrite components	150
7.2	Backscattered electron images of Allende components	156
7.3	Variation in $\delta^{30}\text{Si}$ of the chondrules	160
7.4	$\delta^{30}\text{Si}$ versus major element concentration	162
7.5	$\delta^{30}\text{Si}$ versus $\delta^{29}\text{Si}$ for CAIs	166
7.6	Histogram of $\delta^{30}\text{Si}$ compositions of chondrules	170
7.7	Normal probability plot	171
7.8	$\delta^{30}\text{Si}$ versus Mg/Si for CV3 components	177

List of Tables

1.1	Summary of the main chondrite groups	6
2.1	Cations in sample solutions before and after column chemistry	30
2.2	Column cleaning	30
2.3	Operating conditions for the Nu Plasma	37
3.1	Re-analysis of sample powders	55
3.2	Standard addition measurements	64
4.1	Silicon isotope data of standards, meteorites and terrestrial samples	72
4.2	Comparison of recent high resolution $\delta^{30}\text{Si}$ data	84
4.3	$\delta^{30}\text{Si}$ with BHVO-2 as bracketing standard	90
4.4	Student t-test for BSE versus meteorites	91
4.5	Calculations of Si (wt%) in the Earth's coreS	97
5.1	Silicon isotope data of standards, meteorites and terrestrial samples	106
5.2	Direct measurements of $\Delta^{30}\text{Si}_{\text{BHVO2-lunar}}$	110
6.1	Silicon isotope data for lunar basalt mineral separates	125
6.2	Diffusion data for Si in mineral phases	133
7.1	$\delta^{30}\text{Si}$ and elemental data for components from CV3 meteorites	152

LIST OF TABLES

Chapter 1

Introduction

1.1 Solar System evolution and planetary formation

The chemical composition and make-up of the Earth is the culmination of a series of processes that began even before the start of the solar system. Nuclear processes inside stars and supernovae (collectively known as nucleosynthesis) are responsible for generating the elements and isotopes of the periodic table. Within the interstellar medium dense molecular clouds, formed from a diversity of these stellar sources, are the breeding grounds for young stars (e.g. Messenger et al., 2006). It is thought that the collapse of one such dense molecular cloud core due to self-gravitation formed the protosun and solar nebula (e.g. Boss, 2007). This event is taken to be the start of solar system evolution. The first stages of planetary accretion began with the coagulation of micron-scale particles that settled out into the mid-plane of the nebular disk. This protoplanetary disk of dust and gas was host to a number of processes, such as evaporation, condensation and melting, leading to the formation of refractory calcium-aluminium inclusions (CAIs), which are generally accepted to be the oldest known solids to have formed in the solar system (e.g. McKeegan and Davis, 2007).

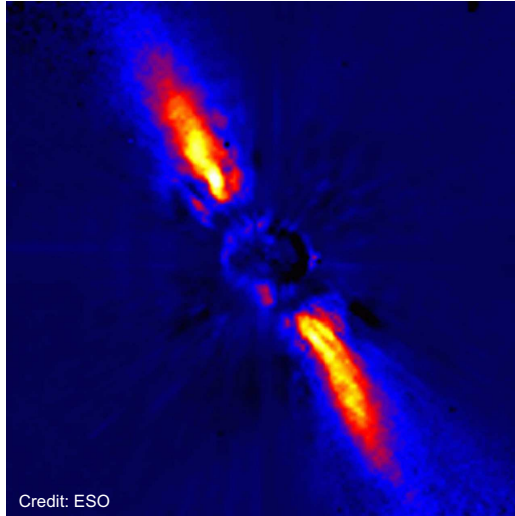


Figure (1.1): This false colour near infrared image shows the dust disk around the young (~ 12 Myr) star Beta Pictoris (ESO, 1997). This well-studied debris disk has also been shown to host at least one planet (Lagrange et al., 2010).

Chondrules, millimetre-scale rounded igneous objects, are also thought to date from this early nebular phase. Once kilometre-scale planetesimals formed, accretion proceeded through gravitational attraction and collision. Following this was a period of “runaway growth” (also gravitationally driven), where planetary embryos, Mercury- to Mars-sized objects, were built over timescales on the order of $\sim 10^5$ yr (Wetherill and Stewart, 1989). The final stages of accretion to form planets the size of Earth and Venus involved stochastic “giant impacts” between the planetary embryos. The remaining planetesimals would have been either swept up or may have been removed either by falling into the Sun or through ejection from the solar system (e.g. Chambers, 2007).

During planetary formation energy released from gravitational accretion and the decay of short-lived radionuclides provided the heat for differentiation of planetesimals and planetary embryos. The most significant chemical differentiation was metal-silicate fractionation or core formation. Hafnium-tungsten dating of iron meteorites,

thought to be the cores of planetesimals, show that core formation happened early on in solar system history within 1.5 Myr of CAI formation (Kleine et al., 2005; Markowski et al., 2006; Scherstén et al., 2006).

The Earth's tectonic activity has erased the first few hundred million years of the Earth's history from the rock record, which limits the use of terrestrial samples to understand the processes in the solar nebula or the earliest history of differentiation on planetary bodies. Therefore, information must be sought from beyond the confines of the terrestrial realm. Astronomical observations of dust and gas disks surrounding other stars are one tool to understand the solar protoplanetary disk (Fig. 1.1). An alternative option is to analyse material from the solar system that has undergone little processing in the past 4.57 Gyr and which can be sampled in the form of meteorites.

1.2 Meteorites

Meteorites are commonly classified based on their textures into three main categories: stones, irons and stony-irons. A more useful division in order to probe planetary formation is the split between primitive and differentiated meteorites. Figure 1.2 gives the classification based on textural categorisation, with the blue boxes indicating those meteorites that are differentiated rather than primitive. Stony-irons contain roughly equal amounts of silicate and Fe-Ni metal. There are two types (i) pallasites, where the silicate is set in an unbroken mesh of metal, and which may sample the core-mantle boundary in an asteroid and (ii) mesosiderites, which probably formed via surface impact processes on the surface of a differentiated asteroid (Mittlefehldt et al., 1998). The information on stony-iron meteorites is very limited relative to other groups of meteorites. Their texture is such that homogeneity of sample material is hard to achieve; hence stony-iron meteorites have not been analysed in this study. Iron meteorites, in most cases, do not contain enough silicon (90- 460ppb, Pack et al.,

2011) to allow for Si isotopic measurements. Therefore, they are also unlikely to be significant in terms of early Earth budgets and hence they will not be discussed in further detail. A brief description of those groups of meteorites that are analysed in this work follows.

1.2.1 Chondrites

The textures of stony chondrites show that they have not undergone melting since the accretion of their constituents. These meteorites are agglomerates of chondrules, CAIs (calcium aluminium inclusions), metal, sulphide and matrix (usually a fine-grained silicate material). Their bulk chemical composition approaches that of the Sun's photosphere apart from the incompletely condensed elements such H, He, N, C, O (Scott and Krot, 2007). It is thought that the best representation of the refractory component that accreted to form the Earth is to be found among the chondrite groups. They are generally thought of as primitive meteorites but most show some degree of alteration, either by aqueous fluids and/or thermal metamorphism. This processing may have happened on the meteorite parent body or from further interaction within the solar nebula (e.g. Brearley, 2003). Primary variations in chemical and isotopic composition have been used to classify these meteorites (Table 1.1; Figure 1.3). The chemical composition of CI chondrites has the closest resemblance to the sun, making CIs the most chemically primitive of all the chondrite groups (e.g Anders and Ebihara, 1982).

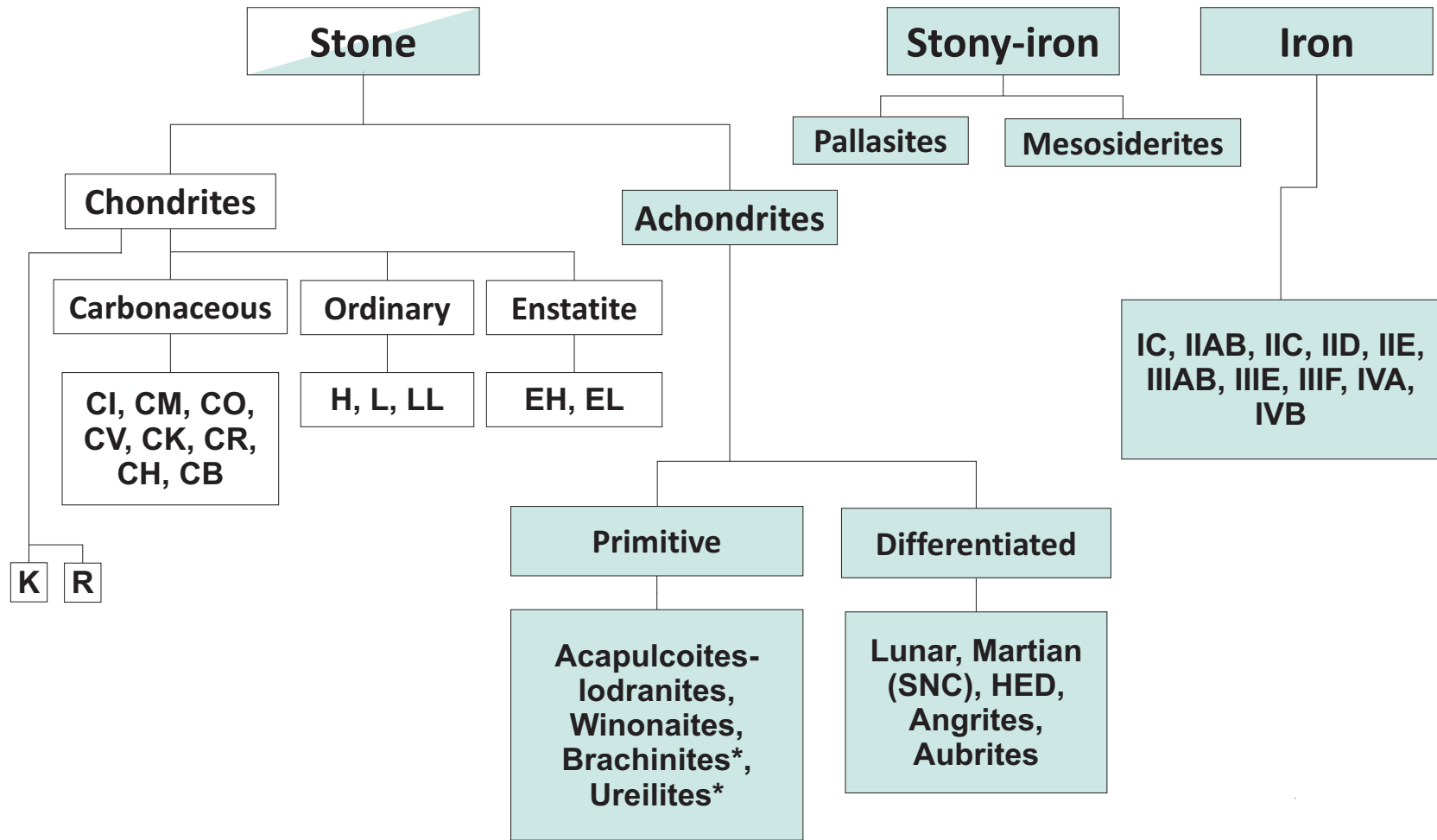


Figure (1.2): Meteorite classification based on texture. The blue shaded boxes indicate those meteorites that have undergone differentiation. The stars designate those groups of achondrites that are sometimes classified as differentiated rather than primitive (Weisburg et al., 2006; Krot et al., 2007)

1.2. Meteorites

Table (1.1): Summary of the main chondrite groups and their petrologic properties (after Scott (2007))

Group	Petrologic type ^a	CAIs and AOAs (vol%) ^b	Chondrules (vol%)	Fe, Ni metal (vol%)	Matrix (vol%)	Examples ^c
Carbonaceous						
CI	1	<0.01	<5	<0.01	95	Orgueil
CM	1-2	5	20	0.1	70	Murchison
CO	3	13	40	1-5	30	Ornans
CV	2-3	10	45	0-5	40	Allende
CK	3-6	4	15	<0.01	75	EET 92002
CR	1-2	0.5	50-60	5-8	30-50	Renazzo
CH	3	0.1	~70	1-5	30	ALH 85085
CB	3	<0.1	30-40	60-70	<5	Bencubbin
Ordinary						
H	3-6	0.01-0.2	60-80	8	10-15	Allegan
L	3-6	<0.1	60-80	3	10-15	Barratta
LL	3-6	<0.1	60-80	1.5	10-15	Parnallee
Enstatite						
EH	3-6	<0.1	60-80	8	<0.1-10	Indarch
L	3-6	<0.1	60-80	15	10-15	Khairpur
Other						
K	3	<0.1	20-30	6-9	70	Kakangari
R	3-6	<0.1	>40	<0.1	35	Rumuruti

^a The numbers refer to a secondary classification scheme for chondrites: 1-2 = aqueous alteration; 3-6 = increasing degrees of thermal metamorphism

^b CAI=calcium aluminium inclusion, AOA= amoeboid-olivine aggregate; both are refractory inclusions

^c When possible, meteorites that are analysed in this thesis have been picked as examples

The components of chondrites can contribute key information when studying nebular processes. Chondrules, from which chondrites derive their name, are sub-millimetre sized spherical objects and in most cases constitute a significant volume of the meteorite (Table 1.1). The defining characteristic of chondrules is that they all appear to have been melted to some degree at some point and most consist of ferromagnesian silicate material (Brearley and Jones, 1998). Some are melt droplets

and others are igneous systems with, for example, olivine and pyroxene phases that have been subsequently rounded (Sears, 2004). The standard model for archetypal chondrule formation involves closed-system crystallisation where volatile loss from chondrules was minimized by flash melting of dust aggregates, lasting only seconds to minutes (Scott and Krot, 2007). Other formation mechanisms that would minimise volatile loss include melting under high dust-gas ratios or high gas pressures.

Other components of interest are CAIs and pre-solar grains. Evidence from short-lived radionuclide chronometers e.g. ^{26}Al – ^{26}Mg , ^{129}I – ^{129}Xe , ^{53}Mn – ^{53}Cr , show that CAIs are the oldest known objects formed in the solar system (McKeegan and Davis, 2007). CAIs are composed dominantly from Al-, Ti-, Ca-rich FeO poor oxide and silicate minerals that are stable at high temperatures. The Mg and Si in CAIs is isotopically heavy relative to bulk chondrites and their mass-dependent fractionations point to evaporative loss during their formation (Clayton et al., 1988; Shahar and Young, 2007).

1.2.2 Achondrites

The achondrite class covers a wide range of mineralogies, petrologies, chemical compositions and likely origins. They make up only $\sim 3\%$ of the known stones category as a whole (Grady, 2000) and can be roughly grouped into differentiated achondrites and ‘primitive’ achondrites. This grouping is based on the degree of melting the meteorite has undergone relative to chondrites. However, the boundary between these two categories is not clear cut, and for some groups of meteorites (see Fig. 1.2) there is no clear consensus as to which category they belong in. Whereas chondrites are often used to study nebular processes, achondrites can inform theories about asteroid and planetesimal differentiation in the solar system.

1.2.2.1 Primitive achondrites

Primitive achondrites are differentiated meteorites that have igneous or metamorphic textures but approximately chondritic bulk composition (Krot et al., 2007). They are generally thought to be ultrametamorphosed chondrites that may also, in some cases, have experienced very low degrees of partial melting (Mittlefehldt et al., 1998). There appears to be a general consensus that acapulcoites-lodranites, winonaites and IAB chondritic silicates (silicate inclusions in iron meteorites) are primitive achondrites, due to their near chondritic mineralogy (olivine, Ca-poor pyroxene, significant metal and sulphide) and chemical composition (Hutchison, 2006).

Brachinites and ureilites do not sit so comfortably in the primitive achondrite category. Brachinites are medium- to coarse-grained olivine-rich rocks. There is some debate over their origin, whether they are partial melt residues or igneous cumulates. If the latter, they should be classified as differentiated achondrites (Weisburg et al., 2006). Ureilites are an unusual group of meteorites due to their combination of primitive and differentiated characteristics. They resemble residual terrestrial peridotites in that they are ultramafic olivine and pyroxene rocks. However, unlike mantle rocks, they contain interstitial material with varying amounts of carbon, metal, sulphides and silicates (Mittlefehldt et al., 1998). The trace element chemistry of ureilites indicates that they are missing a basaltic complement, which in turn implies a large degree of partial melting (Goodrich, 1992). However, their oxygen isotopes compositions display trends with slope ~ 1 on three isotope oxygen plots (Figure 1.4b), which appears to contradict the extensive igneous processing seen in the petrology. This points to either an isotopically heterogeneous parent body or at least 6 distinct oxygen isotope reservoirs (Goodrich, 1992).

1.2.2.2 Differentiated achondrites

The largest suite of crustal igneous rocks available for study from any single solar system body other than the Earth or Moon is the howardite, eucrite and diogenite (HED) suite of meteorites (Mittlefehldt et al., 1998). The Fe/Mn ratios of the pyroxenes and the oxygen isotope ratios support a genetic link between these three types of meteorite (Krot et al., 2007). There is a gradation from the basaltic eucrites into the diogenites, which are coarse-grained orthopyroxenites thought to be cumulates from a fractionally crystallising magma (Mittlefehldt et al., 1998). Howardites are polymict breccias that contain clasts of both eucrite and diogenite lithologies. The HED meteorite group is the only one, other than lunar and martian meteorites, for which there is a candidate parent body: the reflectance spectra of the asteroid 4 Vesta has been shown to match that of a basaltic eucrite (McCord et al., 1970).

The SNC (shergottite-nakhlite-chassignite) meteorites are generally accepted to be Martian igneous rocks (McSween Jr and Treiman, 1998). They are linked as a group due to their common, distinct, mass-dependent oxygen isotope trend (Figure 1.4a). The unique noble gas signature of the Martian atmosphere measured by the Viking spacecraft matches the noble gas ratios in shock-implanted glass in a number of SNC meteorites; hence why SNC meteorites are generally accepted to come from Mars (Marti et al., 1995). With new desert finds, the acronym SNC does not cover the entire range of martian lithologies that have been observed; hence why the term “martian meteorite clan” is sometimes used instead (Weisburg et al., 2006). Martian meteorites are also, in most cases, much younger than other meteorite groups, with crystallization ages for the nakhlites and chassignites being ~ 1.3 Gyr and some shergottites having crystallisation ages of ~ 175 Myr rather than 4.5-4.6Gyr ages of chondritic materials (Nyquist et al., 2001). This implies some form of sustained, ongoing tectonic activity on the parent body after initial accretion. The majority of the Martian meteorites are basaltic shergottites, while the nakhlites are olivine clinopyroxenites that may

1.3. Stable isotopes in meteorites

have a sill or surface lava flow origin (McSween Jr and Treiman, 1998). Chassigny is a unique meteorite made up of $\sim 90\%$ olivine and hence has been interpreted as a cumulate dunite (Hutchison, 2006).

The total mass of known lunar meteorites pales into insignificance in comparison to the amount of material that was returned from the near side of the moon by the six Apollo landings and three robotic Luna missions. However, the composition of some of the lunar meteorites implies that they may be from the far side of the moon (Hutchison, 2006), though the data is not conclusive.

Aubrites are brecciated pyroxenites that formed under very reducing conditions, and are thus FeO poor. A link between aubrites and enstatite chondrites has been proposed on the basis of their reduced mineralogy and oxygen isotope ratios (e.g. Mittlefehldt et al., 1998) but this has yet to be universally accepted due problems of cosmic ray exposure ages and composition (Keil, 2010).

The final group of highly differentiated achondrites are the angrites, which range in texture from basalts to pyroxenites (Mittlefehldt et al., 1998). They have identical oxygen isotope compositions suggesting that they originated on a common body. They are the most highly alkali-depleted basalts in the solar system, hence their use to approximate the Earth's initial $^{87}\text{Sr}/^{86}\text{Sr}$ ratio. Their absolute age can also be precisely determined due to their high U/Pb ratios.

1.3 Stable isotopes in meteorites

Measurements of stable isotope ratios in meteorites allows for the investigation of processes in the solar nebula and primary planetary differentiation. Stable isotopic variations in natural samples can be split into two main categories: those that relate to isotopically distinct sources that have not been completely homogenised, and those that are the result of physical processing of a once homogeneous reservoir. The former

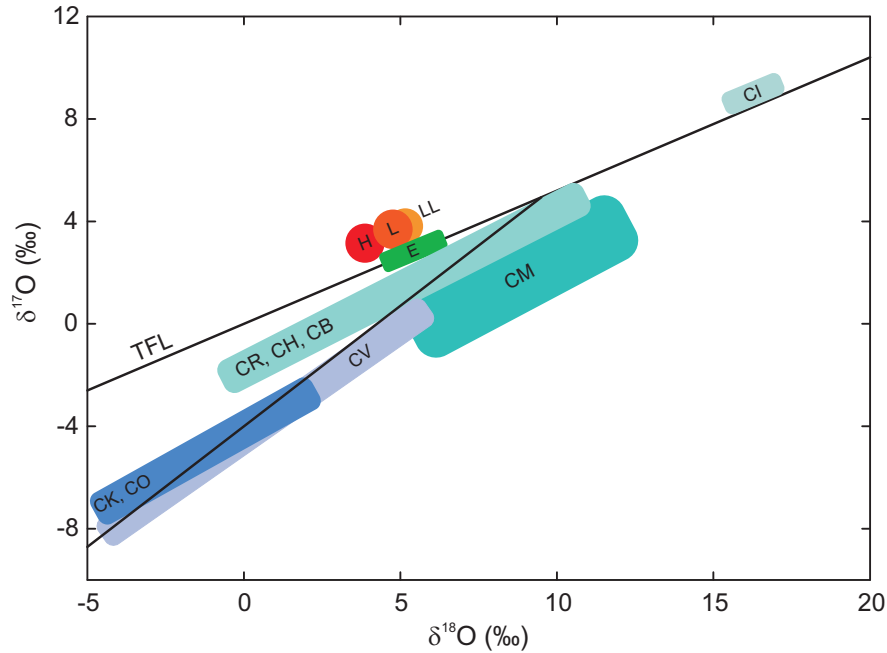


Figure (1.3): Oxygen isotope ranges for whole rock samples from the major chondrite classes. TFL= Terrestrial fractionation line, the other plotted slope is CCAM (carbonaceous chondrite anhydrous mineral). Data are from Clayton et al. (1984, 1991), TFL and CCAM are from Clayton (2003b)

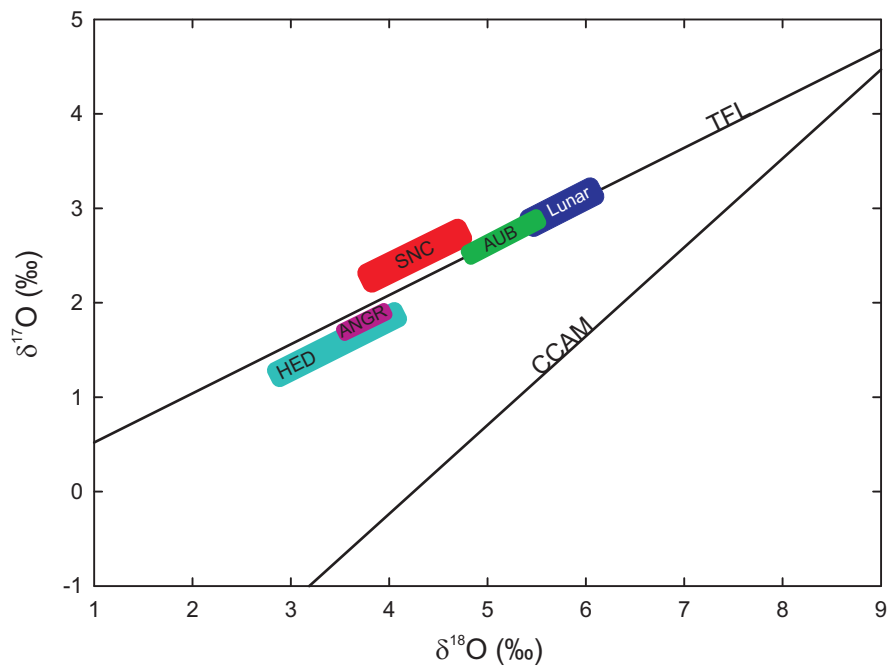
variations are known as mass independent anomalies, whereas the latter variations can be described in terms of mass-dependent fractionation laws.

1.3.1 Mass independent variation

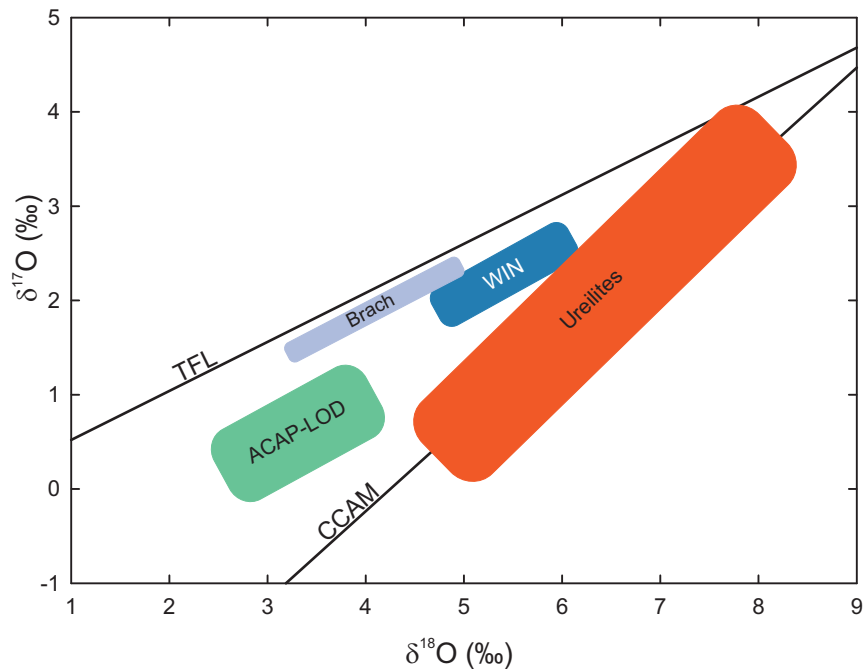
Mass independent isotopic variations usually reflect either different nucleosynthetic formation pathways (e.g. p-, r-, s-process) for the different isotopes, or in some rarer cases chemical reactions (Thiemens, 2006).

Mass-independent anomalies of oxygen isotopes have long been used by meteoritists for discriminating between different parent bodies for meteorites (e.g. Clayton et al., 1976). In the case of oxygen it is thought that the mass independent variations are related to a chemical process rather than nuclear processes (Thiemens,

1.3. Stable isotopes in meteorites



(a) Differentiated achondrites



(b) Primitive achondrites

Figure (1.4): Data are from Clayton and Mayeda (1996, 1999) TFL (terrestrial fractionation line) and CCAM (carbonaceous chondrite anhydrous mineral) slopes are from Clayton (2003b)

2006; McKeegan et al., 2011). The parent bodies for meteorites can be distinguished from each other on a three isotope plot of oxygen (Figure 1.3 and 1.4). In general, mass independent anomalies in meteorites are usually interpreted as the result of large scale isotopic heterogeneity due to inefficient mixing in the protoplanetary disk. Anomalies have been identified in solar system material in the isotopic ratios of O (e.g. Clayton, 2003b), Ti (Leya et al., 2008), Ni (Regelous et al., 2008), Mo (Dauphas et al., 2002), Ru (Chen et al., 2010), Os (Brandon et al., 2005), Sm (Andreasen and Sharma, 2006), Nd (Andreasen and Sharma, 2006), Cr (Trinquier et al., 2009) and Zr (Schönbächler et al., 2005b) among others. However, there are other elements with similar variations in nucleosynthetic origins for their isotopes such Te, which do not show measurable variations (Fehr et al., 2006). This indicates that the portion of the solar nebula where inner solar system bodies accreted was isotopically heterogeneous with respect to some elements but not others. The anomalies in different classes of chondrite can be used to identify likely precursors to the Earth. It can be seen from Figure 1.3, that CI and enstatite chondrites are the only groups that are close to or on the terrestrial fractionation line for oxygen. Enstatite chondrites are the only bulk meteorites that match the Earth as regards the Ni (Regelous et al., 2008), Cr and Ti (Trinquier et al., 2009) mass independent anomalies. Enstatite chondrites as the precursor material to the Earth pose some serious problems, however, with respect to element constraints (Palme and O'Neill, 2003).

Mass-independent Si isotope anomalies have been measured in pre-solar grains. Pre-solar grains are refractory phases that are recognisable due to their extreme isotopic signatures, and are therefore thought to have formed outside of the solar system (Figure 1.5). These nanoparticles, including diamond, graphite and silicon carbide (SiC), are thought to have formed in stellar outflows or the ejecta of stellar explosions (Ott, 2007). The volume of these phases is so small that it is not possible to see traces of their extreme and mass independent signal in bulk meteorite analysis

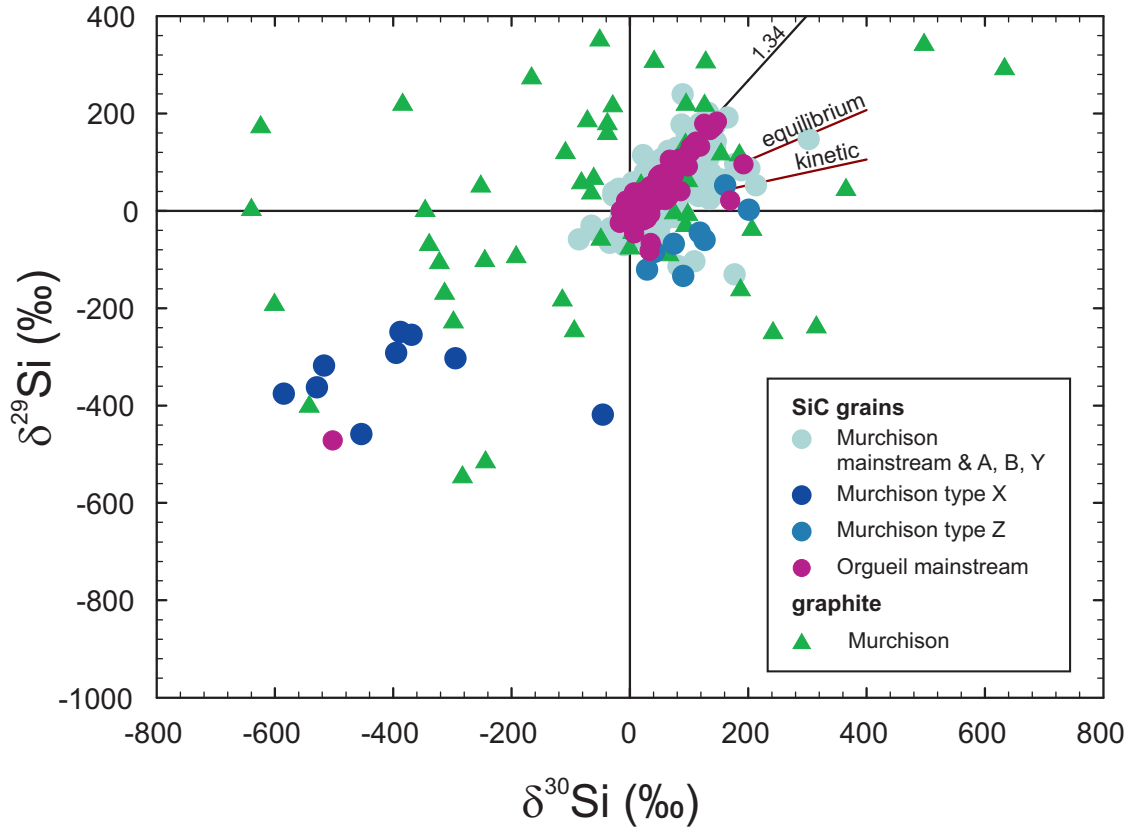


Figure (1.5): The variation in the Si isotopic composition of pre-solar grains is up to three orders of magnitude greater than the variations seen in bulk meteorite samples. The equilibrium and kinetic lines on the figure are the mass dependent fractionation lines (see Section 1.3.2). Mainstream SiC grains follow an approximate trend of 1.34, thought to result from galactic chemical evolution and also that the grains derive from a large number of AGB (asymtotic giant branch) stars (Ott, 2007). A and B subtypes are indistinguishable from mainstream grains as regards their Si isotope composition. Y grains are those that fall on the ^{30}Si -rich side of the mainstream grains (Ott, 2007). The source of the Z grains are thought to be low mass, low metallicity AGB stars (Hoppe et al., 1997), while X grains are have their origins in supernovae Ott (2007). Wolf-Rayet and Type II supernovae are thought to account for the properties of the majority of the graphite grains (Hoppe et al., 1995). Data are from Huss and Hutcheon (1997); Hoppe et al. (1997, 1996); Hoppe et al. (1994); Hoppe et al. (1995)

for Si isotopes.

1.3.2 Mass dependent fractionation

There are two different kinds of mass dependent isotopic fractionation reactions: equilibrium and kinetic. Equilibrium fractionation is a purely quantum phenomenon, driven mainly by differences in the vibrational energies of molecules and crystals containing atoms with different masses (Schauble, 2004). Kinetic fractionation results from motions that can be described classically using effective masses and occurs when there is incomplete isotopic exchange between reactants. Mass dependent fractionations can be described graphically as plotting on a straight line in three isotope space (i.e. a plot of $\delta^{30}\text{Si}$ vs $\delta^{29}\text{Si}$). The slope of the line is the exponent relating to the fractionation factor and is different for kinetic and equilibrium reactions (Young et al., 2002b).

$$\beta_{\text{equi}} = \frac{\left(\frac{1}{m_1} - \frac{1}{m_2}\right)}{\left(\frac{1}{m_1} - \frac{1}{m_3}\right)} \quad (1.1)$$

$$\beta_{\text{kin}} = \frac{\ln\left(\frac{m_1}{m_2}\right)}{\ln\left(\frac{m_1}{m_3}\right)} \quad (1.2)$$

where $m_1 < m_2 < m_3$. For silicon the exponents are $\beta_{\text{equi}} = 0.5178$ and $\beta_{\text{kin}} = 0.5092$ when using the exact atomic masses of $^{28}\text{Si} = 27.97693$, $^{29}\text{Si} = 28.97649$ and $^{30}\text{Si} = 29.97377$ (Audi and Wapstra, 1993). At the current levels of precision it is only possible to distinguish between these two slopes at isotopic variations $> +5\%$ or $< -5\%$. Most of the Si isotopic fractionations in high temperature, abiotic systems are too small to identify the type of the mass dependent fractionation from the Si isotope data. To date no mass-independent fractionations have been measured for Si in terrestrial or bulk meteorite samples; hence the mass dependency of measured

data is often used as a means of quality control.

Recent developments in MC-ICPMS (multi-collector inductively-coupled-plasma mass-spectrometry), have lead to an expansion in the number of studies being carried on stable mass dependent isotope variations in solar system materials. Differentiation on various planetary parent bodies, whether metal-silicate or magmatic, is often an issue investigated with mass dependent isotopic data. The search for the material that accreted to form the Earth is not just confined to mass independent anomalies, but is also within the scope of mass dependent fractionations as well. These fractionations are often very small (on the order $\sim 0.5\%$), so for many elements there is still much vigorous debate as to whether there is any resolvable variation in the inner solar system. Magnesium is a case in point, with at least two recent studies finding a difference between bulk silicate Earth (BSE) and chondrites (Wiechert and Halliday, 2007; Young et al., 2009) and four finding no resolvable difference (Teng et al., 2007; Bourdon et al., 2010; Chakrabarti and Jacobsen, 2010a; Pogge von Strandmann et al., 2011). The Fe story is not much simpler. There appears to be a consensus that chondrites, HED and SNC meteorites are all the same within uncertainty, pointing to a relatively well mixed inner solar system (Zhu et al., 2001; Poitrasson et al., 2004; Weyer et al., 2005; Schoenberg and von Blanckenburg, 2006). The disagreement comes over whether Fe isotopes fractionate during partial melting and therefore the Fe isotopic composition of BSE (Williams et al., 2005; Schoenberg and von Blanckenburg, 2006; Teng et al., 2008). If only peridotites are used for BSE, then BSE is the same as chondrites within uncertainty (Weyer et al., 2005). If a more general compilation of mantle derived rocks is used, the Earth is now heavier than other planetary bodies, which could be ascribed to partial vaporisation in the lunar-forming Giant Impact (Poitrasson et al., 2004).

Outside of these major elements, mass dependent variations in the inner solar system have been observed for a number of other elements. Mass dependent isotopic

variations in Cr between BSE and chondrites point to Cr partitioning into Earth's core (Moynier et al., 2011). For some stable isotope systems, just as with mass dependent anomalies, meteorite groups other than carbonaceous chondrites appear to be the best primary building blocks for Earth. Calcium isotope data indicate that ordinary chondrites represent the best material from which to build the inner planets (Simon and DePaolo, 2010), whereas stable Sr isotopes rule out CV or CO meteorites as Earth precursor material (Moynier et al., 2010). The Li isotopic composition of differentiated materials, such as basalts from Earth, Moon, Mars and other achondrites, is heavier than chondrites. There is also variation in Li isotopic composition between carbonaceous and ordinary chondrites (Seitz et al., 2007; Magna et al., 2006). It is possible that the lighter chondritic values and the variation between the chondrite groups may be caused by secondary processes on their parent bodies. Secondary processes on chondrite parent bodies are also thought to affect Cd isotopes. The inner solar system is homogeneous as regards Cd isotopes with the exception of ordinary and some enstatite chondrites, and these variations are thought to be due to volatilization and redistribution of Cd during open-system metamorphism on the parent bodies (Wombacher et al., 2008).

1.4 Silicon isotopes

Silicon is a ubiquitous element on Earth, being the third most abundant element on the Earth by weight fraction (McDonough, 2003). In the wider cosmos it only places seventh on the list (Clayton, 2003a) but its abundance is still high enough for Si to be adopted as an abundance standard (e.g. Lodders, 2003). There are three stable isotopes of silicon with masses 28, 29 and 30 with the average abundance percentages being 92.2297%, 4.6832% and 3.0875% respectively (Rosman and Taylor, 1998). Silicon isotopic variations are expressed in the conventional δ notation:

1.5. Previous Si isotope data

$$\delta^{30}\text{Si} = \left[\frac{(^{30}\text{Si}/^{28}\text{Si})_{\text{sample}}}{(^{30}\text{Si}/^{28}\text{Si})_{\text{NBS-28}}} - 1 \right] \times 1000 \quad (1.3)$$

or

$$\delta^{29}\text{Si} = \left[\frac{(^{29}\text{Si}/^{28}\text{Si})_{\text{sample}}}{(^{29}\text{Si}/^{28}\text{Si})_{\text{NBS-28}}} - 1 \right] \times 1000 \quad (1.4)$$

where $(^{30}\text{Si}/^{28}\text{Si})_{\text{sample}}$ is the ratio of ^{30}Si to ^{28}Si in the sample of interest and $(^{30}\text{Si}/^{28}\text{Si})_{\text{NBS-28}}$ is the corresponding ratio in the standard reference material, in this case NBS-28. As the variations are usually quite small, the factor of 1000 is used to express variations in a convenient permil (‰) scale. A $\delta^{30}\text{Si}$ or $\delta^{29}\text{Si}$ value greater than 0 means that the sample is “heavier” than the standard (i.e. it has a larger $^{30}\text{Si}/^{28}\text{Si}$ or $^{29}\text{Si}/^{28}\text{Si}$ ratio).

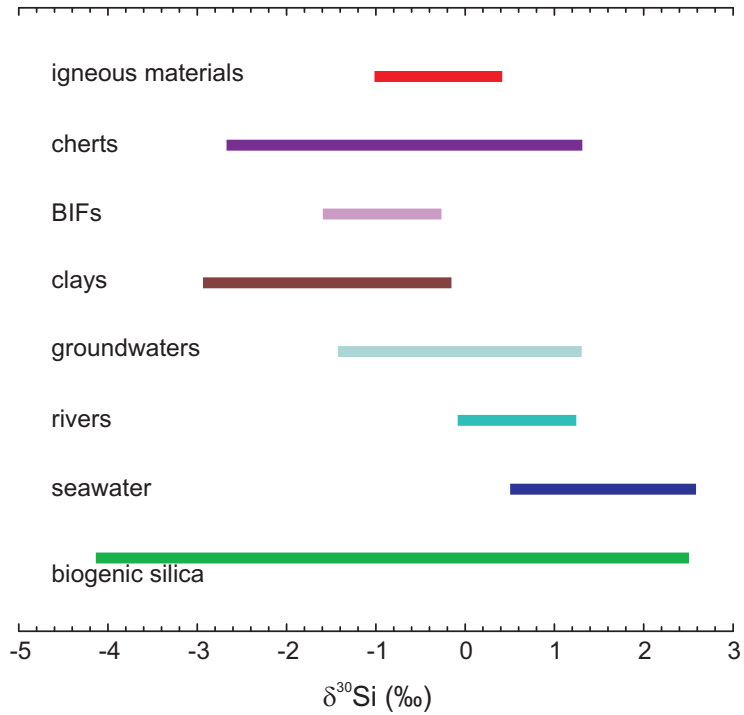
1.5 Previous Si isotope data

There are comprehensive compilations of terrestrial Si data to be found in Douthitt (1982) and Ding et al. (1996). A compilation of the data from these and more recent studies can be seen in Figure 1.6. Biological utilisation is responsible for the largest spread in Si isotope composition with variations up to $\sim 5\%$. However, low temperature Si isotope variation is not wholly dominated by biological fractionation. Clay mineral formation during weathering references is thought to be the key abiotic process responsible for heavier surficial waters relative to igneous materials (Ziegler et al., 2005; Georg et al., 2009a). There is a certain amount of evidence for aqueous alteration and clay formation on other planetary bodies (Bland et al., 2000; Treiman, 2005) and it could be that Si isotope compositions of some meteorites show evidence of secondary alteration effects.

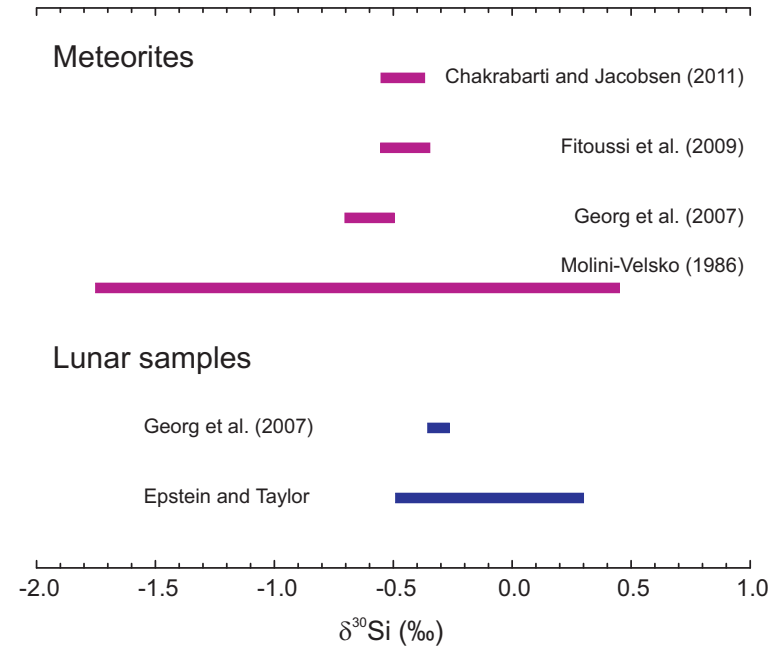
High temperature environments show much more restricted ranges in Si isotope composition (Figure 1.6), therefore there has been little focus on pinning down high

temperature fractionations until recent improvements in Si isotope analysis (e.g. Georg et al., 2006a; Savage et al., 2010). Early analyses of extra-terrestrial samples for their Si isotope composition was often a by-product of oxygen isotope analysis (e.g. Epstein and Taylor Jr., 1970b). As a result there is a significant amount of Si data for lunar samples where the oxygen isotopes were also analysed (Figure 1.6). Much of the initial interest in Si isotopes in meteorites was due to the fact that O and Si are directly bonded in silicates and it was hoped that the Si data could provide more information on oxygen mixing trends. The initial broad survey by Yeh and Epstein (1978) ruled that out however, as no corresponding convincing mass independent Si anomalies were found in bulk samples. The comprehensive study of meteorites by Molini-Velsko et al. (1986) confirmed the mass dependent behaviour of Si isotopes in solar system bulk samples. These relatively early comprehensive studies all show quite broad ranges in Si composition (Figure 1.6), and it is necessary to assess how much of the variation is natural and how much is analytical.

With the recent developments in MC-ICPMS (multi-collector inductively coupled-plasma mass-spectrometry) techniques (e.g. Georg et al., 2006a), there has been a renewed focus on analysing the Si isotope composition of solar system materials. The initial target has been whether BSE and meteorites have a resolvably different Si composition or not. There is the possibility that Si is the major light element in the core as it is known from geophysical studies (e.g. Birch, 1964), that the core is $\sim 10\%$ less dense than a pure Fe-Ni alloy. Experimental work at high temperature and pressure (e.g. Ito et al., 1995; Takafuji et al., 2005; Kilburn and Wood, 1997; Gessmann et al., 2001; Wade and Wood, 2005) has shown that up to $\sim 8\text{wt}\%$ of Si will dissolve into molten iron when in equilibrium with a silicate melt at high temperatures and pressures. The work of Georg et al. (2007a) showed that silicon isotope ratios in chondrites (used as bulk Earth reference material) are lighter than those seen in average BSE. This would imply that Si partitioned into the metal phase



(a) Terrestrial Si reservoirs



(b) Extra-terrestrial samples

Figure (1.6): Typical $\delta^{30}\text{Si}$ ranges of a selection of terrestrial (and extra terrestrial) Si reservoirs. Rivers (De La Rocha et al., 2000; Georg et al., 2006b, 2007b) groundwaters (Georg et al., 2009a,b) seawater (De La Rocha et al., 2000; Beucher et al., 2008; Reynolds et al., 2006) igneous materials (Ding et al., 1996), cherts (Robert and Chaussidon, 2006; van den Boorn et al., 2007; Marin-Carbonne et al., 2011), BIFs (banded iron formations)(André et al., 2006; Steinhoefel et al., 2010) clays (Ziegler et al., 2005; Georg et al., 2009b; Opfergelt et al., 2010) biogenic silica (Douthitt, 1982; Ding et al., 1996; Cardinal et al., 2003; Ding et al., 2008; Hendry et al., 2010), lunar (Epstein and Taylor Jr., 1970a, 1971; Taylor Jr. and Epstein, 1970, 1973a,b)

during core formation. However, as with Mg, a consensus has yet to be reached as to whether this difference is resolvable and how much variation there is between the different meteorite groups (Georg et al., 2007a; Chakrabarti and Jacobsen, 2010b; Fitoussi et al., 2009; Ziegler et al., 2010).

1.6 Motivation for this study

The aims of this thesis were to test, and potentially refine, the method used to analyse stable Si isotopes in light of the recent controversy, and to then use Si measurements in number of extra-terrestrial samples as an interrogative tool for cosmochemical questions such as:

How homogeneous was the region where the inner solar system components accreted?

What are the meteoritic building blocks for the Earth?

How does parent body differentiation, for example core formation, vary between planetary bodies?

How similar (or different) are the Earth and Moon in bulk composition?

To this end, the following studies were carried out:

1. Various sources of inter-laboratory variation in $\delta^{30}\text{Si}$ were investigated to try and reconcile the previous conflicting $\delta^{30}\text{Si}$ data for solar system material. (Chapter 3)
2. A broad range of meteorite bulk samples were analysed, both chondrites and achondrites. This was to assess homogeneity of the inner solar system, and also to look for any parent body differentiation effects. Some BSE samples were also analysed in order to investigate a potential BSE-chondrite offset and the implications for core formation on the Earth. (Chapter 4)

1.6. Motivation for this study

3. A number of lunar samples were analysed in order to assess the degree of lunar homogeneity and its similarity to BSE. This could have implications for the process of lunar formation and its major element budget. (Chapter 5)
4. Mineral separates from lunar basalts were analysed to investigate igneous processes on the Moon such as mare basalt formation and effects of a lunar magma ocean. (Chapter 6)
5. A number of chondrite components (chondrules, CAIs) were analysed both for Si isotope composition and major element concentration in order to understand formation processes of the components and also inner solar system homogeneity. (Chapter 7)

Chapter 2

Method

2.1 Introduction to Si isotope methods

Early studies of Si isotope ratios in natural samples used gas-source mass spectrometry with SiF_4 as the analyte (e.g. Reynolds and Verhoogen, 1953; Allenby, 1954; Tilles, 1961; Epstein and Taylor Jr., 1970b; Taylor Jr. and Epstein, 1970). Reynolds and Verhoogen (1953) used a sodium carbonate flux to extract the Si from the samples which was then converted into BaSiF_6 . This was decomposed by heating to give the SiF_4 and introduced into the mass spectrometer, where it was ionised to give SiF_3^+ . The range of Si isotopic composition in the samples (cherts, mafic and felsic minerals, sedimentary rocks) they analysed was $\sim 3\%$ using olivine as a standard. Allenby (1954) reacted their samples with HF to generate SiF_4 . Their reported range in $^{28}\text{Si}/^{30}\text{Si}$ between their most extreme samples, sinter and biogenic quartz, was close to 14%. Tilles (1961) used a similar method to Reynolds and Verhoogen (1953) and found a range closer to 5%. Interestingly, Tilles (1961) measured all three isotopes of silicon but used a non-standard delta notation:

$$\delta_{\text{sample}} = \left[\frac{(^{30}\text{Si} / [^{28}\text{Si} + ^{29}\text{Si}])_{\text{sample}}}{(^{30}\text{Si} / [^{28}\text{Si} + ^{29}\text{Si}])_{\text{standard}}} - 1 \right] \times 1000 \quad (2.1)$$

2.1. Introduction to Si isotope methods

rather than the now standard:

$$\delta^{30}\text{Si} = \left[\frac{(^{30}\text{Si}/^{28}\text{Si})_{\text{sample}}}{(^{30}\text{Si}/^{28}\text{Si})_{\text{standard}}} - 1 \right] \times 1000 \quad (2.2)$$

The difference between equation 2.1 and 2.2 over the isotopic range of interest is only on the order of 0.01‰, but equation 2.1 excludes the possibility of assessing whether the collected Si isotope data are mass dependent or not. Epstein and Taylor Jr. (1970b) and Taylor Jr. and Epstein (1970) collected the SiF₄ by-product released when fluorinating silicate samples for oxygen isotope analysis. This technique did have the advantage over more modern MC-ICPMS (multi collector inductively-coupled-plasma mass spectrometry) methods, in that direct analysis of both Si and O isotopes on the same sample was possible. The errors on the samples of these early studies were 0.15 to 0.5‰. The first comprehensive studies of the Si isotope compositions of terrestrial and meteoritic samples by Douthitt (1982) and Molini-Velsko et al. (1986) also used gas-source mass spectrometry.

Improvements in methods used to generate SiF₄ (e.g. Ding et al., 1996; Brzezinski et al., 2006) have contributed to the continuing popularity of using gas-source IRMS (isotope ratio mass spectrometry) to analyse Si isotopes, particularly for dissolved and biogenic silica (De La Rocha et al., 1996, 2000; Leng and Sloane, 2008). It still is occasionally used for lithological samples (Ziegler et al., 2005) but this is less common. Modern gas source IRMS does have the advantage that it has high internal precision $2\sigma_{SD} = \pm 0.1\%$ on $\delta^{30}\text{Si}$ (De La Rocha et al., 1996), however it does involve the use of hazardous gases such as F₂ or BrF₅.

There are a number of in-situ techniques that have been used to analyse Si isotopes in a variety of samples. SIMS (secondary ions mass spectrometry) has been used by Basile-Doelsch et al. (2005) to analyses silcretes and by Robert and Chaussidon (2006) to study banded iron formations. Sugiura et al. (2004) and Knight et al. (2009a) are

among the workers who have used SIMS to study CAIs (calcium aluminium inclusions) from chondrites. CAI Si isotopic compositions have also been measured using laser ablation MC-ICPMS (Shahar and Young, 2007). Chmeleff et al. (2008) developed a method of using a UV-femtosecond laser connected to a MC-ICPMS. However, the errors for these in-situ techniques are relatively large at $2\sigma_{SD} = \pm 0.75\%$ on $\delta^{30}\text{Si}$ for the SIMS method (Basile-Doelsch et al., 2005), $\sigma_{SD} = 0.3\%$ on $\delta^{29}\text{Si}$ for LA-MC-ICPMS (Shahar and Young, 2007), and $2\sigma_{SD} = \pm 0.24\%$ on $\delta^{30}\text{Si}$ for the femtosecond laser-ablation MC-ICPMS (Chmeleff et al., 2008). Therefore any spatial advantage gained must be balanced against the amount of variation that can be resolved with these techniques.

MC-ICPMS is a popular method of analysing Si isotopes due to the fast sample throughput and external precision similar to gas-source IRMS. It also avoids the use of complex fluorination techniques that involve hazardous gases. There are many different combinations of sample processing (HF digestion, NaOH digestion, NaOH fusion), chemistry (anion exchange columns, cation exchange columns) and instrument set-ups (wet plasma, dry plasma, Mg doping). Cardinal et al. (2003) achieved $< \pm 0.1\%$ on $\delta^{30}\text{Si}$ using HF to digest the sample and a dry plasma. As their samples were pure silica or opal, column chemistry was not required. They also used Mg isotopes to correct for instrumental mass drift, however some studies have rejected their use due to the significant difference in behaviour between Si and Mg within the plasma (De La Rocha, 2002; Georg et al., 2006a). Engström et al. (2006) also used HF to digest their samples before loading the samples onto an anion exchange resin bed. The fact that they ran in wet plasma without using a desolvation device was probably a contributing factor to their high external precision, which was $> \pm 0.3\%$.

For many of the recent high temperature studies NaOH digestion has been the popular method to decompose the samples, and cation exchange resin has been used (e.g. Georg et al., 2007a; Fitoussi et al., 2009; Savage et al., 2010; Chakrabarti and

2.2. Analytical Method

Jacobsen, 2010b; Armytage et al., 2011). The advantage of non-HF chemistry is that presence of excess F can affect the efficiency of the plasma ionisation leading to loss in beam intensity and mass-bias stability. Van den Boorn et al. (2006) used a NaOH digestion process in which the decomposition occurred in Parr bombs at $\sim 200^{\circ}\text{C}$ in a furnace over a three day period. This method has an advantage over using crucibles as the use of Teflon equipment facilitates low blanks and also maximises silicon recovery. This method has also been used to digest meteorite samples by Chakrabarti and Jacobsen (2010b). However, temperatures this low do not appear to adequately remove sulphur species which can cause offsets in during Si isotope measurements of high sulphur rocks (van den Boorn et al., 2009).

Georg et al. (2007a), Fitoussi et al. (2009) and Savage et al. (2010) have all used NaOH fusion in a silver crucible at $\sim 700^{\circ}\text{C}$, which is detailed in Section 2.2.1.1. Shaha et al. (2009) and Ziegler et al. (2010) used an HF sample digestion but at their low final concentration of fluorosilicate ions (40mM), their data do not show any matrix or plasma instability induced isotopic effects.

2.2 Analytical Method

2.2.1 Chemical preparation

2.2.1.1 Alkaline fusion

The procedure used to analyse samples for Si isotopes in Oxford is based on the NaOH fusion method detailed in Georg et al. (2006a). The ideal amount of Si to allow for multiple repeat analyses was in the range 0.3 to 10 mg. For most silicate samples this corresponded to 1-20 mg of sample. However, in order to keep sample heterogeneity to a minimum for the bulk samples, at least 70-100 mg of sample was usually ground in an alumina mortar with ethanol. An alumina mortar was used in

order to minimise contamination of the samples with contaminant silicon. Some of the samples had been already powdered for previous studies and it is likely that they were crushed in an agate mortar. This is unlikely to present a contamination issue, however, based on the relatively limited Si isotope range in terrestrial non-biogenic samples (Figure 1.6). The silicon contribution from an agate mortar would have to approach 20% of the total mass of silicon while having an isotopic composition on the extreme end of the hard rock range.

The advantage of using an alkaline fusion method to attack the silicate samples is the avoidance of any use of HF during sample processing. As mentioned in Section 2.1, HF can suppress the ionisation efficiency of the plasma as well as being a toxic substance to work with. An additional advantage of this particular fusion method is the quick processing of samples, as a sample can go from rock powder to a solution ready to run through column chemistry within <48 hours. In the first step of the chemistry the powdered silicate sample was fused with solid NaOH (flux) in a silver crucible. The ratio of sample to NaOH was approximately 200mg NaOH per 10mg of sample. A silver crucible was used as it has been shown to be slow to NaOH attack (Potts, 1987). The crucible was subsequently heated at 720°C for 10 minutes in a furnace. After ~5 minutes the crucible, along with the fusion cake, was dropped into 20 ml MQ-e water in a 30ml Teflon vial. The vial was left overnight to allow the fusion cake to dissolve. The fusion cake was transferred into an acidified solution and diluted, with the Teflon vial and crucible being rinsed multiple times with MQ-e to ensure quantitative recovery. Prior to the transference and in between the multiple rinsing stages, the Teflon vial was put in an ultrasonic bath for 5-15 minutes. Either HCl or HNO₃ was used to acidify the fusion cake with flux to acid ratios of 3.5ml of 10 N HCl or 5 ml of 15 N HNO₃ per 200mg NaOH flux. The different amounts of HCl and HNO₃ result from the optimal acid concentrations for introducing the sample solutions into the MC-ICPMS. The final solutions (between 80ml and 1000ml) were stored in pre-

2.2. Analytical Method

cleaned FEP or PP bottles with Si concentrations typically between 5 and 20ppm. The concentrations were measured as coloured Mo-Si complexes using a DR 2800 (Hach Lange) photospectrometer after fusion and prior to loading the solutions on the columns. Multiple aliquots from solutions were run through the column chemistry. Indeed each time the sample was measured during a run on the mass spectrometer it had been newly processed through column chemistry. It was found that storing the purified Si solutions, whether in Teflon or PP, for significant lengths of time (>24hours) would lead to inaccurate measurements on the mass spectrometer.

2.2.1.2 Column chemistry

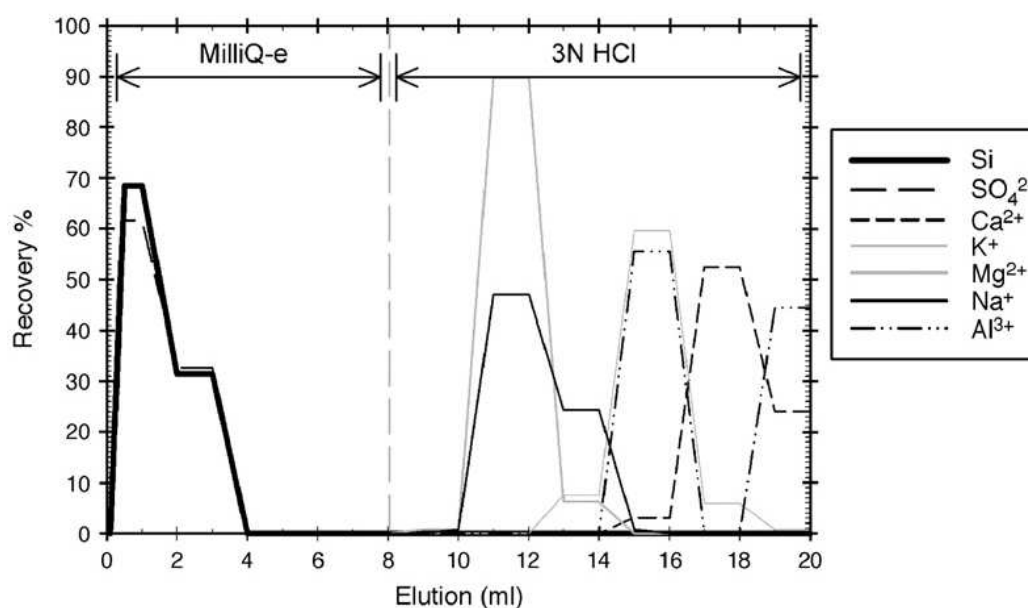


Figure (2.1): Elution curves for the DOWEX 50W-X12 (200-400 mesh) resin from Georg et al. (2006a). The high sulphate concentration is due to this being a river water sample rather than a silicate rock. There is minimal tailing of the Si elution curve, and it is only when the eluent is acidic that the other cations begin to appear.

Using MC-ICPMS for silicon isotopic analysis requires that a pure silicon solution (typically mildly acidic) is introduced into the instrument. If the solution contains other ambient cationic species, typically referred to as “matrix”, the stability and the intensity of the signal, and the peak resolution is often affected. One common

way of separating the element of interest from the other ionic species is via ion-chromatography. The silicon method used here is based on a cation-exchange process (Georg et al., 2006a) as it avoids the use of HF. The sample was loaded onto a stationary phase in a column, in this case resin beads with negatively charged functional groups, which will retain cations. In the solutions Si was in the form $\text{Si}(\text{OH})_4$ which is in equilibrium with the anionic silicate species H_3SiO_4^- in the pH range 2-8. Neither one of these forms will be retained by cation exchange resins; hence Si separation and purification can be achieved using only MQ-e water as the eluent. Figure 2.1 shows published elutions curves for the DOWEX 50W-X12 (200-400 mesh) resin used in this study. Table 2.1 shows the details of some of the cation “impurities” pre- and post- column chemistry. Sodium is clearly the most abundant cation as the result of the NaOH flux used to put the samples into solution, but the post column scans show Na concentrations ~ 3 orders of magnitude smaller. Also the elution curves of Georg et al. (2006a) (Figure 2.1) show that Na^+ only starts to elute once HCl is the eluent. The interfering sulphate ion in Figure 2.1 is not an issue for silicate rock samples due to the high temperatures experienced during fusion. Table 2.1 and Figure 2.1 show the column chemistry method used is effective at removing the “matrix” cations.

The columns used were BioRad polyprep (Hercules, CA, USA) with a 1.8ml resin bed of the cation exchange resin DOWEX 50W-X12 (200-400 mesh) in the H^+ form. The resin was pre-cleaned through several rinses of MQ-e, HNO_3 and HCl to ensure to ensure the complete removal of matrix elements and the efficiency of the exchange process (Table 2.2). Recovery from both the fusion and ion-chromatography stage was $>97 \pm 2\%$. The total procedural blank, including instrument blanks, at Oxford is 13ng where typical analytical amounts are $4.5 \mu\text{g}$, giving a sample to blank ratio of ~ 350 .

2.2. Analytical Method

Table (2.1): Cations in sample solutions before and after column chemistry

Processing	Sample	Na (ppb)	Mg (ppb)	Al (ppb)	Si (ppb)	Ca (ppb)	Fe (ppb)	Ni (ppb)
Pre-column chemistry	Allende I	21130	517	55	821	82	976	59
	Allende-RBG ^a	15792	557	50	904	75	1015	62
	Allegan	40847	437	33	750	38	1595	111
	Allegan-RBG	16404	459	33	814	52	444	16
	Juvinas	30296	104	214	759	187	352	0
Post-column chemistry	Juvinas-RBG	21474	112	167	839	194	391	1
	Allende I	36	0	0	808	7	0	0
	Allende-RBG	91	0	0	861	11	0	0
	Allegan	95	0	0	840	13	0	0
	Allegan-RBG	35	0	1	780	25	0	0
	Juvinas	32	0	0	780	6	0	0
	Juvinas-RBG	112	0	0	901	9	0	0

^a RBG indicates those solutions that had been made up (i.e. the fusion chemistry) for Georg et al. (2007a)

Table (2.2): Si separation process for a meteorite solution with an Si concentration of 11.9 ppm and desired running concentration of 750ppb

Separation stage	Solution	Volume
Pre-cleaning:	3 N HNO ₃	10 ml
	6 N HNO ₃	6 ml
	10 N HCl	5 ml
	6 N HNO ₃	3 ml
	3 N HNO ₃	3 ml
Rinse	MQ-e	3 x 3 ml
Sample load	Acidified sample solution	4.5 μ g (equal to 0.378 ml)
Elution	MQ-e	2 x 2.5 ml
Dilution to running concentration	MQ-e	0.622 ml
Result		6ml at 750ppb Si

2.2.2 Mass spectrometry

2.2.2.1 Principles of MC-ICPMS

The essence of a mass spectrometer is to separate ions based on their m/z (mass to charge ratio), and analyse their relative concentrations. The mass spectrometer

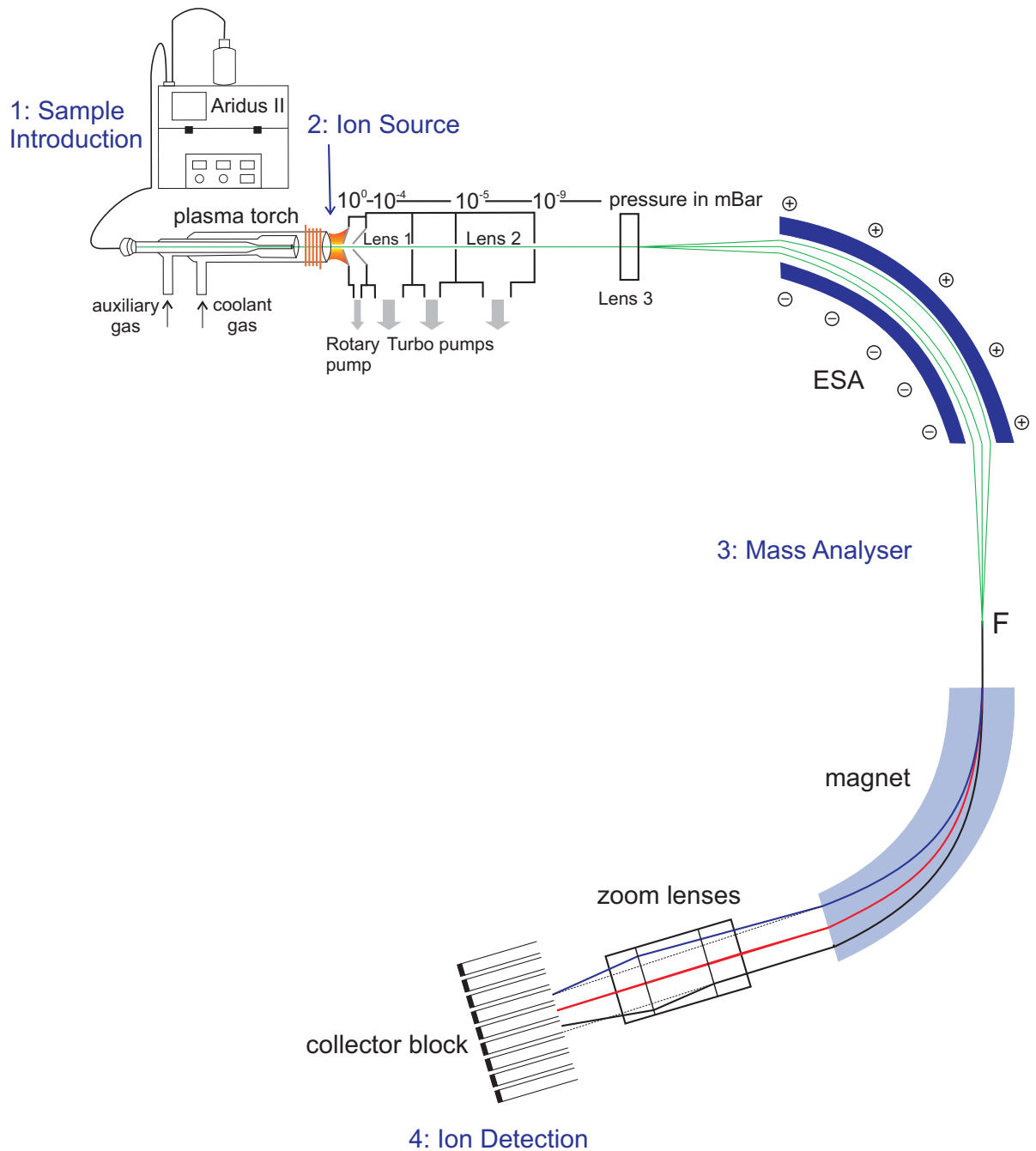


Figure (2.2): Schematic of the Nu Plasma mass spectrometer used during this study. After Nu Plasma schematic from Becker (2007)

used to collect the Si isotopic data in this thesis was a NuPlasma (Nu Instruments, Wrexham, UK) multi-collector inductively-coupled-plasma mass spectrometer (MC-ICPMS). There are four key components to any mass spectrometer: (1) sample introduction; (2) ion source; (3) mass analyser; (4) ion detection system (Figure 2.2). What follows is a description of some of the principles of mass spectrometry (Herbert and Johnstone, 2003; de Hoffmann and Stroobant, 2007) with the focus on analysing Si isotopes using a Nu Plasma.

Sample introduction: The sample for analysis is aspirated into the source as an aerosol. In the case of Si the aerosol that is injected is ‘dry’ due to an Aridus II (CETAC, Omaha, NE, USA) desolvating device that removes up to 99% of the solvent (Figure 2.2). The sample solution is aspirated into a heated (110°C) spray chamber using a self-aspirating concentric microflow PFA nebulizer (Elemental Scientific Inc.) with an uptake rate of 50-80 $\mu\text{l}/\text{min}$. This vaporises the solvent, being mostly water, and also creates small droplets of the aerosol. Any large droplets fall to the bottom of the spray chamber and are pumped out as waste. The sample vapour subsequently enters a heated (also 110°C) PTFE membrane, which has porous and hydrophobic walls. Outside the membrane there is a counterflow of Ar gas, known as the “sweep” gas. This removes the solvent molecules that have permeated through the membrane, which in turn creates a chemical gradient allowing for further loss of solvent vapour. The non-volatile sample components do not pass through the wall but continue on into the ion source via injection through the torch.

The advantage of running using a ‘dry’ plasma is that it enhances the sensitivity for Si while reducing interferences from oxides and hydrides. An increased sensitivity for Si means less sample is required, allowing for analysis of individual chondrules for example. As many of the isobaric interferences for Si are polyatomic solvent based ones (e.g. $^{12}\text{C}^{16}\text{O}^+$, $^{14}\text{N}^{16}\text{O}^+$), the use of a desolvating

device is necessary for high precision Si isotopic measurements.

Ion source: The Ar plasma, the ion source for this mass spectrometer, is a gaseous phase that contains neutral molecules, but also, more importantly, ions and electrons. The Ar is not directly heated but a radio-wave frequency electromagnetic field is applied through a load coil. The RF field is controlled by the RF generator with an output power of 1300W. This rapidly oscillating field interacts inductively with charged particles, speeding them up and increasing their kinetic energy. These fast and free moving ions collide with the neutral particles ionizing them in turn and increasing the energy of the system as a whole. The kinetic energies will eventually become so high that the plasma will reach temperatures in the order of 5,000–10,000K. As long as the RF generator maintains the oscillating electromagnetic field, the plasma will sustain this high energy state. A high-voltage spark is used to provide the initial flux of electrons. Ar is used as the plasma gas as its high ionisation energy, 15.76 eV, allows for ionisation of the majority of the periodic table. Though generally advantageous, this also requires that the sample solution contains only the analyte of interest in order to avoid mass interferences, hence the need for column chemistry.

The plasma is generated at the end of the quartz plasma torch. There are three concentric Ar flows through the torch. The outer gas flow, or coolant gas, acts as the main plasma support gas as well as protecting the tube walls. The auxiliary gas lifts the plasma off the end of the torch, while the inner or nebulizer gas flow carries the sample aerosol through central injector and into the plasma (see Table 2.3 for typical flow rates). Initially a sapphire injector rather than a quartz one was used for Si isotopic analysis due to concerns about blanks. These, however, were not found to be a major issue and a fully quartz torch was used for the majority of the analyses.

2.2. Analytical Method

One of the significant advantages of using an ICP (inductively-coupled-plasma) as an ion source is that the samples are introduced at atmospheric pressure making sample exchange very simple. However, as the mass analysis needs to be done at vacuum pressures, an interface region is necessary to step down the high pressures and temperatures. The first part of the interface is the nickel sampler cone. It has a small hole in the center which impinges on the end of the plasma flame. The other side of the sampler is pumped down to a pressure of 1 mbar, hence the sample-containing gas undergoes supersonic expansions and cools. Behind the sampler is a skimmer cone (also nickel) with a smaller orifice, and the region behind the skimmer is at 10^{-4} mbar. After the skimmer are a series of lenses to focus and align the beam, and the vacuum is strengthened further to $\sim 10^{-9}$ mbar before entering the mass analyser. Approximately 99% of the ions will be lost between the plasma and the region behind the skimmer cones as the transmission through this interface region is very inefficient. The cones also provide the initial accelerating potential of 6 kV.

Mass analyser: The mass analyser is the core of the mass spectrometer where the ions are split based on their m/z or mass to charge ratio. In a Nu Plasma the mass analyser has two main components, the magnet and the ESA (electrostatic analyser). When a moving ion experiences a magnetic field it will be deflected, with the magnitude of the deflection depending on the momentum of the ion as described below. The kinetic energy of the ion will be related to the acceleration through the ion source:

$$E_k = zV_s = \frac{1}{2}mv^2 \quad (2.3)$$

where E_k is the kinetic energy, z is the number of charges on the ion, V_s is the accelerating potential applied to the ion upon leaving the ion source, m is the mass of any one ion, v is the velocity of an ion after acceleration through

V_s . The centrifugal force the ion will experience due to deflection of its path by the magnetic field is equal to the force exerted by the field on a moving charge:

$$\frac{mv}{r} = zB \quad (2.4)$$

with r being the radius of the arc of the ions deflected in the magnetic field of strength B . Combining equation 2.3 and 2.4 by eliminating velocity gives:

$$\frac{E_k}{2m} = \frac{z^2 B^2 r^2}{m^2} \quad (2.5)$$

rearranging for the radius of the arc gives:

$$r = \frac{\sqrt{2mE_k}}{zB} \quad (2.6)$$

From equation 2.6 it is clear that the radius of the arc the ion beam will follow, assuming a charge of unity, will be greater the larger the mass of the ion. However, the radius is also dependent on the kinetic energy of the ion as it enters the magnet. In other words, the magnet is a momentum analyser, not just a mass analyser. The ions leave the plasma with a wide spread of energies but the magnet has no ability to focus any spread in E_k , so the image on the collector will be blurred. This is where the second part of the mass analyser, the ESA, comes in. For a radial electrostatic field, such as in the ESA, the centrifugal force equilibrates the electrostatic force:

$$zE = \frac{mv^2}{r} \quad (2.7)$$

where E is the intensity of the electrical field. If we substitute in the initial kinetic energy and rearrange:

$$r = \frac{2E_k}{zE} \quad (2.8)$$

This gives a trajectory that is independent of the mass (as $E_k = zV_s$), hence the ESA is purely an energy focusing device. In the Nu Plasma it is positioned before the magnet, which provides a beam source that is focused with respect to kinetic energy prior to entry into the magnet (point F in Figure 2.2). If the energy focussing of the ESA and the magnet have the same magnitude, the E_k will cancel out and focus onto the collector slits will only be a function of mass. This forward double focusing or Nier-Johnson geometry allows for high mass resolution and peak shapes.

Ion detection: After the ion beams of different m/z ratio are focused and separated, they need to be detected. For Si isotopes, Faraday cups are used as high sensitivity is not required. Ions, which are travelling at high speed, strike the Faraday cage or cup causing a flow of electrons. This electrical current is typically on the femto- to nano-amp (10^{-15} to 10^{-9} A) scale, and is passed through a large ($10^{11}\Omega$) resistor. This produces a voltage that can be measured on a digital voltmeter. Faraday cups are the simplest and most precise detectors, however, they do have intrinsic background noise that rules out their use for very small ion beams.

The Nu Plasma has 12 Faraday cups in the collector block to allow for collection of multiple ion beams simultaneously. This helps overcome the other major disadvantage of plasma source mass spectrometry: the inherent instability of the plasma. The plasma is subject to fluctuations on the scale of ion beam intensities. As the beam intensities are direct measures of the concentration, this instability limits high precision isotopic ratio analysis. If all the isotopes beams are collected simultaneously, any such fluctuations should not affect the

Table (2.3): Operating conditions for the Nu Plasma

Parameter	Nu Plasma
RF Power	1300 W
1st accelerator potential	6 kV
Sample cone	Type 'B' WA cone (Nu Instruments)
Skimmer cone	Type 'B' WA cone (Nu Instruments)
Coolant flow rate (Ar)	13 l/min
Auxiliary flow rate (Ar)	0.9-1.2 l/min
Nebulizer gas flow rate (Ar)	21-26 l/min
Nebulizer	Self aspirating microflow PFA (Elemental Scientific Inc.)
Nebulizer uptake rate	50-80 $\mu\text{l min}^{-1}$
Resolving power	~ 4000
Cup configuration	L5 (^{28}Si), H1(^{29}Si), H5 (^{30}Si)
Si running concentration	500-1000ppb
Sensitivity on ^{30}Si beam	0.5-1 V/ppm
Desolvating device	Cetac ARIDUS II

ratios of the ion beams. In a Nu Plasma the positions of the collectors are fixed and a system of variable dispersion zoom optics is used to overcome the problem of the separation between isotopes being mass dependent. These do not change the resolution but rather they can change the width of the ion beam at the focal plane at the collectors by magnifying or de-magnifying the beam.

2.2.2.2 Pseudo high resolution analysis

Despite all the effort of removing the cations of interest through column chemistry, and reducing the solvent based interferences by using a desolvator, there are still interferences that need to be dealt with in order to achieve high precision isotopic analysis. For Si, these are polyatomic, generally gaseous species that either form in the plasma or have not been completely removed by the desolvator ($^{12}\text{C}^{16}\text{O}^+$, $^{14}\text{N}^{2+}$, $^{28}\text{Si}^{1}\text{H}^+$, $^{14}\text{N}^{16}\text{O}^+$). Ion beams can be resolved if they are narrower than the distance

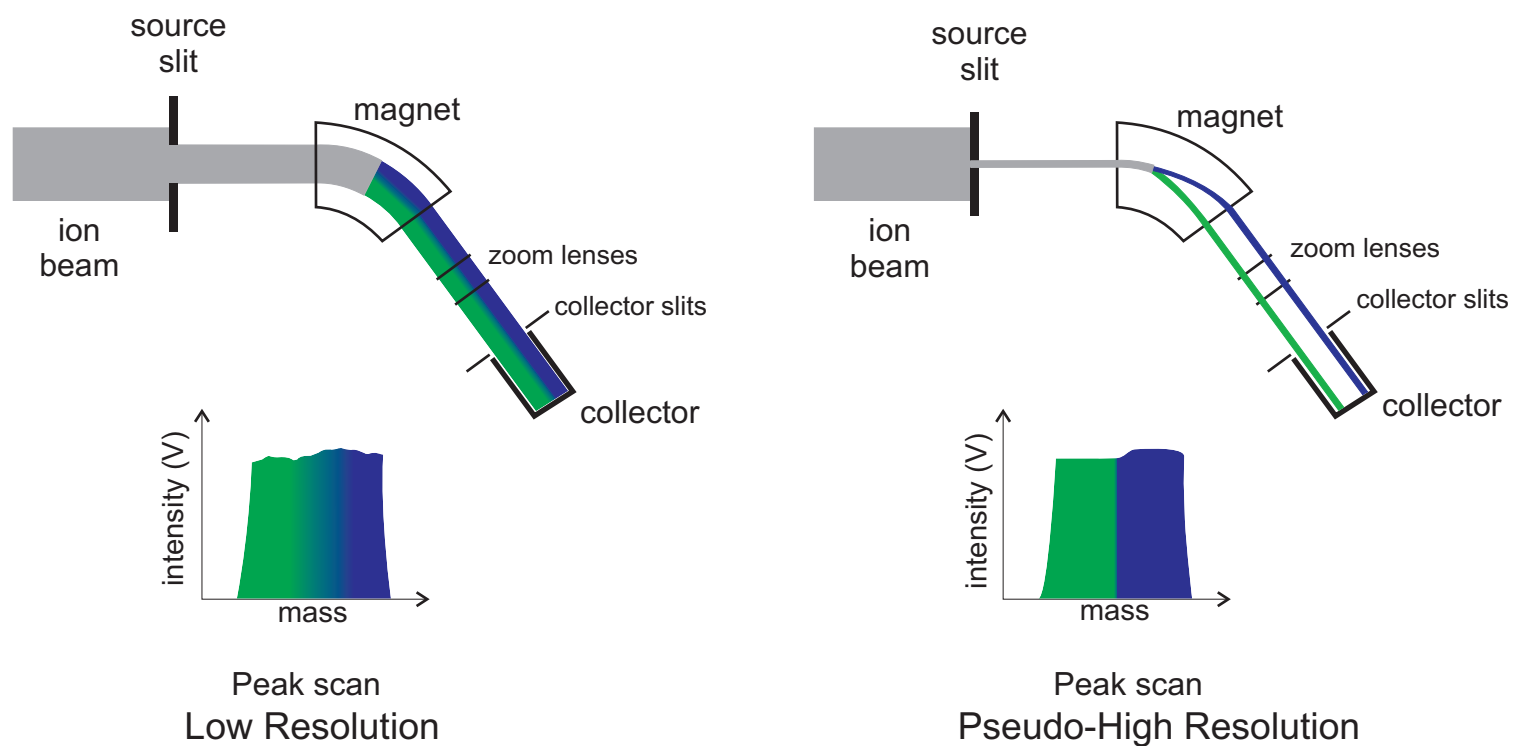


Figure (2.3): Schematic of pseudo high resolution. The mass analyser is represented only by the magnet for simplicity. The diagram on the left shows a low resolution scenario where it is not possible to resolve the analyte ion beam (green) from the interference ion beam (blue). In the pseudo high resolution scenario on the right, it is clear that the two ion beams are resolved from one another. In the mass scan though, the peaks are not resolved from one another. However, there is now a shoulder on the light mass side where it is possible to measure only the analyte. (After Georg, 2006)

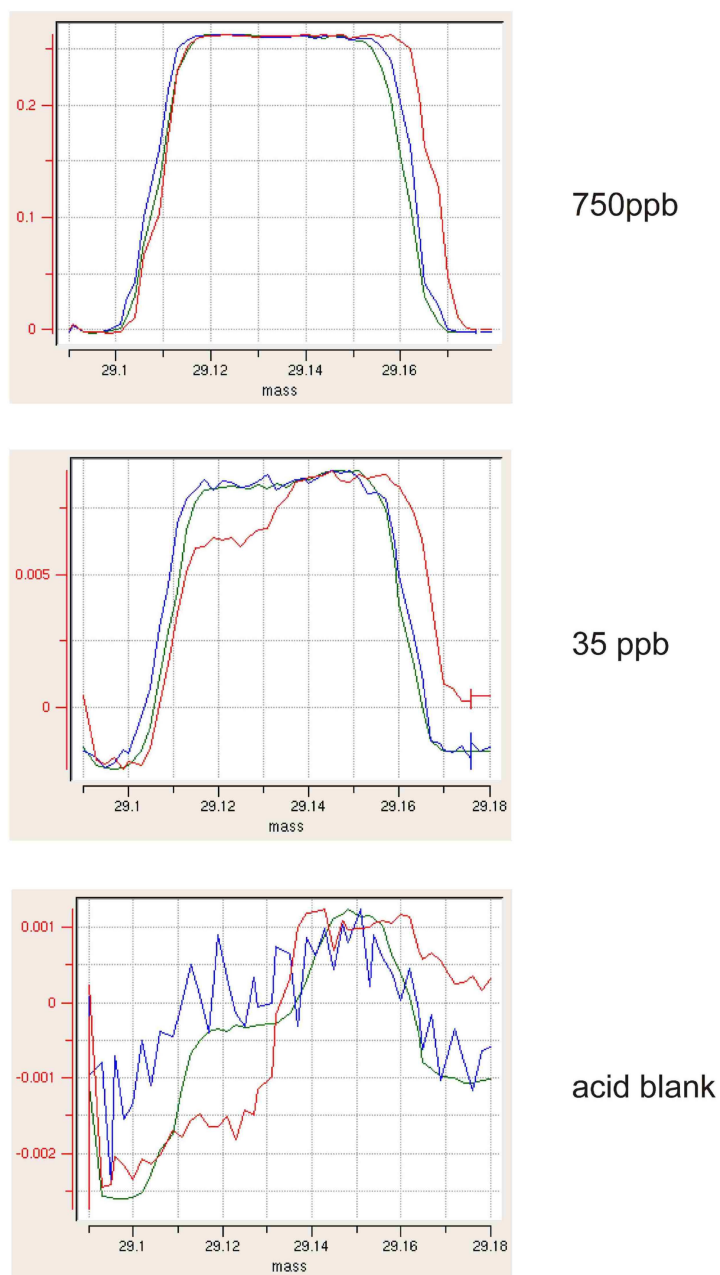


Figure (2.4): Peak scans collected during an analytical session on the Nu Plasma. The red trace is ^{30}Si beam, ^{29}Si beam is blue and ^{28}Si beam is green. The scale on the y-axis is the intensity of ^{30}Si in volts. The top figure is a peak scan at a typical running concentration, and it is hard to see the interferences. If the concentration of the analyte is reduced, the interferences become plainer. In the middle figure the hump on the heavy side of the peak is addition of the interfering beam $^{14}\text{N}^{16}\text{O}^+$. In the bottom figure during uptake of the wash acid, the interferences of $^{14}\text{N}^{16}\text{O}^+$, $^{14}\text{N}^{2+}$, $^{28}\text{Si}^1\text{H}^+$ can be observed in addition to the Si blank

2.2. Analytical Method

between them. Prior to the ion beam entering the ESA it passes through a vertical and horizontal source defining slit which physically cut the beam. These change both the height and the width of the ion beam from the circular beam defined by the skimmer orifice to a oblong beam. The vertical aperture remains fixed, but the horizontal source slit is adjustable to widths of 0.3, 0.05 and 0.03 mm on the Nu Plasma. These correspond to low, medium and high mass resolution respectively. However, the reduction in width causes a concomitant loss in overall sensitivity and transmission of up to 80%. Therefore a compromise is necessary between the resolution needed and the sensitivity required through a combination of adjusting the source slit only as much as needed and increasing the concentration of the running solution. In conjunction with the source slit, Nu Plasma instruments also have Alpha slits which are two metal plates which are controlled by “muscle” wires which expand as a current is applied to them. These further reduce sensitivity by cutting down the beam to reduce beam aberrations that could lead to blurring of the peak image at the collectors. The Alpha slits, like the source defining slit, are located before the electrostatic analyser, before any focusing or dispersion of the beam has occurred.

For Si it is possible to resolve the ^{30}Si beam from $^{14}\text{N}^{16}\text{O}^+$ beam at medium resolution. This corresponds to resolving power of ~ 4000 , where the resolving power is defined as $m/\Delta m$, where Δm is between 5% and 95% of the peak height and m is the mean of the two masses. However, although the beams are resolved from one another, during a mass scan they will simultaneously occupy the same collector for part of the scan. Hence, although the *beams* are resolved, the *peaks* are not (Figure 2.3). There are some physical alterations one can make to overcome this issue. One is to simply increase the size of the geometry of the machine. This forces the ion beams to physically travel further, increasing their separation to the extent that when they reach the plane of the collectors they can be recorded in separate Faraday cups. The Nu Plasma 1700 has a larger geometry than the Nu Plasma, but even

then the separation is not great enough to resolve all peaks in this fashion. What is possible, with the increased geometry, is that peaks can be resolved in a mass scan when combined with fully adjustable collector entrance slits.

With the Nu Plasma in Oxford there is not the capability to do this, as the collector mask is not set up for Si dispersion, and the peaks cannot be fully resolved. Advantageously, however, all of the major interferences on the Si beams lie on the heavy mass side of the peak. As the ion beams themselves are completely resolved (Figure 2.4), there will be a flat topped region or shoulder on the light side of the peak where it is possible to measure and be free of interferences. This type of set-up is sometimes referred to as “pseudo” high resolution.

2.2.2.3 Data collections protocols

We are interested in measuring the Si isotopic fractionations in different natural materials with the MC-ICPMS. However, the mass fractionations that occur within the instrument will be much larger than any natural variation we would hope to measure. For Si double spiking, perhaps the best method for correcting instrumental mass bias, is not possible as there are only two stable isotope ratios. The external mass bias correction using Mg isotopes, which seems to work very well on the ThermoFinnegan Neptune MC-ICPMS with wet plasma (Zambardi and Poitrasson, 2010), has not been shown to work particularly well on the Nu Plasma (Georg et al., 2006a). Therefore, simple standard sample bracketing was used, with the international Si standard NBS-28 as the bracketing standard. Silicon isotope variations are reported as the deviations of $^{30}\text{Si}/^{28}\text{Si}$ and $^{29}\text{Si}/^{28}\text{Si}$ from the NBS-28 standard in parts per thousand using:

$$\delta^{30}\text{Si} = \left[\frac{(^{30}\text{Si}/^{28}\text{Si})_{\text{sample}}}{(^{30}\text{Si}/^{28}\text{Si})_{\text{NBS-28}}} - 1 \right] \times 1000 \quad (2.9)$$

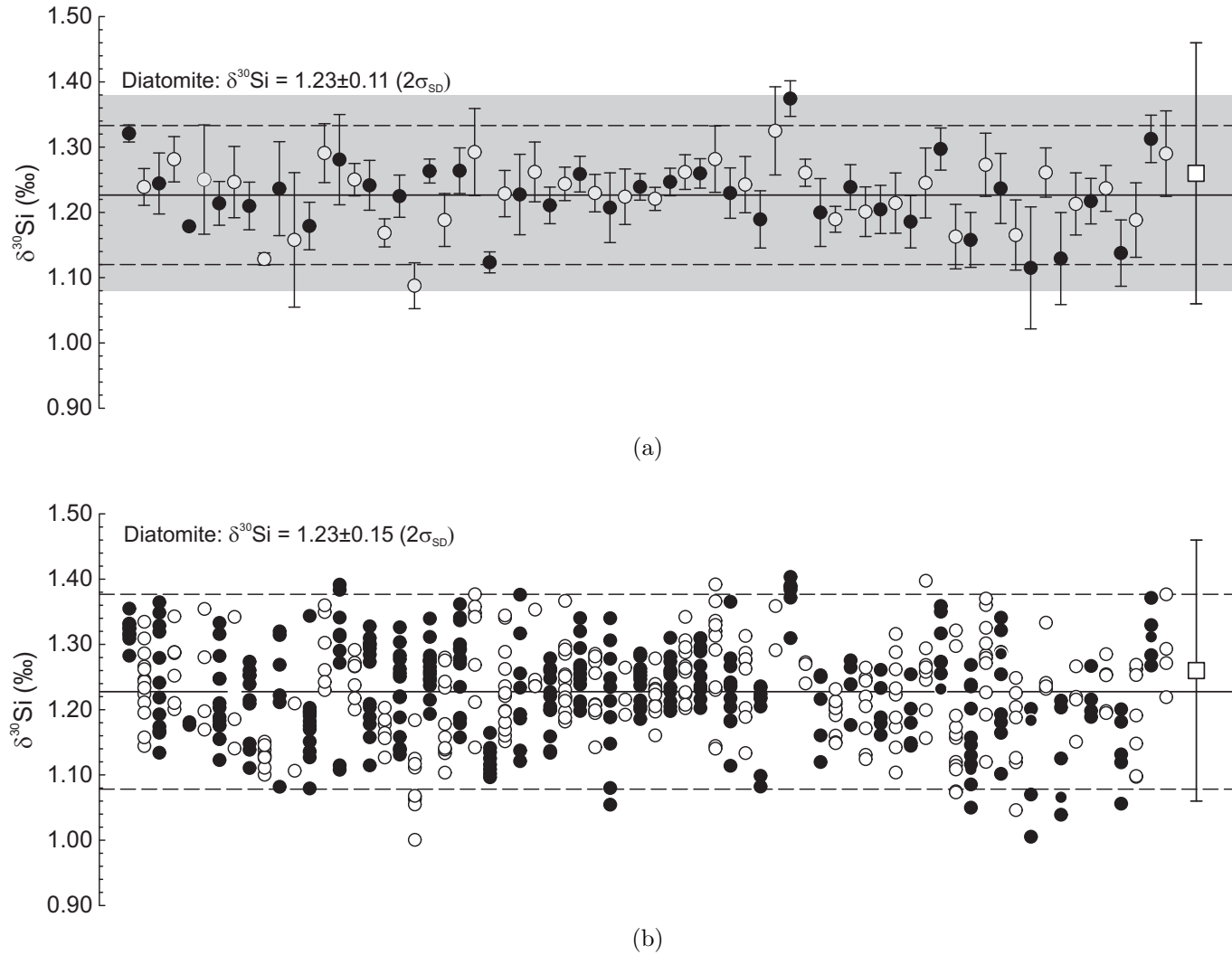


Figure (2.5): $\delta^{30}\text{Si}$ of Diatomite over a 36 month period. Only $\delta^{30}\text{Si}$ is plotted for clarity as all the data is mass dependent, and the difference in symbol colour is purely for clarity of comparison between (a) and (b). The white square data point in both (a) and (b) is the calibrated composition from Reynolds et al. (2006) $\pm 2\sigma_{SD}$. (a) shows the average $\delta^{30}\text{Si}$ composition for Diatomite per run $\pm 2\sigma_{SEM}$. The grey band is $\pm 2\sigma_{SD}$ from (b). (b) shows every individual $\delta^{30}\text{Si}$ measurement of Diatomite, with the each position on the x-axis corresponding to a different analytic session.

$$\delta^{29}\text{Si} = \left[\frac{(^{29}\text{Si}/^{28}\text{Si})_{\text{sample}}}{(^{29}\text{Si}/^{28}\text{Si})_{\text{NBS-28}}} - 1 \right] \times 1000 \quad (2.10)$$

Each silicon isotope ratio measurement (standard or sample) represents 20 cycles with an integration time of 10s for each cycle. The in run instrumental precision on the $^{30}\text{Si}/^{28}\text{Si}$ and $^{29}\text{Si}/^{28}\text{Si}$ ratios is on the order of $\pm 9 \times 10^{-7}$ (σ_{SEM}). In a typical run the sample would be analysed 6 times and the bracketing standard 7 times. The average of the two standards bracketing the sample was used to calculate the $\delta^{30}\text{Si}$ and $\delta^{29}\text{Si}$ values as above. As the bracketing standard is also bracketed by two adjacent samples, the number of $\delta^{30}\text{Si}$ and $\delta^{29}\text{Si}$ values for a run of a sample is 11 rather than 6. In general, the reported sample data were the result of more than one run, with the uncertainty of the average $\delta^{30}\text{Si}$ or $\delta^{29}\text{Si}$ values quoted as the standard error of the mean (standard deviation/ \sqrt{n}) (e.g. Taylor, 1997) for all the data across the multiple runs. Reporting $2\sigma_{SEM}$ is the convention in the majority of the recent high temperature Si literature (Georg et al., 2007a; Fitoussi et al., 2009; Chakrabarti and Jacobsen, 2010b; Savage et al., 2010; Ziegler et al., 2010).

To verify the accuracy of the measurements, various calibrated standards such as IRMM-018, Diatomite and BHVO-1 and -2 were included in each run. Each run also represented a separate column chemistry repeat for the samples, standards and bracketing standard. Two different calibrated standards were typically run in each measurement session. The standard that was most frequently run was Diatomite (Figure 2.5). The reproducibility of Diatomite ($2\sigma_{SD}$) over a 36 month period was ± 0.11 $\delta^{30}\text{Si}$ and ± 0.06 $\delta^{29}\text{Si}$; or ± 0.15 $\delta^{30}\text{Si}$ and ± 0.09 $\delta^{29}\text{Si}$ depending whether the average of each run was averaged ($n = 70$) or whether the average of ever single measurement was used ($n = 585$). The Diatomite values of $\delta^{30}\text{Si} = 1.23 \pm 0.15\text{‰}$ and $\delta^{29}\text{Si} = 0.62 \pm 0.09\text{‰}$ are consistent with the calibrated values of $\delta^{30}\text{Si} = 1.23 \pm 0.20\text{‰}$ and $\delta^{29}\text{Si} = 0.64 \pm 0.14\text{‰}$ (Reynolds et al., 2007). Similarly the Si isotope values for IRMM-018 and BHVO-1,-2 are in agreement with the published values (see Figure

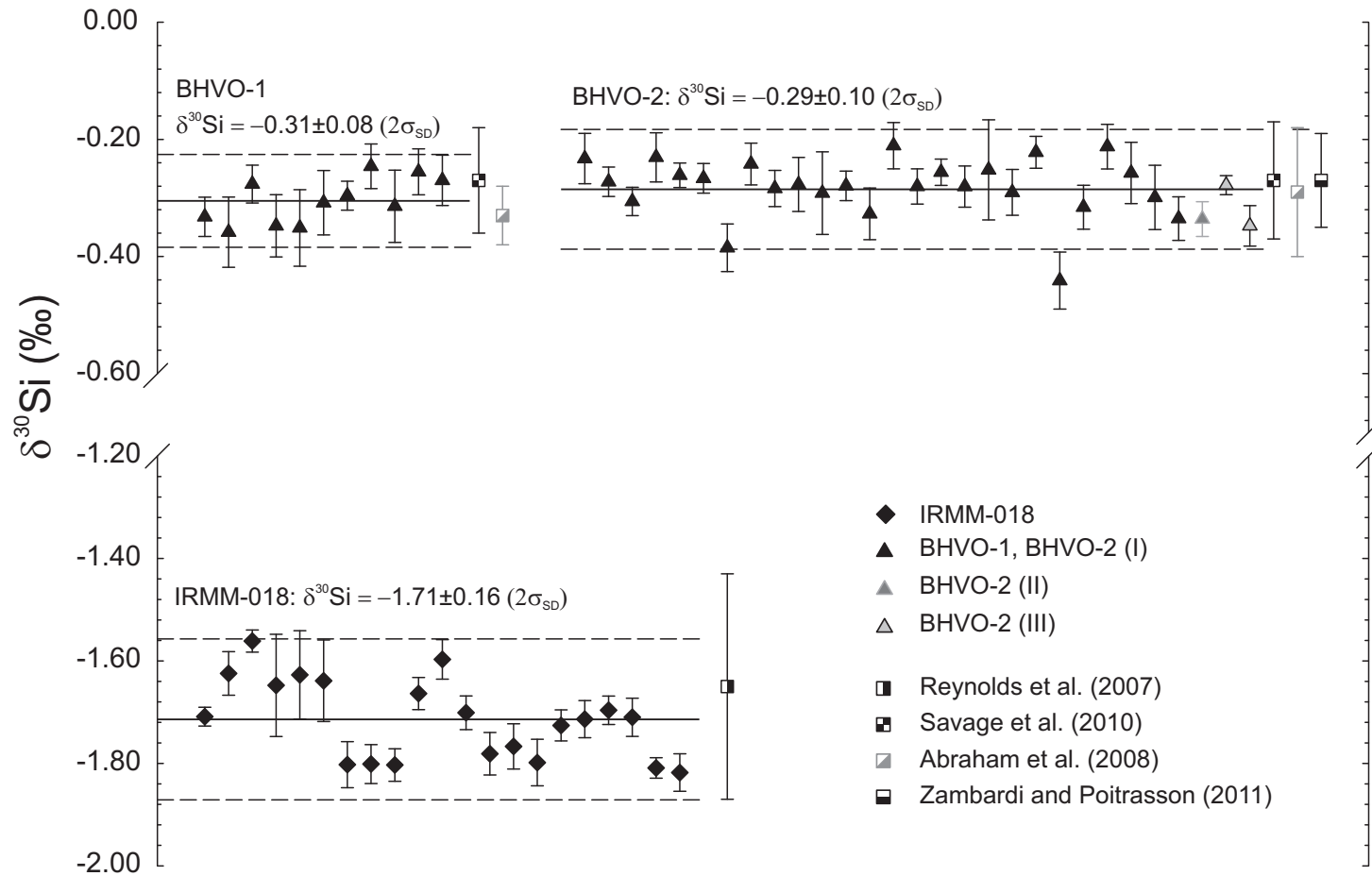


Figure (2.6): $\delta^{30}\text{Si}$ of the pure Si standard IRMM-018 and the USGS rock standard BHVO (batches 1 and 2). IRMM-018 has been shown to be a relatively heterogeneous standard (Reynolds et al., 2006), hence it was only run a limited number of times. The dashed lines show the $2\sigma_{SD}$ envelopes. The standard data from the other studies are plotted with $\pm 2\sigma_{SD}$ error bars.

2.6). All fractionations measured were mass dependent; indeed mass dependence was used as a data quality check by constructing three-isotope plots of the data (see Chapter 4 and 5).

Chapter 3

Assessing potential sources of inter-laboratory variation in $\delta^{30}\text{Si}$ ¹

3.1 Introduction

In 2007, Georg et al. reported a measurable difference between the Si isotopic composition of meteorites, including both chondrites and achondrites, ($\delta^{30}\text{Si} = -0.58 \pm 0.06\text{‰}$, $1\sigma_{SD}$), and mantle-derived materials representative of the bulk silicate Earth (BSE) ($\delta^{30}\text{Si} = -0.38 \pm 0.06\text{‰}$, $1\sigma_{SD}$). The uniqueness of BSE in contrast to the other differentiated bodies indicates that there was a process, or series of processes, that fractionated Si isotopes only in the Earth as opposed to the rest of sampled inner solar system. It was suggested that the fractionation was the result of Si entering the core at high temperature and pressure (Georg et al., 2007a). Contrary to the data of Georg et al. (2007a), Fitoussi et al. (2008) found barely resolvable differences between the Si isotopic signatures of carbonaceous chondrites and terrestrial samples and concluded that Si isotopes per se did not provide evidence for or against Si in the Earth's core. Subsequently Fitoussi et al. (2009) did report a difference between carbonaceous chondrites and terrestrial samples but one that was smaller than that reported by Georg et al. (2007) by a factor of ~ 2.5 .

¹Parts of this chapter have been published as "Silicon isotopes in meteorites and planetary core formation" R. M. G. Armytage, R. B. Georg, P.S. Savage H. M. Williams, A. N. Halliday. *Geochimica et Cosmochimica Acta* (2011) **75**, 3662-3676

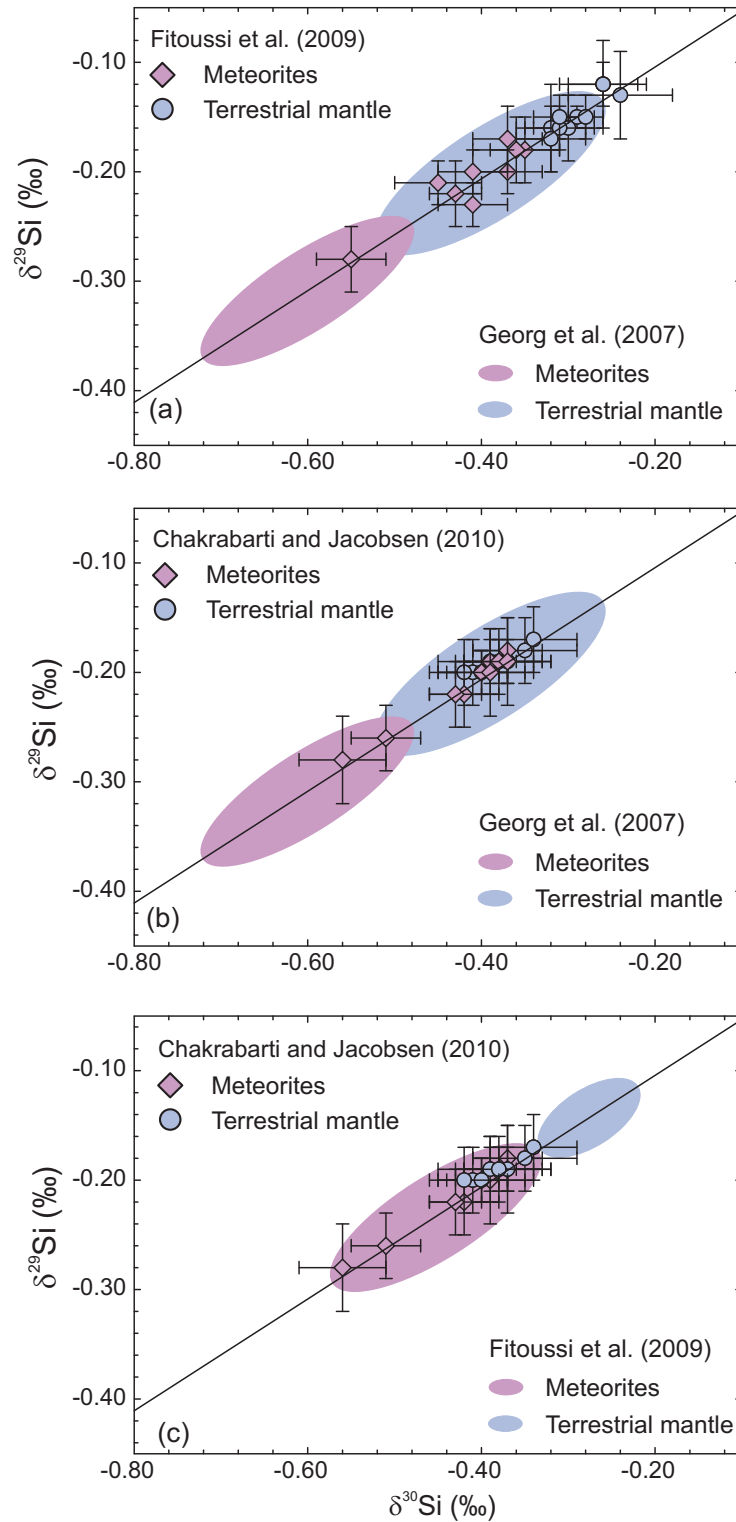


Figure (3.1): $\delta^{30}\text{Si}$ versus $\delta^{29}\text{Si}$ data for meteorites and terrestrial mantle samples from three recently published studies. The error bars on the data points are $\pm 2\sigma_{SEM}$

Another laboratory group reported conclusions similar to the earlier Fitoussi et al. (2008) study, that there is no offset between meteorites and terrestrial mantle in their Si isotope compositions (Chakrabarti and Jacobsen, 2009, 2010b). The differences between all these studies is not only the magnitude of $\Delta^{30}\text{Si}_{\text{BSE-meteorite}}$ but also differences in the absolute $\delta^{30}\text{Si}$ compositions for both the meteorite and terrestrial populations (Figure 3.1).

One notable aspect of this Si isotope debate is that the studies of Georg et al. (2007a) and Fitoussi et al. (2009) were carried out in the same laboratory, using the same method and on the exact same multi-collector inductively-coupled-plasma mass spectrometer (MC-ICPMS) instrument (Nu 1700). Therefore it is possible that the variation in published $\Delta^{30}\text{Si}_{\text{BSE-meteorite}}$ or in absolute $\delta^{30}\text{Si}$ values could be linked to some small systematic variation in the method or the samples themselves.

A number of tests were carried out in order to interrogate potential causes of the Si isotope variations and to try and reproduce the $\delta^{30}\text{Si}$ compositions from Georg et al. (2007a).

3.2 Compositional effects

One possibility is that the offset $\Delta^{30}\text{Si}_{\text{BSE-meteorite}}$, is not linked to core formation, but instead is the result of meteorites and terrestrial samples behaving differently during chemical processing, generating isotopic offsets. This difference in behaviour could be the result of the different major and minor element compositions in meteorites relative to terrestrial mantle samples. Even if $\Delta^{30}\text{Si}_{\text{BSE-meteorite}}$ is not affected, compositional causes may be one of the reasons for the discrepancy in the measured $\delta^{30}\text{Si}$ between the previous datasets (Georg et al., 2007a; Fitoussi et al., 2009; Chakrabarti and Jacobsen, 2010b)

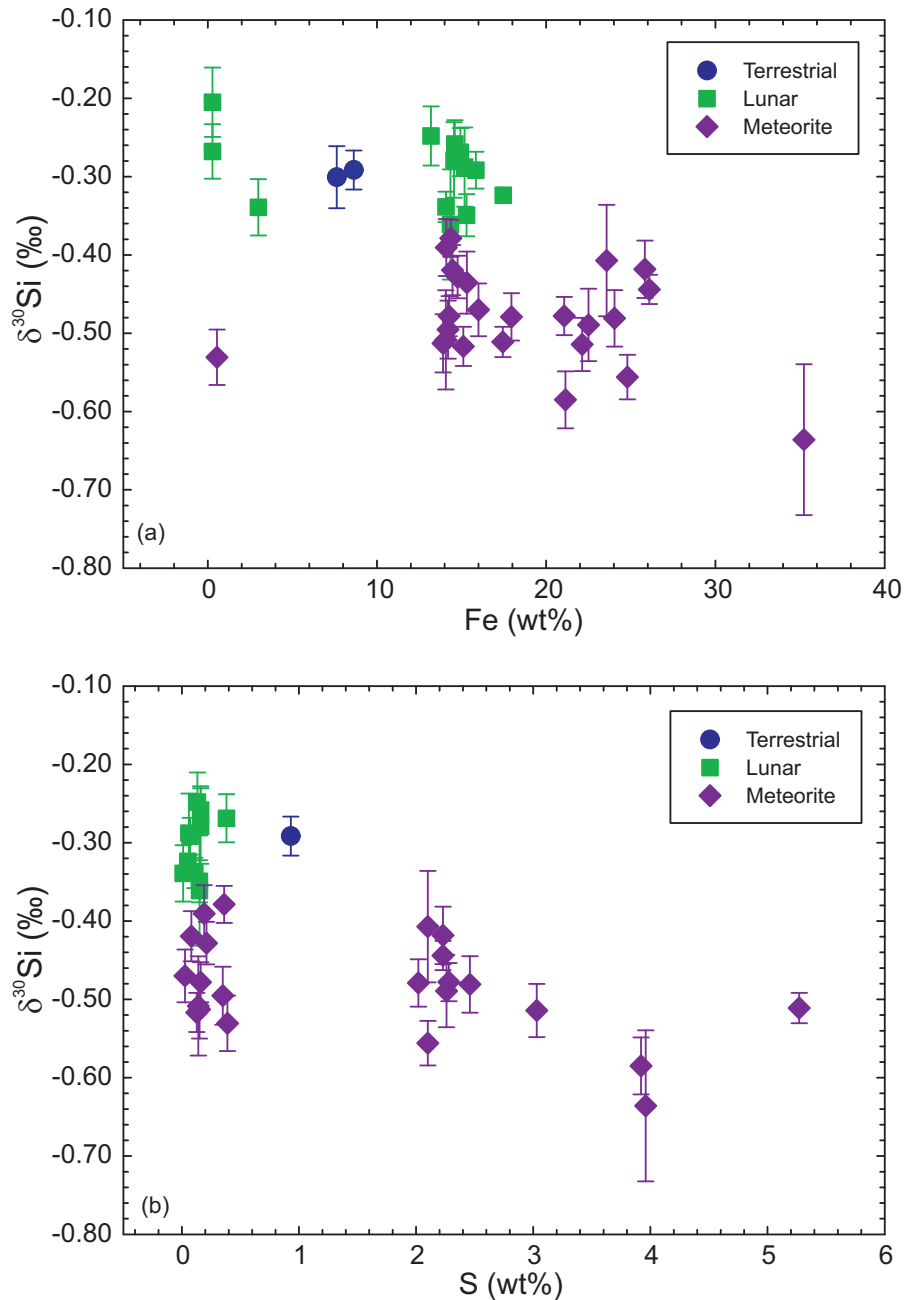


Figure (3.2): $\delta^{30}\text{Si}$ compositions from Chapters 4 and 5 vs Fe and S contents of the samples. There is a suggestion of a negative correlation, but a wide range in $\delta^{30}\text{Si}$ is seen at Fe \sim 14 wt% and S \sim 0.3 wt% ruling out any convincing trend. Iron and S concentration data is from Galer and O’Nions (1989); Wilson (1997); Makishima and Nakamura (2001); Beatty and Albee (1978); Rhodes et al. (1977); Willis et al. (1972); Rhodes and Hubbard (1973); Laul and Schmitt (1973); Apollo 16 Preliminary Examination (1973); Rhodes et al. (1976); Jarosewich et al. (1987); Mason (1963); Jarosewich (1990); Dreibus et al. (1995); Jarosewich and Mason (1969); Mason and Wiik (1966a,b); Easton (1985b); Kitts and Lodders (1998); Jochum et al. (1980); Lodders (1998); Dreibus et al. (2000); Gibson and Moore (1983). The errors on the literature Fe and S data are small and omitted for the sake of clarity

3.2. Compositional effects

Fitoussi et al. (2009) mention the possibility of the higher Fe contents in the meteorites being responsible for large discrepancy between the two datasets for meteorites in particular. Figure 3.2a plots $\delta^{30}\text{Si}$ data from this study against Fe contents from the literature (see figure caption for references). A weighted-fit line through the data would have the equation $y = -0.0425 \pm 0.0008x - 0.2630 \pm 0.014$ with an $r^2=0.38$. The meteorite Fe concentrations span the entire range of the plotted Fe data from 0 to 36wt%, but none of the $\delta^{30}\text{Si}$ meteorite compositions are heavier than -0.36‰ . Equally there are a number of samples, both meteoritic and lunar, that have an Fe concentration of $\sim 14\text{wt}\%$ but range in $\delta^{30}\text{Si}$ from -0.26‰ to -0.55‰ . Clearly, Fe content is not responsible for $\Delta^{30}\text{Si}_{\text{BSE-meteorite}}$. If Fe was causing the variation between the laboratories in $\delta^{30}\text{Si}$ of meteorites, one would expect to see that achondrites (typical Fe concentrations 13 – 14wt%) would reproduce better than chondrites (22 – 24wt% Fe). Figure 4.6 shows this not to be the case as there is almost as much inter-laboratory variation in Juvinas (a eucrite) and Murchison (a carbonaceous chondrite).

The ion-chromatography that is used by Georg et al. (2007a), Fitoussi et al. (2009) and Chakrabarti and Jacobsen (2010b) to analyse Si isotopes involves only a cation-exchange column. Therefore, it is possible that the presence of anions in variable concentrations could cause a matrix effect in the MC-ICPMS. One possible culprit could be SO_4^{2-} . Figure 3.2b shows a plot of $\delta^{30}\text{Si}$ against Swt%, which would have a regression line of $y = -0.0502 \pm 0.0028x - 0.325 \pm 0.002$ with the correlation similar to Fe at $r^2=0.37$. In any case, it is expected that sulphur would be lost during the fusion process as its boiling point is 718K, while the alkaline fusion occurs at $\sim 1000\text{K}$. Georg et al. (2006a) tested a sulphate spiked Si standard and did not find any offset due to SO_4^{2-} in the plasma. Van den Boorn et al. (2009) did find sulphur effects when measuring a S doped basalt standard (BHVO-2) but their alkaline digestion technique involved lower temperatures. They found that an additional high temperature

($\sim 1600\text{K}$) “ignition” step was required to avoid sulphur-induced offsets. Chakrabarti and Jacobsen (2010b) used the same technique, but without the high-temperature step. However, this cannot be the sole cause of the variation seen in Figure 3.1 as the meteorites would be the most affected, yet their meteorite data are very similar to Fitoussi et al. (2009), who also use the high temperature alkaline fusion of Georg et al. (2006a).

Carbon could be another element creating a “matrix” effect during analysis of Si isotopes. If one compares the carbon contents of the chondrite Orgueil, 3.45wt% (Anders and Ebihara, 1982), the martian meteorite Shergotty, 0.05wt% (Lodders, 1998) and the terrestrial basalt BHVO-1 0.011wt% (Kubota, 2009), it is clear that the carbon content of the achondrite is more similar to BHVO-1 than to the carbonaceous chondrite. However, the Si isotopes tell a different story (Table 4.1) with Shergotty ($\delta^{30}\text{Si} = -0.52 \pm 0.02\text{‰}$) being nearly identical to Orgueil ($\delta^{30}\text{Si} = -0.51 \pm 0.02\text{‰}$) in composition and very different to BHVO-1 ($\delta^{30}\text{Si} = -0.30 \pm 0.01\text{‰}$).

There is, therefore, no evidence of compositional effects on the chemistry from any of the likely candidates and other sources for the cause of the discrepancy should be sought.

3.3 Re-analysis of samples

3.3.1 Sample powders

One potential cause for the variation could be sample heterogeneity. Meteorite “bulk” sample powders can often only derive from a few 100s of mg, rather than result from crushing 5–10g of material. Sample heterogeneity, as a contributor to inter-laboratory variation, is also supported by the fact that the differences in the $\delta^{30}\text{Si}$ compositions for the terrestrial samples are less pronounced than for the meteorites. The variation that is seen in Figure 3.1 could simply be the result of different meteorite powder

3.3. Re-analysis of samples

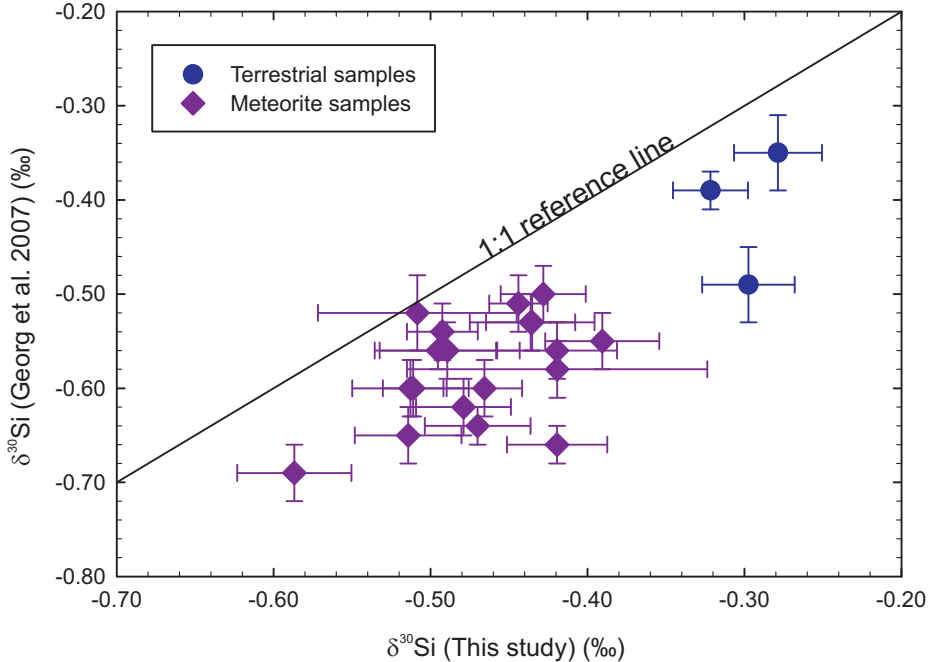


Figure (3.3): $\delta^{30}\text{Si}$ from Georg et al. (2007) versus $\delta^{30}\text{Si}$ measured on the same meteorites and terrestrial samples in this study.

aliquots being analysed.

For a number of both the terrestrial and meteoritic samples analysed in Georg et al. (2007a), there was remaining sample powder which was processed and analysed in Oxford (see Table 3.1 for data). When plotted against the $\delta^{30}\text{Si}$ compositions from Georg et al. (2007a) the Oxford data is consistently heavier, both for the meteorite and the terrestrial samples (Figure 3.3) though the correlations within the groups are weak ($r^2 = 0.22$ for the meteorites and $r^2 = 0.04$ for the terrestrial samples). As this work is not able to reproduce the measured compositions from Georg et al. (2007a) despite the use of the exact same sample powders, indicates that part of the variation must be linked to chemical processing or the mass spectrometry of the samples. Sample heterogeneity may still play some role however, which is explored further in section 3.4.

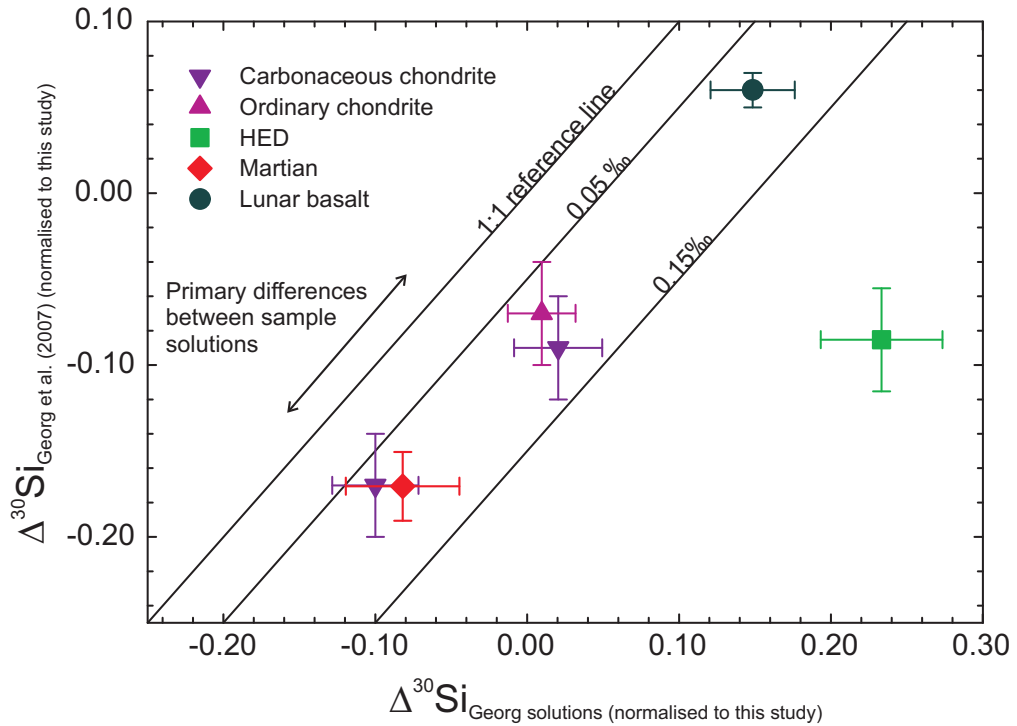


Figure (3.4): The $\delta^{30}\text{Si}$ values from Georg et al. (2007a) have been normalised to the values measured in this study ($\Delta^{30}\text{Si}_{\text{Georg2007}}$) and plotted against the normalised $\delta^{30}\text{Si}$ compositions ($\Delta^{30}\text{Si}_{\text{Georg solutions}}$) measured for the meteorite sample solutions from Georg et al. (2007) that had been processed through column chemistry and measured on the MC-ICPMS in Oxford. Variations in the x-direction should only be the result of fusion effects or initial sample heterogeneity. Variations in the y-direction correspond to differences in ion-chromatography and mass spectrometry, as well as fusion and heterogeneity effects.

3.3.2 Sample solutions

Some of the solutions (meteoritic, terrestrial and lunar) that had been prepared and analysed in Georg et al. (2007a) were re-measured. In addition to running on a different MC-ICPMS instrument, this also included putting the solutions through column chemistry. The solutions were approximately three years old and were analysed in the same measurement session as the same samples processed from scratch (i.e. including fusion) in Oxford. On re-analysis, two of the solutions are slightly lighter, two are identical and two are heavier than the analysis of fresh sample material reported here (Figure 3.5 and Table 3.1).

At first glance, there does not appear to be anything systematically different that can be ascribed to the results of the ion exchange and mass spectrometry conducted by Georg et al. (2007) versus that conducted in Oxford. It can be seen from Figure 3.4, that there is a suggestion of a correlation between the $\Delta^{30}\text{Si}_{\text{Georg et al. (2007)}}$ and the $\Delta^{30}\text{Si}_{\text{Georg solutions}}$, with 5 out of the 6 samples plotting along a line with an offset of about 0.1‰. The alignment of the data parallel to the 1:1 line provides evidence that there are systematic differences to do with the samples or their fusion and not purely the mass spectrometry or solution processing (ion exchange). These effects have been investigated further with additional studies as described in the following.

Table (3.1): Silicon isotope data for samples freshly prepared from powder at Oxford and for Georg et al. (2007a) solutions measured in Oxford

Sample	Source/Study	$\delta^{30}\text{Si}$ ‰	$2\sigma_{SEM}$	$\delta^{29}\text{Si}$ ‰	$2\sigma_{SEM}$	N
Orgueil (CI)	This study	-0.51	0.02	-0.27	0.01	25
	RBG solution ^a	-0.49	0.02	-0.27	0.01	7
	Georg et al. 2007a	-0.60	0.03	-0.30	0.01	40
Allende (CV3)	This study ^b	-0.41	0.07 ^c	-0.22	0.04 ^c	7
	RBG solution	-0.52	0.03	-0.28	0.01	43
	Georg et al. 2007a	-0.58	0.03	-0.29	0.01	39
Bath (H4)	This study	-0.44	0.02	-0.23	0.01	22
	RBG solution	-0.43	0.02	-0.22	0.01	9
	Georg et al. 2007a	-0.51	0.03	-0.22	0.02	20
Nakhla (SNC)	This study	-0.47	0.03	-0.24	0.01	24
	RBG solution	-0.55	0.04	-0.28	0.02	11
	Georg et al. 2007a	-0.64	0.02	-0.35	0.02	13
Juvinas (HED)	This study	-0.51	0.03	-0.26	0.02	47
	RBG solution	-0.26	0.05	-0.14	0.02	11
	Georg et al. 2007a	-0.60	0.03	-0.28	0.02	25
Lunar basalt 70035 (High Ti basalt)	This study ^b	-0.36	0.07 ^c	-0.18	0.06 ^c	2
	RBG solution	-0.21	0.03	-0.11	0.01	11
	Georg et al. 2007a	-0.30	0.01	-0.16	0.02	11

^a The RBG solutions are the sample solutions that were initially processed for Georg et al. (2007) but have been re-measured, including processing over the ion-exchange columns, at Oxford

^b The Allende value is the average of eight Allende aliquots and the lunar basalt 70035 is the average of two aliquots.

^c The uncertainties on the means of Allende and 70035 are given as $\pm 2\sigma_{SD}$.

3.4 Sample heterogeneity and sample preparation

With any bulk meteorite study for which small aliquots are analysed there is always the potential for effects from sample heterogeneity. This is a particular problem in dealing with CV chondrites, which are known to contain a relatively large proportion of calcium-aluminium refractory inclusions (CAIs) with isotopically heavy fractionated Si (Clayton et al., 1988; Shahar and Young, 2007). Therefore, five samples were taken from a powder, derived from crushing a ~ 500 g piece of the CV3 chondrite Allende from the Smithsonian and compared with other samples from the same Natural History Museum, London cut (BM1981. M5) used by Georg et al. (2007a). In addition one more fusion was carried out on an aliquot of a powder of a 5g Allende fragment from the Natural History Museum (BM.1969,148). Two of the sample solution aliquots were filtered in a similar fashion to that deployed for some of the Georg et al. (2007a) measurements using a $< 0.1\mu\text{m}$ filter to remove any opaque particles that may not have been attacked by the NaOH fusion. The opaques usually dissolved within 24hrs of being made up in an acidified solution so the filtering was done immediately after transferring the fusion cake. This was to see if Si might have been adsorbed leading to fractionation of the isotopes (Delstanche et al., 2009). However, no effects were observed (Fig. 3.6) and indeed the fractionation would have to be very large for the very small amounts of particulate material to significantly affect the Si isotope composition. It can be seen also that the 5 aliquots of the Smithsonian sample are identical within uncertainty and show no systematic offset from the 2 aliquots of BM1981. M5 or the aliquot of BM.1969,148.

In Georg et al. (2007a), all the rock samples had HCl as their running acid to avoid additional formation of $^{14}\text{N}^{16}\text{O}^+$, which interferes with ^{30}Si . Some recent Si isotope work has used HNO_3 as a running acid (Savage et al., 2010; Ziegler et al., 2010), which could potentially lead to an increase in interfering peaks, and hence be responsible for the $\delta^{30}\text{Si}$ offsets reported between these studies and Georg et al. (2007a). Therefore

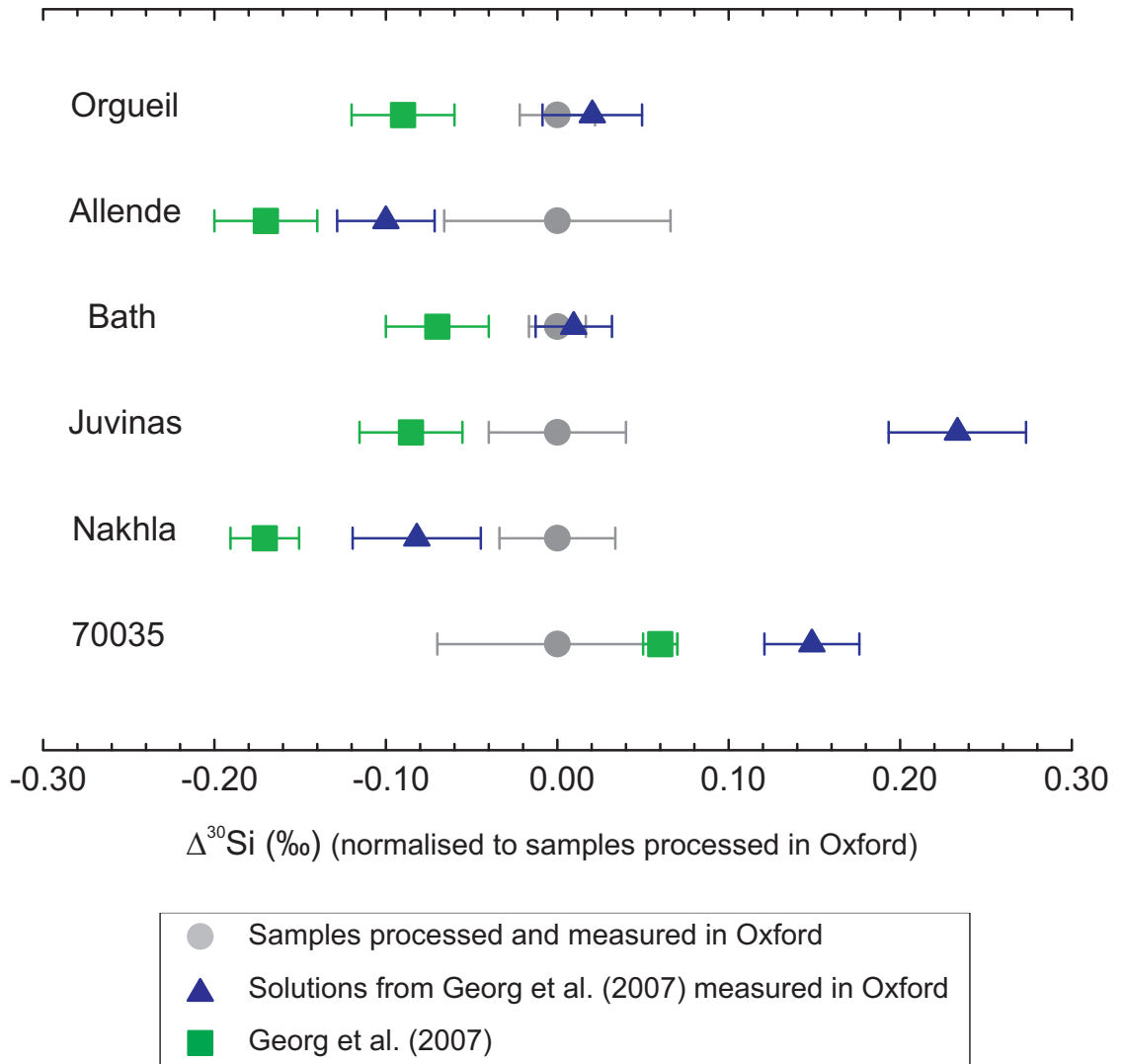


Figure (3.5): $\delta^{30}\text{Si}$ of samples processed from scratch in Oxford, solutions from Georg et al. (2007a) re-analysed (including column chemistry) in Oxford, and the original $\delta^{30}\text{Si}$ compositions measured by Georg et al. (2007a) all normalised to $\delta^{30}\text{Si}_{\text{Oxford}}$ samples

3.4. Sample heterogeneity and sample preparation

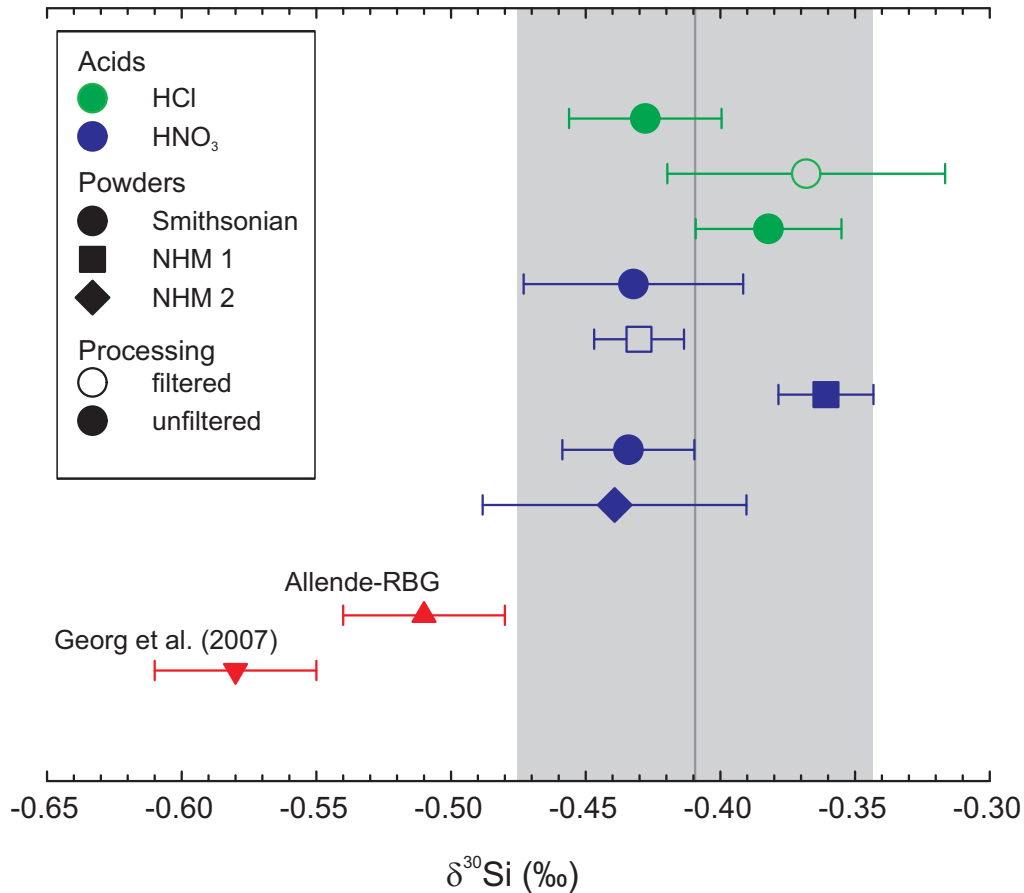


Figure (3.6): $\delta^{30}\text{Si}$ of Allende aliquots of different meteorite cuts with differing processing histories. The error bars represent two standard errors of the mean ($2\sigma_{SEM}$). Allende-RBG refers to the split that was processed through the fusion step by Georg et al. (2007a) but the column chemistry and mass spectrometry occurred as part of this study. The data point labelled Georg et al. (2007a) is the value obtained in that study on the same solution as Allende-RBG. Both Allende-RBG and Georg et al. (2007) had HCl as their solvent. NHM 1 refers to the BM1981.M5 Allende split from the NHM, London (the same powder as was used in Georg et al. (2007)) and NHM2 is the other NHM, London split, BM.1969,148. The grey band is the average of all the Allende aliquots processed from scratch in Oxford $\pm 2\sigma_{SD}$ (-0.41 ± 0.07)

weak (2%v/v) HNO₃ was tested as an analytical medium (in addition to HCl) but no systematic differences were observed (Fig. 3.6).

The $2\sigma_{SD}$ for all eight Allende aliquots is $\pm 0.07\%$ $\delta^{30}\text{Si}$, which is smaller than the external reproducibility for any of the pure Si standards such as Diatomite and IRMM-018 (Table 4.1). It is larger than the error quoted on the meteorite and rock samples (Table 4.1), with two exceptions. This points to small isotopic effects as a result of slight variations in sample processing, though nothing systematic. The $2\sigma_{SD}$ for the two sets of repeat samples that were treated in an identical manner (i.e. same running acid, filtration state and initial powder) are 0.06 and 0.02% $\delta^{30}\text{Si}$ which points to a good reproducibility for the method.

The only Allende sample analysed in Oxford that appears to be significantly offset is Allende-RBG, the original sample solution from Georg et al. (2007a) but processed here through ion chromatography columns and MC-ICPMS analysis in Oxford (Section 3.3). It is not as negative as the value reported by Georg et al. (2007a) (Fig. 3.6) which implies that both sample preparation and the ion-chromatography/mass spectrometry are contributing to the variation between the Allende data in this study and Georg et al. (2007). However, the cause in either case is still not clear despite these tests.

3.5 Sample solution pH

Fitoussi et al. (2009) assert that to avoid offsets in $\delta^{30}\text{Si}$ related to the yield, the pH of the Si solutions loaded onto the ion-exchange columns must lie within the limited pH range of 2.1-2.4. As the Georg et al. (2007a) solutions had a pH value of 1.6 this could be the cause of the discrepancy between those two datasets. This was tested by adding either HCl or NaOH to various aliquots of BHVO-2 to give a range of pH values of ~ 0.5 to 11 when measured using a pH meter. The solutions were allowed

3.5. Sample solution pH

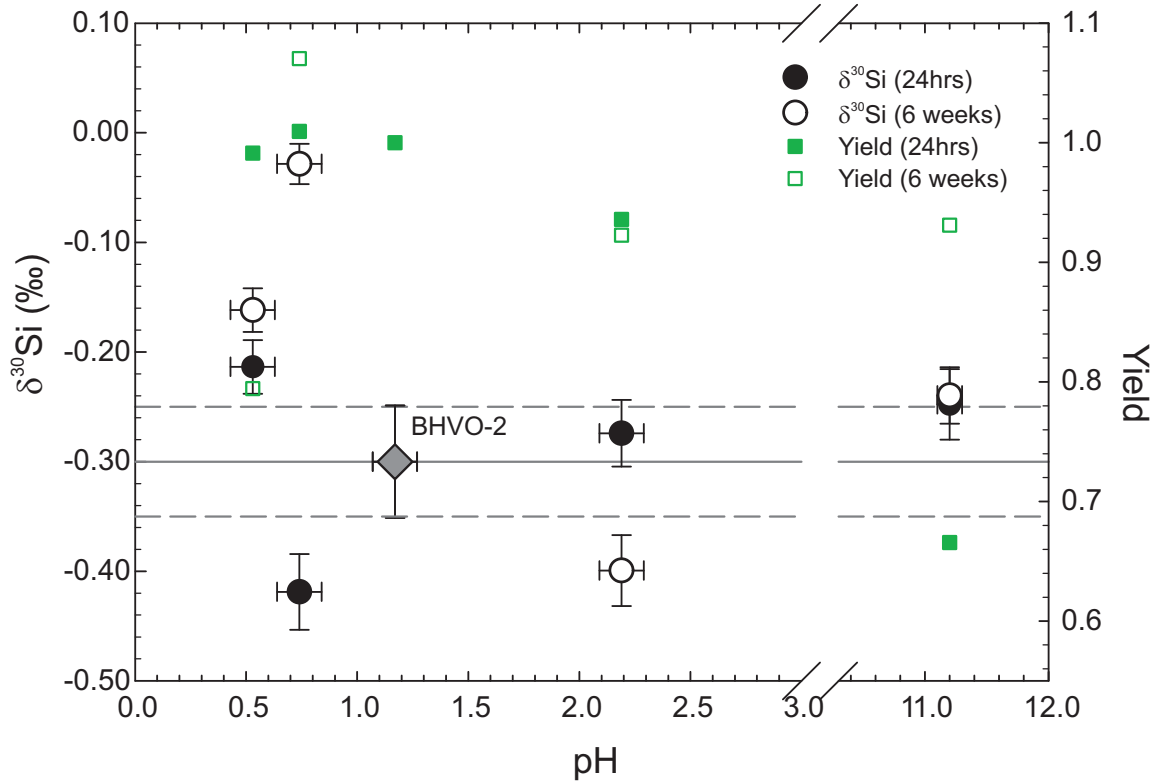


Figure (3.7): $\delta^{30}\text{Si}$ data for BHVO-2 aliquots from two measurement sessions and their yields plotted against pH. 24hrs and 6 weeks refer to the length of time the samples had to equilibrate after HCl or NaOH was added. The point labelled as “BHVO-2” is the original aliquot that has not been altered since the initial fusion and acidification.

to equilibrate for 24 hours before being loaded onto the columns. During the MC-ICPMS run, the original BHVO-2 solution was bracketed against NBS-28 while the other aliquots were bracketed against BHVO-2 and subsequently corrected to NBS-28. The $\delta^{30}\text{Si}$ of the aliquots were analysed again 6 weeks later. The yields were based on the intensities recorded for the Si beams on the Nu Plasma. The pH results (Fig. 3.7) do not appear to support the findings of Fitoussi et al. (2009) The original BHVO-2 solution has a pH of 1.2, which is lower than their specified pH range, but its $\delta^{30}\text{Si}$ is the same within error of the previously published values (Abraham et al., 2008; Fitoussi et al., 2009). The solutions with low pH do show offsets from BHVO-2 in $\delta^{30}\text{Si}$ but can have very high yields which rules out effects due to adsorption on the column resulting from positively charged polymerized chains resulting from the acidic

conditions (Fitoussi et al., 2009). Furthermore, the direction and the magnitude of the offsets are not consistent between the two measurement sessions. This may point to some instability in these particular aliquots, as the majority of the sample solutions have similar pH values but these effects are not seen. Another problem could be the lack of “matrix” matching during analysis on the MC-ICPMS between sample and the bracketing standard due to the differing pHs. The aliquot with a pH of 2.2 does show consistently high yields but its $\delta^{30}\text{Si}$ is not always within zero of BHVO-2. In fact it is the sample with a pH of ~ 11 that is the most consistent in its $\delta^{30}\text{Si}$ value though its yields vary dramatically. As the offsets of low pH solutions tend to be towards heavier $\delta^{30}\text{Si}$ values, it makes it unlikely that low pH is the sole cause of the discrepancy between the Fitoussi et al. (2009) and Georg et al. (2007a) datasets as the $\delta^{30}\text{Si}$ values in the latter are *lighter* than subsequent Si isotope measurements. Indeed the solutions measured here (e.g. Table 4.1) are more acidic than those of Georg et al. (2007a) but the heavier data are more consistent with Fitoussi et al. (2009). Neither Zambardi and Poitrasson (2010) nor Savage et al. (2010) observe an isotopic effect related to pH.

3.6 Standard Addition

The most effective method to assess and correct for any potential matrix effects is to double spike the element of interest with a known isotopic ratio (e.g. Dodson, 1963; Siebert et al., 2001; Fantle and Bullen, 2009) The sample is spiked at the beginning of the sample processing, allowing for correction of any isotopic fractionation due to incomplete recovery or instrumental mass fractionation. To do this, however, requires at least three isotopic ratios and hence four stable isotopes, ruling out its use for Si isotope analysis. Sample-standard bracketing allows for corrections of instrumental mass bias, but there is the potential for differences in mass to emerge if there is any

3.6. Standard Addition

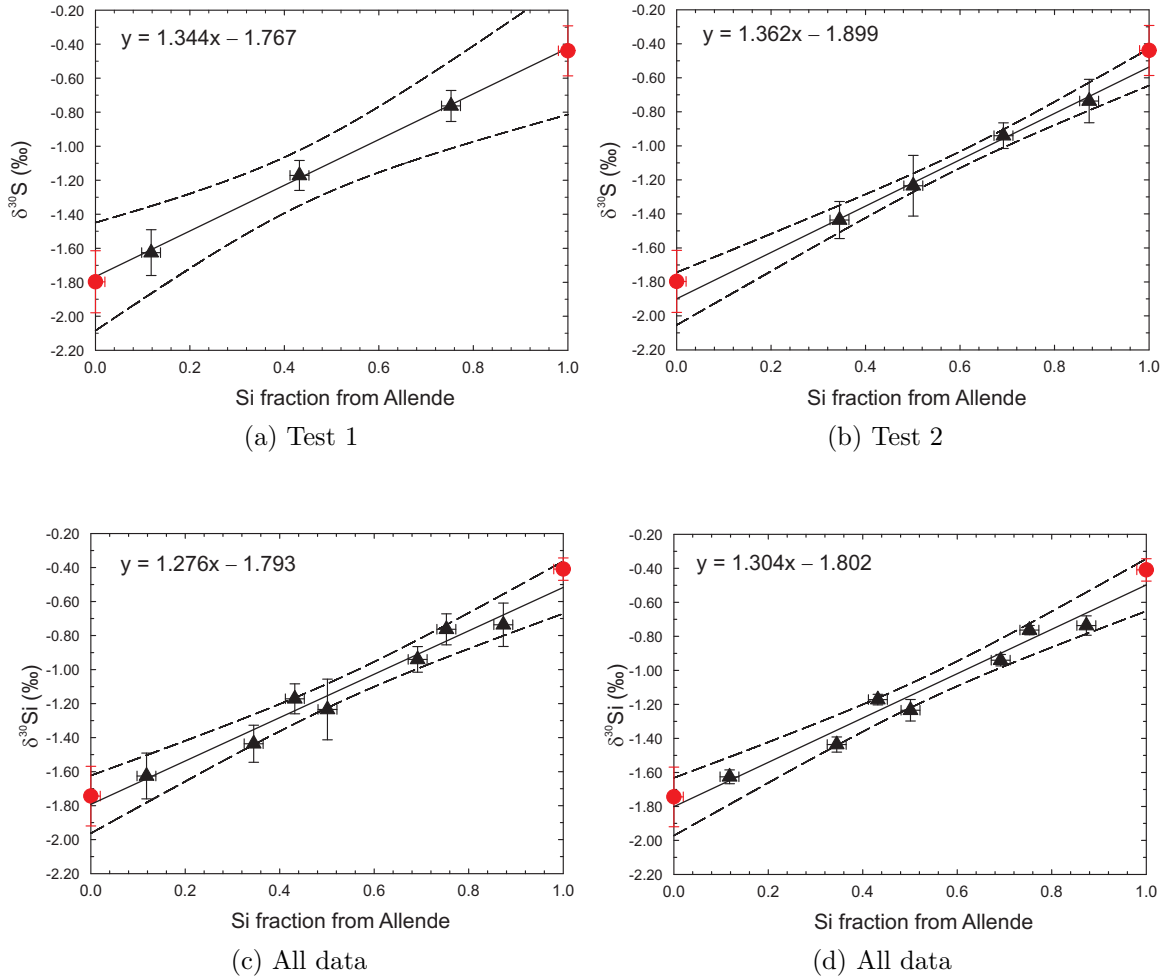


Figure (3.8): $\delta^{30}\text{Si}$ of mixtures with different proportions of the meteorite Allende and the Si isotopic standard, IRMM-018, plotted against the fraction of Si derived from Allende. (a) and (b) represent two different standard addition tests, while (c) and (d) are a compilation of (a) and (b). All the mixtures in each test were processed at the same time and represent one analytical session. Plotted in red are the isotopic compositions of the pure end-member aliquots of Allende and IRMM-018 from multiple measurement sessions. The end member compositions are different in (a) and (b) as they represent two different aliquots of Allende and IRMM-018 that were each digested at the same time as the mixtures. The values in (c) and (d) are the long term averages for multiple aliquots of IRMM-018 and Allende. The error envelopes are the 95% confidence interval for the line of best fit. The plotted error bars are $2\sigma_{SD}$ in all but (d) (see text for detail)

residual matrix left after processing the sample. This has been highlighted as a potential cause for the inter-laboratory variation in Mg isotopes studies of silicate material (Tipper et al., 2008). One method to assess the degree of potential matrix effects on isotope samples is to do “mixing” experiments, also known as standard addition tests. Various mixtures of sample and standard are prepared in known proportions, their isotopic compositions measured, and the data is regressed to calculate the isotopic compositions of the pure sample and pure standard.

Chakrabarti and Jacobsen (2010a) used aliquots of stock solutions of olivine and pure Mg standards to conduct their standard addition tests. Prytulak et al. (2011) added their V isotopic spike during the dissolution stage to allow for optimal spike-solution equilibration. For the Si tests, the “spiking” occurred during the primary processing stage with the IRMM-018 silica standard powder added to the Allende powder prior to the mixture’s fusion. As much of the debate over $\delta^{30}\text{Si}$ composition of silicates centers on the meteorite data, Allende was chosen for the sample to spike. IRMM-018 was chosen for the standard as it would allow for a range of isotopic compositions for the mixes, but not so extreme so as to create long-term memory effects in the MC-ICPMS. It could be argued that mixing the standard and the sample post-fusion, in liquid form, would allow for better equilibration. However, as the source of the conflict between the datasets is not known, it is useful to test for matrix effects from the whole of the procedure.

Two sets of standard addition tests were carried out (Table 3.2 and Fig 3.8), with two different Allende powders (Smithsonian and NHM 2). Each test was performed in one analytical session, with pure samples and standards also processed through chemistry and run at the same time. The regressions (through the mixtures only) were carried out using the Deming regression facility of SigmaPlotv12. Deming regression differs from simple linear regression as it takes into account measurement errors on both variables (Cornbleet and Gochman, 1979). Due to the nature of the data,

Table (3.2): Standard addition measurements

	$X_{\text{Si-sam}}$	$X_{\text{Si-std}}$	$\delta^{30}\text{Si}_{\text{meas.}}$ (‰)	$2\sigma_{SD}$	$2\sigma_{SEM}$	n	$\delta^{30}\text{Si}_{\text{calc.}}$ (‰) Allende ^a	$\delta^{30}\text{Si}_{\text{calc.}}$ (‰) IRMM-018 ^a
Test 1	0.75	0.25	-0.76	0.09	0.03	11	-0.46	-1.77
	0.43	0.57	-1.17	0.09	0.03	8	-0.47	-1.73
	0.12	0.88	-1.63	0.13	0.04	11	-1.06	-1.78
Regr. 1 ^b							-0.42	-1.77
Allende IV	1.00	0.00	-0.43	0.18				
IRMM-018 α	0.00	1.00	-1.70	0.20				
Test 2	0.87	0.13	-0.74	0.13	0.06	5	-0.58	-2.78
	0.69	0.31	-0.94	0.08	0.03	5	-0.56	-2.07
	0.50	0.50	-1.23	0.18	0.06	8	-0.67	-2.03
	0.34	0.66	-1.44	0.11	0.04	6	-0.75	-1.96
Regr. 2 ^c							-0.54	-1.90
Allende VIII	1.00	0.00	-0.44	0.15				
IRMM-018 β	0.00	1.00	-1.80	0.18				
Regr. 3 ^d							-0.52	-1.79
Regr. 4 ^e							-0.50	-1.80
Allende ^f			-0.42	0.07				
IRMM-018 ^f			-1.74	0.17				

^a Calculated $\delta^{30}\text{Si}$ composition of the pure sample and pure spike based on $X_{\text{Si-sam}}$ and $X_{\text{Si-std}}$ and $\delta^{30}\text{Si}_{\text{meas.}}$ of the mixture and either IRMM-018 or Allende.

^b Calculated value for Allende and IRMM-018 using the Deming regression based on $\delta^{30}\text{Si}_{\text{meas.}}$ from Test 1 (at $2\sigma_{SD}$ uncertainty levels) and $X_{\text{Si-sam}}$ and $X_{\text{Si-std}}$.

^c Same as Regr. 1 but using the Test 2 data.

^d Same as Regr. 1 but using the data from Test 1 and 2 combined.

^e Same as Regr. 3 but using $2\sigma_{SEM}$ uncertainties.

^f Long term averages of multiple aliquots.

it is possible that the simple least-squares regression would suffer from significant error (Cornbleet and Gochman, 1979), hence the Deming method was chosen. The regression was then used to calculate the Si isotopic composition of the pure standard and pure sample (Regr. 1 and Regr. 2 in Table 3.2)

$\delta^{30}\text{Si}_{\text{calc.}}$ is the calculated $\delta^{30}\text{Si}$ for the pure sample or spike based on the measured $\delta^{30}\text{Si}$ of the mixture and $X_{\text{Si-std}}$ or $X_{\text{Si-sam}}$. Table 3.2 shows that there is significant variation in $\delta^{30}\text{Si}_{\text{calc.}}$ relative to $\delta^{30}\text{Si}_{\text{mesu.}}$ for both the pure standard and the pure sample. $\delta^{30}\text{Si}_{\text{calc.}}$ is highly dependent on the sample:standard ratio. The less sample the mixture contains, the less accurate it generally is in predicting the $\delta^{30}\text{Si}_{\text{mesu.}}$ of Allende. Even with offsets of up to -0.59% , however, the $\delta^{30}\text{Si}_{\text{calc.}}$ compositions for Allende always fall within the 95% confidence limits. This is not the case for IRMM-018, the pure silica standard. This larger variation in IRMM-018 relative to Allende is also seen in the long term averages. It is also known from inter-laboratory studies of Si isotope standards that IRMM-018 is somewhat heterogeneous (Reynolds et al., 2006). The fact that for both Allende and IRMM-018 the predictions based on the regressions are well within error of $\delta^{30}\text{Si}_{\text{mesu.}}$ demonstrates, despite the heterogeneity of the standard, the accuracy of the data.

In the meteorite versus bulk silicate Earth $\delta^{30}\text{Si}$ literature (e.g. Georg et al., 2007a; Fitoussi et al., 2009; Chakrabarti and Jacobsen, 2010b) the uncertainty on the $\delta^{30}\text{Si}$ data is usually quoted in $2\sigma_{SEM}$ rather than $2\sigma_{SD}$. The standard error of the mean (σ_{SEM}) describes the uncertainty of how well the sample mean represents the population mean. In other words, what the uncertainty is on x_{best} where $x_{\text{best}} = \bar{x}$ (Taylor, 1997). In discussing potential sources of variability of the data, it is worth assessing how much variation there is from the average value, i.e. using σ_{SD} instead of σ_{SEM} when regressing the data. Figure 3.8 (c) & (d) show that the difference in regression between the two different kinds of uncertainty is minimal, with little change in the position of the confidence intervals. What is noticeable is that where σ_{SEM} is used

3.7. Conclusions

(Fig. 3.8 (d)), the data points are no longer all within error of the regression line. This could indicate that using σ_{SEM} underestimates the uncertainty in $\delta^{30}\text{Si}$ compositions of the samples.

3.7 Conclusions

These tests on some of the putative causes for $\delta^{30}\text{Si}$ interlaboratory variation have found no source for systematic offsets when using the method of Georg et al. (2006a). There is nothing in these tests that clearly indicates the scale of the discrepancies between the Georg et al. (2007a) and Fitoussi et al. (2009) data in particular. Further and more detailed testing is required to fully understand the interlaboratory variation in the meteorite and terrestrial data.

Chapter 4

Silicon isotopes in meteorites and planetary core formation¹

4.1 Introduction

The compositional differences between the rocky bodies in the solar system are the result of both accretionary and planetary processes with metal-silicate differentiation playing a key role (e.g. Righter et al., 2006). It has long been proposed that the Earth's core must contain a significant percentage of a light element (or elements) to fit the density inferred from seismic studies (Birch, 1964). Hydrogen, carbon, oxygen, silicon and sulphur have been proposed as potential candidates (Poirier, 1994) in the ongoing debate. The superchondritic Mg/Si of the terrestrial mantle has been used to argue that Si in particular is an important component in the core (Allègre et al., 1995; Drake and Righter, 2002). Recent estimates indicate that the core might contain as much as 6wt% Si in comparison with 21wt% Si in the primitive mantle (e.g. McDonough, 2003). Partitioning experiments show that Si becomes more siderophile with increasing temperature and pressure and with decreasing oxygen fugacity (e.g. Kilburn and Wood, 1997; Gessmann et al., 2001; Wade and Wood, 2005); therefore, it is a likely candidate for entering the core during metal-silicate differentiation of

¹The majority of this chapter has been published as “Silicon isotopes in meteorites and planetary core formation” R. M. G. Armytage, R. B. Georg, P.S. Savage H. M. Williams, A. N. Halliday. *Geochimica et Cosmochimica Acta* (2011) **75**, 3662-3676

the Earth. Equilibrium isotope fractionation is driven by differences in bonding environment; hence the differences in structure between silicate and metallic liquids could lead to Si isotope fractionation (Georg et al., 2007a). Theoretical calculations, along with partitioning experiments, provide evidence that Si isotopes fractionate between metal and silicate with fractionation factors (ϵ) in the range of 0.4 to 2‰ (Schauble et al., 2007; Shahar et al., 2009). If Si isotopes are fractionated by core formation, there should be a difference between the Si isotope composition of bulk, undifferentiated chondrites and that of the Earth’s mantle. It is widely assumed that the refractory element composition of the bulk Earth is approximated by that of chondrites (Palme and O’Neill, 2003 and references therein). Therefore, the superchondritic Mg/Si ratio in the bulk silicate Earth (BSE) has long been used to argue for the presence of silicon in the core (e.g. Ringwood, 1959). The advantage of using Si isotope data, rather than superchondritic Mg/Si arguments, is that the fractionation factors should be dependent on temperature and pressure. Therefore, measurements of Si isotopes in meteorites and the terrestrial mantle can complement partitioning data from metal-silicate equilibration and provide constraints on mass balance and/or core formation conditions.

The work of Molini-Velsko et al. (1986) is the most comprehensive study of Si isotope variation in meteorites to date. However, at the level of their external precision, $\delta^{30}\text{Si} = \pm 0.4\text{‰}$ ($2\sigma_{SD}$), it was not possible to resolve any potential differences between meteorite groups or between meteorites and terrestrial samples. With improvements in multi collector ICPMS (MC-ICPMS) over the past decade there have been a number of studies of non-traditional stable isotope systems in meteorites e.g. Weyer et al., 2005; Moynier et al., 2007; Seitz et al., 2007; Teng et al., 2007; Wombacher et al., 2008. The higher precision that is now technically achievable provides the ability to resolve small, sub-permil isotopic differences such as those expected in high temperature systems. Using MC-ICPMS, Georg et al. (2007a) reported a mea-

sureable difference, $\delta^{30}\text{Si} = 0.20\text{‰} \pm 0.11$ ($1\sigma_{SD}$), between the Si isotopic composition of chondrites, a proxy for Earth's precursor material, and mantle-derived materials as representatives of BSE. It was also found that differentiated achondrites from Mars and the HED parent body (Vesta) have the same average Si isotope signature as chondrites, while the Moon is similar to the silicate Earth. The fact that meteorites are different from the silicate Earth, points to a fractionation event or series of events that was unique to the Earth-Moon system, in contrast to other differentiated bodies that have been sampled. It was proposed that the fractionation was the result of Si entering the core at high temperature and pressure.

More recently Fitoussi et al. (2009) reported a difference between carbonaceous chondrites and terrestrial samples that was smaller than that reported by Georg et al. (2007a) by a factor of ~ 2 and with differences in absolute $\delta^{30}\text{Si}$ values. Other recent Si isotope work (Ziegler et al., 2010) found clear offsets in the Si isotope composition of meteorites relative to terrestrial samples, more than twice that observed by Georg et al. (2007a). The data of Chakrabarti and Jacobsen (2010b) do not display a Si isotope offset between meteorites and terrestrial mantle but report similar absolute terrestrial $\delta^{30}\text{Si}$ values to Georg et al. (2007a).

Here we set out to extend the high precision Si isotope meteorite dataset, especially for achondrites. We also assess what effect the differences between the reported $\delta^{30}\text{Si}$ compositions for meteorites and BSE have on the amount of Si in the core, and how useful Si isotopes are in constraining this.

4.2 Samples and analytical methods

4.2.1 Sample preparation

The meteorites and terrestrial samples analysed were, in the most part, the same samples as had been analysed by Georg et al. (2007). A minimum mass of 70-100 mg

4.2. Samples and analytical methods

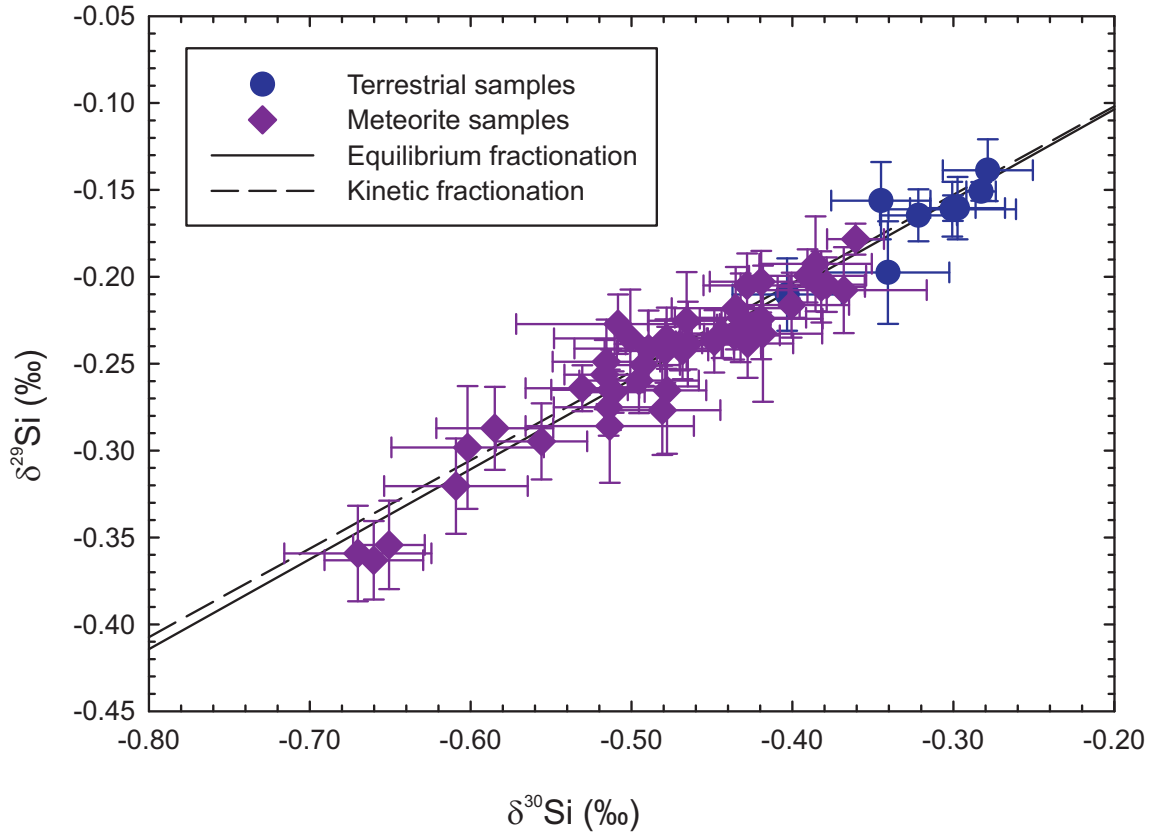


Figure (4.1): $\delta^{29}\text{Si}$ versus $\delta^{30}\text{Si}$. The error bars represent $\pm 2\sigma_{SEM}$ unless multiple aliquots have been processed (see Table 4.1) when the error plotted is $\pm 2\sigma_{SD}$. The calculated slopes for mass dependent equilibrium fractionation (0.5178) and mass dependent kinetic fractionation (0.5092) are also plotted.

of sample was ground in an alumina mortar with ethanol. Ideally larger masses on the order of grams would have been used in order to minimise sample heterogeneity, however a key aim was to reproduce the measurement conditions of Georg et al. (2007a) as closely as possible, including the same sample powders. The procedure used in this study is based on the method detailed in Georg et al. (2006a) and in Chapter 2.

The solid Si isotope standards NBS-28, IRMM-018 and Diatomite were processed in exactly the same manner as the rock and meteorite samples. The total procedural blank, including instrument blanks, at Oxford is 13ng where typical analytical amounts are $4.5\mu\text{g}$, giving a sample to blank ratio of ~ 350 .

To correct for instrumental mass drift, sample-standard bracketing was used with

the international standard NBS-28 as the bracketing standard. Silicon isotope variations are reported as the deviations of $^{30}\text{Si}/^{28}\text{Si}$ and $^{29}\text{Si}/^{28}\text{Si}$ from the NBS-28 standard in parts per thousand using:

$$\delta^{30}\text{Si} = \left[\frac{(^{30}\text{Si}/^{28}\text{Si})_{\text{sample}}}{(^{30}\text{Si}/^{28}\text{Si})_{\text{NBS28}}} - 1 \right] \times 1000 \quad (4.1)$$

$$\delta^{29}\text{Si} = \left[\frac{(^{29}\text{Si}/^{28}\text{Si})_{\text{sample}}}{(^{30}\text{Si}/^{28}\text{Si})_{\text{NBS28}}} - 1 \right] \times 1000 \quad (4.2)$$

where NBS28 is the standard reference material used for Si isotopes. Each measurement represents 20 cycles with an integration time of 10 s for each cycle. The reported sample data are the result of more than one run (~ 9 measurements per run) and the accuracy of the measurements in each run was verified with various calibrated standards such as IRMM-018, Diatomite and BHVO. Each run also represents a separate column chemistry repeat for both the samples, standards and bracketing standard. The reproducibility of Diatomite over a 18 month period is $\pm 0.15\%$ $\delta^{30}\text{Si}$ and $\pm 0.10\%$ $\delta^{29}\text{Si}$ ($\pm 2\sigma_{SD}$, $n = 400$). The Diatomite values of $\delta^{30}\text{Si} = 1.23 \pm 0.15\%$ and $\delta^{29}\text{Si} = 0.63 \pm 0.10\%$ are consistent with the calibrated values of $\delta^{30}\text{Si} = 1.26 \pm 0.20\%$ and $\delta^{29}\text{Si} = 0.64 \pm 0.14\%$ (Reynolds et al., 2007). Similarly the Si isotope values for IRMM-018 and BHVO-1,-2 are in agreement with the published values (data in Table 4.1). All fractionations measured were mass dependent; indeed mass dependence was used as a data quality check. Therefore only $\delta^{30}\text{Si}$ is discussed in the text though all three isotopes were measured. The mass dependence was checked by constructing a three isotope plot of all the data (Fig 4.1) which was regressed to give a slope of $0.508^{+0.024}_{-0.036}$. This is within error of the calculated equilibrium (0.5178) and kinetic (0.5092) fractionation slopes.

4.2. Samples and analytical methods

Table (4.1): Silicon isotope data of standards, meteorites and terrestrial samples

Standards		$\delta^{30}\text{Si}$ (‰)	$2\sigma_{SD}$	$\delta^{29}\text{Si}$ (‰)	$2\sigma_{SD}$	N	SiO_2 (wt%)
Diatomite		1.23	0.15	0.63	0.10	400	99.3
<i>Diatomite^a</i>		<i>1.26</i>	<i>0.2</i>	<i>0.64</i>	<i>0.14</i>	<i>100</i>	
IRMM-018		-1.69	0.19	-0.87	0.12	152	99.2
<i>IRMM-018^a</i>		<i>-1.65</i>	<i>0.22</i>	<i>-0.85</i>	<i>0.14</i>	<i>740</i>	
BHVO-1		-0.30	0.15	-0.16	0.08	117	49.3
BHVO-2		-0.28	0.14	-0.15	0.08	223	
BHVO-2 (II)		-0.34	0.07	-0.16	0.06	6	
BHVO-2 (III)		-0.30	0.09	-0.18	0.07	11	
BHVO-1 and -2 average		-0.31	0.04	-0.16	0.02	4	
<i>BHVO-1 and -2 average^b</i>		<i>-0.31</i>	<i>0.26</i>	<i>-0.17</i>	<i>0.13</i>	<i>19</i>	
Samples		$\delta^{30}\text{Si}$ (‰)	$2\sigma_{SEM}^c$	$\delta^{29}\text{Si}$ (‰)	$2\sigma_{SEM}$	N	SiO_2 (wt%)
Carbonaceous Chondrites							
Orgueil	CI1	-0.52	0.02	-0.27	0.01	25	22.6
Murchison	CM2	-0.52	0.03	-0.28	0.02	20	27.4
Allan Hills 83108	CO3.5	-0.49	0.02	-0.25	0.01	24	32.7
Allende I		-0.43	0.03	-0.24	0.02	14	33.0
Allende II		-0.37	0.05	-0.21	0.02	13	32.9
Allende III		-0.38	0.03	-0.21	0.02	23	33.5
Allende IV		-0.43	0.04	-0.22	0.03	20	33.2
Allende V		-0.43	0.02	-0.23	0.01	70	34.1
Allende VI		-0.36	0.02	-0.18	0.01	37	33.9
Allende VII		-0.45	0.05	-0.24	0.02	9	35.5
Allende mean ($\pm 2\sigma_{SD}$)	CV3	-0.41	0.07	-0.22	0.04	7	
Grosnaja	CV3	-0.56	0.03	-0.29	0.02	16	30.0
Mokoia	CV3	-0.48	0.04	-0.28	0.03	8	32.1
Elephant Moraine	CK4						
92002		-0.44	0.03	-0.23	0.01	24	36.2
Carbonaceous chondrite mean ($\pm 2\sigma_{SD}$)							
		-0.48	0.10	-0.26	0.05	8	
Ordinary Chondrites							
Bath	H4	-0.44	0.02	-0.23	0.01	22	37.2
Allegan	H5	-0.48	0.03	-0.24	0.02	10	40.7
Cereseto	H5	-0.42	0.04	-0.22	0.02	19	37.3
Épinal	H5	-0.47	0.02	-0.23	0.03	11	38.9

Continued on Next Page...

Table 4.1 – Continued

Samples		$\delta^{30}\text{Si}$ (‰)	$2\sigma_{SEM}$	$\delta^{29}\text{Si}$ (‰)	$2\sigma_{SEM}$	N	SiO_2 (wt%)
Barratta	L4	-0.48	0.02	-0.27	0.04	10	40.6
Plainview (d)	L6	-0.47	0.05	-0.24	0.02	11	37.2
Parnallee	LL3.6	-0.40	0.04	-0.22	0.02	11	40.8
Ordinary chondrite							
mean ($\pm 2\sigma_{SD}$)		-0.46	0.06	-0.24	0.03	8	
Enstatite Chondrites							
Indarch I		-0.66	0.03	-0.36	0.02	29	39.1
Indarch II		-0.65	0.02	-0.35	0.03	19	39.1
Indarch mean ($\pm 2\sigma_{SD}$)	EH4	-0.66	0.01	-0.36	0.01	2	
St. Mark's I		-0.60	0.05	-0.30	0.04	8	39.5
St. Mark's II		-0.67	0.04	-0.36	0.03	10	38.9
St. Mark's mean ($\pm 2\sigma_{SD}$)	EH5	-0.64	0.10	-0.33	0.09	2	
Khairpur	EL6	-0.58	0.04	-0.29	0.02	20	43.0
Enstatite chondrite							
mean ($\pm 2\sigma_{SD}$)		-0.63	0.07	-0.32	0.07	3	
Chondrite average ($\pm 2\sigma_{SD}$)		-0.49	0.15	-0.26	0.08	19	
HED meteorites							
Pasamonte	EUC-P ^d	-0.42	0.03	-0.20	0.02	30	46.5
Béréba	EUC-M ^e	-0.43	0.03	-0.20	0.02	0	47.3
Bouvante	EUC-M	-0.44	0.04	-0.22	0.02	21	50.7
Juvinas	EUC-M	-0.51	0.04	-0.27	0.02	29	45.9
Sioux County	EUC-M	-0.52	0.04	-0.27	0.02	24	52.0
Johnstown	DIO	-0.51	0.06	-0.23	0.02	9	47.1
Kapoeta	HOW	-0.38	0.02	-0.20	0.02	16	47.9
HED meteorite average ($\pm 2\sigma_{SD}$)		-0.45	0.10	-0.23	0.05	7	
Martian meteorites							
Governador Valadares I		-0.61	0.04	-0.32	0.03	12	46.4
Governador Valadares II		-0.51	0.05	-0.29	0.03	8	49.9
Governador Valadares							
mean ($\pm 2\sigma_{SD}$)	Nakhlite	-0.56	0.14	-0.30	0.04	2	
Nakhla	Nakhlite	-0.47	0.03	-0.24	0.01	24	47.4
Sayh al Uhaymir 005	Shergottite	-0.48	0.03	-0.24	0.02	11	51.0
Shergotty	Shergottite	-0.52	0.02	-0.26	0.02	20	50.1
Zagami	Shergottite	-0.39	0.04	-0.20	0.02	14	49.3
Martian average ($\pm 2\sigma_{SD}$)		-0.48	0.13	-0.25	0.08	5	

Continued on Next Page...

4.2. Samples and analytical methods

Table 4.1 – Continued

Samples	$\delta^{30}\text{Si}$ (‰)	$2\sigma_{SEM}$	$\delta^{29}\text{Si}$ (‰)	$2\sigma_{SEM}$	N	SiO_2 (wt%)	
Ureilites							
Allan Hills A77257	-0.52	0.03	-0.25	0.02	20	44.1	
Dhofar 132	-0.39	0.03	-0.19	0.03	18	42.2	
Elephant Moraine 96042	-0.50	0.05	-0.24	0.03	14	37.2	
Pecora Escarpment 82506	-0.47	0.02	-0.24	0.02	9	40.9	
Ureilite average ($\pm 2\sigma_{SD}$)	-0.47	0.12	-0.23	0.05	4		
Mayo Belwa	Aubrite	-0.53	0.04	-0.26	0.01	11	55.0
Achondrite average ($\pm 2\sigma_{SD}$)							
Meteorite average ($\pm 2\sigma_{SD}$)							
Terrestrial basalts							
A12 D5-5							
Atlantic MORB glass	-0.28	0.03	-0.14	0.02	23	47.4	
P13							
Basalt Principe	-0.30	0.03	-0.16	0.02	18	41.1	
R937							
East Pacific Rise MORB glass	-0.32	0.02	-0.16	0.01	22	47.6	
Terrestrial peridotites							
C235A							
Cameroon line spinel lherzolite	-0.40	0.04	-0.20	0.02	18	43.1	
San Carlos Olivine							
Spinel lherzolite	-0.30	0.04	-0.16	0.02	19		
BSE average ($\pm 2\sigma_{SD}$)^f							
<i>BSE mean^g</i>							
	-0.29	0.08	-0.15	0.05	35		

^a Value from an inter-laboratory comparison study (Reynolds et al., 2007)

^b Data for the BHVO-1 and -2 mean comes from Abraham et al. (2008)

^c The subscript SEM refers to the standard error of the mean, which is calculated from $\sigma_{SD}/N^{1/2}$

^d EUC-P denotes a polymict eucrite

^e EUC-M denotes a monomict eucrite

^f A mean value for BHVO-1-2 is included in this average

^g The value for the bulk silicate Earth average ($\pm 2\sigma_{SD}$) comes from Savage et al. (2010)

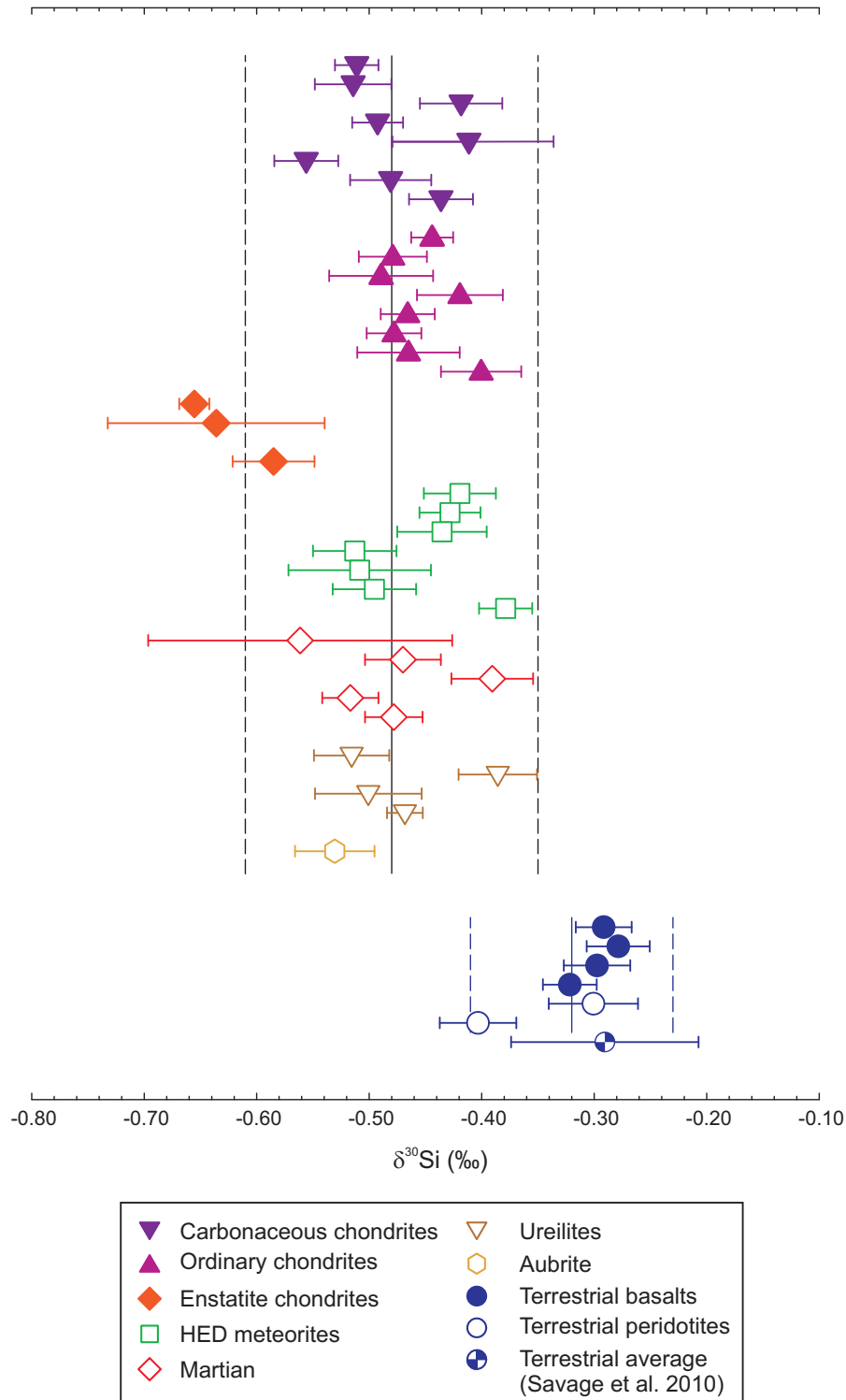


Figure (4.2): $\delta^{30}\text{Si}$ silicon isotope compositions of meteorites and terrestrial samples. The error bars represent $\pm 2\sigma_{SEM}$ unless multiple aliquots have been processed (see Table 4.1) when the error plotted is $\pm 2\sigma_{SD}$. The solid lines are the mean values for meteorites and terrestrial samples, while the dashed lines are $\pm 2\sigma_{SD}$.

4.3 Results and Discussion

4.3.1 Introduction

The silicon isotope data for the 42 different bulk rock (including the USGS basalt standard BHVO) and meteorite samples are given in Table 4.1 and in Figure 4.2.

4.3.1.1 Chondrites

The $\delta^{30}\text{Si}$ of the CV3 chondrites measured in this study scatter over the entire range of $\delta^{30}\text{Si}$ compositions for carbonaceous chondrites. Heavy $\delta^{30}\text{Si}$ signatures for CAIs (calcium-aluminium inclusions) have been reported (Clayton et al., 1988; Shahar and Young, 2007) so it could be expected that the variation is related to CAI proportions in the meteorite analysed. If this is the case, it must be due to heterogeneity at the sampling level, as no systematic variation in $\delta^{30}\text{Si}$ can be seen between the different carbonaceous chondrite groups with their differing proportions of CAIs (Scott and Krot, 2007).

The average composition of the ordinary chondrites is within error to that of the carbonaceous chondrites but with less scatter ($\delta^{30}\text{Si}_{\text{Carb. chondrite}} = -0.48 \pm 0.10\text{‰}$, and $\delta^{30}\text{Si}_{\text{Ord. chondrite}} = -0.46 \pm 0.06\text{‰}$, both expressed as $2\sigma_{SD}$). This lack of significant offset in $\delta^{30}\text{Si}$ between the two chondrite classes is in accord with some of the previous Si isotope studies (Georg et al., 2007a; Chakrabarti and Jacobsen, 2010b). There is no significant variation between the ordinary chondrite groups either. Parnallee, the only LL chondrite analysed, is the heaviest of all of them but as no other LL chondrites have been analysed in recent studies (Fitoussi et al. (2009) also only measured Parnallee), it is not possible to attach any significance to the value.

Enstatite chondrites are known to contain significant (on the order of $\sim 2\text{wt}\%$), and variable proportions of Si dissolved in the metal phases (Krot et al., 2007). It has also been shown that the $\delta^{30}\text{Si}$ of the metal is fractionated relative to the composition of the

silicate phase (Ziegler et al., 2010). Due to the complications of trying to homogenise metal and silicate in bulk samples, repeat fusions were performed on the majority of the samples to test for sample heterogeneity effects. In all cases the $2\sigma_{SD}$ was $<0.10\text{‰}$, i.e. better than the external reproducibility for pure Si standards. This demonstrates the robustness of the analytical preparation techniques. The enstatite chondrites analysed here are lighter than the other chondrites with an average $\delta^{30}\text{Si}$ of $-0.63 \pm 0.07\text{‰}$ ($2\sigma_{SD}$) and within uncertainty of the other chondrite classes. Student t-tests show that the enstatite mean is different from the mean Si isotopic composition of the other chondrites at $>99\%$ probability level. In every other recent bulk meteorite Si isotope study (Georg et al., 2007a; Fitoussi et al., 2009; Chakrabarti and Jacobsen, 2010b) one bulk enstatite chondrite (EH class) has been analysed and it is always the lightest chondrite measured. Fitoussi et al. (2009) highlighted the correlation of their $\delta^{30}\text{Si}$ compositions with chondritic Mg/Si ratios.

Figure 4.3 shows that this correlation carries less significance in the studies involving more samples, which show more dispersion in the data. However, it is a trend common to the 3 recent bulk meteorite studies, despite the inter-lab differences in $\delta^{30}\text{Si}$. It has been suggested (Fitoussi et al., 2009), that this is the result of a kinetic isotope fractionation mechanism from the reaction of olivine and SiO(g) to form enstatite during the early solar nebula. Another possible explanation for the light $\delta^{30}\text{Si}$ composition of bulk enstatite chondrites is that the bulk meteorites analysed by the different laboratory groups are not the total original “bulk” composition. If significant amounts of silicate material were lost after metal silicate partitioning, the bulk Si isotope composition of enstatite chondrites could shift to lighter values due to the metal preferentially taking in lighter silicon. No clear correlations between $\delta^{30}\text{Si}$ and volatile element content or Mg# are observed however, lending weight to the explanation of Fitoussi et al. (2009).

Two additional enstatite chondrite samples, Abee and Hvittis, were analysed.

4.3. Results and Discussion

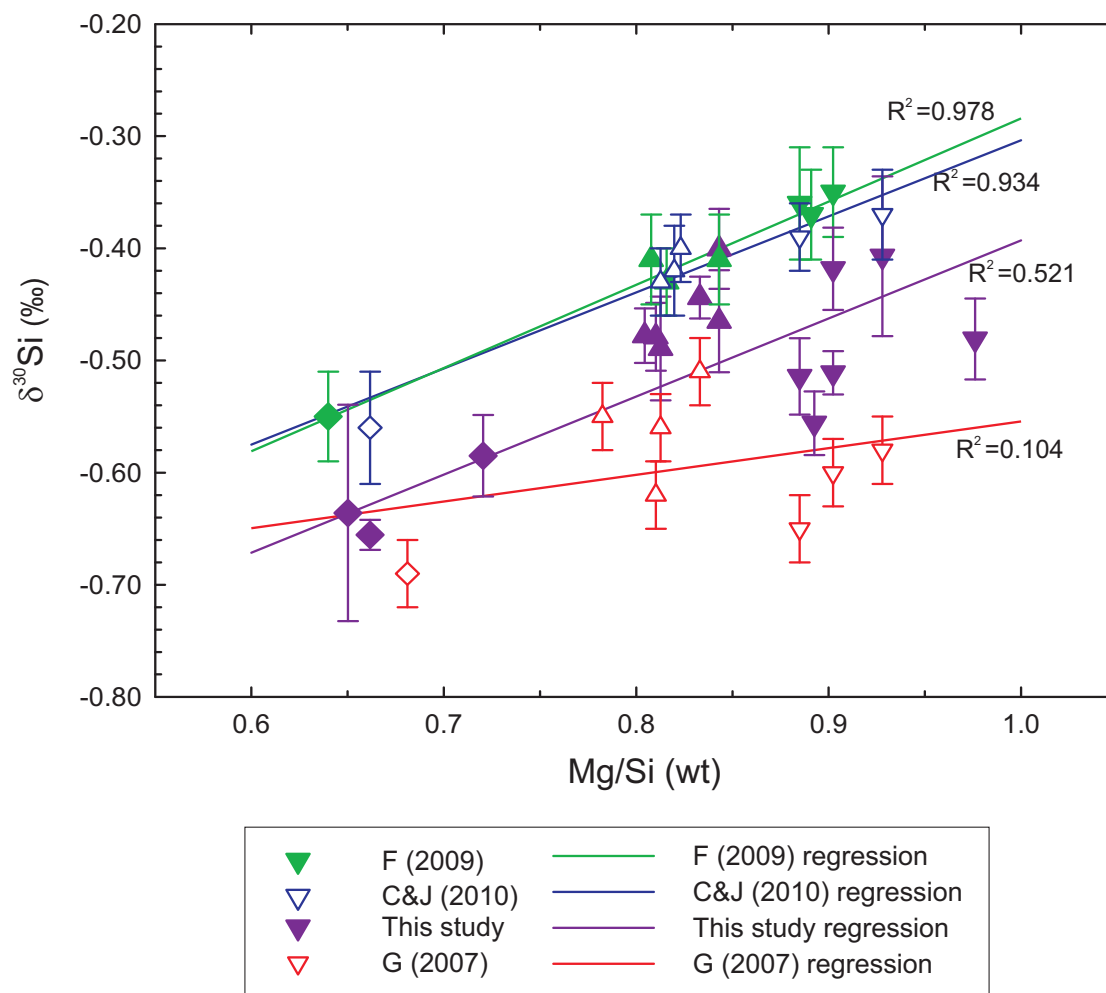


Figure (4.3): $\delta^{30}\text{Si}$ vs. Mg/Si ratios in chondritic samples from: Fitoussi et al. (2009); Chakrabarti and Jacobsen (2010b); this study; Georg et al. (2007a). The point-down triangles are the carbonaceous chondrites, the point-up triangles are the ordinary chondrites and the diamonds are the enstatite chondrites. The regression lines are weighted fit lines for each individual dataset. The errors on the literature Mg/Si data are small and omitted for the sake of clarity (Mason, 1963; Mason and Wiik, 1966a; Jarosewich, 1967; Mason and Wiik, 1967; Von Michaelis et al., 1968; Ahrens et al., 1969; Graham et al., 1976; Fulton and Rhodes, 1984; Easton, 1985a; Jarosewich, 1990; Leya et al., 2001; Fitoussi et al., 2009)

They had both been previously processed for an earlier W isotope study (Lee and Halliday, 2000) and were analysed due to their availability. The Abee (EH4) sample analysed here is the non-magnetic fraction whereas Hvittis (EL6) was part of an initial crudely separated magnetic fraction but then was the semi-magnetic residue of a more thorough magnetic separation. (D. C. Lee pers. comm. 2010). Abee is one of the heavier enstatite chondrites with regards to $\delta^{30}\text{Si}$, which is consistent with it being the non-magnetic (i.e. silicate) fraction of a meteorite where the lighter silicon isotopes have preferentially partitioned into Si-bearing kamacite (Figure 4.4). The reason for the heavy $\delta^{30}\text{Si}$ composition of Hvittis is unclear as its preparation involved concentrating the metal phase which should be lighter, relative to the bulk sample. It could be that in the EL6 chondrites, the metal contains so little Si, that it is hard to resolve an isotopic fractionation between two phases. Further work on separate metal and silicate phases needs to be done to understand this issue. It is possible that the difference between Khairpur (EL6) and Hvittis (EL6) is due to bulk sample variation rather than due to their different processing histories.

With the addition of these two enstatite chondrite samples, there is a hint that the more reduced EH chondrites have the lightest $\delta^{30}\text{Si}$ compositions (Figure 4.4). The EH chondrites also contain more Si in the metal phase (1.6 - 4.9wt% versus 0.2 - 1.2 wt.% Krot et al., 2007) as a consequence of being more reduced than the EL group. However, if the variation was directly related to oxidation state, one might expect to see similar effects in the ordinary and carbonaceous chondrite classes, which are not observed (Figure 4.2). Hence the variation in $\delta^{30}\text{Si}$ is quite possibly due to sampling differing proportions of the metal between the different enstatite chondrite groups groups.

4.3. Results and Discussion

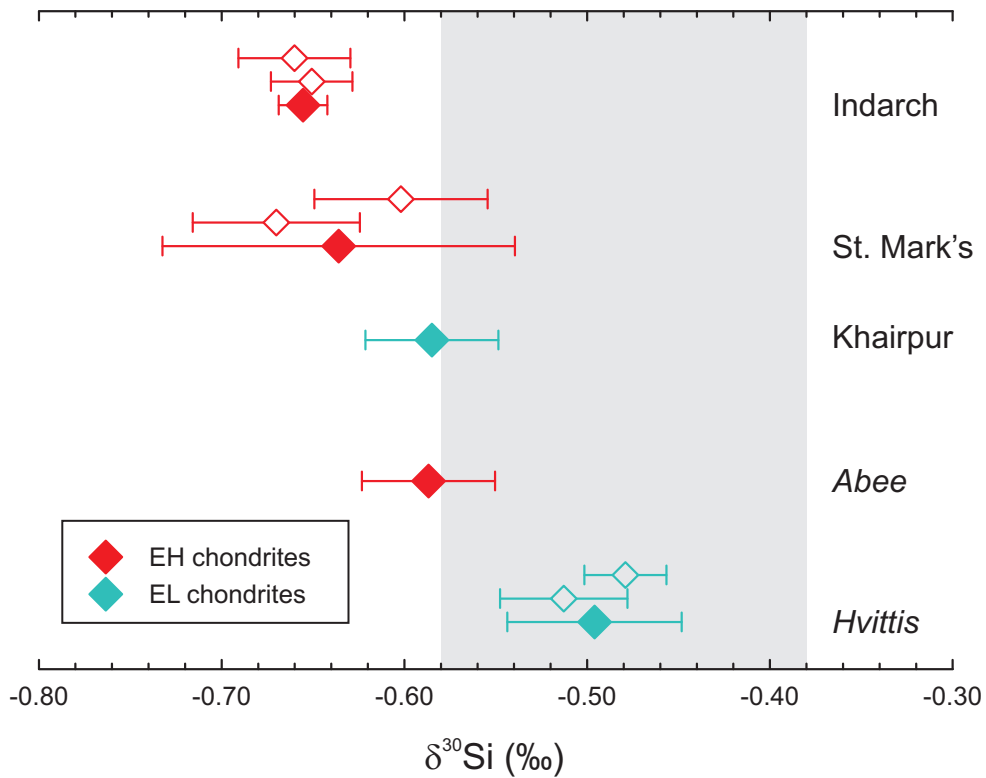


Figure (4.4): $\delta^{30}\text{Si}$ of enstatite chondrite samples. The italic names indicate those that have been previously processed and are not bulk samples. The open symbols where present are different bulk aliquots (i.e. different fusions) from the same meteorite with the large solid symbol being the mean of the two values $\pm 2\sigma_{SD}$. The error bars on the open symbols and those meteorites where only one aliquot was processed are $2\sigma_{SEM}$. The shaded grey area is the average $\delta^{30}\text{Si}$ for carbonaceous chondrites $\pm 2\sigma_{SD}$.

4.3.1.2 Achondrites

The chondrites and the differentiated achondrites averages (Table 4.1) are identical within error with $\delta^{30}\text{Si}_{\text{Chondrite}} = -0.49 \pm 0.15\text{‰}$ ($2\sigma_{SD}$) and $\delta^{30}\text{Si}_{\text{Achondrite}} = -0.47 \pm 0.11\text{‰}$ ($2\sigma_{SD}$). This similarity is as described by previous studies (Georg et al., 2007a; Fitoussi et al., 2009; Chakrabarti and Jacobsen, 2010b). In terrestrial settings, Savage et al. (2010) observed no resolvable Si isotope difference between the compositions of basalts and peridotites. This lack of Si isotopic fractionation as the result of magma generation in the terrestrial mantle, makes it reasonable, therefore, to assume that the $\delta^{30}\text{Si}$ compositions for the mafic SNC (Shergottite, Nakhilite, Chassignite) and HED (Howardite, Eucrite, Diogenite) meteorites are representative of the mantles of Mars and Vesta respectively. The variation that is seen in the HED samples appears unrelated to lithological type; much of the scatter lies within the eucrites. The one howardite, Kapoeta, is the heaviest of the HED samples but as only one sample has been analysed it is not possible to draw any firm conclusions. It has been suggested that eucrites are heterogeneous with respect to their $\Delta^{17}\text{O}$ values (Wiechert et al., 2004) and hence may come from different parent bodies. The only anomalous eucrite that has been measured in Oxford however is Pasamonte, whose $\Delta^{17}\text{O}$ anomaly is thought to be related to a chondritic impactor (Greenwood et al., 2005). As chondrites have been shown to have the same $\delta^{30}\text{Si}$ as achondrites, this is unlikely to be the cause of any of the variation seen in the data. Also when the $\delta^{30}\text{Si}$ values are plotted against major and trace element data for the eucrites (Kitts and Lodders, 1998) no correlations emerge.

There is slightly more scatter among the martian samples, $\delta^{30}\text{Si}_{\text{martian}} = 0.48 \pm 0.13\text{‰}$ ($2\sigma_{SD}$), than is observed for the HED meteorites, $\delta^{30}\text{Si}_{\text{HED}} = 0.45 \pm 0.10\text{‰}$ ($2\sigma_{SD}$). The large difference within the martian sample Govenador Valadares, is likely to be a result of heterogeneity in the sample as the two separate fusions gave such different results. No systematic differences are observed between the martian lithologies.

Governador Valadares and Nakhla are both nakhlites (olivine clinopyroxenites) and contain smectite-rich aqueous alteration minerals (Treiman, 2005). It is known from terrestrial settings that clay minerals are generally isotopically lighter than basaltic igneous rocks (Douthitt, 1982; Ding et al., 1996), which could potentially give rise to variation between the nakhlites and the shergottites (basalts). However, mass balance calculations make this unlikely as the “iddingsite” alteration product is present in very low (<1wt%) amounts (Bunch and Reid, 1975).

The petrogenesis of ureilites is still poorly understood (Goodrich, 1992) as they are coarse-grained ultramafic rocks that contain primitive characteristics such as slope ~ 1 trends on the 3 isotope oxygen plot. The ureilite average $\delta^{30}\text{Si} = -0.47 \pm 0.12\text{‰}$ ($2\sigma_{SD}$) is within error of the other achondrite bodies analysed and is not resolvable from chondrites. It appears that melt extraction on differentiated meteorite parent bodies does not fractionate Si isotopes relative to other basaltic achondrites e.g. those of Mars and Vesta. For this first high precision study of the Si isotope composition ureilites were picked that showed a range of chemical variability, for example in their olivine Mg# (Lee et al., 2009). However, no correlation is found with Si isotope composition.

The sole aubrite (enstatite achondrite) analysed was one of the lightest achondrites with respect to its $\delta^{30}\text{Si}$ composition. This is in accord with the data of Georg et al. (2007a). The oxygen isotope compositions and reduced nature of aubrites and enstatite chondrites appear to suggest some kind of kinship between the two classes (Clayton et al., 1984). The light Si isotope values are consistent with this, even though problems have been raised concerning the cosmic ray exposure ages and composition that make it unlikely that aubrites are derived by melting and differentiation of EH and EL type materials (Keil, 2010).

4.3.1.3 Terrestrial rocks

The terrestrial mean is heavier than any of the meteorite groups, with $\delta^{30}\text{Si} = -0.32 \pm 0.09\text{‰}$ ($2\sigma_{SD}$). Within the terrestrial samples analysed, the basalts are tightly clustered, $\delta^{30}\text{Si} = -0.30 \pm 0.04\text{‰}$ ($2\sigma_{SD}$), while the peridotites show more variation with $\delta^{30}\text{Si} = -0.35 \pm 0.14\text{‰}$ ($2\sigma_{SD}$). These values for the limited number of terrestrial samples analysed in this study, are in excellent agreement with the average BSE (bulk silicate Earth) value of $\delta^{30}\text{Si} = -0.29 \pm 0.08\text{‰}$ ($2\sigma_{SD}$) of Savage et al. (2010), the result of a more extensive study of mantle rocks.

4.3.1.4 Comparison with previous studies

There is a difference in the $\delta^{30}\text{Si}$ values of both meteorites and terrestrial samples between this study and those data reported in previous studies (Georg et al., 2007a; Fitoussi et al., 2009; Chakrabarti and Jacobsen, 2010b; Ziegler et al., 2010). However, in common with all of these studies, apart from Chakrabarti and Jacobsen (2010b), a difference in $\delta^{30}\text{Si}$ is measured between meteorites and terrestrial samples. The $\delta^{30}\text{Si}$ for meteorites and terrestrial samples reported here range from -0.67 to -0.36‰ and -0.40 to -0.28‰ respectively. This compares well with previously reported ranges based on far fewer meteorite samples of -0.55 to -0.35‰ and -0.32 to -0.24‰ (Fitoussi et al., 2009) and -0.56 to -0.37‰ and -0.42 to -0.34‰ (Chakrabarti and Jacobsen, 2010b). The contrast between this study and the -0.70 to -0.50‰ and -0.51 to -0.31‰ obtained by Georg et al. (2007a) is the most striking; in many cases the same sample powders were used in this study yet the ranges for the Si isotope data are noticeably offset. Potential causes for this variation has been explored in detail in Chapter 3.

4.3. Results and Discussion

Table (4.2): Comparison of recent high resolution $\delta^{30}\text{Si}$ data

	Meteorite average $\delta^{30}\text{Si}$ (‰) ^a	BSE average $\delta^{30}\text{Si}$ (‰) ^{a,b}	$\Delta^{30}\text{Si}_{\text{BSE-Meteorite}}$ ^a
This study	-0.48 ± 0.06	-0.32 ± 0.05	0.17 ± 0.11
Chakrabarti and Jacobsen (2010)	-0.42 ± 0.06	-0.38 ± 0.03	0.04 ± 0.09
Ziegler et al., (2010)			0.45 ± 0.10^c
Fitoussi et al., (2009)	-0.41 ± 0.06	-0.29 ± 0.03	0.12 ± 0.09
Georg et al., (2007)	-0.58 ± 0.06	-0.29 ± 0.03	0.38 ± 0.06
Savage et al., (2010)		-0.29 ± 0.04	
All data ^d	-0.50 ± 0.09	-0.34 ± 0.06	0.16 ± 0.15

^a The majority of the previous studies have used $\pm 1\sigma_{SD}$ when discussing the meteorite and BSE populations, hence the same approach is adopted here for consistency.

^b Includes BHVO-2 in BSE estimates, which has been excluded from some published values.

^c There is only one bulk meteorite and one terrestrial sample from this study

^d This includes all the data from all the studies in the table apart from Savage et al. (2010)

4.3.2 Assessment of recent of Si isotope data

4.3.2.1 Meteorite and terrestrial mean values

There is disagreement between all of the recently published high resolution and high precision Si data, both when it comes to the $\delta^{30}\text{Si}$ compositions for meteorite and terrestrial samples and for $\Delta^{30}\text{Si}_{\text{BSE-meteorite}}$ (Table 4.2).

Figure 4.5 shows a comparison of the recent studies where significant numbers of bulk meteorites were analysed, along with averages of all the data across the studies (This study, (Georg et al., 2007a; Fitoussi et al., 2009; Chakrabarti and Jacobsen, 2010b)). The mean terrestrial values for all the studies lie within 1 standard deviation of each other, but there is more discrepancy when it comes to the meteorites. The average values from this study for both meteorite and terrestrial samples correspond well to the global averages. The data of Georg et al. (2007a) are noticeably offset to lighter values in comparison to the global means. The Chakrabarti and Jacobsen (2010b) study is notable as it is the only recent work that does not resolve a difference between meteorite and terrestrial samples (Table 4.2, Fig. 4.5). Their meteorite

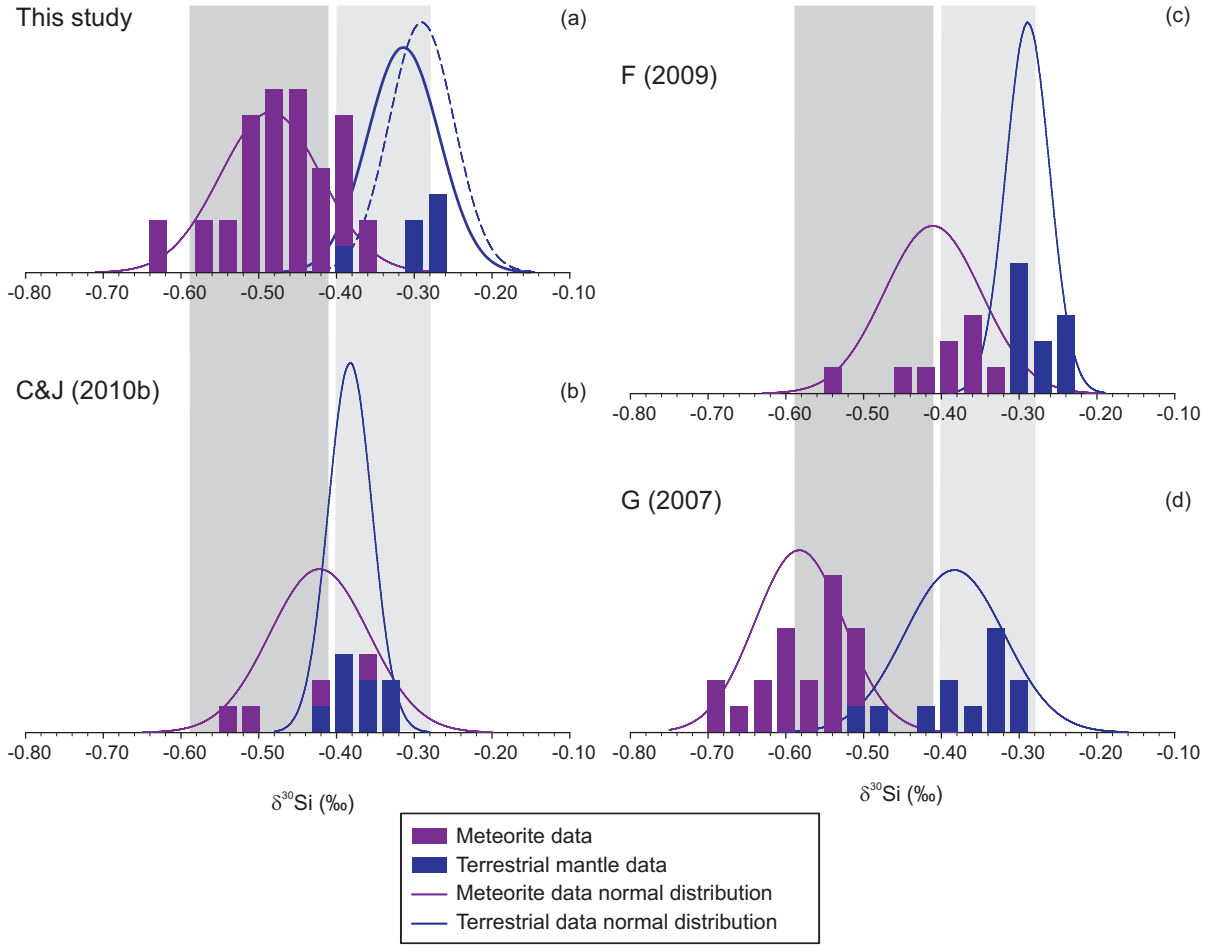


Figure (4.5): Histograms and calculated normal distributions of $\delta^{30}\text{Si}$ values for meteorites and terrestrial samples from a) this study, b) Chakrabarti and Jacobsen (2010), c) Fitoussi et al (2009), d) Georg et al. (2007). The blue dashed line in a) is the calculated normal distribution for the terrestrial data of Savage et al. (2010). The dark and light grey bands are the mean $\pm 1\sigma_{SD}$ for the pooled recent $\delta^{30}\text{Si}$ data (Table 4.2) for meteorites and terrestrial samples respectively.

values are similar to those of Fitoussi et al. (2009) but theirs are the only terrestrial data that are as light as Georg et al.'s. The majority of recent studies report $\delta^{30}\text{Si}$ compositions for BHVO in the order of -0.27‰ to -0.33‰ (Abraham et al., 2008; Fitoussi et al., 2009; Savage et al., 2010; Zambardi and Poitrasson, 2010) in contrast to the -0.41‰ value of Chakrabarti and Jacobsen (2010b). Therefore, the lack of measurable offset appears to reflect their terrestrial data rather than the meteorite compositions.

4.3.2.2 Sample by sample comparison

Just as there are major differences between all the recent Si isotope studies on the large scale, so too are the discrepancies observed on the sample by sample basis. Figure 4.6 plots the values of Murchison (CM2), Juvinas (EUC), EH chondrite and terrestrial rocks from all the recent studies. A key initial observation is the large scatter seen both in Murchison and Juvinas between the studies, despite the similarity in the measured values between these meteorites within a given laboratory. If the discrepancy between the laboratories was an issue of sample heterogeneity, the Si isotope composition of Juvinas would not be expected to follow that of Murchison so closely. Juvinas is a basalt from a differentiated body; its major element composition (Kitts and Lodders, 1998) is much closer to that of BHVO-2 than it is to Murchison. All the bulk enstatite chondrites analysed in previous studies were EH chondrites. These reproduce much better between the labs than either Murchison or Juvinas, for reasons yet unknown.

The reproducibility of the terrestrial samples is much better between the studies. However even then two terrestrial basalts from two of the studies still fall outside of the BSE value defined by Savage et al. (2010). The studies of Fitoussi et al. (2009) and Georg et al. (2007a) are the most similar in terms of sample preparation and the exact same MC-ICPMS instrument was used in both cases, but with regards to the data, they are some of the most dissimilar $\delta^{30}\text{Si}$ compositions both in the magnitude of the meteorite-terrestrial offset and individual samples. It is clear that there needs to be sample exchange, both of powdered and processed samples, to determine the cause of this inter-laboratory discrepancy for meteorites in particular.

Amidst all this disagreement there is still cause for optimism with regards the use of Si. The spread of meteorite data from all these studies is limited in comparison with the Molini-Velsko et al. (1986) $\delta^{30}\text{Si}$ data; though interestingly the mean composition has not substantially changed (Fig. 4.7).

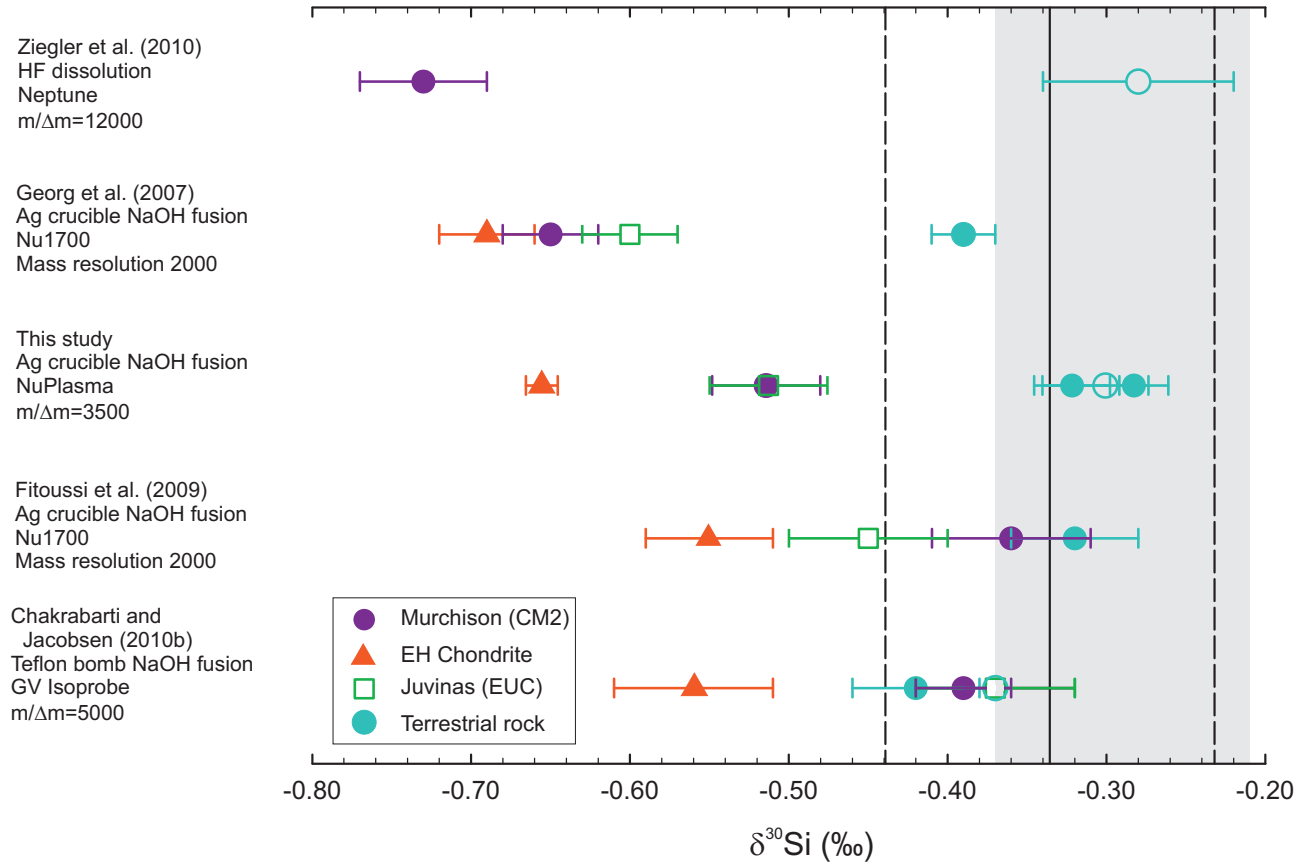


Figure (4.6): Comparison of $\delta^{30}\text{Si}$ for Murchison, EH chondrites, Juvinas and terrestrial samples from different lab groups. The EH chondrites plotted are: Indarch (This study, Chakrabarti and Jacobsen, 2010b); Abee (Georg et al., 2007); Sahara 97158 (Fitoussi et al., 2009). The solid line is the mean of all the plotted terrestrial samples and the dashed lines are $\pm 2\sigma_{SD}$. The shaded grey band is the Si isotope composition for BSE ($\pm 2\sigma_{SD}$) from Savage et al. (2010). The open terrestrial symbol is for San Carlos Olivine; all the other terrestrial samples are basalts. The basalts are BHVO-1,-2 (This study, Fitoussi et al., 2009; Chakrabarti and Jacobsen, 2010) and R937 (This study, Georg et al., 2007) The resolving power is given for all the studies apart from Fitoussi et al. (2009) and Georg et al (2007) where the true resolution is given.

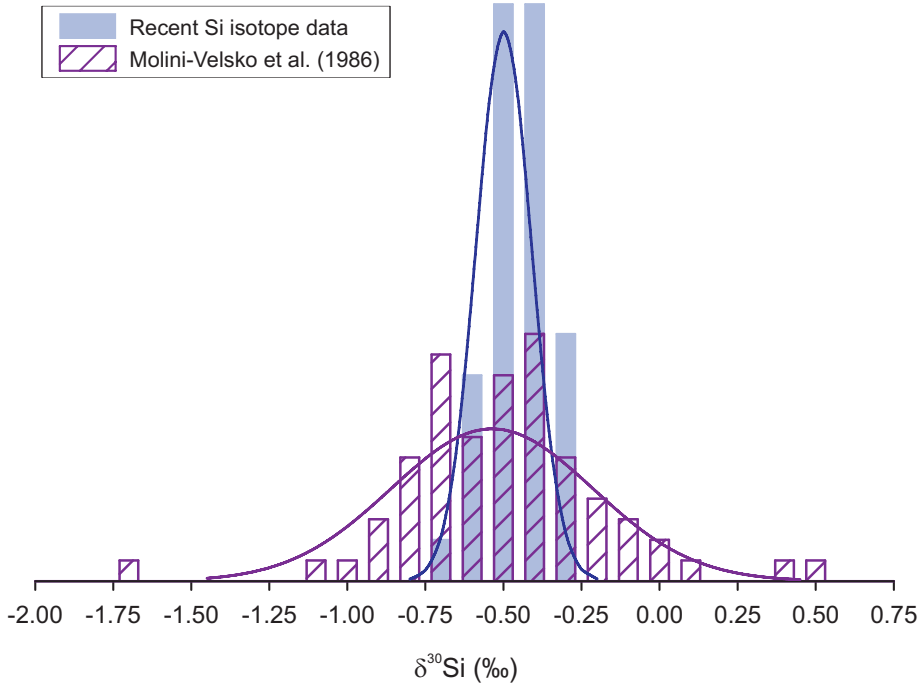


Figure (4.7): Histogram and calculated normal distribution of $\delta^{30}\text{Si}$ for meteorites from all the recent studies (This study, Georg et al., 2007; Fitoussi et al., 2009; Chakrabarti and Jacobsen, 2010b; Ziegler et al., 2010) compared to the Molini-Velsko et al. (1986) meteorite data.

4.3.3 $\Delta^{30}\text{Si}_{\text{BSE-meteorite}}$

The meteorite Si isotope data reported here are on average lighter than the compositions of the terrestrial mantle samples. However, there are inconsistencies in the literature as to how $\Delta^{30}\text{Si}_{\text{BSE-Meteorite}}$ should be calculated; whether it should be the difference between bulk silicate Earth (BSE) and chondrites; or between BSE and only carbonaceous chondrites. This was not a consideration in Georg et al. (2007a) as the mean values of these different meteorite populations were the same. There are two aspects to consider: firstly which meteorites are most likely to be the building blocks for Earth; and secondly whether the number of samples analysed is sufficient to make a categorical assessment that the meteorite populations are different.

With regards to the refractory lithophile elemental ratios in the Earth (Palme and O'Neill, 2003), carbonaceous chondrites are the best match for the precursor material, which would argue for the use of $\Delta^{30}\text{Si}_{\text{BSE-Carb.chondrite}}$ in calculations. Sr isotopes,

however, rule out CV or CO meteorite as primary building blocks of Earth (Moynier et al., 2010). Measurements of stable Ca isotopes suggest that ordinary chondrites represent the best material from which to build the differentiated bodies (Simon and DePaolo, 2010). Conversely enstatite chondrites are a better match for Earth when it comes to mass independent isotope anomalies (Clayton, 2003b; Regelous et al., 2008; Trinquier et al., 2009).

Fitoussi et al. (2009) used a value of $0.08 \pm 0.04\%$ ($1\sigma_{SD}$) for $\Delta^{30}\text{Si}$ using only carbonaceous chondrite compositions to define the chondritic mean value. Their study, however, is the only one that finds resolvable differences between the $\delta^{30}\text{Si}$ compositions of ordinary and carbonaceous chondrites and is based on only 3 samples of each. As this difference is not observed in this study, $\Delta^{30}\text{Si}_{\text{BSE-meteorite}^*}$ rather than $\Delta^{30}\text{Si}_{\text{BSE-Carb.chondrite}}$ is used. Meteorite* is defined as the average of the $\delta^{30}\text{Si}$ of all the meteorites (including achondrites) except for the enstatite chondrites. All the recent Si isotope studies report significantly lighter values for enstatite chondrites relative to all other meteorites (see section 4.3.1.1), therefore there is a strong argument that they are sampling a different Si isotope reservoir from the other inner solar system objects that have been measured. The achondrites are included as they cannot be resolved as being different from the carbonaceous or ordinary chondrites. The fact that chondrites and differentiated achondrites have similar $\delta^{30}\text{Si}$, different to that found for BSE, points to there being some fractionation event unique to the Earth that did not affect the other differentiated bodies of Mars and Vesta. One possible option for these isotopic effects is partial loss due to evaporation and condensation as the result of the Moon-forming giant impact. However, recent isotopic data for Mg and Li, which have similar volatilities to Si, do not support impact related fractioning losses (Seitz et al., 2007; Teng et al., 2007; Chakrabarti and Jacobsen, 2010a). The Mg isotope studies of Wiechert and Halliday (2007) and Young et al. (2009) report terrestrial mantle derived rocks with a slightly heavier Mg isotopic composition than

4.3. Results and Discussion

Table (4.3): $\delta^{30}\text{Si}$ with BHVO-2 as bracketing standard

		$\delta^{30}\text{Si}_{\text{BHVO2}}$	$2\sigma_{SEM}$	$\delta^{29}\text{Si}_{\text{BHVO2}}$	$2\sigma_{SEM}$	N
Allende VII	CV3	-0.14	0.04	-0.07	0.05	8
Mokoia	CV3	-0.17	0.03	-0.10	0.02	8
St Mark's I	EH5	-0.33	0.03	-0.20	0.03	8

chondrites. However, the effect, if real, is small and other differentiated bodies have a Mg isotopic signature similar to terrestrial rocks, which suggests that it cannot be caused by a process that is responsible for generating the Si isotope difference of the BSE. In addition, the most recent Mg isotope studies imply that the bulk silicate Earth is chondritic in its Mg isotope composition (Teng et al., 2007; Chakrabarti and Jacobsen, 2010a; Bourdon et al., 2010).

Our meteorite mean $\delta^{30}\text{Si}$ of $-0.48 \pm 0.07\text{‰}$ ($1\sigma_{SD}$) compares with the terrestrial mean of $-0.32 \pm 0.04\text{‰}$ ($1\sigma_{SD}$). The terrestrial mean we measure is consistent with the BSE composition ($-0.29 \pm 0.04\text{‰}$ ($1\sigma_{SD}$)) from the extensive study of terrestrial rocks by Savage et al. (2010) measured in the same lab in Oxford. Removing the enstatite chondrites gives a meteorite* mean of $\delta^{30}\text{Si}$ of $-0.47 \pm 0.05\text{‰}$ ($1\sigma_{SD}$). Therefore our $\Delta^{30}\text{Si}_{\text{BSE-meteorite}^*} = 0.15 \pm 0.10\text{‰}$ which is consistent with the Georg et al. (2007a) value for $\Delta^{30}\text{Si}_{\text{BSE-meteorite}^*} = 0.20 \pm 0.11(1\sigma_{SD})$ and also with the value calculated for the compiled published data, $\Delta^{30}\text{Si}_{\text{BSE-meteorite}^*} = 0.15 \pm 0.15 (1\sigma_{SD})$ (This study, Chakrabarti and Jacobsen, 2010b; Georg et al., 2007a; Fitoussi et al., 2009; Ziegler et al., 2010). As another check on the difference between the terrestrial and meteorite data we measured three meteorite samples, Mokoia (CV3), Allende (CV3), St Mark's (EH5) using BHVO-2 as the bracketing standard on the MC-ICPMS (Table 4.3). The $\delta^{30}\text{Si}$ compositions (relative to BHVO-2) supports the robustness of our non-zero $\Delta^{30}\text{Si}_{\text{BSE-meteorite}^*}$.

Another way to evaluate whether the means of two data populations are different is to carry out a student t-test. The parameter, t , for two sample populations is

Table (4.4): Student t-test for BSE versus meteorites

	Calculated t value	P=0.001 (99.9% confidence interval)
This study	t=6.57	$t_{crit} = 5.04$
Chakrabarti and Jacobsen (2010b)	t=1.76	$t_{crit} = 4.22$
Fitoussi et al. (2009)	t=5.42	$t_{crit} = 4.44$
Georg et al. (2007)	t=8.99	$t_{crit} = 3.82$
All data	t=8.05	$t_{crit} = 3.4$

calculated by:

$$t = \frac{\bar{x}_1 - \bar{x}_2}{\sqrt{\frac{s_1^2}{n_1} + \frac{s_2^2}{n_2}}} \quad (4.3)$$

where the subscripts 1 and 2 refer to the two populations (in this case BSE and meteorite*), s is the standard deviation of the population and n is the number of values in the population. The degrees of freedom can be calculated as below:

$$\text{degrees of freedom} = \frac{\left(\frac{s_1^2}{n_1} + \frac{s_2^2}{n_2}\right)^2}{\left[\frac{s_1^2/n_1}{n_1-1}\right] + \left[\frac{s_2^2/n_2}{n_2-1}\right]} \quad (4.4)$$

For a certain number of degrees of freedom there is a t_{crit} for the null hypothesis at certain confidence level. In this case the null hypothesis is that the means of the two populations are the same. If the calculated t value is greater than t_{crit} , for the appropriate degrees of freedom, then the two populations are not the same at the confidence level. Table 4.4 shows the calculations at the 99.9% confidence level. All the datasets bar Chakrabarti and Jacobsen (2010b) are shown to have different means. The student t-test therefore shows that using only $1\sigma_{SD}$ errors to assess the uncertainty on $\Delta^{30}\text{Si}_{\text{BSE-meteorite}^*}$ is valid approach. When the populations become larger e.g. $\Delta^{30}\text{Si}_{\text{BSE-meteorite}^*}$ for the compiled data, the student t-test shows that the means truly are different, which could not be seen just by looking at the standard deviations ($\Delta^{30}\text{Si}_{\text{BSE-meteorite}} = 0.15 \pm 0.15, 1\sigma_{SD}$).

4.3.4 Evidence for silicon in the Earth's core

Both Georg et al. (2007) and Fitoussi et al. (2009) suggest that the most likely cause of a non-zero $\Delta^{30}\text{Si}_{\text{BSE-meteorite}^*}$ is Si entering the metal phase during core formation. There have been a number of experimental studies that show that Si displays siderophile behaviour under certain conditions applicable to terrestrial core formation (Kilburn and Wood, 1997; Gessmann et al., 2001; Takafuji et al., 2005; Wade and Wood, 2005). Depending on the oxygen fugacity, the pressures (2.5 – 97 GPa) and temperatures (2000–3150K) required for Si to enter the metal phase during metal-silicate equilibration are higher than would be expected for Mars (Kong et al., 1999) or would be predicted for Vesta based on its small size. This fits very well with the observation from this, and previous studies (Georg et al., 2007a; Fitoussi et al., 2009; Chakrabarti and Jacobsen, 2010b), that HED and Martian meteorites have similar $\delta^{30}\text{Si}$ values to chondrites.

The percentage of Si in the core can be calculated using the following series of equations. We assume that the $^{30}\text{Si}/^{28}\text{Si}$ fractionation between metal and silicate is the result of isotopic equilibrium, and use a simple mass balance:

$$\delta^{30}\text{Si}_{\text{meteorite}^*} = f\delta^{30}\text{Si}_{\text{BSE}} + (1 - f)\delta^{30}\text{Si}_{\text{core}} \quad (4.5)$$

where f is the fraction of Si in the silicate phase. The fractionation factor ϵ between silicate and metal is $\epsilon_{\text{sil-met}} = 10^3 \ln \alpha_{\text{sil-met}}$. This can be approximated by $\epsilon_{\text{sil-met}} \sim \delta^{30}\text{Si}_{\text{silicate}} - \delta^{30}\text{Si}_{\text{metal}} = \delta^{30}\text{Si}_{\text{BSE}} - \delta^{30}\text{Si}_{\text{core}}$. If ϵ and $\Delta^{30}\text{Si}_{\text{meteorite}^*} = \delta^{30}\text{Si}_{\text{BSE}} - \delta^{30}\text{Si}_{\text{meteorite}^*}$ are substituted into equation 4.5:

$$\Delta^{30}\text{Si}_{\text{BSE-meteorite}^*} = \epsilon(1 - f) \quad (4.6)$$

There is also the mass balance:

$$M_{\text{BE}} C_{\text{BE}}^{\text{Si}} = M_{\text{BSE}} C_{\text{BSE}}^{\text{Si}} + M_{\text{core}} C_{\text{core}}^{\text{Si}} \quad (4.7)$$

where the subscripts BE, BSE and core refer to the bulk Earth, bulk silicate Earth and the Earth's core respectively. M and C^{Si} refer to the mass and concentration of Si in the reservoirs. The fraction of the bulk Earth's Si in the silicate phase (f) is:

$$f = \frac{M_{\text{BSE}} C_{\text{BSE}}^{\text{Si}}}{M_{\text{BE}} C_{\text{BE}}^{\text{Si}}} \quad (4.8)$$

We can combine equations 4.8 and 4.7 by getting rid of the bulk Earth terms. Substituting in c for $C_{\text{BSE}}^{\text{Si}}$ and replacing $C_{\text{core}}^{\text{Si}}$ by $X/100$ gives the core's weight percentage of Si (X):

$$X = 100 \left(\frac{M_{\text{BSE}}}{M_{\text{core}}} \right) \left[\frac{c}{f} - c \right] \quad (4.9)$$

with c being the measured Si fraction in BSE with a value of 0.212 (Palme and O'Neill, 2003). Combining equations 4.6 and 4.9:

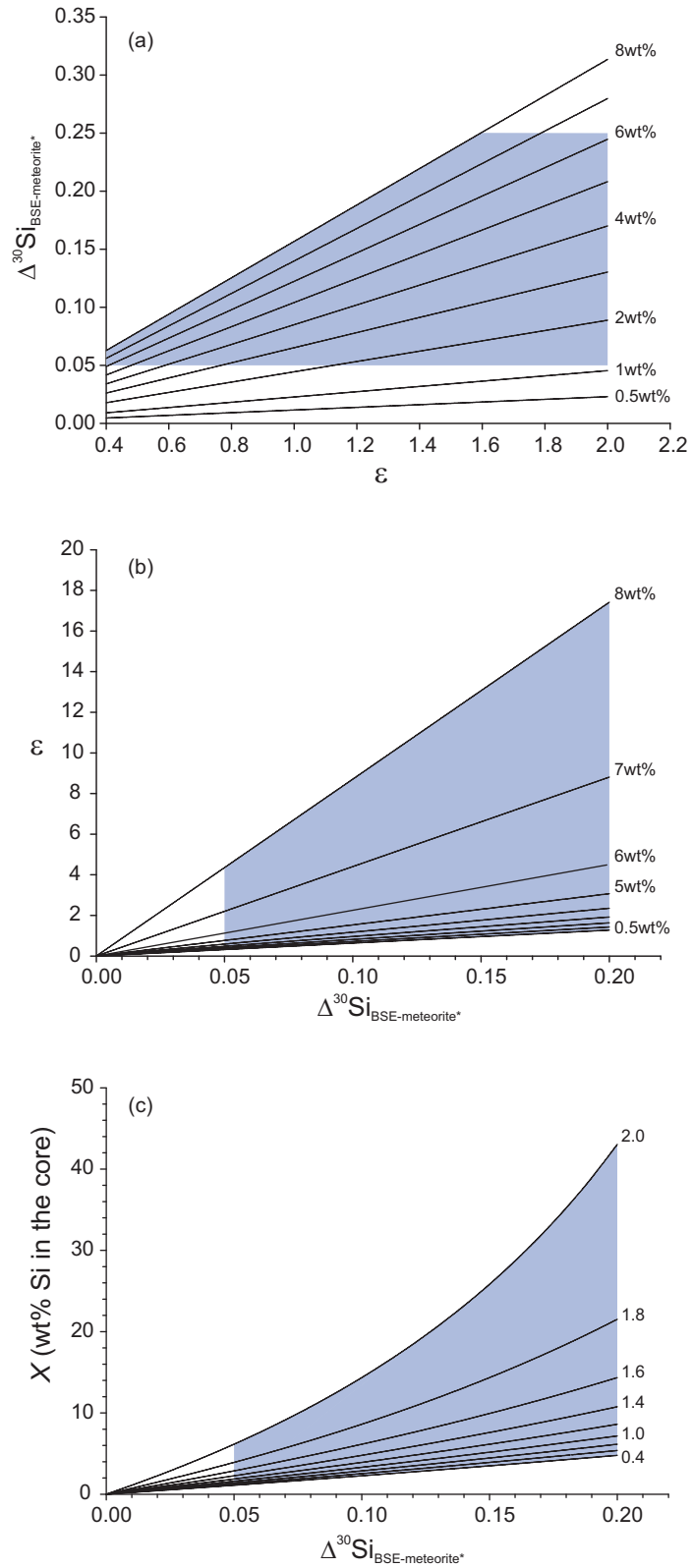
$$X = 100 \left(\frac{M_{\text{BSE}}}{M_{\text{core}}} \right) \left[\frac{c}{1 - \frac{\Delta^{30}\text{Si}_{\text{BSE-meteorite}^*}}{\epsilon}} - c \right] \quad (4.10)$$

The three variables in equation 4.10, X , ϵ and $\Delta^{30}\text{Si}_{\text{BSE-meteorite}^*}$, are all independently constrained by different methods. The range of X can be found either through partitioning experiments, or constraints from chondrite models of bulk Earth chemistry. ϵ can be arrived at either through first principles lattice dynamical models or can be experimentally determined, while $\Delta^{30}\text{Si}_{\text{BSE-meteorite}^*}$ is found by measuring the $\delta^{30}\text{Si}$ of appropriate samples. The series of plots in Figure 4.8 shows the possible range (on the y-axis) of one of the variables in equation (4.10) when plausible ranges for the other two variables are used.

It is interesting to note that in Figure 4.8a, the calculated range for $\Delta^{30}\text{Si}_{\text{BSE-meteorite}^*}$

4.3. Results and Discussion

Figure (4.8): The y-axes are always the dependent variables, whereas the x-axes are the dependent variables. (a) Calculated $\Delta^{30}\text{Si}_{\text{BSE-meteorite}^*}$ using equation (4.10) and a range for ϵ from 0.4 to 2.0 (Schauble et al., 2007; Shahar et al., 2009). The plot is contoured in wt% Si in the core from 0.5 – 8wt% (Kilburn and Wood, 1997; Gessmann et al., 2001) (0.5 was chosen rather than 0 for the lower limit so as to avoid undefined answers). The grey shaded area corresponds to the measured $\Delta^{30}\text{Si}_{\text{BSE-meteorite}^*}$ value from this study with uncertainties at the $1\sigma_{SD}$ level. (b) Calculated ϵ with $\Delta^{30}\text{Si}_{\text{BSE-meteorite}^*}$ from 0.00 – 0.20‰ (This study, Georg et al., 2007a; Chakrabarti and Jacobsen, 2010b; Fitoussi et al., 2009). The contours are as in (a). The shaded area should extend beyond the plot to $\Delta^{30}\text{Si}_{\text{BSE-meteorite}^*} = 0.25\text{‰}$. (c) Calculated wt%Si in the core with $\Delta^{30}\text{Si}_{\text{BSE-meteorite}^*}$ from 0.00 - 0.20‰ and contours of ϵ from 0.4-2.0



is not that dissimilar from what has been measured across the different laboratory groups. It is clear, however that the constraints that $\Delta^{30}\text{Si}_{\text{BSE-meteorite}^*}$ can put on either the wt% of Si in the core, or the metal-silicate fractionation factor, ϵ , are limited (Figure 4.8b & c), as the shaded areas are much larger than physical plausibility. ϵ is a parameter of interest as it can help constraint the conditions of core formation.

It has known for some time that the fractionation factor for isotope exchange reactions is related to temperature by an A/T^2 (Bigeleisen and Mayer, 1947). Ziegler et al. (2010) found the temperature dependence (in Kelvin) for the $^{30}\text{Si}/^{28}\text{Si}$ fractionation factor of

$$\epsilon = \frac{8.04 \pm 0.47 \times 10^6}{T^2} \quad (4.11)$$

when anchored to the experimental data of Shahar et al. (2009). Taking $\Delta^{30}\text{Si}_{\text{BSE-meteorite}^*} = 0.15$ from this study and using 8wt% Si in the core is taken as a working maximum for X (e.g. Gessmann et al., 2001), equation (4.10) gives us a minimum value for ϵ of 0.957. From equation 4.11, the maximum temperature of core formation is therefore $2898\text{K}^{+83.5}_{-86.0}$, which is in the range of the expected temperature (e.g. Gessmann and Rubie, 2000; Wade and Wood, 2005) for metal-silicate equilibration in the terrestrial magma ocean. However, these errors on the temperature do not include the uncertainties on $\Delta^{30}\text{Si}_{\text{BSE-meteorite}^*}$. If these are included (e.g. Figure 4.9), the new temperature estimate becomes $2898\text{K}^{+2122}_{-653}$. Therefore, at current levels of precision, Si isotope data cannot be used to put significant constraints on the temperature of core formation.

From partitioning studies (e.g. Wade and Wood, 2005) it is known that a good assumption is to fix the maximum temperature of core formation to lie on the peridotite liquidus. At core formation pressures of 40GPa this would be $\sim 3000\text{K}$. Using equation (4.11), this gives $\epsilon = 0.89$, and this can be used along with the measured $\Delta^{30}\text{Si}_{\text{BSE-meteorite}^*}$ to constrain the amount of Si in the core rather than using the isotope data to constrain the temperature of core formation.

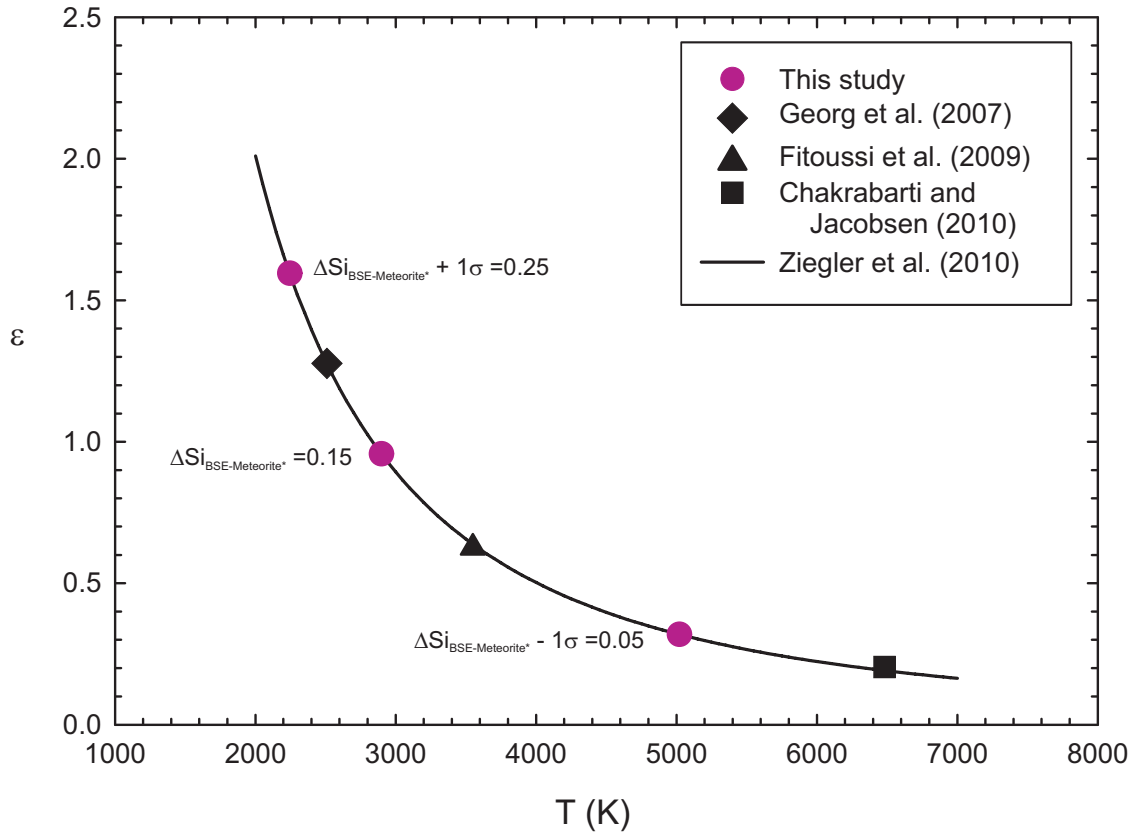


Figure (4.9): The fractionation factor ϵ plotted against temperature. The solid line is equation 4.11 (Ziegler et al., 2010), which is also the equation used to calculate the rest of the symbols on the plot. The purple circles correspond to ϵ values calculated from equation (4.10) for $\Delta^{30}\text{Si}_{\text{BSE-meteorite}^*} = 0.05, 0.15, 0.25$ (from this study $\pm 1\sigma_{SD}$) assuming 8wt% Si in the core. The black symbols are the ϵ values calculated in the same way from the mean values of $\Delta^{30}\text{Si}_{\text{BSE-meteorite}^*}$ from previously published studies. The errors on T from 4.11 are on the order of the symbol size.

Table (4.5): Calculations of Si (wt%) in the Earth's core assuming $\epsilon = 0.89$ (see text for details)

	$\Delta^{30}\text{Si}_{\text{BSE-Meteorite}^*}$	Si in core (wt%)	$\Delta^{30}\text{Si}_{\text{BSE-Carb. chondrite}}$	Si in core (wt%)	$\Delta^{30}\text{Si}_{\text{BSE-En. chondrite}}$	Si in core (wt%)
This study	0.15 ± 0.10	$8.7^{+8.1}_{-6.2}$	0.17 ± 0.10	$9.4^{+8.3}_{-6.3}$	0.31 ± 0.12	$23.0^{+17.2}_{-11.3}$
Chakrabarti and Jacobsen (2010)	0.03 ± 0.07	$1.5^{+3.9}_{-3.4}$	0.00 ± 0.04	$0.0^{+2.1}_{-1.9}$	$0.18 \pm 0.08^{\text{a}}$	$10.9^{+6.9}_{-5.5}$
Ziegler et al. (2010)			0.45 ± 0.10	$11.0^{+25.6}_{-16.1}$		
Fitoussi et al., (2009) ^b	0.10 ± 0.07	$5.4^{+4.7}_{-3.9}$	0.07 ± 0.04	$3.7^{+2.4}_{-2.2}$	$0.26 \pm 0.07^{\text{a}}$	$17.8^{+7.6}_{-6.1}$
Georg et al., (2007)	0.20 ± 0.11	$12.5^{+10.5}_{-7.6}$	0.20 ± 0.11	$12.5^{+10.5}_{-7.6}$	$0.31 \pm 0.09^{\text{a}}$	$23.0^{+12.1}_{-8.9}$
All data	0.15 ± 0.15	$8.7^{+13.2}_{-8.7}$	0.14 ± 0.15	$8.0^{+12.8}_{-8.5}$	0.25 ± 0.12	$16.8^{+13.8}_{-9.5}$

^a As only one enstatite chondrite was measured in this study the error on the enstatite chondrite reservoir comes from the $2\sigma_{SEM}$ for the meteorite rather than $1\sigma_{SD}$ of the enstatite chondrite population.

^b Including BHVO-2 in BSE estimates

4.3. Results and Discussion

Table 4.5 shows the calculated range of wt% Si in the core based on the range of published $\Delta^{30}\text{Si}_{\text{BSE-meteorite}^*}$, $\Delta^{30}\text{Si}_{\text{BSE-Carb. chondrite}}$, $\Delta^{30}\text{Si}_{\text{BSE-En. chondrite}}$ values. It is clear that there is considerable uncertainty for the amount of Si in the core resulting from errors in $\Delta^{30}\text{Si}_{\text{BSE-meteorite}^*}$. Based on the range of published values the core could contain anywhere from 0 to 44wt%, though the higher values are implausible based on chemical and physical constraints.

The $\Delta^{30}\text{Si}_{\text{BSE-En. chondrite}}$ values give a relatively high average of $16.8_{-9.5}^{+13.8}$ wt% Si in the core. This is in a similar range to the result of major element calculations that use enstatite chondrites as the precursor to bulk Earth. If a simple mass balance calculation is carried out using a Si concentration in bulk enstatite chondrites of 0.206 (Javoy et al., 2010, and references therein) and a Si fraction of 0.212 in BSE (Palme and O'Neill, 2003), this gives ~ 19 wt% of Si in the core.

The mean measured offset of $\Delta^{30}\text{Si}_{\text{BSE-meteorite}^*} = 0.15\text{‰}$ from this study gives the amount of Si in the core as $8.7_{-6.2}^{+8.1}$ wt% (Table 4.5). The “correct” value for $\Delta^{30}\text{Si}_{\text{BSE-meteorite}^*}$ and hence putting tight limits on the amount of Si in the core is still an open question. Silicon isotopes show that it is likely that there may be a significant amount of Si in the core but the current inter-lab reproducibility limits any further constraints.

Chapter 5

Silicon isotopes in lunar rocks: implications for the Moon's formation and the early history of the Earth¹

5.1 Introduction

The Moon is generally thought to be the result of a large body striking the proto-Earth with a glancing blow, spinning off material that re-accreted to form the Moon (e.g. Hartmann and Davis, 1975). Smoothed particle hydrodynamic (SPH) models of Cameron (2000) and Canup and Asphaug (2001), indicate that such a blow from a Mars-sized body is sufficient to explain the high angular momentum of the Earth-Moon system and the Moon's Fe deficiency. Another constraint on any Moon-forming model is that lunar rocks have $\Delta^{17}\text{O}$ compositions that are indistinguishable from the terrestrial fractionation line (Wiechert et al., 2001; Spicuzza et al., 2007). $\Delta^{17}\text{O}$ variations in extra-terrestrial material are thought to be linked to their accretion source regions in the early solar nebula, and are used to distinguish different parent bodies (e.g. Clayton, 2003b). The SPH models indicate that the Moon is mostly derived from material from the impactor; however the likelihood of such a large late

¹Currently in review in *Geochimica et Cosmochimica Acta* as "Silicon isotopes in lunar rocks: implications for the Moon's formation and the early history of the Earth" R. M. G. Armytage, R. B. Georg, H. M. Williams, A. N. Halliday

impactor having the same $\Delta^{17}\text{O}$ as the proto-Earth is very low. Hence, Pahlevan and Stevenson (2007) proposed a model that explains the similarity of the O isotopic composition of the Earth and Moon by homogenisation across a vapour cloud in the aftermath of the Giant Impact. The liquid-vapour exchange processes in such a vapour cloud and the subsequent partial separation of reservoirs could potentially lead to chemical variations and mass-dependent isotopic differences between the Earth and Moon. Pahlevan et al. (2011) modelled such a scenario looking at the evolution of lunar FeO/MgO via rainout from a partially vaporised magma ocean, which gives rise to a predicted offset ($\sim 0.14\%$) between the bulk Moon and bulk silicate Earth (BSE) in silicon (Si) isotope composition.

The Si isotopic composition of meteorites has been the focus of a number of high-precision studies in recent years (Georg et al., 2007a; Fitoussi et al., 2009; Chakrabarti and Jacobsen, 2010b; Ziegler et al., 2010; Armytage et al., 2011). All but one study (Chakrabarti and Jacobsen, 2010b) find that Si in the terrestrial mantle is isotopically heavier than chondrites and differentiated achondrites, making the BSE Si isotopic composition unique in comparison to undifferentiated chondritic bodies as well as to Mars and Vesta. The range of average $\delta^{30}\text{Si}$ compositions from the studies are: BSE -0.38 to -0.29% (Georg et al., 2007a; Fitoussi et al., 2009; Chakrabarti and Jacobsen, 2010b; Armytage et al., 2011); chondrites -0.58 to -0.41% (Georg et al., 2007a; Fitoussi et al., 2009; Chakrabarti and Jacobsen, 2010b; Armytage et al., 2011); Mars -0.48 to -0.59% (Georg et al., 2007a; Armytage et al., 2011); Vesta -0.56 to -0.38% (Georg et al., 2007a; Fitoussi et al., 2009; Chakrabarti and Jacobsen, 2010b; Armytage et al., 2011). The offset between meteorites and BSE also varies between the studies from ~ 0 (Chakrabarti and Jacobsen, 2010b) to 0.2% (Georg et al., 2007a). The best explanation for the data is isotopic fractionation when Si entered the Earth's core during metallic liquid-silicate liquid partitioning at high temperatures and pressures (Gessmann et al., 2001).

The only published high precision lunar Si isotope data to date are from lunar basalts and one lunar breccia. Georg et al. (2007a) analysed four basalt samples with an average $\delta^{30}\text{Si} = -0.31 \pm 0.07\text{‰}$ ($2\sigma_{SD}$) and Fitoussi et al. (2010) measured an average lunar basalt composition of $\delta^{30}\text{Si} = -0.30 \pm 0.05\text{‰}$ ($2\sigma_{SD}$). The current best estimate for the Si isotopic composition of BSE is $-0.29 \pm 0.08\text{‰}$, $\pm 2\sigma_{SD}$ (Savage et al., 2010); therefore the data of Georg et al. (2007a) and Fitoussi et al. (2010) provide provisional evidence that the Moon, unlike any other measured inner solar system body, has a Si isotope composition similar to BSE. Chakrabarti and Jacobsen (2010b) found a much lighter composition for the lunar breccia 14304 of $\delta^{30}\text{Si} = -0.45 \pm 0.05\text{‰}$ ($2\sigma_{SEM}$), but their average BSE composition was also much lighter ($-0.38 \pm 0.06\text{‰}$, $2\sigma_{SD}$), so is therefore consistent with the previous conclusion. This implies that Si isotopes, like O isotopes, were possibly equilibrated in the aftermath of the Giant Impact, and did not experienced any subsequent fractionation due to processes in the proto-lunar disk. This latter point, however, conflicts with the prediction of Pahlevan et al. (2011). It needs to be assessed how representative lunar basalts are of the bulk Moon Si isotope composition, and whether it matches BSE. The information from lunar samples brought back by the Apollo and Luna missions, augmented by a wealth of remote sensing data, points to something beyond a simple globally stratified lunar crust and interior (e.g. Jolliff et al., 2000). Epstein and Taylor analysed the Si composition of a number of lunar samples (including both basalts and anorthosites) in a series of studies in the 1970s (Epstein and Taylor Jr., 1970a,b; Taylor Jr. and Epstein, 1970; Epstein and Taylor Jr., 1971, 1972; Taylor Jr. and Epstein, 1973a,b) and found a range for whole rock samples of $\delta^{30}\text{Si} = -0.49\text{‰}$ to $+0.30\text{‰}$. They did not find any consistent offsets linked to different rock types. However, their precision, approximately a factor of two larger than current external precision ($\sim \pm 0.16\text{‰}$: e.g. Fitoussi et al., 2009; Savage et al., 2010; Ziegler et al., 2010; Armytage et al., 2011) does not allow for small differences to be confidently resolved.

The aim of this study is to place better constraints on the Si composition of the lunar mantle. In particular it is necessary to understand whether the narrower range of lunar Si isotope composition measured by Georg et al. (2007a) and Fitoussi et al. (2010) in comparison to Epstein and Taylor (Epstein and Taylor Jr., 1970a,b; Taylor Jr. and Epstein, 1970; Epstein and Taylor Jr., 1971, 1972; Taylor Jr. and Epstein, 1973a,b), is purely the result of technological improvements or is partly a function of sample population size. A well-characterised lunar mantle with regards to Si isotopes could help to further constrain lunar formation and the conditions of terrestrial core formation.

5.2 Method

5.2.1 Samples

The lunar samples were chosen to represent all the Apollo landing sites and a range of rock types from high-Ti basalts, anorthosites, olivine-normative basalts, through to lunar picritic glasses. The four basalts analysed by Georg et al. (2007a) (15555, 70035, 75075 and 77516) and one of the whole rock lunar samples from Epstein and Taylor's dataset (60025 Taylor Jr. and Epstein, 1973b) were also analysed in this sample set. Millimetre-scale whole glass spherules were handpicked from the 74220 soil that had been previously processed (sieved and washed) by Lee et al. (1997) and also from the powdered "green glass clods" 15425 and 15426.

5.2.2 Analytical methods

The method used to determine the Si isotopic composition of the samples has been used previously to analyse meteoritic samples (Armytage et al., 2011) and is based on Georg et al. (2006a). For the bulk lunar samples (15058, 15118, 15668, 65035, 60015) that had not already been powdered in previous studies (e.g. Lee et al., 1997;

Wiechert et al., 2001; Schönbacher et al., 2005a) at least ~ 60 mg of sample material was crushed in an alumina mortar. Alumina was used as a cleaning abrasive in between samples. 5-10mg of the homogenised sample material was subsequently fused with ~ 200 mg solid NaOH in a silver crucible at 720°C for 10min in a furnace. The resulting fusion cake was stored in 20ml of deionised water (18.2m , MQ-e, Milli Pore) in a Teflon beaker overnight, before being transferred into a weak (~ 0.2 M) HCl solution. The acid to flux ratio was 3.5ml of 10 N HCl to ~ 200 mg NaOH. The final solutions (60ml to 500ml) were stored in pre-cleaned PP bottles with Si concentrations typically between 2.5 and 15ppm. The ion-chromatography to separate Si from the other cations used BioRad polyprep columns (Hercules, CA, USA) filled with 1.8ml strong acidic cation exchange DOWEX 50W-X12 (200-400 mesh) resin in the H^+ form (Georg et al., 2006a). The resin was pre-cleaned through several rinses of MQ-e, HNO_3 (3 M, 6 M) and HCl (10 M) to ensure the complete removal of matrix elements and the efficiency of the exchange process. The Si concentrations were measured as coloured Mo-Si complexes using a DR 2800 (Hach Lange) photospectrometer after fusion and prior to loading the solutions on the columns. Recovery from both the fusion and ion-chromatography stage, was $>97 \pm 2\%$. The solid Si isotope standards NBS-28 and Diatomite, and the rock standard BHVO-2 were processed in exactly the same manner as the lunar samples. The total procedural blank, including both the powdering and the instrument blanks, at Oxford is 13ng where typical analytical amounts are $4.5\mu\text{g}$, giving a sample to blank ratio of ~ 350 .

The solutions were analysed on a Nu Plasma (Nu Instruments, Wrexham, UK) multi-collector inductively-coupled-plasma mass spectrometer (MC-ICPMS) at the Department of Earth Sciences, University of Oxford. The instrument was operated in medium resolution mode, which allows for all three Si masses to be resolved from interferences (e.g. $^{12}\text{C}^{16}\text{O}^+$, $^{14}\text{N}^{2+}$, $^{28}\text{Si}^1\text{H}^+$, $^{14}\text{N}^{16}\text{O}^+$) on the low mass side of the peak plateau. The resolving power ($R = m/\Delta m$) is ~ 4000 , where Δm is between

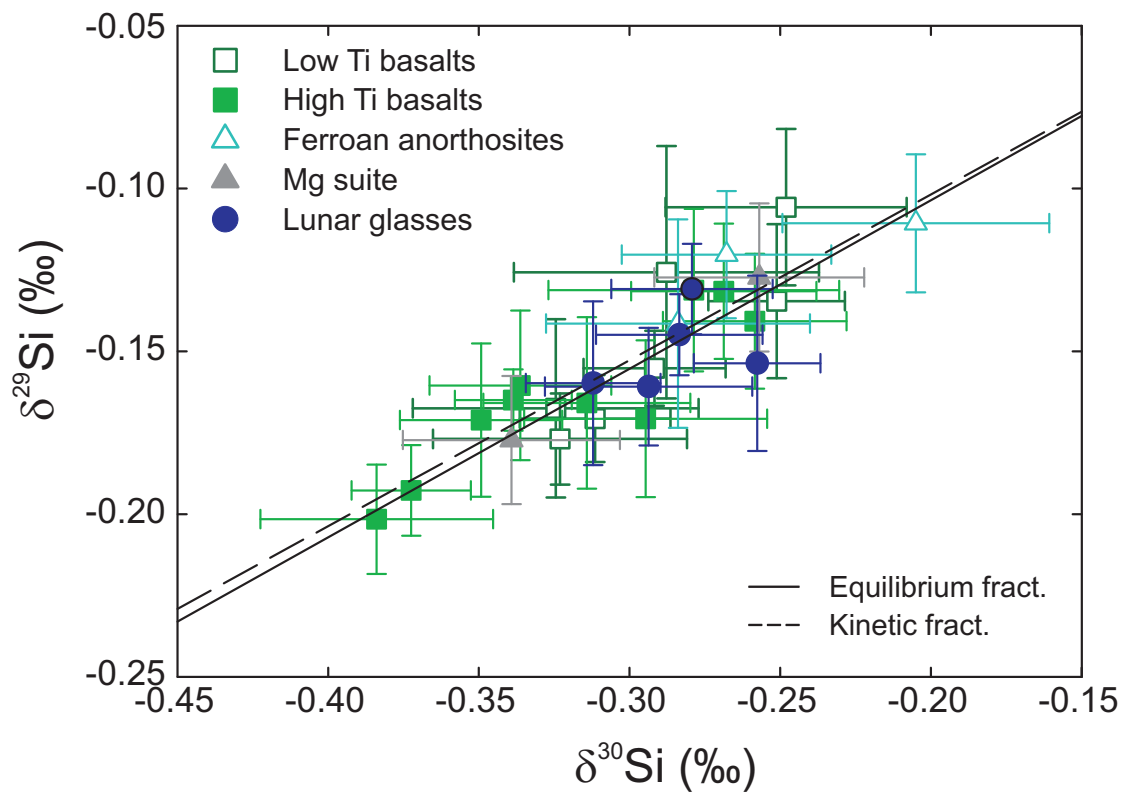


Figure (5.1): $\delta^{30}\text{Si}$ versus $\delta^{29}\text{Si}$ plot. The error bars represent $\pm 2\sigma_{SEM}$ for the samples. The calculated slopes for mass dependent equilibrium fractionation (0.5178) and mass dependent kinetic fractionation (0.5092) are also plotted.

5% and 95% peak height and m is the mean of these two masses. A self aspirating concentric microflow PFA nebulizer (Elemental Scientific Inc.) with an uptake rate of $\sim 75 \text{ l min}^{-1}$ was used to aspirate the samples into an Aridus II (CETAC, Omaha, NE, USA) desolvator. The typical sensitivity was $\sim 10\text{V}$ total per ppm on Faraday collectors with $10^{11}\Omega$ resistors. To correct for instrumental mass drift, sample-standard bracketing was used with the international Si standard NBS-28 as the bracketing standard. Each measurement represents 20 cycles with an integration time of 10 s for each cycle. The in run instrumental precision on the $^{30}\text{Si}/^{28}\text{Si}$ and $^{29}\text{Si}/^{28}\text{Si}$ ratios is typically $\pm 9 \times 10^{-7}$ (σ_{SEM}). The accuracy of the measurements in each run was checked using various calibrated standards such as Diatomite and BHVO-2. Samples were repeated in different sessions, and the reported data represent average $\delta^x\text{Si}$ values of multiple runs. Each N in Table 1 represents one sample run and two bracketed standard runs. Silicon isotope variations are reported as the deviations $^{30}\text{Si}/^{28}\text{Si}$ and $^{29}\text{Si}/^{28}\text{Si}$ from the international standard NBS-28 in parts per thousand using:

$$\delta^x\text{Si} = \left[\frac{(^x\text{Si}/^{28}\text{Si})_{\text{sample}}}{(^x\text{Si}/^{28}\text{Si})_{\text{NBS-28}}} - 1 \right] \times 1000 \quad (5.1)$$

where $^x\text{Si}/^{28}\text{Si}_{\text{sample}}$ is the ratio of $^{29,30}\text{Si}$ to ^{28}Si in the sample of interest and $^x\text{Si}/^{28}\text{Si}_{\text{NBS-28}}$ is the corresponding ratio in the standard reference material. The Si isotopic composition of Diatomite standard for the 12 month period when the samples were analysed was $\delta^{30}\text{Si} = 1.23 \pm 0.14\text{‰}$ and $\delta^{29}\text{Si} = 0.63 \pm 0.09\text{‰}$ ($\pm 2\sigma_{SD}$, N= 250). These values are consistent with the calibrated value from Reynolds et al. (2006) as shown in Table 5.1. Similarly the long term average for the rock standard BHVO-2 $\delta^{30}\text{Si} = -0.28 \pm 0.14\text{‰}$ and $\delta^{29}\text{Si} = -0.15 \pm 0.08\text{‰}$ ($\pm 2\sigma_{SD}$, N= 210) is in agreement with the previously published values (Abraham et al., 2008; Savage et al., 2010; Zambardi and Poitrasson, 2010) (Table 5.1). All fractionations measured were mass dependent, indeed mass dependence was used as a data quality check to ensure complete reso-

lution of the Si mass spectrum from polyatomic interfering species. Mass dependent mass bias was checked by constructing a three isotope plot of all the data (Figure 5.1), which was regressed to give a slope of 0.520 ± 0.015 . This is within error of the calculated equilibrium (0.5178) and kinetic (0.5092) fractionation slopes.

5.3 Results

The Si isotopic data for the 20 bulk lunar rocks and 4 lunar glasses are given in Table 5.1 and Figure 2. The average of all the bulk lunar samples is $\delta^{30}\text{Si} = -0.29 \pm 0.08\text{‰}$ ($2\sigma_{SD}$), which is identical to the recent value of Savage et al. (2010) for bulk silicate Earth of $\delta^{30}\text{Si} = -0.29 \pm 0.08\text{‰}$ ($2\sigma_{SD}$). The average of the four lunar basalts ($\delta^{30}\text{Si} = -0.31 \pm 0.07\text{‰}$, $2\sigma_{SD}$) from Georg et al.'s (2007a), and Fitoussi et al.'s (2010) mean lunar composition ($\delta^{30}\text{Si} = -0.30 \pm 0.05\text{‰}$, $2\sigma_{SD}$) are consistent with the narrow observed range of Si isotope compositions across the variety of samples observed in this study (Figure 3). The lunar lithologies analysed in this study are identical within error ($\pm 2\sigma_{SD}$): $\delta^{30}\text{Si}_{\text{Low-Ti basalt}} = -0.29 \pm 0.06\text{‰}$; $\delta^{30}\text{Si}_{\text{High-Ti basalt}} = -0.32 \pm 0.09\text{‰}$; $\delta^{30}\text{Si}_{\text{Lunar glass}} = -0.29 \pm 0.05\text{‰}$; $\delta^{30}\text{Si}_{\text{Highland Rocks}} = -0.27 \pm 0.10\text{‰}$. The similarity of the whole rock data from across the landing sites and lithologies is consistent with the initial conclusion from the Si isotopic work done on the Apollo samples (e.g. Taylor Jr. and Epstein, 1973a).

Table (5.1): Silicon isotope data of standards, meteorites and terrestrial samples

Standards	$\delta^{30}\text{Si}$	$2\sigma_{SD}$	$\delta^{29}\text{Si}$	$2\sigma_{SD}$	n ^a	N ^b	SiO ₂
	(‰)	(‰)	(‰)	(‰)			(wt%)
Diatomite	1.23	0.14	0.63	0.09	33	250	99.3
<i>Diatomite^c</i>	<i>1.26</i>	<i>0.20</i>	<i>0.64</i>	<i>0.14</i>	<i>100</i>		
BHVO-2	-0.28	0.14	-0.15	0.08	26	210	49.3
<i>BHVO-2^d</i>	<i>-0.28</i>	<i>0.27</i>	<i>-0.17</i>	<i>0.11</i>		<i>6</i>	
<i>BHVO-2^e</i>	<i>-0.27</i>	<i>0.10</i>	<i>-0.14</i>	<i>0.05</i>		<i>59</i>	

Continued on Next Page...

Table 5.1 – Continued

Samples	$\delta^{30}\text{Si}$	$2\sigma_{SEM}$ (‰)	$\delta^{29}\text{Si}$	$2\sigma_{SEM}$ (‰)	n ^a	N ^b	SiO ₂ (wt%)
<i>BHVO-2^f</i>	<i>-0.27</i>	<i>0.08</i>	<i>-0.14</i>	<i>0.05</i>		<i>42</i>	
12011 Pigeonite basalt	-0.29	0.05	-0.13	0.04	1	9	48.5
14053 Aluminous basalt	-0.25	0.04	-0.11	0.02	2	18	48.9
15058 Quartz normative basalt	-0.31	0.02	-0.17	0.01	3	25	47.7
15118 Quartz normative basalt	-0.29	0.02	-0.16	0.05	3	19	49.4
15555 Olivine normative basalt	-0.32	0.05	-0.17	0.03	3	25	45.7
15555 (II) ^h	-0.32	0.04	-0.18	0.03	1	5	45.7
15668 Olivine normative basalt	-0.25	0.02	-0.13	0.02	2	16	47.2
<i>Low-Ti basalt mean ($\pm 2\sigma_{SD}$)ⁱ</i>	<i>-0.29</i>	<i>0.06</i>	<i>-0.14</i>	<i>0.05</i>		<i>6</i>	
10049 High-Ti basalt	-0.27	0.03	-0.13	0.02	1	11	45.4
70035 High-Ti basalt	-0.39	0.02	-0.20	0.01	3	24	36.7
70035 (II)	-0.34	0.03	-0.16	0.02	1	9	36.7
70135 High-Ti basalt	-0.35	0.03	-0.17	0.02	1	11	36.8
71047 High-Ti basalt	-0.31	0.03	-0.17	0.03	1	11	40.7
71539 High-Ti basalt	-0.38	0.04	-0.20	0.02	2	17	37.0
71566 High-Ti basalt	-0.28	0.05	-0.13	0.02	2	19	48.5
74255 High-Ti basalt	-0.33	0.02	-0.16	0.01	2	18	41.0
75075 High-Ti basalt	-0.26	0.03	-0.14	0.02	1	11	40.3
77516 High-Ti basalt	-0.29	0.04	-0.17	0.02	1	9	40.7
<i>High-Ti basalt mean ($\pm 2\sigma_{SD}$)ⁱ</i>	<i>-0.32</i>	<i>0.09</i>	<i>-0.16</i>	<i>0.05</i>		<i>8</i>	
60015 Ferroan-anorthosite	-0.27	0.03	-0.12	0.02	3	22	45.0
60025 Ferroan-anorthosite	-0.20	0.04	-0.11	0.02	2	18	44.8
65035 Ferroan-anorthosite	-0.28	0.04	-0.14	0.02	1	11	45.6
67955 Norite (Mg-granulite)	-0.34	0.04	-0.18	0.02	1	11	46.4
77215 Norite	-0.26	0.03	-0.13	0.02	1	11	57.1
<i>Highland suite mean ($\pm 2\sigma_{SD}$)ⁱ</i>	<i>-0.27</i>	<i>0.10</i>	<i>-0.14</i>	<i>0.05</i>		<i>5</i>	
15425 Green glass	-0.31	0.02	-0.16	0.03	1	11	43.1
15426 Green glass	-0.29	0.03	-0.16	0.02	2	19	43.2
15426 Brown glass	-0.26	0.02	-0.15	0.03	1	9	39.9
74220 Orange glass (picked)	-0.28	0.03	-0.14	0.01	2	16	38.9

Continued on Next Page...

5.3. Results

Table 5.1 – Continued

Samples		$\delta^{30}\text{Si}$	$2\sigma_{SEM}$ (‰)	$\delta^{29}\text{Si}$	$2\sigma_{SEM}$ (‰)	n ^a	N ^b	SiO ₂ (wt%)
74220	Orange glass (bulk fraction)	-0.28	0.03	-0.13	0.01	1	9	39.5
	<i>Glass mean</i> ($\pm 2\sigma_{SD}$) ⁱ	-0.29	0.05	-0.14	0.02		4	
	Lunar mean ($2\sigma_{SD}$) ⁱ	-0.29	0.05	-0.15	0.05		24	
	BSE mean ^j	-0.29	0.08	-0.15	0.05		35	
	Meteorite mean ^k	-0.48	0.13	-0.25	0.07		38	

^a Number of measurement sessions, which necessarily means column chemistry repeats

^b Number of measurements of $\delta^{30,29}\text{Si}$ in total

^c Value from inter-laboratory comparison study (Reynolds et al., 2006)

^d Data for BHVO-2 mean from Abraham et al. (2008)

^e Data for BHVO-2 mean from Savage et al. (2010)

^f Data for BHVO-2 mean from Zambardi and Poitrasson (2010)

^g The subscript SEM refers to the standard error of the mean, which is calculated from $\sigma_{SD}/N^{1/2}$

^h II designates separates fusion i.e. an individually prepared aliquot of basalt powder

ⁱ When there are duplicate fusions the average of their values is used when calculating the mean.

^j Bulk silicate Earth average from Savage et al. (2010)

^k From Chapter 4

To confirm the similarity of the terrestrial and lunar data, five of the lunar samples (basalts and a glass) were analysed using the USGS basalt BHVO-2 as the bracketing standard (Table 5.2). These took place over five different analytical sessions. The average $\Delta^{30}\text{Si}_{\text{BHVO2-Lunar}}$ measured this way was $0.01 \pm 0.08\text{‰}$ ($\pm 2\sigma_{SD}$), which adds support to the similarity of the Si compositions of the Moon and the BSE.

Georg et al. (2007a) reported Si isotope data for lunar basalts that were within error identical to BSE, later corroborated by Fitoussi et al. (2010) and now by our more detailed study. It is interesting to note that the lunar data of Georg et al. (2007a), Fitoussi et al. (2010) and this study are identical, when the corresponding meteorite and terrestrial data do not always agree (Georg et al., 2007a; Fitoussi et al., 2009; Armytage et al., 2011). The key issue is why the Georg et al. (2007a) lunar data can be replicated when their meteorite and terrestrial data have not been. There is no clear reason why this should be the case, as it is more likely that there would

be homogeneity issues for lunar rocks in comparison to terrestrial samples, due to constraints on sample size. On closer examination, the differences between these different lab groups in terms of their terrestrial data is not that significant as the Georg et al. (2007a) $\delta^{30}\text{Si}_{\text{BSE}} = 0.38 \pm 0.06\text{‰}$ is within one standard deviation of $0.32 \pm 0.05\text{‰}$ (Armytage et al., 2011) and almost within one standard deviation of other studies: $0.28 \pm 0.03\text{‰}$ (Fitoussi et al., 2009), $0.29 \pm 0.04\text{‰}$ (Savage et al., 2010). The light Si compositions of meteorites from Georg et al. (2007a) ($\delta^{30}\text{Si}_{\text{meteorite}} = -0.58 \pm 0.05\text{‰}, \pm 1\sigma_{SD}$) have only been replicated by Ziegler et al. (2010) (Murchison, CM2 chondrite, $\delta^{30}\text{Si} = -0.73 \pm 0.04\text{‰}, \pm 1\sigma_{SEM}$), indicating that it is the difference in the meteorite data that is more of an issue rather than the similarities in the lunar samples. However, Georg et al.’s (2007a) conclusion of a clearly resolvable isotopic offset between BSE and meteorites is replicated in magnitude and direction by later studies (Fitoussi et al., 2009; Ziegler et al., 2010; Armytage et al., 2011). Armytage et al. (2011) investigated the reason for the differences between the Georg et al. (2007a) and (Fitoussi et al., 2009) meteorite data and was able to rule out several putative explanations but unable to establish a cause. The only recent study that does not find a difference between meteorites and BSE is Chakrabarti and Jacobsen (2010b). Their study, reproduces the heavier meteorite data of Fitoussi et al. (2009) and Armytage et al. (2011), but gives an estimate for BSE that is significantly lighter than the estimate for BSE from a more detailed study by Savage et al. (2010). In addition, the Si isotope composition of their lunar sample is much lighter than any of the compositions measured by Georg et al. (2007a), Fitoussi et al. (2010) or this study (Figure 5.3). The reason for the discrepancy of the data from Chakrabarti and Jacobsen (2010b), in particular BSE and the USGS rock standard, could be due to the chosen analytical approach. Unlike Georg et al. (2007a); Fitoussi et al. (2009); Savage et al. (2010); Armytage et al. (2011), Chakrabati and Jacobsen use a NaOH dissolution technique in sealed Teflon at $\sim 200^\circ\text{C}$ (van den Boorn et al., 2006) rather

5.4. Discussion

than a crucible NaOH fusion at $\sim 720^\circ\text{C}$. Van den Boorn et al. (2009) later found that the dissolution technique, as applied by Chakrabarti and Jacobsen, is not suitable to provide accurate basalt data unless an additional ignition step is used. Chakrabarti and Jacobsen (2010b) did not include any extra ignition steps and it may be that the lack of a high temperature step in their dissolution process that may be causing the discrepancy between their terrestrial basalt data and conclusions of other lab groups.

Table (5.2): Direct measurements of $\Delta^{30}\text{Si}_{\text{BHVO2-lunar}}$

		$\delta^{30}\text{Si}$	$2\sigma_{SEM}$	$\delta^{29}\text{Si}$	$2\sigma_{SEM}$	n	N
Measurements of $\Delta^{30}\text{Si}_{\text{BHVO2-Lunar}}$							
15058	Quartz normative basalt	0.03	0.04	0.02	0.02	1	11
10049	High-Ti basalt	0.04	0.04	0.04	0.02	1	11
75075	High-Ti basalt	0.01	0.05	-0.03	0.02	1	5
77516	High-Ti basalt	0.01	0.03	0.02	0.05	1	10
15426	Green glass	-0.06	0.05	-0.03	0.02	1	9
Average $\Delta^{30}\text{Si}_{\text{BHVO2-lunar}}$ ($\pm 2\sigma_{SD}$)		0.01	0.08	0.00	0.06		1

All these samples have been analysed on the MC-ICPMS using the USGS basalts standard BHVO-2 as the bracketing standard rather than NBS-28, giving a direct measurement of the offset between terrestrial and lunar basalts.

5.4 Discussion

5.4.1 Lunar mantle composition

Mare basalts are exposed over 17% of the Moon's surface and are thought to be the product of highly effusive eruptions from relatively deep sources (Head and Wilson, 1992). Previous work has shown that Si isotopes do not measurably fractionate during mantle melting in a terrestrial setting (e.g. Savage et al., 2010). In terms of crystallisation processes, it is observed that fractionation of Si isotopes can occur with evolution from parental magmas (Savage et al., 2011), which is consistent with

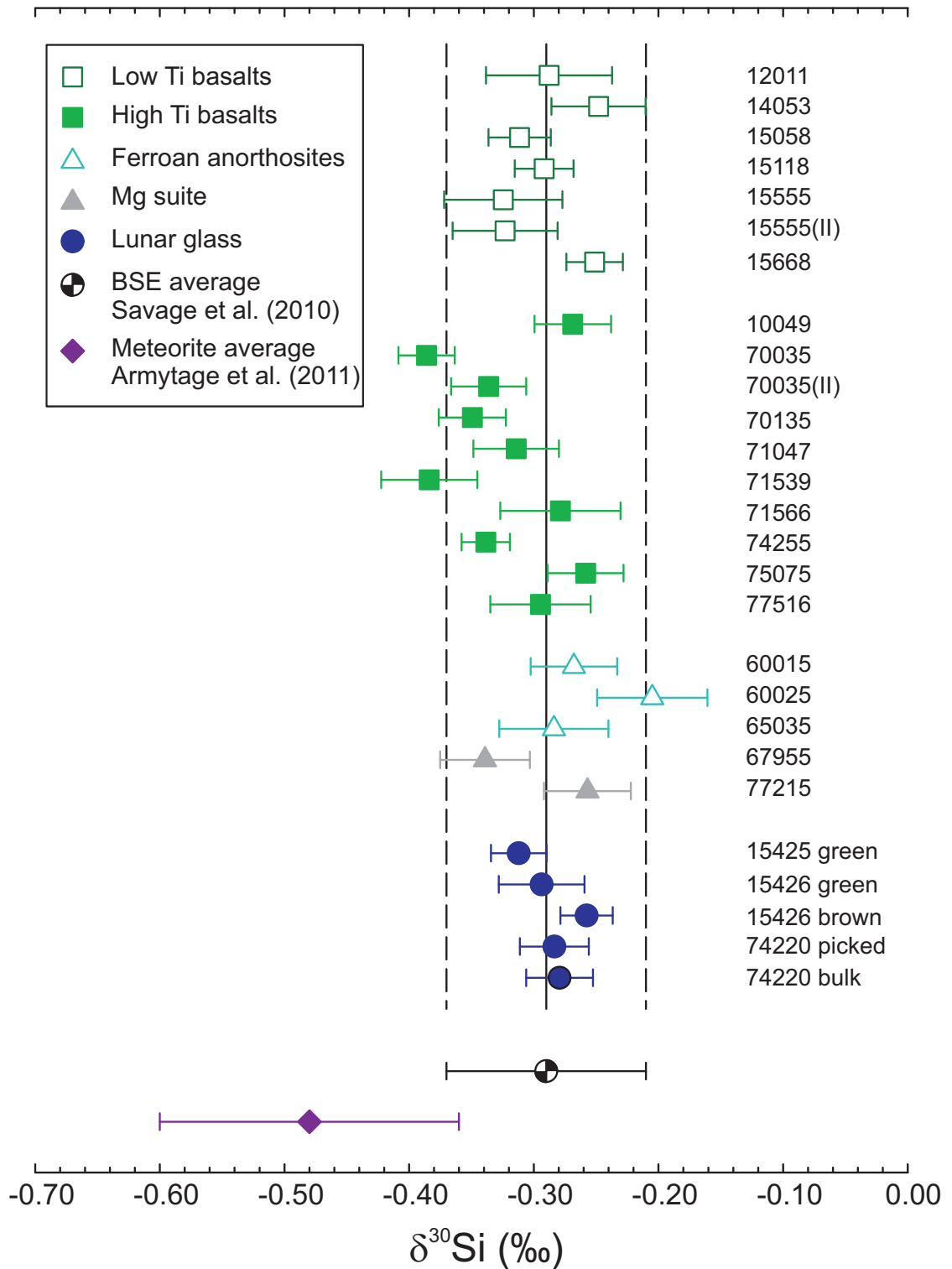


Figure (5.2): $\delta^{30}\text{Si}$ isotope compositions of bulk lunar samples. The error bars represent $\pm 2\sigma_{SEM}$. (II) designates a separate fusion of another aliquot of sample powder. The solid line is the mean of the lunar samples, while the dashed lines are $\pm 2\sigma_{SD}$.

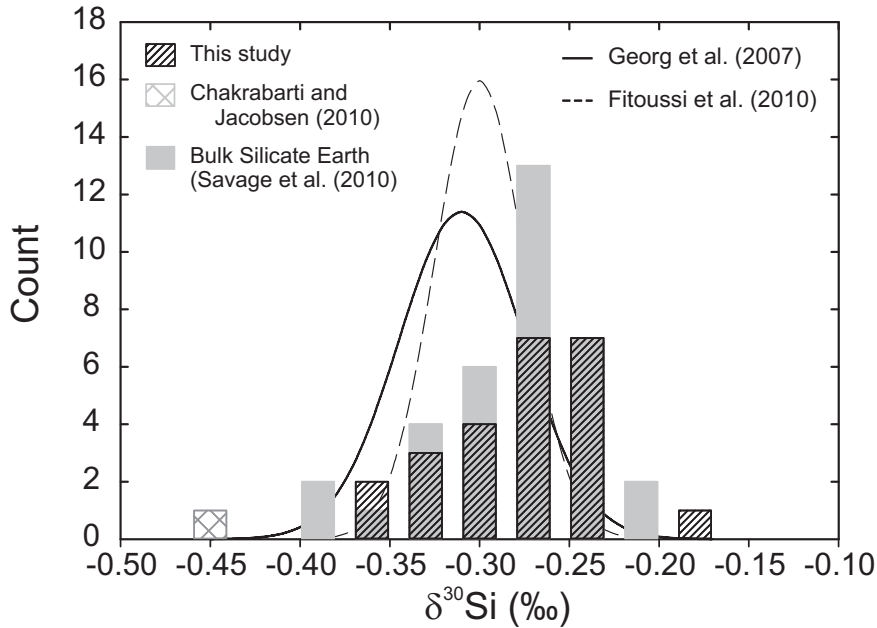


Figure (5.3): Histograms of $\delta^{30}\text{Si}$ values lunar samples from this study and bulk silicate Earth samples (BSE) from Savage et al. (2010). The lunar breccia from Chakrabarti and Jacobsen (2010b) has also been plotted. The solid black line is the calculated normal distribution of the Georg et al. (2007a) lunar basalt data while the dashed black is the calculated normal distribution of mare basalts of Fitoussi et al. (2010)

recent theoretical calculations (Méheut et al., 2009). The evolutionary igneous trend has the empirical relationship $\delta^{30}\text{Si} = 0.0056 \times \text{SiO}_2 - 0.567$ (2 standard error on the regression: $\pm 0.05\text{‰}$) (Savage et al., 2011). However, as all of the rocks derived from the lunar mantle have relatively low SiO_2 , no trend in $\delta^{30}\text{Si}$ can be resolved. Therefore it is reasonable to assume that the Si isotope compositions of the mare basalts reflect their mantle sources.

The mare basalts were initially divided by Papike et al. (1976) into high and low-Ti basalts. The low Ti-basalts have an average $\delta^{30}\text{Si} = -0.29 \pm 0.06\text{‰}$ ($\pm 2\sigma_{SD}$, $N=6$), while the high Ti-basalts are indistinguishable within error with $\delta^{30}\text{Si} = -0.32 \pm 0.09\text{‰}$ ($\pm 2\sigma_{SD}$, $N=8$). It has been suggested that the variation in Ti content of the mare basalts is the result of distinct source regions (Papike et al., 1976), which is

supported by their distinct correlations in ϵNd and ϵHf (Unruh et al., 1984). As this distinction is not apparent in the Si isotope composition (Figure 5.2), it implies that these source regions are homogeneous in terms of Si isotopes at the current levels of precision.

The picritic glasses analysed in this study have a mean Si isotopic composition of $\delta^{30}\text{Si} = -0.29 \pm 0.05\text{‰}$ ($\pm 2\sigma_{SD}$, $N = 4$), which is identical to the mare basalts within error. As there is no measurable difference in the Si isotope composition of the sources between the low-Ti mare basalt, high-Ti basalts or the picritic glasses, it is likely that their homogeneous Si composition is an inherited signature from processes early in lunar history with no subsequent fractionation between these sources in the lunar mantle during differentiation.

For isotope systems such as Fe (Poitrasson et al., 2004), Cu and Zn (Moynier et al., 2006), the pyroclastic glasses are lighter in isotope composition compared to the mare basalts. The Cu and Zn glass data can be explained by isotopic fractionation during formation due to fire fountaining (Moynier et al., 2006). This is consistent with the lack of variation in Si composition between mare basalts and the lunar glasses. Firstly, Si is significantly less volatile than Zn or Cu with a 50% condensation temperature of 1310K rather than 726K (Zn) or 1034 (Cu) (Lodders, 2003). Secondly, Si, being a major element, is also much more abundant than Zn or Cu, therefore coating the surfaces of the glasses with condensed fractionated vapour (Moynier et al., 2006), will not perturb the bulk composition of the glass to a measurable extent (coatings are on the order of 0.06% by volume, (Meyer et al., 1975)). Explaining the lack of consistency between the Fe isotope glass data and the Si isotope data is more problematic. Silicon and Fe are both major elements in the volcanic glasses and have a similar volatility, with 50% condensation temperatures of 1310K and 1334K, respectively (Lodders, 2003). One explanation for the glass Fe data involves the sampling of a deeper source that accreted from material that did not experience a full scale evaporation and hence

is isotopically lighter than the mare basalt source (Poitrasson et al., 2004). However, this interpretation is not consistent with the similar condensation temperatures of Fe and Si. A subsequent study found that the same lunar glasses had the same Fe isotope composition, within error, as the low-Ti basalts (Weyer et al., 2005), which would be more consistent with the Si isotope compositions.

5.4.2 Highland rocks

The idea of a lunar magma ocean (LMO) has existed in one form or another since the return of the first Apollo 11 samples (e.g. Smith et al., 1970; Wood et al., 1970). The abundant plagioclase-rich crust suggests flotation in a global magma ocean and its antiquity (e.g. Norman et al., 2003) points to a primordial event. Although the expected concomitant olivine and pyroxene cumulates have yet to be discovered and sampled, the rare earth element (REE) patterns show that the mare basalts sources are complementary to the feldspathic crust (e.g. Taylor, 1982). There is a hint that the ferroan anorthosites (60015, 60025 and 65035) are on average slightly heavier ($\delta^{30}\text{Si}_{\text{FAN}} = -0.25 \pm 0.08\text{‰}$, $\pm 2\sigma_{SD}$) than the lunar mantle ($\delta^{30}\text{Si} = -0.30 \pm 0.08\text{‰}$ $\pm 2\sigma_{SD}$) as represented by mare basalts and picritic glasses, but they are still the same within error.

Samples from lunar highland rocks must be considered with care, as there is always the possibility of chemical contamination through addition of meteorite material and the issue of whether or not they possess primary compositions resulting from endogenous lunar igneous processes (Warren and Wasson, 1977). As the mean Si isotopic composition of meteorites is lighter than that of lunar samples (Georg et al., 2007a; Fitoussi et al., 2009, 2010; Armytage et al., 2011), the Si isotope data would seem to suggest that 67955 is the highland sample most likely to be affected by meteorite contamination (see Table 5.1). Norman et al. (2007) found that the PGE (platinum group elements) and Fe-Ni-Co concentrations of sample 67955 indicated meteoritic

contamination. However, for a number of reasons it is likely that the lighter composition of 67955 ($\delta^{30}\text{Si} = -0.34 \pm 0.04\text{‰}$, $\pm 2\sigma_{SEM}$) in comparison to other highland rocks is due to variation from causes other than meteorite contamination. Firstly, the Si isotope composition of 67955 is the same or heavier (Table 5.1) than a number of high-Ti basalt samples (e.g. 70035, 74255, 70135), which are known not to show any evidence of meteoritic contamination (Day et al., 2007). Secondly, mass balance calculations between the most “pristine” highland sample 60025 (Day et al., 2010) and 67955 require that $\sim 80\%$ of chondritic material would be needed to explain the Si isotope variation. High abundances of siderophile elements, e.g. >130 pg Ir, are used as indicators of meteoritic contamination (Warren and Wasson, 1977). Using 1 part per trillion in 60025 from Day et al. (2010) and 456ppb for Orgueil from Horan et al. (2003), 80% meteoritic contamination of 67955 would give an expected composition >350 ppb Ir. The maximum Ir concentration that has been measured in 67955 is 11ppb (Lindstrom and Lindstrom, 1986). Hence, Si isotopic compositions of lunar rocks are not very sensitive to meteoritic contamination, and Si isotope variations can therefore be interpreted in terms of endogenous lunar processes.

5.4.3 Moon formation

The lunar mean ($\delta^{30}\text{Si} = -0.29 \pm 0.08\text{‰}$, $\pm 2\sigma_{SD}$) is heavier than the stony meteorite average of $\delta^{30}\text{Si} = -0.48 \pm 0.13\text{‰}$ ($\pm 2\sigma_{SD}$) (Armstrong et al., 2011), which includes chondrites (carbonaceous, ordinary, enstatite) and achondrites (HED, martian, ureilites, an aubrite). Hence the Moon is the only extraterrestrial body measured to date that is like bulk silicate Earth (BSE) with regard to its Si isotope composition ($\delta^{30}\text{Si} = -0.29 \pm 0.08\text{‰}$, $\pm 2\sigma_{SD}$, Savage et al., 2010). The heavy $\delta^{30}\text{Si}$ of the BSE relative to chondrites is thought to result from terrestrial core formation with lighter Si isotopically fractionating into metal (e.g. Georg et al., 2007a; Fitoussi et al., 2009). The simplest explanation for the uniqueness of the Earth-Moon system, therefore,

would be that the Moon formed from the Earth's mantle after terrestrial core formation took place (e.g. Ringwood, 1986). If the hydrodynamic simulations of moon formation by a giant impact (e.g. Canup and Asphaug, 2001) are correct in showing that most lunar material should have derived from the impactor, the similarity of BSE and the Moon Si isotopic composition requires further explanation. It is thought that Mars-sized bodies, would, in most core accretion scenarios, not be large enough to create the pressure and hence temperature conditions necessary for Si to enter the core (Gessmann et al., 2001). This makes it irrelevant whether the whole impactor or just the silicate portion is homogenised, as both will have a chondritic Si isotope composition. Therefore, the identical $\delta^{30}\text{Si}$ of the BSE and the Moon is likely unique to the Earth-Moon system and the result of isotopic homogenization in the aftermath of the Giant Impact, as was proposed to explain the identical oxygen isotopic composition (Pahlevan et al., 2011).

The similarity (or not) of the Moon to the Earth in terms of major element budgets provides key information as regards the composition of the Moon-forming impactor and/or the processes operating during lunar formation. The estimates of lunar $\text{Fe}/(\text{Fe}+\text{Mg})$ fall into two categories: those that have $\text{Fe}/(\text{Fe}+\text{Mg})$ ratios close to that of the silicate Earth (e.g. Warren, 2005) and others that suggest $\text{Fe}/(\text{Fe}+\text{Mg})$ ratios greater than that of the BSE (e.g. Taylor et al., 2006). The bulk Moon composition estimates of Warren (2005) predict Earth-like ratios ($\text{Fe}/(\text{Fe}+\text{Mg})\sim 0.1$) on the basis of Al_2O_3 -Mg# systematics in highland samples constraining different lunar source region budgets. Taylor et al.'s (2006) $\text{Fe}/(\text{Fe}+\text{Mg})$ ratio of 0.18, on the other hand, is based on bulk geophysical properties of the Moon. Pahlevan et al. (2011) developed their 2007 homogenization model further to explore such potential chemical differences between the Moon and the silicate Earth. In the model the Earth is characterized by a single convective column from the deep magma ocean to the top of a two-phase atmosphere, which exchanges with the proto-lunar disk. Changes in the $\text{Fe}/(\text{Fe}+\text{Mg})$

ratios are predicted during rainout of liquid from the two phase atmosphere with concomitant fractionation of Si isotopes. This fractionation is predicted from SiO (Si valence of +2) being the dominant species in the vapour phase, while the Si in the melt (liquid fraction) presumably exists as SiO_4^{4-} (+4 valence) (Pahlevan et al., 2011). A higher degree of liquid rainout corresponds to increased Fe/(Fe+Mg) values in the proto-lunar disk and larger magnitude $\Delta^{30}\text{Si}_{\text{BSE-lunar}}$, where $\Delta^{30}\text{Si}_{\text{BSE-lunar}} = \delta^{30}\text{Si}_{\text{BSE}} - \delta^{30}\text{Si}_{\text{lunar}}$. The Si measurements from this study combined with the BSE data of Savage et al. (2010) show that $\Delta^{30}\text{Si}_{\text{BSE-lunar}} = 0.00 \pm 0.16\text{‰}$ ($\pm 2\sigma_{SEM}$). Therefore in theory, it is not possible to distinguish between liquid rainout fractions of 0 or 40%, which would correspond to lunar Fe/(Fe+Mg) ratios of BSE to $\times 2$ BSE (Pahlevan et al., 2011). However the $\pm 0.16\text{‰}$ uncertainty on $\Delta^{30}\text{Si}_{\text{BSE-lunar}}$ is somewhat of an overestimate of the level at which differences in the mean values of $\delta^{30}\text{Si}_{\text{lunar}}$ and $\delta^{30}\text{Si}_{\text{BSE}}$ can be assessed.

One way to assess how well the means of the Si isotope datasets are known is to carry out a student t-test calculation on the lunar data from this study and the BSE population from Savage et al. (2010). This can give the maximum $\Delta^{30}\text{Si}_{\text{BSE-lunar}}$ at the 99% confidence interval that cannot be resolved based on current analytical precision.. The student t-test equation, for equal variance but different sample size, can be rearranged to calculate the minimum $\Delta^{30}\text{Si}_{\text{BSE-lunar}}$ that is resolvable at current levels of precision:

$$\Delta^{30}\text{Si}_{\text{BSE-lunar}} = t_{crit} S_{x_1, x_2} \sqrt{\frac{1}{n_1} + \frac{1}{n_2}} \quad (5.2)$$

where

$$S_{x_1, x_2} = \sqrt{\frac{(n_1 - 1)s_1^2 + (n_2 - 1)s_2^2}{n_1 + n_2 - 2}} \quad (5.3)$$

t_{crit} is the t-test value at the 99% confidence interval for the appropriate degree of

freedom, $(n_1 + n_2 - 2)$, x is the mean, $s^2 =$ variance of the sample population (same for the datasets of both this study and Savage et al., 2010), $n =$ number of samples and the subscripts 1 and 2 correspond to groups 1 and 2 respectively. Hence equation 5.2 with $s_2 = 0.042$ and $t_{crit} = 2.67$ gives the minimum absolute value of $\Delta^{30}\text{Si}_{\text{BSE-lunar}} = 0.03\text{‰}$. In other words, any offset in $\Delta^{30}\text{Si}_{\text{BSE-lunar}} > 0.03\text{‰}$ should be detectable from the currently available datasets. Another way to constrain the uncertainty on $\Delta^{30}\text{Si}_{\text{BSE-lunar}}$ is to use the standard error of the mean σ_{SEM} . This is defined as σ/\sqrt{N} , where σ is the standard deviation of the sample population and N is the number of samples in the population, and is a better estimate of how well the mean is known, as it describes the uncertainty of how well the sample mean represents the population mean. The Si isotope BSE data of Savage et al. (2011) has an uncertainty of $\pm 0.01\text{‰}$ at the 2 standard error of the mean level ($2\sigma_{SEM}$) and the lunar data from this study, $\pm 0.02\text{‰}$ ($2\sigma_{SEM}$). This gives $\Delta^{30}\text{Si}_{\text{BSE-lunar}} = 0.00 \pm 0.022\text{‰}$, which concurs with the previous method. This means that liquid rainout fractions greater than 0.2 can be ruled out from the Pahlevan et al. (2011) model, constraining the Fe/(Fe+Mg) of the Moon to be no more than 1-1.3 times that of the BSE. This favours the bulk Moon composition estimates of Warren (2005) which predict Earth-like ratios, whereas Taylor et al.'s (2006) Fe/(Fe+Mg) ratio is only achievable in Pahlevan et al.'s (2011) model, at high degrees ($>40\%$) of liquid rainout, which is not consistent with the isotope data.

5.4.4 Core formation post lunar formation?

The results from this study imply that the Si isotope compositions for BSE and the Moon were homogenised as a result of equilibration in a vapour atmosphere in the aftermath of the Giant Impact. Silicon isotopes have the potential to assess the degree to which lunar formation is the last terrestrial core formation event for Si as the non-chondritic Si isotope composition of the BSE-Moon system is thought to result

from terrestrial metal-silicate partitioning. Using $\Delta^{30}\text{Si}_{\text{BSE-lunar}}$ as the “initial” bulk Earth Si isotopic composition (i.e. prior to any post equilibration core formation), the following mass balance equation can be constructed for the BSE:

$$\Delta^{30}\text{Si}_{\text{BSE-lunar}} = \epsilon(1 - f) \quad (5.4)$$

where $\Delta^{30}\text{Si}_{\text{BSE-lunar}}$ is the maximum unresolvable offset calculated from equation 5.2, ϵ is the metal-silicate fractionation factor (0.89 from Ziegler et al., 2010 after the data of Shahar et al., 2009) and f is the fraction of Si in the silicate phase of the bulk Earth. Solving equation 5.4 for f , gives $f = 0.966$. Therefore, terrestrial metal-silicate partitioning of Si is $\sim 97\%$ complete by the end of BSE-lunar Si isotope equilibration. It could be that the remaining $\sim 3\%$ of Si partitioning could be related to post equilibration core formation. Estimates for the amount of Si in the core generally lie in the range 0-10wt%, with the estimates deriving from many different kinds of data such as the superchondritic Mg/Si ratio of BSE (e.g. Palme and O’Neill, 2003), Si isotope offsets between chondrites and BSE (e.g. Georg et al., 2007a; Fitoussi et al., 2009; Chakrabarti and Jacobsen, 2010b; Armytage et al., 2011), and Si partitioning behaviour (e.g. Gessmann et al., 2001; Tuff et al., 2010). This range would correspond to deficits of 0-4.8wt% Si in the BSE, with the unaccounted for 3% corresponding to 0-0.14wt% Si in the mantle that could be transferred to the core post-equilibration. No matter what the estimate of Si in the core, these are very small fractions in comparison to the size of the reservoirs so as to be negligible. There are compelling physical constraints for only minimal Si metal-silicate partitioning after equilibration associated with the Giant Impact. The segregation models of Wade and Wood (2005) have oxygen fugacity increasing towards the end of accretion, which would not favour the partitioning of Si into metal Kilburn and Wood (1997). The non-zero $\Delta^{30}\text{Si}_{\text{BSE-lunar}}$ could also be the result of a small degree of rainout in the

two phase model atmosphere of Pahlevan et al. (2011). In addition the value of $\Delta^{30}\text{Si}_{\text{BSE-lunar}}$ is defined as the “maximum unresolvable offset” and as such can either take a negative or a positive value. Therefore equation 5.4 can give the maximum possible amount of Si metal-silicate partitioning post lunar formation but can also just be an assessment of the uncertainty on the amount of Si in the core based on Si isotopic constraints (in this case an uncertainty of up to 0.3wt% Si in the core).

5.5 Conclusions

1. The Si isotopic compositions of a range of lunar rock types, from anorthosites to low-Ti and high-Ti mare basalts, were analysed with MC-ICPMS. The average of all the bulk lunar samples was $\delta^{30}\text{Si} = -0.29 \pm 0.08\text{‰}$ ($2\sigma_{SD}$) with no resolvable differences between the different lithologies. The homogeneity of the lunar mantle with respect to Si isotopes, while Ti contents in lunar basalts point to multiple source regions, implies that the signature was probably inherited from the proto-lunar disk and has not been subsequently modified by later differentiation.
2. $\Delta^{30}\text{Si}_{\text{BSE-lunar}}$ is the same as the value for the bulk silicate Earth $\delta^{30}\text{Si} = -0.29 \pm 0.08\text{‰}$ ($2\sigma_{SD}$) (Savage et al., 2010). The lunar Si signature is therefore unique among extra-terrestrial bodies in having the same signature as Earth. The most likely reason is that Si isotopes were homogenised in the aftermath of the Moon forming Giant Impact, after Si had fractionated into the Earth’s core.
3. At the current precision, the differences in the mean $\delta^{30}\text{Si}_{\text{BSE}}$ and $\delta^{30}\text{Si}_{\text{lunar}}$ ($\Delta^{30}\text{Si}_{\text{BSE-lunar}}$) can be resolved to $\pm 0.03\text{‰}$. According to the chemical fractionation models of (Pahlevan et al., 2011) in the aftermath of the Giant Impact, the current Si dataset constrains the $\text{Fe}/(\text{Fe}+\text{Mg})$ of the Moon to be $1-1.3 \times$

silicate Earth. Also only limited Si partitioning into the Earth's core ($<0.3\text{wt}\%$) is possible post lunar formation.

Chapter 6

Silicon isotopic composition of lunar basalt mineral separates

6.1 Introduction

The Moon, out of all bodies in the solar system, is the one we have the most igneous samples from after the Earth. One of the key observations is that the variation in composition of the lunar volcanic products is significantly greater than what is generated by terrestrial mantle melts (e.g Taylor, 1982; Grove and Krawczynski, 2009). Since the return of lunar rocks from the Apollo 11 site, the hypothesis that the Moon experienced a significant early global melting event, the lunar magma ocean (LMO), has been a key feature of our models of understanding the Moon (e.g. Wood et al., 1970; Smith et al., 1970). One of the strongest lines of evidence is the rare earth element (REE) patterns, in particular the ubiquitous negative Eu anomaly, observed across the mare basalts and glasses (e.g. Papike et al., 1998). As there is no evidence of plagioclase being present on the liquidus during melting for primitive mare basalts and picritic glasses, it is likely that the Eu anomaly is an intrinsic source effect resulting from plagioclase fractionating to form the floated anorthosite crust during the LMO (see summaries by Shearer et al., 2006; Grove and Krawczynski, 2009). The mare basalts therefore reflect, to some degree, the complementary olivine and pyroxene cumulates. The variation in Ti content of the mare basalts (Papike et al., 1976),

coupled with their disparate correlations in ϵNd and ϵHf (Unruh et al., 1984) provides evidence for different source regions among the mare basalts.

The stable isotopic ratios for a number of elements show variability between high-Ti and low-Ti mare basalts. Lithium (Magna et al., 2006) and Mg (Wiechert and Halliday, 2007) both show isotopic variability thought to relate to mare basalt source heterogeneity. Oxygen and Fe isotopic ratios both show variations between the high Ti and low Ti basalts. Liu et al. (2010) reported coupled isotopic data for O and Fe in mare basalt samples, with the variation between the isotopic ratios being related to the presence or absence of ilmenite in the source. With all these records of variation in the lunar interior, Si is somewhat of an outlier as the Si isotopic composition of lunar rocks is remarkably homogeneous, with no variations that can be linked to lithology (see Chapter 5). The average Si isotopic composition of a number of mare basalt samples (both high and low Ti) and also anorthosite crustal rocks is $\delta^{30}\text{Si} = -0.29 \pm 0.08\text{‰}$ ($2\sigma_{SD}$), which is the same as the average Si isotopic composition of bulk silicate Earth (BSE), $\delta^{30}\text{Si} = -0.29 \pm 0.08\text{‰}$ ($2\sigma_{SD}$) (Savage et al., 2010). This Moon-Earth similarity is thought to arise from the same processes that is responsible for generating a lunar $\Delta^{17}\text{O}_{\text{lunar}} = 0$ relative to the terrestrial fractionation line. Currently, the cause is thought to be homogenisation in a vapour cloud in the aftermath of the Moon-forming giant impact (Pahlevan and Stevenson, 2007) (see Chapter 5 for a detailed discussion). It has been shown that Si isotopes do not measurably fractionate during mantle melting (e.g. Savage et al., 2010), however analyses of mineral separates from the Skaergaard intrusion (Savage et al., 2011) display $\delta^{30}\text{Si}$ fractionations between the mafic minerals, olivine and pyroxene, and plagioclase on the order of $\sim 0.3\text{‰}$. Therefore one might expect, at the very least, an offset in Si isotope composition between the anorthosite samples and the mare basalts due to fractionation of mineral phases in the LMO.

To gain further insight into the behaviour of Si isotopes in lunar processes, we

analysed the mineral separates from a number of lunar basalts. Variations in isotopic composition of igneous minerals can contribute key evidence to understanding the origin and evolution of magmas.

6.2 Method

Mineral separates from three high-Ti basalts (74255, 70135, 70035) and three low-Ti basalts (14053, 15555) were measured for their Si isotopic composition. Approximately 1mg of plagioclase, pyroxenes and, where present, olivines were hand picked under a microscope from samples that had been crushed and in some cases previously sieved (Schönbächler et al., 2005a). The samples were subsequently processed according to the method described in Chapter 2.

6.3 Results

The $\delta^{30}\text{Si}$ composition of mineral separates from five lunar basalts were analysed (Figure 6.1, Table 6.1). Plagioclase and pyroxene phases were analysed from each sample, but there were only three $\delta^{30}\text{Si}$ data for olivine (14053, 15555, 74255). $\delta^{30}\text{Si}$ compositions of the corresponding bulk basalt samples had been previously analysed (Chapter 5).

The plagioclase separates have the heaviest and most uniform $\delta^{30}\text{Si}$ of all the mineral phases analysed with $\delta^{30}\text{Si} = -0.27 \pm 0.04\text{‰}$ ($2\sigma_{SD}$). The mafic minerals, by contrast, are lighter and more variable in their Si isotopic composition with the averages for the phases being $\delta^{30}\text{Si}_{\text{pyroxene}} = -0.43 \pm 0.14\text{‰}$ ($2\sigma_{SD}$) and $\delta^{30}\text{Si}_{\text{olivine}} = -0.37 \pm 0.09\text{‰}$ ($2\sigma_{SD}$). Pyroxene, in addition to being the mineral phase that shows the most variability, also shows within sample variability (14053, Table 6.1). Olivine and pyroxene also exhibit variability relative to each other as in 74255, the olivine $\delta^{30}\text{Si}$ is lighter (-0.45 ± 0.03 , $2\sigma_{SEM}$) than the pyroxene (-0.33 ± 0.03 , $2\sigma_{SEM}$)

with no overlap in uncertainty, whereas in 15555 the olivine and pyroxene have the same $\delta^{30}\text{Si}$ composition of -0.35‰ . The two separate picked samples of pyroxene that were analysed from 14053, which are not the same within $2\sigma_{SEM}$ (pyroxene-1: $\delta^{30}\text{Si} = -0.36 \pm 0.03$; pyroxene-2 $\delta^{30}\text{Si} = -0.43 \pm 0.03$), are both heavier than the olivine phase from the same basalt (-0.48 ± 0.03 , $2\sigma_{SEM}$). The direction of Si isotopic fractionation between mafic and felsic mineral is similar to that observed previously in low precision studies of lunar basalts e.g. 15058 ($\delta^{30}\text{Si}_{\text{pyroxene}} \sim -0.35$; $\delta^{30}\text{Si}_{\text{plagioclase}} \sim -0.14$) and 75055 ($\delta^{30}\text{Si}_{\text{pyroxene}} \sim -0.31$; $\delta^{30}\text{Si}_{\text{plagioclase}} \sim -0.14$) (Epstein and Taylor Jr., 1972; Taylor Jr. and Epstein, 1973a). However, the magnitude of the inter-mineral fractionations observed in this higher precision study are, on average, smaller and also the $\delta^{30}\text{Si}$ of all the phases tend to be lighter.

Table (6.1): Silicon isotope data for lunar basalt mineral separates

Samples	$\delta^{30}\text{Si}$ (‰)	$2\sigma_{SEM}$	$\delta^{29}\text{Si}$ (‰)	$2\sigma_{SEM}$	N	SiO_2 (wt%)
Low Ti-basalts						
14053						
Olivine	-0.48	0.03	-0.24	0.02	20	50.5
Pyroxene-1	-0.36	0.03	-0.21	0.03	17	46.6
Pyroxene-2	-0.43	0.03	-0.22	0.02	25	46.3
Plagioclase	-0.25	0.04	-0.12	0.03	20	45.8
Bulk	-0.25	0.04	-0.11	0.02	18	45.7
15555						
Olivine	-0.35	0.03	-0.18	0.02	18	38.5
Pyroxene	-0.35	0.01	-0.20	0.01	18	43.0
Plagioclase	-0.29	0.03	-0.15	0.01	20	42.9
Bulk I	-0.32	0.05	-0.17	0.03	25	45.7
Bulk II	-0.32	0.04	-0.18	0.01	5	45.7
High Ti-basalts						
74255						
Olivine	-0.45	0.03	-0.24	0.02	17	34.6
Pyroxene	-0.33	0.04	-0.18	0.02	9	47.4
Plagioclase	-0.29	0.04	-0.17	0.02	17	37.5
Bulk	-0.34	0.02	-0.16	0.03	22	42.0

Continued on Next Page...

6.3. Results

Table 6.1 – Continued

Samples	$\delta^{30}\text{Si}$ (‰)	$2\sigma_{SEM}$	$\delta^{29}\text{Si}$ (‰)	$2\sigma_{SEM}$	N	SiO_2 (wt%)
70135						
Pyroxene	-0.31	0.03	-0.17	0.02	18	45.8
Plagioclase	-0.27	0.04	-0.12	0.02	18	45.6
Bulk	-0.35	0.03	-0.17	0.02	11	36.3
70035						
Pyroxene	-0.41	0.05	-0.20	0.04	13	48.1
Plagioclase	-0.27	0.04	-0.16	0.03	14	42.7
Bulk I	-0.39	0.02	-0.11	0.02	18	36.7
Bulk II	-0.34	0.03	-0.11	0.02	18	36.7
Terrestrial Samples						
Skaergaard (Savage et al., 2011)						
2307						
Olivine	-0.42	0.01	-0.23	0.04	30	36.28
Clinopyroxene	-0.50	0.04	-0.25	0.01	21	52.00
Plagioclase	-0.15	0.02	-0.07	0.01	22	55.78
5181						
Olivine	-0.45	0.01	-0.22	0.01	31	33.20
Plagioclase	-0.21	0.03	-0.11	0.01	20	58.08
Spinel lherzolites (Georg et al., 2007a)						
C 235 A						
Olivine	-0.35	0.03	-0.16	0.02	9	n.d.
Clinopyroxene	-0.41	0.03	-0.23	0.02	11	n.d.
C 271 I						
Olivine	-0.31	0.03	-0.14	0.03	11	n.d.
Clinopyroxene	-0.42	0.04	-0.23	0.03	9	n.d.

Bulk lunar values from Chapter 5

There are some similarities between this new lunar mineral separate data and high precision $\delta^{30}\text{Si}$ data for mineral separates from terrestrial settings (Figure 6.1, Table 6.1). The mafic minerals are always lighter in $\delta^{30}\text{Si}$ than the felsic minerals. The average olivine Si isotopic composition of the Skaergaard samples from Savage et al. (2011) of -0.44‰ is the same within uncertainty of the olivine compositions from 14053 (-0.48 ± 0.03 , $2\sigma_{SEM}$) and 74255 (-0.45 ± 0.03 , $2\sigma_{SEM}$). The olivine $\delta^{30}\text{Si}$ composition of 15555 (-0.35 ± 0.03 , $2\sigma_{SEM}$), on the other hand, is closer to the average olivine composition of the peridotites, -0.33‰ , as measured by Georg et al.

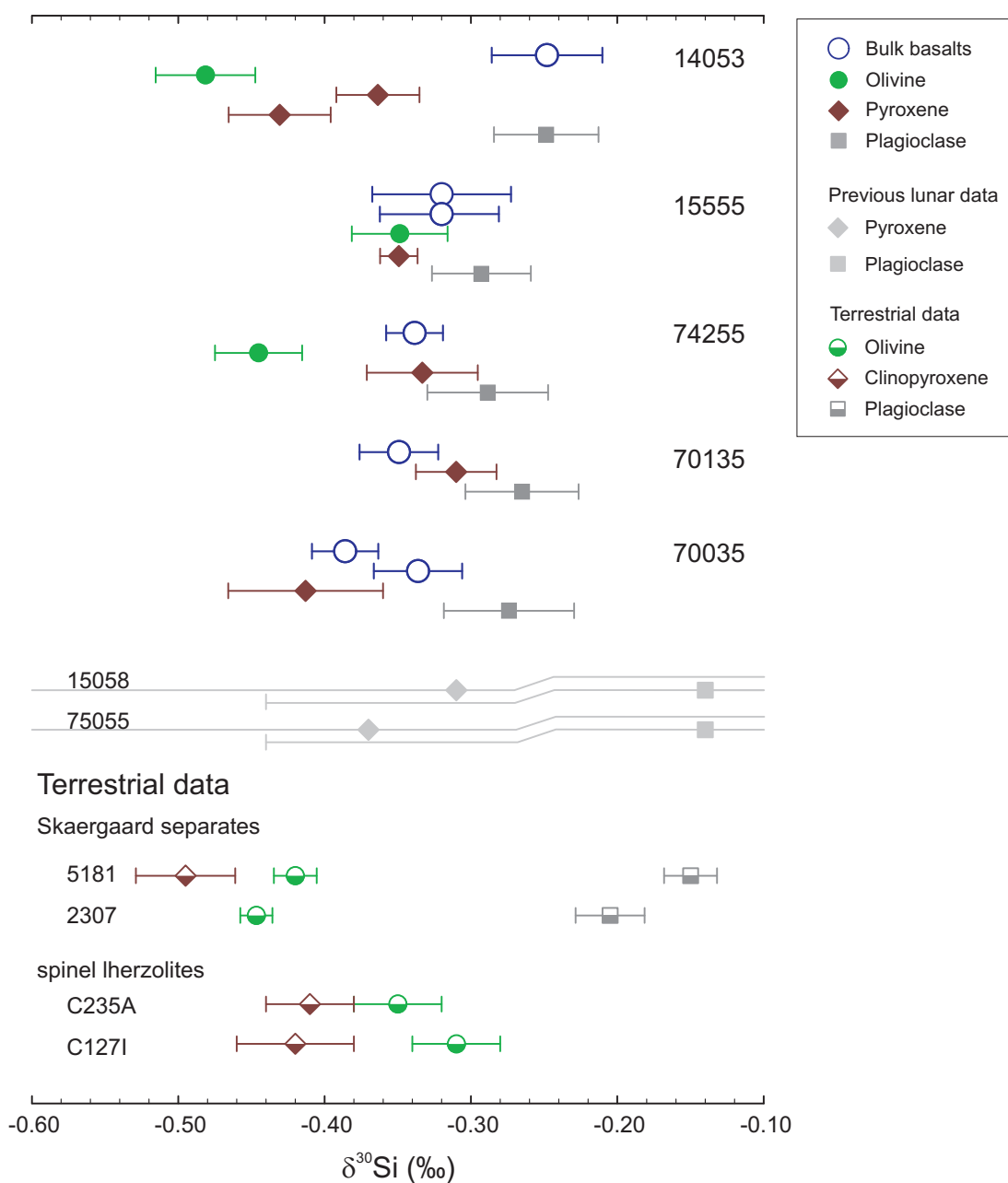


Figure (6.1): $\delta^{30}\text{Si}$ mineral separates data for five lunar basalts. 14053 and 15555 are low-Ti basalts while 74255, 70135 and 70035 are high-Ti basalts. The error bars represent $\pm 2\sigma_{SEM}$. The previous lunar data plotted here (Epstein and Taylor Jr., 1972; Taylor Jr. and Epstein, 1973a) are only two representative basalts selected from the large mineral dataset from Epstein and Taylor's work. 15058 is a low-Ti basalt and 75053 is a high-Ti basalt. As Taylor and Epstein did not publish their reproducibility for these data, the uncertainty is taken to be 0.3‰ ($\pm 2\sigma_{SD}$) from Douthitt (1982) as Douthitt used the same analytical method. The Skaergaard data is from Savage et al. (2011), while the spinel lherzolite data is from Georg et al. (2007a). The error bars on the terrestrial data are $\pm 2\sigma_{SEM}$.

(2007a). Conversely, the terrestrial plagioclases from Skaergaard have considerably heavier compositions, $-0.15 \pm 0.02\text{‰}$; $-0.21 \pm 0.03\text{‰}$ ($2\sigma_{SEM}$), than the lunar samples analysed here (heaviest lunar $\delta^{30}\text{Si}_{\text{plagioclase}} = -0.25 \pm 0.04$). The most noticeable difference between the terrestrial and lunar data is the direction of the fractionation between olivine and pyroxene. In all of the terrestrial samples, where both phases have been analysed, the pyroxene is always lighter than the olivine in $\delta^{30}\text{Si}$ composition by up to $\sim 0.11\text{‰}$. Whereas in the lunar samples the olivine can be up to $\sim 0.12\text{‰}$ lighter than the pyroxene in Si isotopic composition. First principles calculations by Méheut et al. (2009) predict small and positive Si isotope fractionations between forsterite and clinopyroxene, which is consistent with the terrestrial mineral data but not the lunar samples (Figure 6.2).

6.4 Discussion

6.4.1 Variations in fractionation factors in lunar basalts

In Figure 6.2 it is clear that the mineral-mineral $\delta^{30}\text{Si}$ offsets in the lunar basalts are not particularly consistent due to the variability in the $\delta^{30}\text{Si}$ of the individual phases. The degree and direction of the variability does not appear to correlate with the Ti content of the basalts, hence cannot be simply linked to source differences. Despite the pyroxenes having the greatest range in $\delta^{30}\text{Si}$ (Table 6.1), it is the olivine-plagioclase fractionations that display the largest range ($\sim 0.18\text{‰}$). However, the range of olivine-plagioclase $\delta^{30}\text{Si}$ compositions do overlap with terrestrial compositions. On the other hand the range of lunar olivine-pyroxene $\delta^{30}\text{Si}$ offsets are the same as the terrestrial compositions within uncertainty, however as mentioned previously the direction of offset is not the same. The pyroxene-plagioclase fractionations are consistent in direction between the lunar and terrestrial data but there is no overlap in the high resolution datasets within uncertainty.

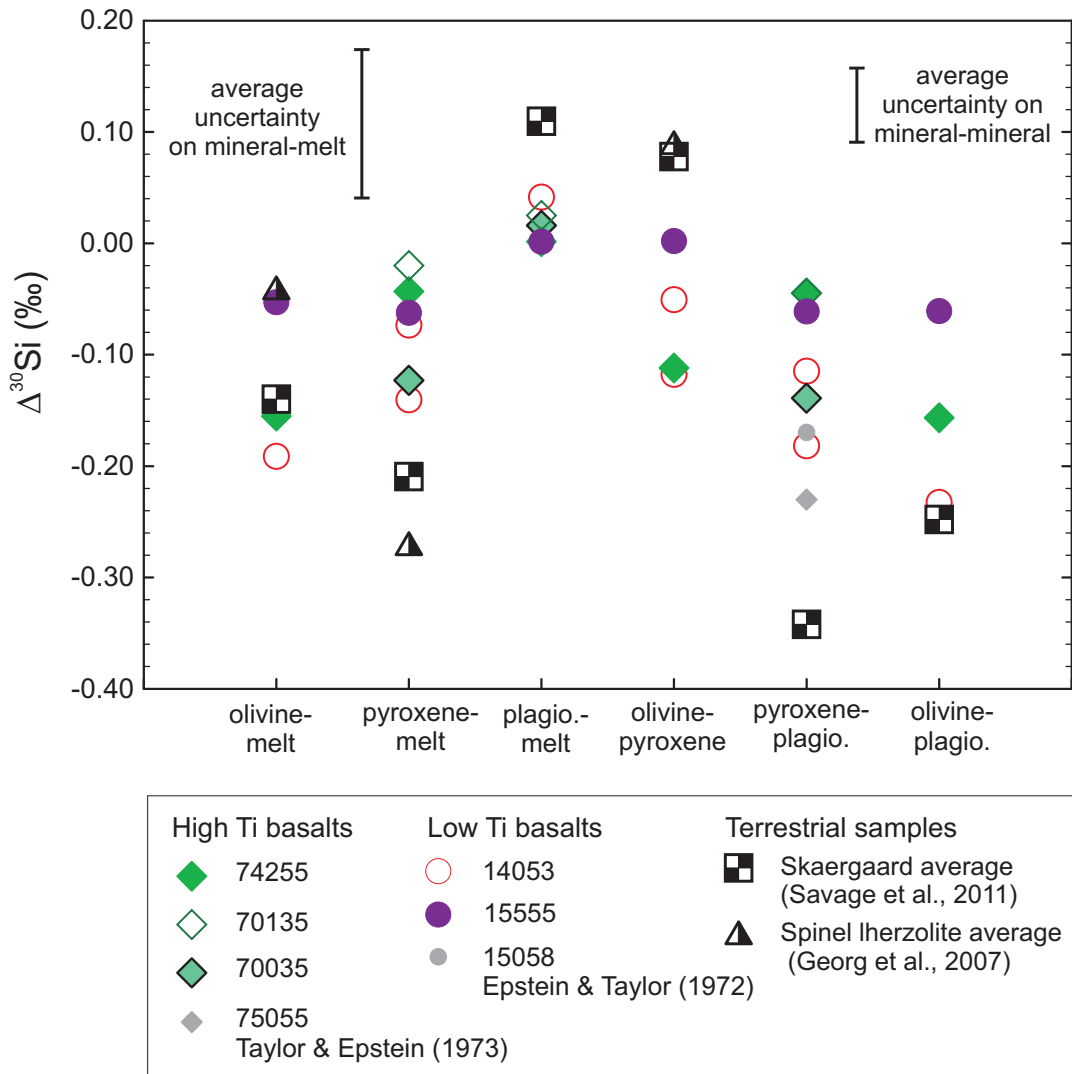


Figure (6.2): $\Delta^{30}\text{Si}_{\text{mineral-mineral}}$ and $\Delta^{30}\text{Si}_{\text{mineral-melt}}$ for lunar mineral separates from Figure 6.1. The $\delta^{30}\text{Si}$ composition of the melt is taken to be the bulk silicate Earth average of -0.29‰ (Savage et al., 2010) as formation of melt does not measurably fractionate Si isotopes (Savage et al., 2010). Average error bars rather than individual ones are plotted for clarity.

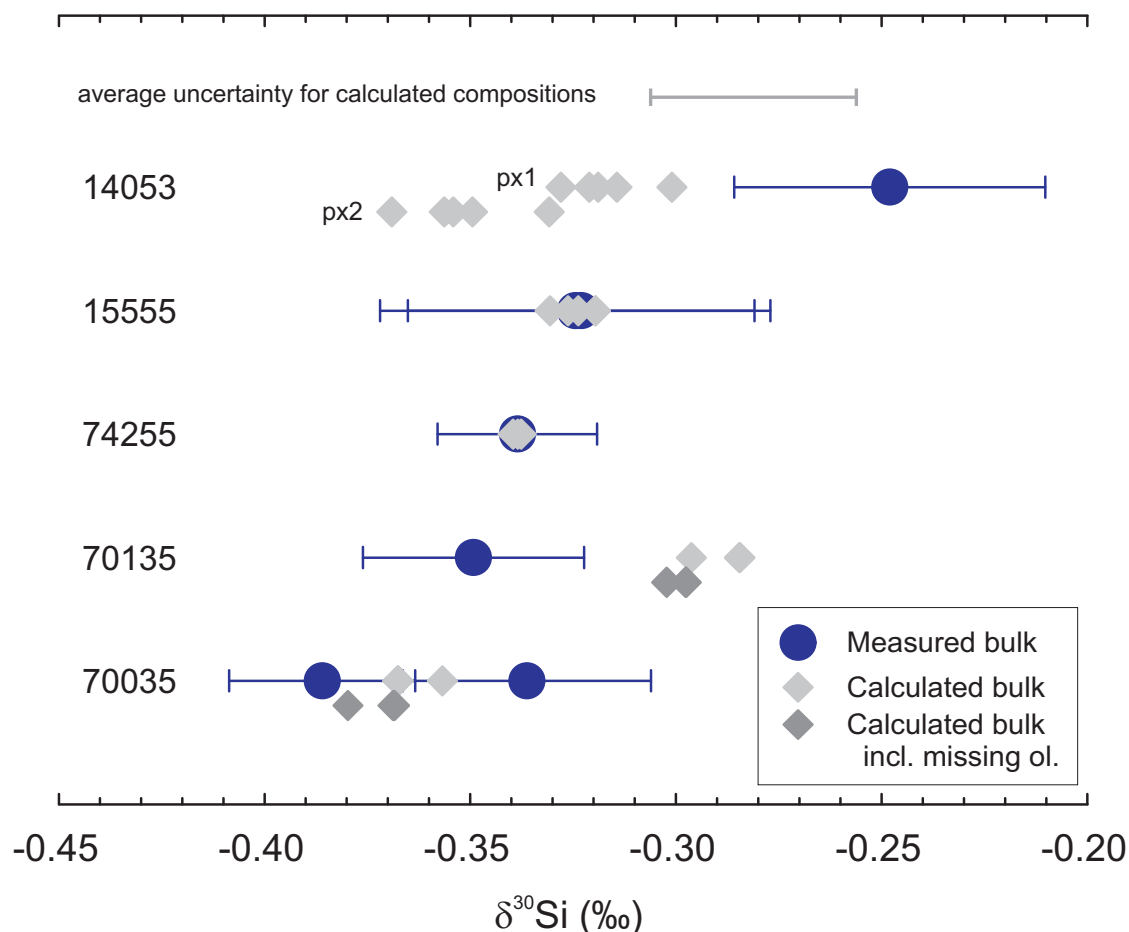


Figure (6.3): Calculated bulk $\delta^{30}\text{Si}$ lunar basalt separates plotted with the measured bulk values. The spread of calculated values for each basalt is from using different literature estimates of modal abundances. px1 and px2 refer to using the two different measured pyroxene $\delta^{30}\text{Si}$ compositions to calculate the bulk. For 70135 and 70035, not enough olivine could be picked for analysis; hence there are two different bulk calculations, one using only pyroxene and plagioclase and the other including an estimated Si concentration and $\delta^{30}\text{Si}$ for olivine. The Si concentrations of the mineral phases came from the measured Si concentrations of the solutions. Modal abundance references: 14053 (Hallis et al., 2010; Gancarz et al., 1971; Patchen and Taylor, 2004); 15555 (Hallis et al., 2010; Longhi et al., 1972; McGee et al., 1977; Heuer et al., 1972; Nord Jr. et al., 1973); 74255 (LSPET, 1973; Dymek et al., 1975; Brown et al., 1975); 70135 (Roedder and Weiblen, 1975; Brown et al., 1975); 70035 (Roedder and Weiblen, 1975; Brown et al., 1975; Weigand, 1973)

Despite this variation in fractionation factors, it does appear that the mineral separates data is internally consistent and there does not appear to be a major Si-bearing phase with an extreme $\delta^{30}\text{Si}$ composition missing (Figure 6.3). The bulk $\delta^{30}\text{Si}$ compositions of the lunar basalts were recalculated from the mineral $\delta^{30}\text{Si}$ data and modal abundances from the literature (see Figure 6.3 caption for details). All the bulk measured $\delta^{30}\text{Si}$ compositions can be recovered within uncertainty,

6.4.1.1 Thermal effects

One of the striking features of Figure 6.1 is the lack of inter-mineral fractionation measured in the low-Ti basalt 15555. This could be related to the thermal history of 15555 as opposed to the other basalts: either that the cooling rate allowed for a different degree of inter-mineral fractionation; or that there was some later thermal metamorphism and re-equilibration of the minerals. However, there is no evidence of post crystallisation metamorphism in this well-studied basalt (e.g. Papanastassiou and Wasserburg, 1973), which rules out that option. The likelihood of any thermal effects playing a role is dependent on the diffusion behaviour of Si. Silicon is known to be a slow diffusing species in minerals, making measurements of the diffusion coefficient relatively tricky (e.g. Chakraborty, 2010). One way to assess whether differing thermal histories played a role in the variation of inter-mineral fractionation within the lunar basalts is to look at the closure temperatures for these phases. Dodson (1973) derived an equation to determine the closure temperature for thermally activated diffusion for a particular cooling rate:

$$T_c = \frac{E}{R \ln \left[\frac{-ART_c^2 D_o}{Ea^2 s} \right]} \quad (6.1)$$

where T_c is the closure temperature, R is the gas constant, E is the activation energy, D_o is the pre-exponential factor diffusion parameter (from $D = D_o e^{-E/RT}$), a is the

characteristic diffusion size, s is the cooling rate and A is a numerical constant based on the geometry; when modelled as a sphere $A = 55$.

Figure 6.4 shows the closure temperatures for Si plotted as a function of cooling rate for the three mineral species for different diffusion sizes. Also plotted are estimated cooling rates for 15555 (Bianco and Taylor, 1977; Walker et al., 1977) and 74255 (Usselman et al., 1975) as well as their liquidus (Grove and Krawczynski, 2009). For olivine and plagioclase, at the range of cooling rates for both rocks, the range of closure temperatures lies well above the liquidus. Cooling rates would have to be on the order of 1-100 K/Myr for there to be significant diffusion of Si, unlike the $\sim 10,000$ K/yr rates that are likely (Usselman et al., 1975; Bianco and Taylor, 1977; Walker et al., 1977). Therefore, the $\delta^{30}\text{Si}$ compositions of olivine and plagioclase are likely to reflect fractionations from the melt composition rather than inter-mineral fractionations during sub-solidus cooling.

Due to the difficulties in analysing Si diffusivities, Béjina and Jaoul (1996), could only constrain the activation energy for diffusion in diopside with quite a large uncertainty, 211 ± 110 kJ/mol. They also suggested that Si may self-diffuse by an interstitial mechanism, which would be dependent on oxygen fugacity, and hence calculated such a “corrected” activation energy of 280 kJ/mol. In Figure 6.4, the lower limit of the activation energy and the “corrected” value are both plotted for illustration. What is noticeable is that if the lower limit of the activation energy is used and a characteristic diffusion scale of 0.1 mm, the cooling rate of 15555 does intersect the closure temperature curve of pyroxene. However as olivine and plagioclase have much higher closure temperatures, it is unlikely to lead to any significant inter-mineral diffusion of Si.

Estimated cooling rates for the Skaergaard samples are in the order of ~ 1 K/kyr (Ganguly and Domeneghetti, 1996) and recent estimates of the liquidus temperature are $< 1250^\circ\text{C}$ (Thy et al., 2009). Again, the closure temperature curves for the

Table (6.2): Diffusion data for Si in olivine, plagioclase and diopside

Phase	D_o (m ² /s)	E (kJ/mol)	Ref.
Olivine	6.31×10^{-5}	338 ± 14	Dohmen et al. (2002)
Plagioclase (An ₉₃)	3.79×10^{-7}	465 ± 50	Cherniak (2003)
Diopside	3.79×10^{-7}	211 ± 110	Béjina and Jaoul (1996)
		280	“corrected” value

mineral phases only intersect at the 0.1mm diffusion scale, if at all. Hence the $\delta^{30}\text{Si}$ compositions of the Skaergaard samples are also probably reflecting mineral-melt fractionations rather than the inter-mineral fractionation exchange.

The limited fractionations displayed by the mineral separate data from 15555 still needs to be explained. Examining the data in Figure 6.1 more closely, it is apparent that the olivine is the mineral phase that is the least consistent with the other basalts. One attractive explanation would be that the olivine in this sample is xenocrystic, that is represents fractionation from a different liquid $\delta^{30}\text{Si}$ composition and has later been entrained. For 15555, however there does not seem to be any evidence to suggest that it contains any significant amount of accumulated olivine (e.g. Walker et al., 1977; Ryder and Schuraytz, 2001). Hence, the limited inter-mineral fractionation observed in 15555 is yet to be fully explained.

6.4.2 Variation between terrestrial and lunar mineral-melt fractionation factors

The key question raised by the mineral separates data is what could account for the difference in direction of offset of olivine-pyroxene between the terrestrial and lunar samples.

Figure 6.2 shows calculated mineral-liquid fractionation factors in addition to the inter-mineral fractionation factors. The melt Si isotope composition has been taken to be the $\delta^{30}\text{Si}$ of bulk silicate Earth (BSE) $-0.29 \pm 0.08\%$ from Savage et al. (2010)

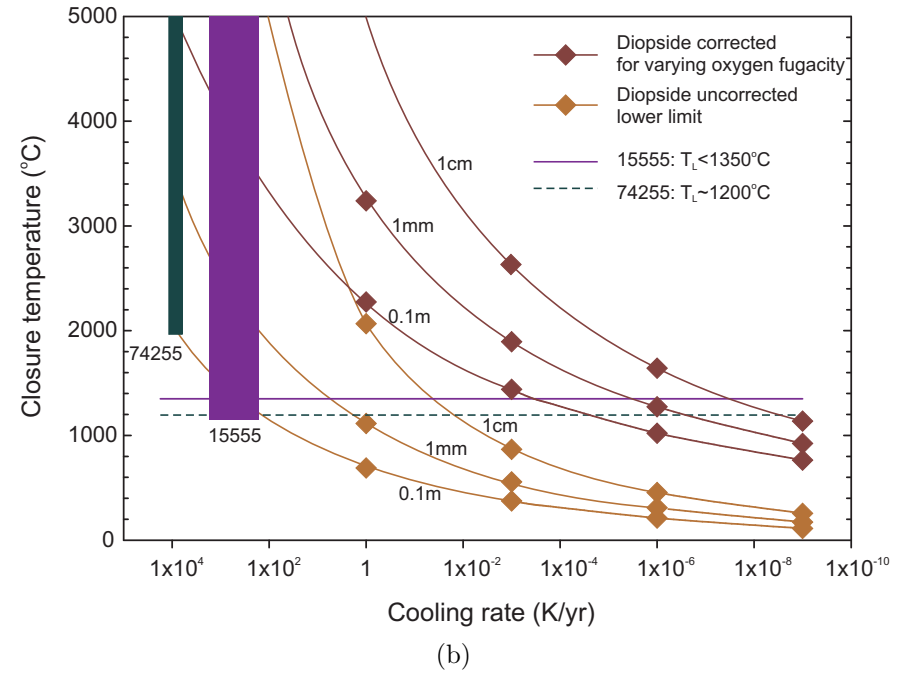
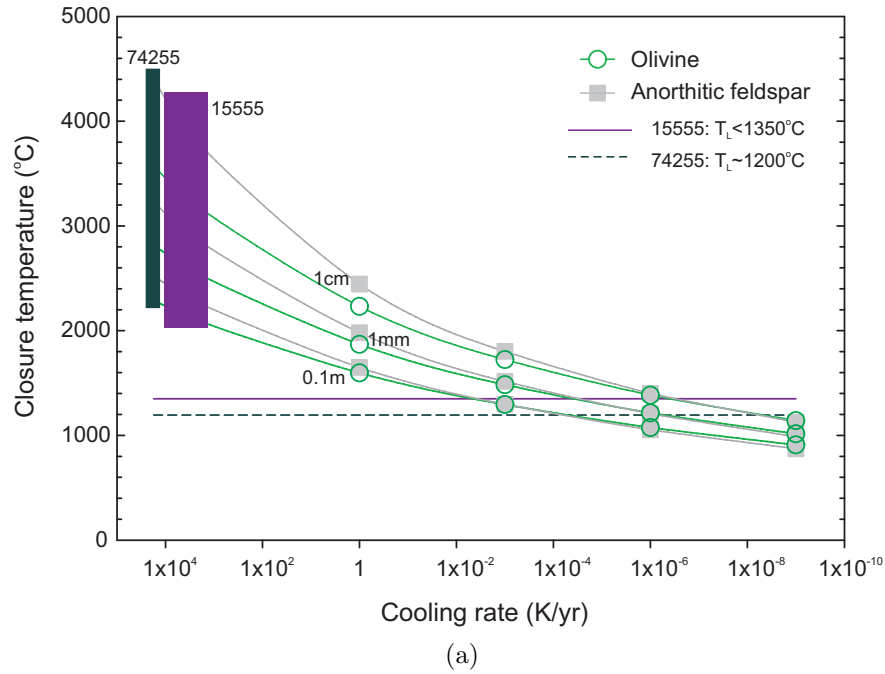


Figure (6.4): Closure temperatures for Si plotted as a function of cooling rate. The contours are from different values of a , the characteristic diffusion size, in metres. The rectangles are estimated cooling rates from the literature (see text for details), and T_L is the liquidus temperature. (a) Closure temperature curves for olivine and anorthitic feldspar. (b) Closure temperature curves for diopside. Both sets of curves are based on diffusion data from B ejina and Jaoul (1996), but one uses their postulated corrected activation energy based on the fact that varying oxygen fugacity may have an effect on the diffusion of Si in diopside

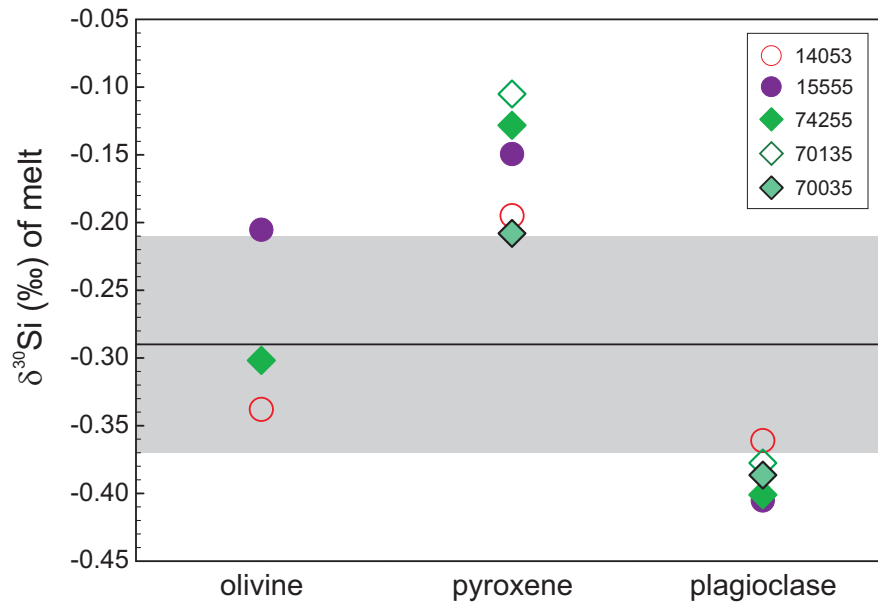


Figure (6.5): $\delta^{30}\text{Si}$ of melts in equilibrium with the mineral $\delta^{30}\text{Si}$ compositions using fractionation factors calculated from the Skaergaard mineral data (Savage et al., 2011). The black line is $\delta^{30}\text{Si} = -0.29\text{‰}$, the mean composition of bulk silicate Earth. The grey band is the $2\sigma_{SD}$ uncertainty on this composition. The error bars on the plotted melt compositions are $\sim \pm 0.05\text{‰}$

as in that study they showed that melting does not fractionate Si isotopes. This is also taken to be the melt composition for the lunar basalts based on the similarity of the lunar average to the BSE $\delta^{30}\text{Si}$ composition (See Chapter 5). The direction of the mineral melt fractionations are consistent between the lunar and terrestrial studies; however there is still significant discrepancy in the magnitude of the fractionation factors.

This could either result from crystallisation and removal of early formed phases in the mare basalts, or it could be that the inter-mineral $\delta^{30}\text{Si}$ fractionation factors are different in lunar settings. These two possibilities are explored in greater detail in the subsequent sections.

6.4.2.1 Crystallisation of the lunar basalts

Figure 6.5, shows the calculated $\delta^{30}\text{Si}$ melt compositions that are in equilibrium with the measured lunar mineral compositions assuming the Skaergaard mineral-liquid fractionation factors calculated from the Skaergaard data of Savage et al. (2011). The first thing to note is that the olivine-melt compositions are within uncertainty of the BSE $\delta^{30}\text{Si}$ for the initial melt composition. This is consistent with olivine being the first crystallising phase from a mare basalt source possessing a Si isotopic composition similar to that of BSE. This in turn would imply limited to no fractional crystallisation and removal from these basalts, which is consistent with the interpretation for some of the samples (e.g. Walker et al., 1977). The pyroxene data is not consistent with this interpretation, as somewhere between 45 – 75% fractional crystallisation of olivine is required to generate the liquid compositions associated with the pyroxene (-0.11 to -0.21%) from an initial source composition of $\delta^{30}\text{Si} = -0.29\%$. Therefore, previous fractionation crystallisation of olivine for these mare basalts is not sufficient to generate the difference in the direction of the olivine-pyroxene offset in $\delta^{30}\text{Si}$ between the terrestrial and lunar samples.

If the Rayleigh evolution curves for the mineral ($\delta^{30}\text{Si}_{melt} = \delta^{30}\text{Si}_0 - \epsilon_{melt-min.} \ln f$) and melt ($\delta^{30}\text{Si}_{min.} = \delta^{30}\text{Si}_{melt} - \epsilon_{melt-min.}$) compositions are plotted for olivine and pyroxene, there is a crossover in the composition of the instantaneous phase (Figure 6.6). This crossover is absent if plagioclase is crystallising in a 50:50 ratio with the pyroxene, affecting the melt composition. We know plagioclase only appears late on the liquidus for the lunar basalts, which is not the case for the Skaergaard samples (e.g. Wager, 1960), and therefore might shed some light on why the lunar olivines are lighter than the pyroxenes. However, as this only happens at very high crystallisation fractions ($>60\%$) it is unlikely to explain the fact that the Si isotopic compositions of pyroxene are heavier than those in olivine in these lunar basalts.

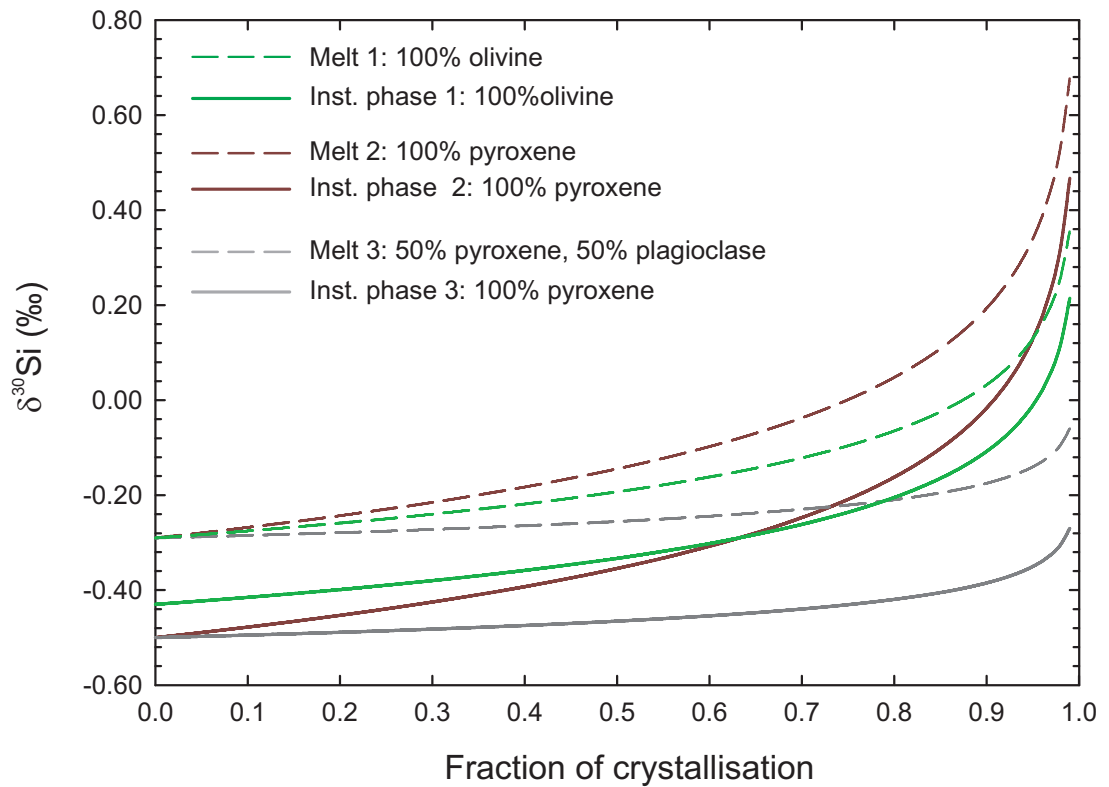


Figure (6.6): Rayleigh fractionation curves for olivine and pyroxene and the corresponding melt $\delta^{30}\text{Si}$ compositions. For melt 3, the melt $\delta^{30}\text{Si}$ evolution was calculated with a fractionation factor $\Delta^{30}\text{Si}_{\text{melt-mineral}} = 0.5\epsilon_{\text{plag.}} + 0.5\epsilon_{\text{pyx.}}$, where $\epsilon_{\text{plag.}}$ and $\epsilon_{\text{pyx.}}$ are the Skaergaard melt-mineral fractionation factors from Savage et al. (2011). The corresponding instantaneous phase curve for Melt 3 is calculated with a fractionation factor of $\epsilon_{\text{pyx.}}$.

6.4.2.2 Different lunar fractionation factors

In the preceding section, it was assumed that the Skaergaard fractionation factors (Savage et al., 2011) are the “true” mineral-melt $\delta^{30}\text{Si}$ fractionation factors. As shown above however, the Skaergaard fractionation factors cannot be used satisfactorily to explain the measured lunar mineral $\delta^{30}\text{Si}$ compositions in terms of their likely crystallisation history. Therefore, the simplest conclusion is that the inter-mineral fractionations are different in lunar settings. It may not, perhaps, be surprising that the mineral $\delta^{30}\text{Si}$ compositions of lunar basalts and a terrestrial layered intrusion show some variation, despite having similar $\delta^{30}\text{Si}$ source compositions. It is unfortunate that at present, no high precision $\delta^{30}\text{Si}$ data exist for mineral separates from terrestrial basalts. If they did, there would be the potential to distinguish between $\delta^{30}\text{Si}$ variations due simply to basalt formation and those variations related to the different basalt forming environments existing on the Earth and Moon.

The main problem with citing different fractionation behaviours in terrestrial and lunar settings is providing any obvious physical basis. The primary issue is explaining why lunar olivines have lighter $\delta^{30}\text{Si}$ compositions than pyroxenes in direct contrast to the terrestrial mineral data (Table 6.1). The terrestrial data are consistent with the theoretical calculations that predict a positive fractionation factor between olivine and pyroxene (Méheut et al., 2009). These calculations are based on density-functional theory (DFT), and as such should not be different for terrestrial and lunar settings.

The mare basalts are thought to have experienced much lower oxygen fugacities than their terrestrial counterparts ($\Delta\text{IW}-2$ to ΔIW) (e.g Taylor, 1982; Papike et al., 2005). This could potentially alter $\delta^{30}\text{Si}$ fractionation factors in lunar settings if some of the Si partitioned into the Fe metal that is present in many of the samples (Taylor, 1982). However, the pressures are not high enough for this to be a significant effect at these oxygen fugacities (Ziegler et al., 2010). If changes in inter-mineral partitioning behaviour were linked in some way to the presence of phases such as ilmenite in the

lunar basalts, one would expect to see significant variations between low-Ti and high-Ti basalts. Table 6.1 shows that this is not the case. It is clear more data in the form of Si isotopic composition of terrestrial basalt mineral separates and also some experimental investigation is needed to fully understand the lunar mineral $\delta^{30}\text{Si}$ data.

6.4.3 Lunar magma ocean and source variation in $\delta^{30}\text{Si}$?

The mare basalt source is thought to reflect the complementary cumulates to the anorthositic crust (e.g. Papike et al., 1998), and plagioclase shows up to $\sim 0.11\%$ offsets relatively to $\delta^{30}\text{Si}_{\text{BSE}}$ (Figure 6.2). Yet bulk $\delta^{30}\text{Si}$ compositions of the lunar basalts and anorthosites do not show any resolvable variation (see Chapter 5). They are, however, slightly heavier ($\delta^{30}\text{Si}_{\text{FAN}} = -0.25 \pm 0.08\%$, $\pm 2\sigma_{SD}$) relative to the bulk lunar mantle (basalts and glasses) $\delta^{30}\text{Si}$ composition ($\delta^{30}\text{Si} = -0.30 \pm 0.08\%$ $\pm 2\sigma_{SD}$), which could indicate some faint lunar magma ocean (LMO) differentiation signature. Starting from a melt with an initial BSE $\delta^{30}\text{Si}$ composition (-0.29% Savage et al., 2010), and melt-plagioclase fractionation factors from Savage et al. (2011) ($\Delta^{30}\text{Si}_{\text{melt-min.}} = 0.11$) and the maximum from this study ($\Delta^{30}\text{Si}_{\text{melt-min.}} = 0.04$), it is clear that $\delta^{30}\text{Si}_{\text{inst.}}$ and $\delta^{30}\text{Si}_{\text{accm. prod.}}$ are consistent with the range in bulk anorthosites for most degrees of fractionation of plagioclase (green and red curves in Figure 6.7). Therefore, the unresolvable degree of offset between the LMO-formed anorthosites and the basalts derived from their complementary cumulates is consistent with the measured inter-mineral fractionation for $\delta^{30}\text{Si}$. The actual proportion of the lunar magma ocean removed into the crust as anorthosite is likely to be in the range of 13%, based on Al constraints from Warren (1985). For the curves calculated using $\Delta^{30}\text{Si}_{\text{min.-melt}} = 0.11$, the region $< 20\%$ crystallisation is where $\delta^{30}\text{Si}_{\text{inst.}}$ and $\delta^{30}\text{Si}_{\text{accm. prod.}}$ are heavier than the BSE range (defined by the two black solid lines), but still within the range of bulk anorthosites (grey horizontal band). Using the maximum $\Delta^{30}\text{Si}_{\text{min.-melt}}$ from this study, the plagioclase $\delta^{30}\text{Si}$ composition is never

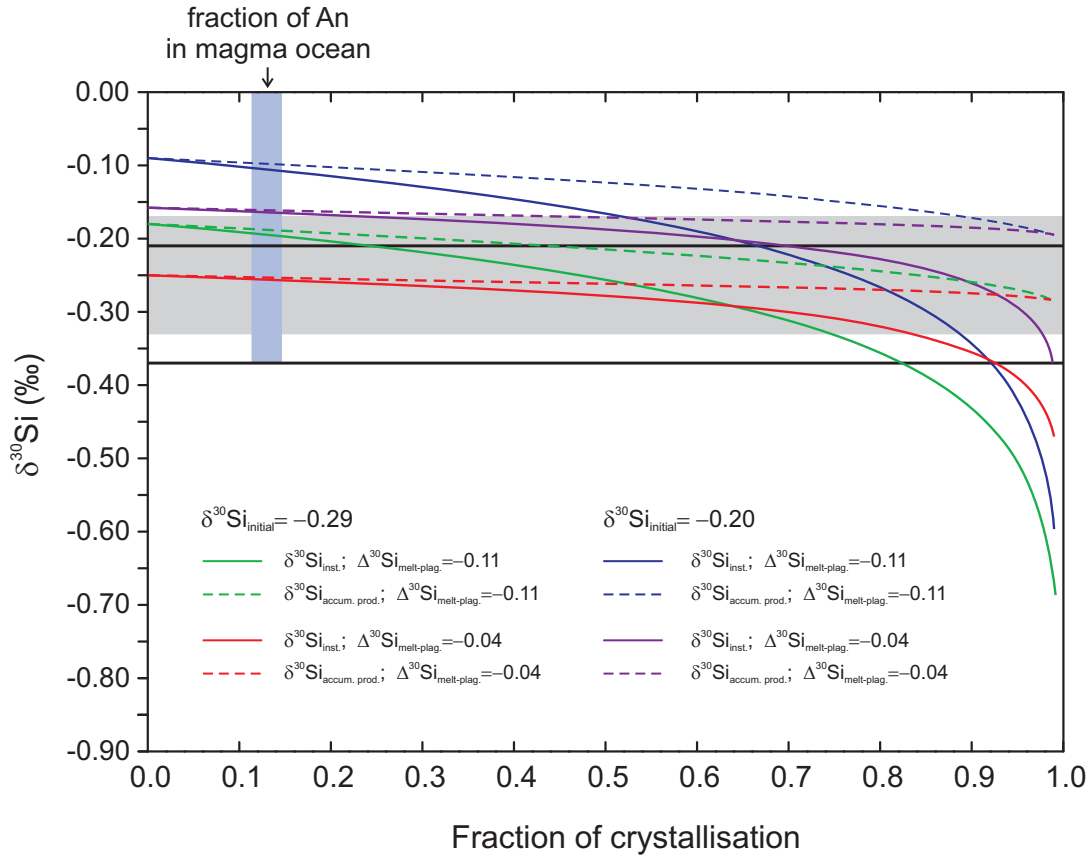


Figure (6.7): Plagioclase fractionation in the LMO. The fraction of An (anorthosite) in the magma ocean is estimated from data from Warren (2005). $\Delta^{30}\text{Si}_{\text{min.-melt}} = 0.11$ is from Savage et al. (2011) and $\Delta^{30}\text{Si}_{\text{min.-melt}} = 0.04$ is the maximum melt-plagioclase offset from this study. The solid curves are the $\delta^{30}\text{Si}$ composition of the instantaneous plagioclase crystallising from a melt with the specified initial $\delta^{30}\text{Si}$ composition. The dashed lines are the accumulated or integrated plagioclase. The grey band is the $2\sigma_{SD}$ envelope on the average of the bulk anorthosites (data from Chapter 5). The black horizontal lines are the $2\sigma_{SD}$ envelope for the $\delta^{30}\text{Si}$ of the bulk silicate Earth (=bulk Moon)

heavier than the BSE (bulk moon range). This could imply that in the LMO, the $\Delta^{30}\text{Si}_{\text{min.-melt}}$ fractionation factors for plagioclase were closer to what is observed in Skaergaard than what is recorded for the lunar basalts.

In the scenario above, the initial $\delta^{30}\text{Si}$ of the melt at the time of plagioclase crystallisation was taken to be that of BSE or of the bulk Moon due to the Giant Impact. However, plagioclase is only thought to have appeared in the crystallisation sequence of the LMO after 70-80% crystallisation of olivine and pyroxene (Snyder et al., 1992). This much fractional crystallisation of the mafic minerals would drive the $\delta^{30}\text{Si}_{\text{initial melt}}$ to compositions on the order of 0‰. As is clear in Figure 6.7, even at an initial $\delta^{30}\text{Si}$ of only -0.20‰ the plagioclase compositions no longer fall within the range of the measured anorthosites. This points perhaps to a more complex story for $\delta^{30}\text{Si}$ in the LMO, than this simple fractionation model.

6.5 Conclusions

The $\delta^{30}\text{Si}$ compositions of plagioclase, pyroxene and olivine (where present) separates from five lunar basalts were measured. Plagioclase was consistently the heaviest phase measured with an average $\delta^{30}\text{Si}$ of $-0.27 \pm 0.04\text{‰}$. The mafic mineral were heavier and more variable in composition with $\delta^{30}\text{Si}_{\text{pyroxene}} = -0.43 \pm 0.14\text{‰}$ and $\delta^{30}\text{Si}_{\text{olivine}} = -0.37 \pm 0.09\text{‰}$. The $\delta^{30}\text{Si}$ compositions of the mafic minerals from the lunar basalts analysed here did not reflect the same direction of offset between the olivine and pyroxene as recorded by Skaergaard mineral separates (Savage et al., 2011).

The slow diffusion rate and consequent high closure temperatures of Si in minerals makes it unlikely that any of the variation in $\delta^{30}\text{Si}$ observed in phases between lunar basalts, or between terrestrial and lunar samples, is linked to variable cooling rates. The $\Delta^{30}\text{Si}_{\text{mineral-melt}}$ fractionation factors for olivine are relatively consistent between the different samples, confirming the similarity in $\delta^{30}\text{Si}$ composition of the mare basalt

source and that of bulk silicate Earth. This is not the case for pyroxene, which would require extensive early crystallisation and removal of olivine for which there is no strong evidence in these samples (e.g. Walker et al., 1977). With thermal diffusive effects being ruled out and no clear effects related to crystallisation history, the most likely interpretation is that fractionation factors for $\delta^{30}\text{Si}$ are different on the Moon. Whether this would apply to different isotopic systems is something that would need to be investigated further. However, there is the caveat that the Si isotopic comparison so far has not been on products of similar terrestrial and lunar settings but between mineral separates from layered intrusion and from erupted basalt.

The lack of currently resolvable differences between the $\delta^{30}\text{Si}$ composition of the bulk anorthosites and the lunar basalts, despite the large-scale differentiation of the lunar magma ocean, is consistent with the measured $\Delta^{30}\text{Si}_{\text{melt-mineral}}$ from both the terrestrial and lunar settings.

Chapter 7

Silicon isotopic variation in chondrules: evidence of nebular formation

7.1 Introduction

Chondrites are essentially “cosmic sediments” (Sears, 2004), being as they are, aggregates of a number of different components (refractory inclusions, chondrules, matrix) of differing ages and genesis. Isotopic analyses of bulk chondrites represent a cumulative average of all the fractionating processes these particles have undergone. Through analysis of populations of the individual components, there is the potential to acquire more specific information about nebular and parent-body processes.

Refractory CAIs (calcium aluminium inclusions) make up to a few vol% in chondrites and are generally accepted to be the oldest known solids in the solar system (e.g. Amelin et al., 2002). Initially thought to be primitive condensates from a gas of solar nebula composition, many are now recognised as having complex histories including many episodes of melting and modification due to interactions with gases or liquids in the nebula or on asteroids (e.g. MacPherson, 2003). Many CAIs display strong positive correlations between the mass dependent fractionations of $\delta^{30}\text{Si}$ and $\delta^{25}\text{Mg}$ consistent with evaporation fractionation processes (Clayton et al., 1988). The levels of enrichment in the heavy isotopes is similar to what has been observed

in laboratory experiments (Davis et al., 1990; Wang et al., 2001), implying that for this type of CAI the bulk isotope systematics of Mg and Si are fairly well understood in terms of formation processes. This is not the case for chondrules, however.

Chondrules are the dominant constituent in chondrites (Brearley and Jones, 1998; Sears, 2004; Scott, 2007). Chondrules are slightly younger than CAIs (e.g. Amelin et al., 2010) and appear to represent solidified partial or completely molten 0.1 – 1mm sized silicate spherules (e.g. Sears, 2004). They consist predominantly of ferromagnesian silicate material (olivine, pyroxene and feldspathic mesostasis) (Brearley and Jones, 1998) and are thought to have cooled in a matter of hours, making it unlikely they were cooling in free space (e.g. Desch and Connelly, 2002).

There are numerous theories to explain the origin of chondrules (see reviews by Boss, 1996; Sears, 2004), which can be broadly divided into two groups: nebular models and planetesimal models. The nebular theories include lightning discharge or shock waves to melt the dust in the early solar nebula. Impact melts or volcanism related processes are the primary contenders among planetary models. The nebular models appear to be currently favoured (e.g. Ciesla and Hood, 2002; Cuzzi and Alexander, 2006; Krot et al., 2009); though the debate is far from over (e.g. Asphaug et al., 2011).

For a number of isotope systems such as K (Alexander et al., 2000), Fe (Zhu et al., 2001) and Mg (Galy et al., 2000), bulk chondrules show relatively limited fractionations ($< 1\text{‰ amu}^{-1}$), particularly when compared with igneous CAIs ($\sim 5\text{‰ amu}^{-1}$). The chondrule fractionations are not just simple isotopic variations arising tied to variations in chondrule composition. Their isotope compositions cannot be linked to simple evaporation residues from a gas of solar composition unlike CAIs (e.g. Davis et al., 2005). The isotopic composition of an individual chondrule, however, could be the result of one or more than one fractionation event. The possible mechanisms to generate isotopic fractionation in chondrules include (i) closed system formation

from isotopically heterogeneous (though still mass-dependent) precursor material; (ii) fractionation during chondrule formation (whether nebular or planetesimally based); (iii) secondary alteration processes, on the chondrite parent body or in the nebula, that are either aqueous or thermally metamorphic in nature. For example, in studies of $\delta^{25}\text{Mg}$ of Allende chondrule, evidence for secondary alteration causing isotopic variation has been identified (Young et al., 2002a); as well as variation resulting from suppressed isotopic fractionation during evaporation within the nebula (Galy et al., 2000). The limited fractionation in the isotopes of the moderately volatile K have been explained by equilibration with the evaporated gas (Alexander et al., 2000). The Mg and K isotopic data are in line with open system behaviour during chondrule formation, rather than closed system behaviour as advocated by Grossman and Wasson (1982).

The gas-source mass spectrometry Si isotopic data of Clayton et al. (1991) for chondrules, also showed a limited isotopic range, $\delta^{30}\text{Si} \sim 1.9\text{‰}$, compared to CAIs, $\delta^{30}\text{Si} \sim 20\text{‰}$ (Clayton et al., 1988). They did not observe any simple correlations of $\delta^{30}\text{Si}$ with chondrule texture, mineralogy or size. However, the chondrule range in $\delta^{30}\text{Si}$ was somewhat greater than the range in bulk chondrites measured by Molini-Velsko et al. (1986) ($\delta^{30}\text{Si} \sim 1.2\text{‰}$), using similar analytical methods. The external precision at that time, using SiF_4 as the analyte, was $\pm 0.4\text{‰}$ ($2\sigma_{SD}$). Modern multi-collector inductively-coupled-plasma mass spectrometry (MC-ICPMS) and alkali fusion preparation methods currently have an external precision for meteoritic samples of $\sim \pm 0.15\text{‰}$, ($2\sigma_{SD}$) (e.g. Georg et al., 2007a; Fitoussi et al., 2009; Chakrabarti and Jacobsen, 2010b; Ziegler et al., 2010; Armytage et al., 2011). These studies have focussed primarily on the the Si isotopic composition of bulk meteorites, and the total range in $\delta^{30}\text{Si}$ composition of bulk meteorites across all these studies was only $\sim 0.5\text{‰}$. This is approximately a factor of four smaller than the range found by Molini-Velsko et al. (1986), and it may be that chondrule $\delta^{30}\text{Si}$ range of Clayton et al. (1991) is

similarly inflated.

There is a limited amount of high-precision Si isotopic data from chondrules. Georg et al. (2007a) analysed four chondrules from the LL3 chondrite Chainpur. The range of $\delta^{30}\text{Si}$ compositions they found was -0.24‰ to -0.75‰ ; by contrast the range of Si compositions of their bulk meteorite samples was -0.50‰ to -0.70‰ . The data from Hezel et al. (2010), analysed in Oxford, seemed to confirm that this large range was not unique to chondrules from ordinary chondrites with measurements of $\delta^{30}\text{Si}$ of a number of chondrules from the CV3 meteorites Mokoia and Grosnaja with a range in compositions of $+1.11\text{‰}$ to -0.36‰ . However, the number of chondrules from an individual meteorite was still limited with only three from Grosnaja and four from Mokoia.

The aim of this study was to investigate the extent and cause of Si isotopic variability in chondrules. One focus was to determine how consistent the greater $\delta^{30}\text{Si}$ variability in chondrules relative to chondrites was, and whether this variability was the result of precursor heterogeneities or open system chondrule formation with suppressed isotopic fractionation. To this end we analysed a series of bulk chondrules from the CV3 meteorite Allende as well as other components from the same sample for their $\delta^{30}\text{Si}$ and major element composition.

7.2 Method

The CV3 carbonaceous chondrite Allende was chosen for analysis as it is a well studied meteorite with a large grain size (up to few mm). We also had some chondrule and CAI sample solutions from other CV3 chondrites, Grosnaja and Mokoia, where the Si isotopic composition had been previously determined in Oxford (Hezel et al., 2009; Hezel et al., 2010), and which were also analysed for their elemental concentrations. This would allow for comparison of the variation in the components of different

meteorites in the same carbonaceous chondrite group.

7.2.1 Sample preparation

An Allende fragment of approximately 7g from cut USNM 3937, was lightly struck by an alumina pestle, while sitting in a cleaned alumina mortar. The rock dust that was produced was transferred to a clear petri dish and the chondrules were handpicked under a binocular microscope using steel tweezers. Occasionally the edge of a steel spatula was used to remove any adhering matrix. One matrix sample (05r) was collected in this way. Only large ($> 2\text{mg}$) chondrules were picked due to the minimum mass requirements for isotopic and elemental analysis and petrological examination. Light coloured irregular shaped inclusions were also picked from the rock dust. Some $\sim 2\text{g}$ of the rock dust was powdered further (prior to picking) in order that a bulk sample of this particular Allende fragment could be analysed.

The individual picked components were then split into two fragments. This was accomplished using a light tap from a much smaller alumina pestle. Often the component would split into more than one fragment; in this case the best looking part would be preserved for mounting and petrological examination and the other fragments, making up at least 1mg, were used for the isotopic and elemental analysis. This method obviously has its limitations as there is no guarantee of the homogeneity of the chondrule or refractory inclusion so linking the solution and any SEM data must be done with care.

The four Mokoia chondrules that were newly analysed in this study were separated, in a very similar procedure, by Dominik Hezel in the manner described in (Hezel et al., 2010).

7.2.2 Petrological examination

Acrylic mounts of all of the picked Allende components, except for the matrix sample 05r, were prepared for petrological examination under the SEM. There was not enough sample to make a mount for 05r, and also the nature of the material meant that it would be very hard to properly polish. The petrological analysis was primarily qualitative in nature as “bulk” elemental analyses are hard to collect from mounted samples.

The mounted samples were examined under the SEM (scanning electron microscope). Backscatter electron images were collected using the JEOL JSM-840A scanning electron microscope at the University of Oxford, equipped with a Tetra backscatter electron detector. To determine the major phases present in the chondrules an Oxford Instruments Isis 300 energy-dispersive analytical system, which gives spatial resolution near $1\mu\text{m}$, was used in conjunction with the detector.

7.2.3 Isotopic and elemental analysis

The fragments of the individual Allende components that were not used for petrographic examination were put into solution using the fusion method outlined in Chapter 2. Aliquots of these solutions were analysed for their Si isotope composition and major element concentration. The Si isotope composition was measured using MC-ICMS and the Si concentration was analysed by photospectrometry according to the procedure in Chapter 2. The primary advantage of using solution mass spectrometry for the isotopic analysis over in-situ techniques is the precision. Our current external reproducibility for $\delta^{30}\text{Si}$ is $\pm 0.15\text{‰}$ ($2\sigma_{SD}$), whereas LA-MC-ICPMS is $\pm 0.40\text{‰}$ ($2\sigma_{SD}$) (Shahar and Young, 2007), SIMS is on the order of $\pm 0.52\text{‰}$ ($2\sigma_{SD}$) (Knight et al., 2009b) and UV-femtosecond LA-MC-ICPMS is $\pm 0.24\text{‰}$ ($2\sigma_{SD}$) (Chmeleff et al., 2008). However, any evidence of internal fractionation, which can inform any evaporation or condensation history, is lost with solution chemistry.

The Mg, Al, Fe and Ca concentrations of the solutions were analysed by inductively-coupled-plasma mass-spectrometry. Aliquots of the solutions (already diluted by ~ 500 during preparation) were diluted by 1000 for Mg, Al, Fe and by 100 for Ca and run on the Thermo Finnigan Element 2 ICP-MS in medium resolution mode at the University of Oxford. Hence the Mg, Al and Fe data were collected in a separate run to the Ca data for samples. ^{115}In was used as an internal standard. Standard addition was used on one sample (a bulk meteorite sample in each case) in each run, in order to ensure the calibration curve was corrected for the sample matrix. A number of blank spikes were also run to give a measure of the reproducibility, and the 2RSD for the elemental concentrations were: Mg=2.8%, Al=4.9wt%, Fe=3.1% and Ca=1.9%. A total procedural blank was also analysed and the concentrations were corrected appropriately. The blank levels were: 16ppb Mg, 750ppb Al, 6.5ppb Fe and 367ppb Ca.

Chondrules and CAIs from samples other than Allende were also analysed for their major element concentrations. The Mokoia chondrules m-a, m-c, m-e and m-f that had not been previously analysed for their Si isotopic composition were treated in the exact manner as the Allende samples, excepting the removal of a fragment for petrological examination. In addition, the solutions of one chondrule and one CAI from Grosnaja, and two chondrules and one CAI from Mokoia, which had been analysed for their Si isotopic composition by us in Oxford for previous studies (Hezel et al., 2009; Hezel et al., 2010), were analysed for their major element concentrations.

7.3 Results

The Si isotopic composition of ten chondrules, one CAI, four unclassified inclusions, and one matrix sample from Allende, and four chondrules from Mokoia were newly determined in this study. Major element concentration data were collected for all

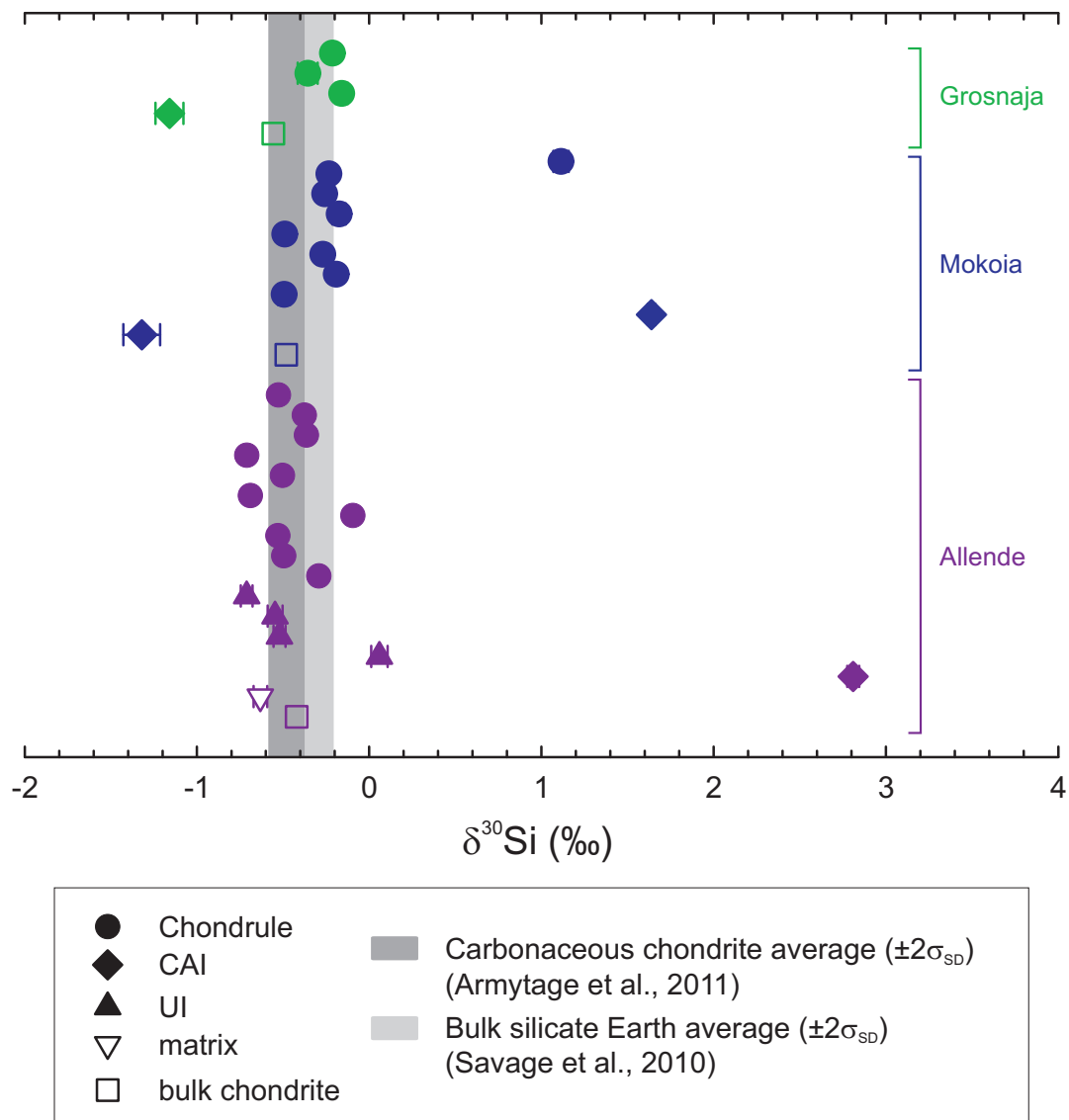


Figure (7.1): $\delta^{30}\text{Si}$ of CV3 chondrite components. All the samples analysed were mass dependent so only $\delta^{30}\text{Si}$ is plotted. All the Allende data are from this study as are four of the Mokoia chondrules (see Table 7.1 for details). The bulk Grosnaja and Mokoia data are from Armytage et al. (2011) or chapter 4. The remaining Grosnaja and Mokoia data are from Hezel et al. (2009) and Hezel et al. (2010). The error bars are $2\sigma_{SEM}$, which is most cases is smaller than the data symbol. The darker grey bar is the carbonaceous chondrite average from Armytage et al. (2011) (same as in chapter 4), which is the same as the meteorite average (same references), but with an uncertainty of $2\sigma_{SEM} = \pm 0.10$, rather than $2\sigma_{SEM} = \pm 0.13$.

these samples as well as for one chondrule and one CAI from Grosnaja and two chondrules and two CAIs from Mokoia where the Si isotopic composition had been measured in previous studies (Hezel et al., 2009; Hezel et al., 2010). Major element data were also collected for bulk samples of Allende, Mokoia and Grosnaja, and in the case of Mokoia and Gronaja the bulk $\delta^{30}\text{Si}$ compositions are from Armytage et al. (2011). Figure 7.1 plots the Si isotopic data for all the samples and Figure 7.4 shows $\delta^{30}\text{Si}$ plotted against Mg, Si, Al, Ca and Fe for the samples for which the elemental composition was analysed.

7.3.1 Petrological examination

Backscatter electron images were taken of fifteen of the components picked from Allende (Figure 7.2). Qualitative EDS spectra were collected to check mineralogy. The majority of the chondrules show the effects of some degree of recrystallisation. Two of the chondrules (04a and 05o) are porphyritic olivine and pyroxene chondrules and two are barred olivine chondrules (04b and 05p). Four of the chondrules (04c, 04e, 04g and 05q) are porphyritic olivine chondrules with significant amounts of Fe-metal. The classification of 04f and 04d as to type of chondrule is less straight forward. 04f is very fine grained with the mineralogy dominated by pyroxene and 04d could probably be classified as a radial pyroxene chondrule. The mounting, however was not ideal. 05m is a moderately coarse grained CAI with an igneous appearance (as opposed to “fluffy”). The nature of 04jh, 04j, 04k and 05l is less clear. During picking, their pale colour and irregular appearance suggested that they were CAIs. However, the mineralogy appeared to be dominated by olivine. It could be that they are amoeboid olivine aggregates (AOAs), but the olivine grains in these are typically $< 20\mu\text{m}$ (e.g. Scott and Krot, 2007). The finer grained 04j could therefore potentially be an AOA, but the other olivine inclusions need further investigation. They are therefore henceforth referred to as UIs (unidentified inclusions).

Table (7.1): Silicon isotope and elemental data from CV3 meteorites

Sample	Type	$\delta^{30}\text{Si}$ (‰)	$2\sigma_{SEM}$	$\delta^{29}\text{Si}$ (‰)	$2\sigma_{SEM}$	N	Mg (wt%)	Al (wt%)	Si (wt%)	Ca (wt%)	Fe (wt%)
Grosnaja											
<i>I</i>	<i>IA</i>	<i>-0.21</i>	<i>0.03</i>	<i>-0.10</i>	<i>0.01</i>	<i>15</i>	<i>17.98</i>	<i>5.70</i>	<i>19.23</i>	<i>11.44</i>	<i>6.10</i>
<i>II</i>	<i>IA</i>	<i>-0.36</i>	<i>0.03</i>	<i>-0.20</i>	<i>0.03</i>	<i>17</i>			<i>19.33</i>		
<i>III</i>	<i>IA</i>	<i>-0.16</i>	<i>0.04</i>	<i>-0.10</i>	<i>0.02</i>	<i>27</i>			<i>17.19</i>		
<i>IV</i>	<i>CAI</i>	<i>-1.16</i>	<i>0.08</i>	<i>-0.59</i>	<i>0.04</i>	<i>23</i>	<i>10.12</i>	<i>12.93</i>	<i>15.99</i>	<i>6.82</i>	<i>6.00</i>
bulk powder		-0.56	0.03	-0.29	0.02	16	12.82	1.46	14.02	2.74	21.58
Mokoia											
m-a	Chd	-0.49	0.04	-0.25	0.02	24	20.66	0.68	18.62	17.08	10.50
m-c	Chd	-0.19	0.02	-0.11	0.02	11	21.60	2.13	14.44	6.70	7.00
m-e	Chd	-0.27	0.03	-0.15	0.03	11	20.61	6.70	15.88	10.71	9.48
m-f	Chd	-0.49	0.02	-0.22	0.01	10	25.68	11.97	26.03	4.68	3.36
<i>VIII</i>	<i>IAB</i>	<i>-0.26</i>	<i>0.02</i>	<i>-0.17</i>	<i>0.01</i>	<i>15</i>	<i>22.57</i>	<i>9.54</i>	<i>18.71</i>	<i>10.26</i>	<i>5.25</i>
<i>IX</i>	<i>IA</i>	<i>-0.23</i>	<i>0.03</i>	<i>-0.13</i>	<i>0.02</i>	<i>15</i>	<i>18.98</i>	<i>4.90</i>	<i>17.51</i>	<i>5.90</i>	<i>11.74</i>
<i>VI</i>	<i>IA</i>	<i>1.11</i>	<i>0.04</i>	<i>0.55</i>	<i>0.02</i>	<i>20</i>			<i>19.72</i>		
<i>XII</i>	<i>IA</i>	<i>-0.17</i>	<i>0.04</i>	<i>-0.11</i>	<i>0.02</i>	<i>15</i>			<i>18.02</i>		
<i>X</i>	<i>CAI</i>	<i>1.64</i>	<i>0.02</i>	<i>0.83</i>	<i>0.02</i>	<i>15</i>	<i>8.51</i>	<i>13.58</i>	<i>14.35</i>	<i>17.85</i>	<i>1.30</i>
<i>XI</i>	<i>CAI</i>	<i>-1.32</i>	<i>0.11</i>	<i>-0.68</i>	<i>0.05</i>	<i>19</i>	<i>9.48</i>	<i>n.d.</i>	<i>23.72</i>	<i>28.11</i>	<i>3.80</i>
bulk powder		-0.48	0.04	-0.28	0.03	8	15.87	3.46	14.49	9.61	21.70
Allende											
04a	Chd	-0.53	0.04	-0.25	0.04	15	21.93	1.60	21.28	3.76	7.40
04b	Chd	-0.38	0.03	-0.20	0.03	18	18.10	7.17	17.81	21.89	4.68
04c	Chd	-0.36	0.04	-0.19	0.04	15	20.75	2.59	16.97	2.99	10.51

Continued on Next Page...

Table 7.1 – Continued

Sample	Type	$\delta^{30}\text{Si}$ (‰)	$2\sigma_{SEM}$	$\delta^{29}\text{Si}$ (‰)	$2\sigma_{SEM}$	N	Mg (wt%)	Al (wt%)	Si (wt%)	Ca (wt%)	Fe (wt%)
04d	Chd	-0.71	0.03	-0.39	0.03	14	12.95	8.38	16.33	7.86	6.32
04e	Chd	-0.50	0.02	-0.27	0.02	14	19.01	5.38	16.57	12.32	9.87
04f	Chd	-0.69	0.03	-0.35	0.02	17	15.17	10.79	18.04	19.88	11.84
04g	Chd	-0.10	0.03	-0.06	0.02	27	21.75	3.19	18.14	5.41	7.60
05o	Chd	-0.53	0.04	-0.28	0.02	20	20.19	1.67	21.38	5.03	8.23
05p	Chd	-0.50	0.04	-0.24	0.04	16	21.03	13.63	17.36	5.33	9.44
05q	Chd	-0.29	0.03	-0.16	0.04	14	23.09	4.08	19.65	4.35	3.91
Chondrule average ($\pm 2\sigma_{SD}$) ^b		-0.46	0.36	-0.24	0.19						
04h	UI ^a	-0.71	0.03	-0.39	0.03	14	23.96	2.01	18.94	15.54	8.81
04j	UI	-0.55	0.04	-0.29	0.03	15	21.76	1.52	17.90	5.23	11.74
04k	UI	-0.52	0.03	-0.30	0.03	25	21.11	2.00	17.01	5.18	11.55
04l	UI	0.06	0.05	-0.01	0.03	12	23.41	1.18	19.49	3.39	9.93
05m	CAI	2.81	0.03	-1.41	0.02	23	2.40	14.82	10.82	23.00	1.36
05r	matrix	-0.63	0.04	-0.35	0.03	17	12.08	6.53	15.99	4.62	27.31
bulk powder		-0.42	0.04	-0.27	0.04	11	14.62	2.98	16.33	2.03	24.99

All samples in italics have been previously analysed for Si composition in Hezel et al. (2009); Hezel et al. (2010)

^a UI=unidentified inclusion. See text for details.

^a Mean composition of Allende chondrules only.

7.3.2 Chondrules

Figure 7.3 shows the variation in $\delta^{30}\text{Si}$ in the chondrule population. The average Si isotopic composition for the Allende chondrules is $\delta^{30}\text{Si} = -0.46 \pm 0.36 (2\sigma_{SD})$. This is a similar average value to that of bulk carbonaceous chondrites ($-0.48 \pm 0.10, 2\sigma_{SD}$) (Chapter 4), bulk chondrites ($-0.49 \pm 0.15, 2\sigma_{SD}$) (Chapter 4), or the average of eight bulk Allende aliquots ($-0.41 \pm 0.07, 2\sigma_{SD}$) (Chapter 3), though with much greater variation. The average chondrule composition from Mokoia (including previous data) is $\delta^{30}\text{Si} = -0.12 \pm 1.11(2\sigma_{SD})$, though it is clear from Figure 7.1 and Figure 7.3 that there is one rather extreme outlier. If this is removed the average becomes $\delta^{30}\text{Si} = -0.32 \pm 0.27(2\sigma_{SD})$. The Grosnaja chondrule average is $\delta^{30}\text{Si} = -0.24 \pm 0.20 (2\sigma_{SD})$ and the average of all the chondrules (with the one outlier removed) is $\delta^{30}\text{Si} = -0.38 \pm 0.35(2\sigma_{SD})$. A student t-test for two-tailed significance shows that the bulk CV3 chondrule average is different from that for bulk chondrites at the 95% level, which is not the conclusion when just the Allende data are used. Further student t-tests show that the means of the Allende and the Mokoia (with the one outlier removed) chondrule data are different at the 90% confidence level but not at 95%. Allende and Grosnaja are different at the 95% level but not at 99%, while Grosnaja and Mokoia do not have different means. As the sample populations are limited in size, especially for Grosnaja, it is risky to draw firm conclusions from these tests. However, it is clear that there is limited variation in the average $\delta^{30}\text{Si}$ of the different chondrule populations from these three CV3 chondrites. What is also evident is that the variation in $\delta^{30}\text{Si}$ seen in the chondrules within one carbonaceous chondrite is greater than the variation of bulk carbonaceous chondrites. Indeed the range of chondrules values scatters over the range of variation in the bulk silicate Earth $\delta^{30}\text{Si}$ as well (Figure 7.1).

The similarity between the mean of the chondrule $\delta^{30}\text{Si}$ data and the average bulk chondrite composition was previously observed by Georg et al. (2007a) for chondrules from the ordinary chondrite Chainpur (LL3). Their chondrule average was $\delta^{30}\text{Si}$

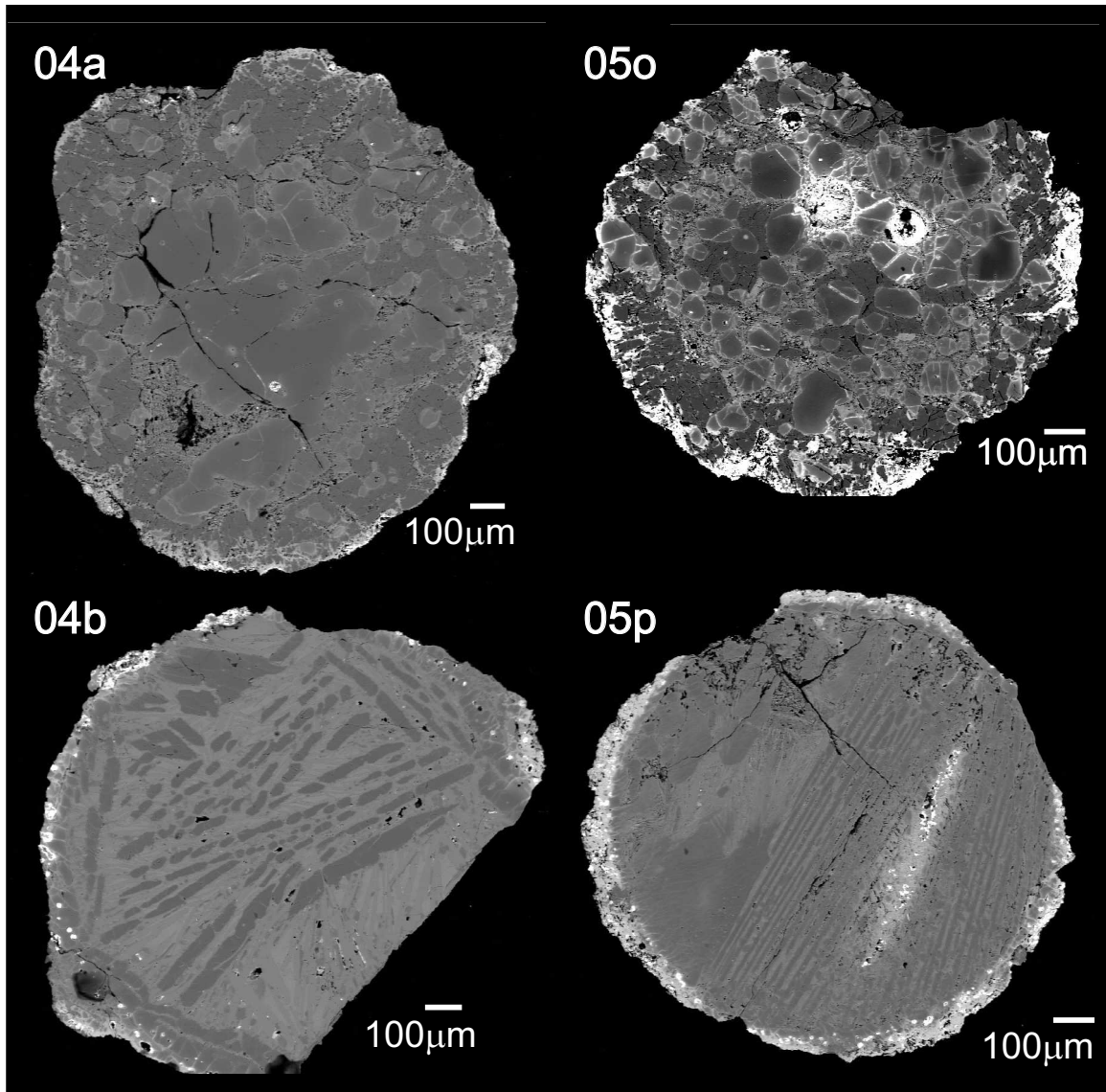


Figure (7.2): Backscattered electron images of Allende chondrules. 04a and 05o are porphyritic olivine and pyroxene chondrules, with the darker regions that are more noticeable towards the rim being the pyroxene. 04b and 05p are barred olivine chondrules with melilite and pyroxene

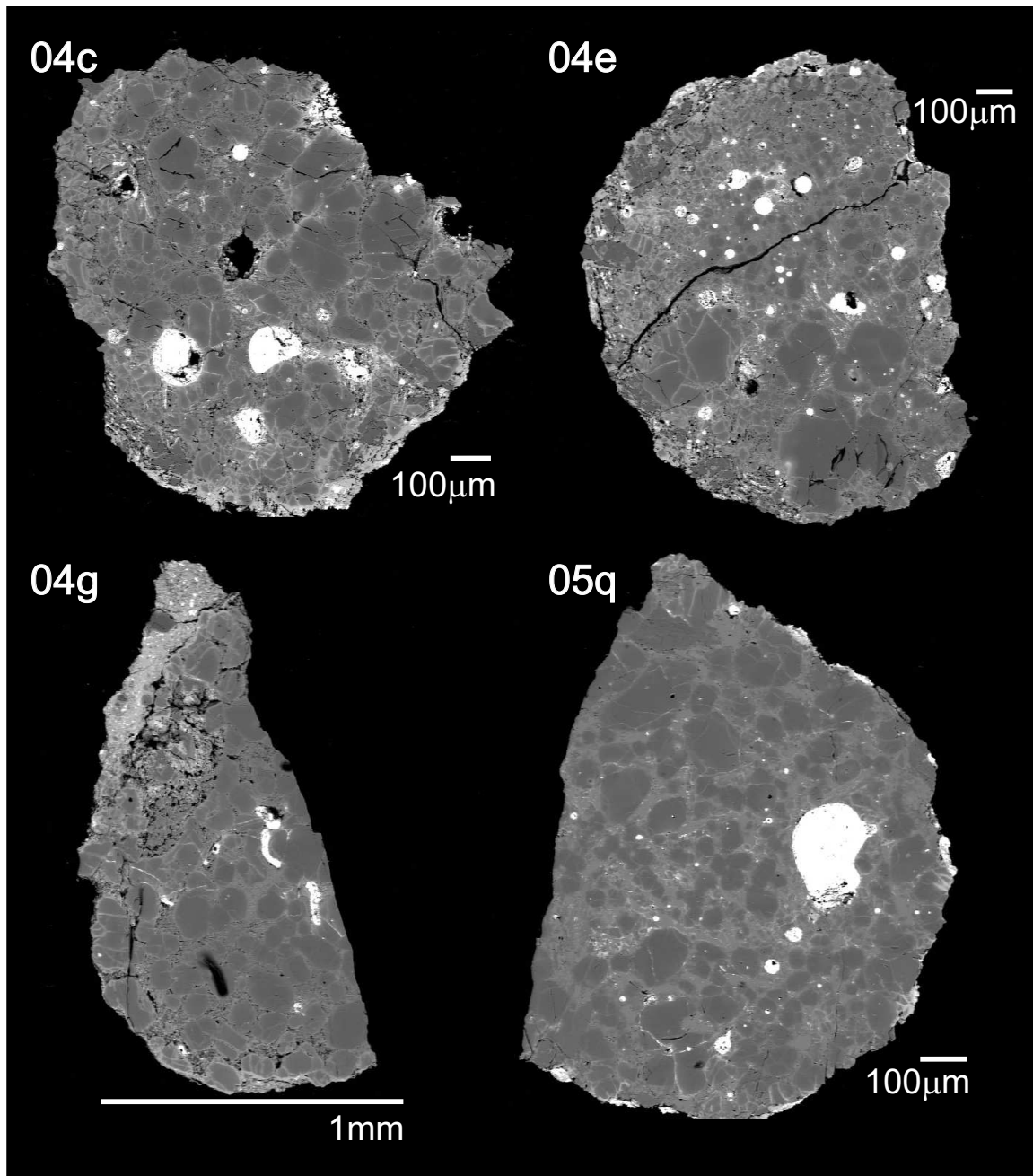


Figure (7.2): Backscattered electron images of Allende chondrules. All these chondrules are porphyritic olivine with varying amount of Fe-Ni metal and Fe-sulphides

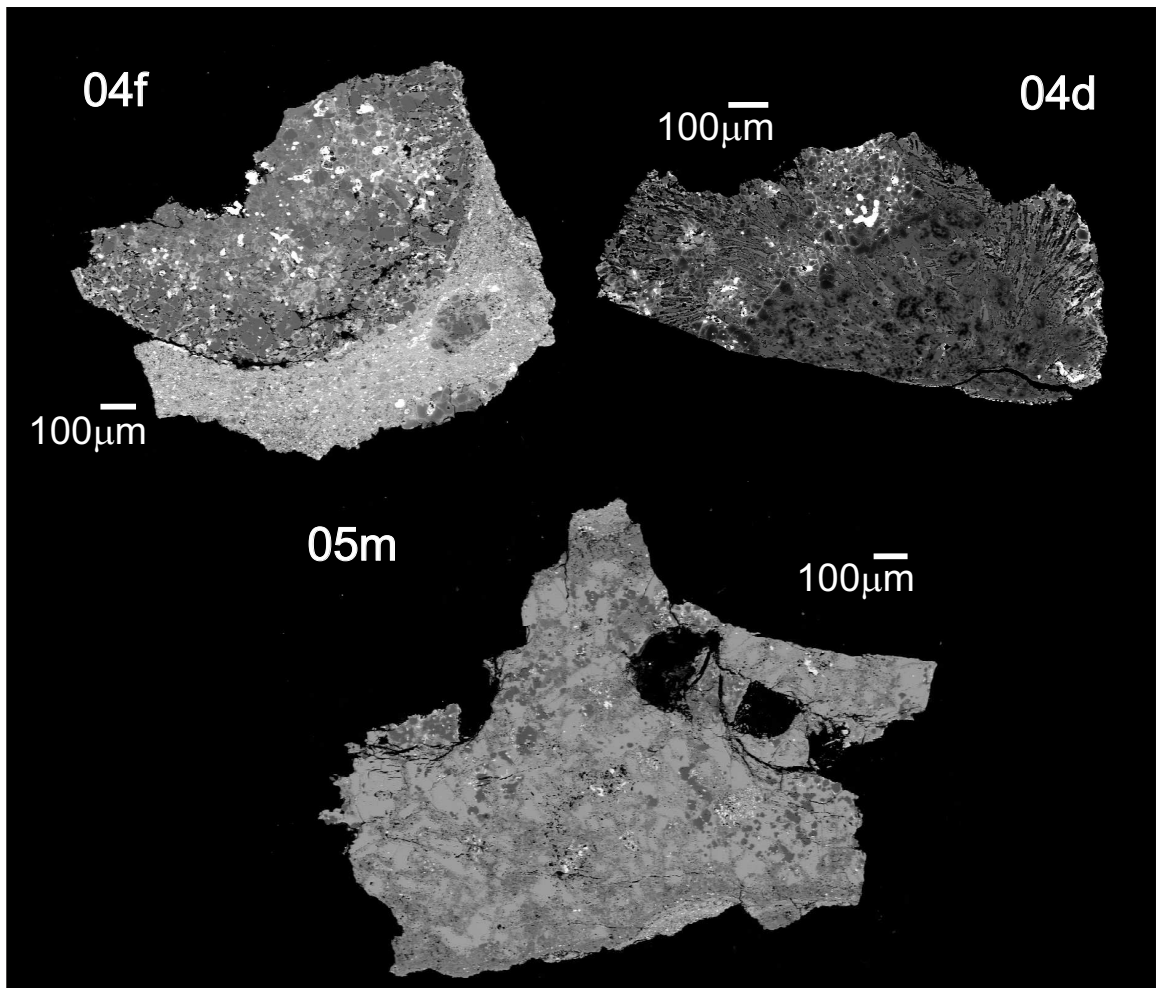


Figure (7.2): Backscattered electron images of Allende components. 04f shows some attached matrix (light coloured-finer grained material), though the fragment that was put into solution was matrix-free. 04f is very fine grained with the dominant mineral being pyroxene. 04d was pyroxene and olivine. 05m is the CAI

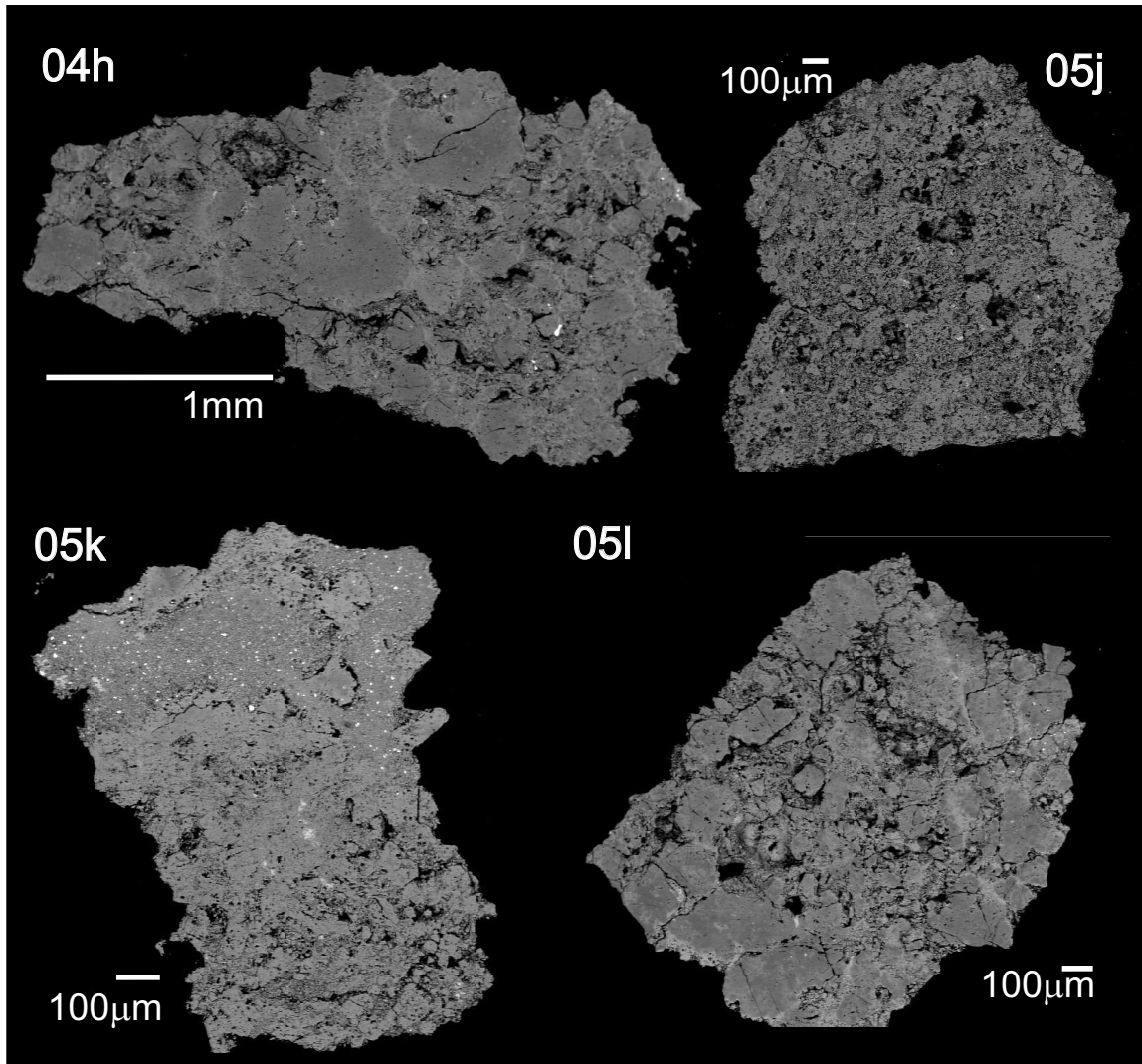


Figure (7.2): Backscattered electron images. Undefined inclusions (UI) that are dominated by olivine. 05j is the finest grained and could possibly be an amoeboid olivine aggregate. The finer grained brighter regions in the top and top left of 05k are matrix material.

$= -0.51 \pm 0.38$ ($2\sigma_{SD}$) and their chondrite mean was $\delta^{30}\text{Si} = -0.58 \pm 0.12$ ($2\sigma_{SD}$) (Figure 7.3). The Chainpur chondrule average $\delta^{30}\text{Si}$ is somewhat lighter than the Grosnaja and Mokoia or the Allende data from this study, but the mean is not different from any of the CV3 chondrules at the 99% level. It is known however, that the Si isotopic compositions of bulk meteoritic and terrestrial samples from Georg et al. (2007a) are offset towards lighter $\delta^{30}\text{Si}$ values compared to the majority of subsequent studies (e.g. Fitoussi et al., 2009; Chakrabarti and Jacobsen, 2010b; Armytage et al., 2011, also see Chapter 3 for more details). It is possible that the chondrule data are reflecting a similar effect, which makes it impossible to say with any certainty whether Si isotopic chondrule data from high precision studies shows any variation with different types of host meteorite. However, the conclusion that the Si isotopic composition of chondrules shows a greater range ($\sim 0.6\%$ discounting the outlier; Table 7.1) than bulk meteorites ($\sim 0.3\%$, Chapter 4) appears robust.

The relationship between the $\delta^{30}\text{Si}$ composition of the bulk meteorites and the distribution of the chondrules is not consistent for all the samples (Figure 7.1). For Grosnaja, the chondrules are at least 0.2% heavier than the bulk $\delta^{30}\text{Si}$ composition. Mokoia's chondrules have the the same, within uncertainty, or heavier $\delta^{30}\text{Si}$ in comparison to the bulk composition for Mokoia. The bulk Si isotopic composition of Allende is only slightly heavier than the mean of its chondrule data.

There are no systematic differences in elemental concentration between the chondrules from the different meteorites, and there are no clear correlations between major element abundance and Si isotopic composition (Figure 7.4). The Mg concentrations for the Allende chondrules range over approximately 10wt% from 13 to 23wt% Mg. The Mokoia chondrules have a slightly higher overall average Mg wt% with a range 19-26wt%. The only Grosnaja chondrule has 13wt% Mg. The bulk samples of Allende and Mokoia have Mg concentrations that are lower than the average chondrule Mg concentrations from those meteorites. The Si concentrations for the Allende chon-

7.3. Results

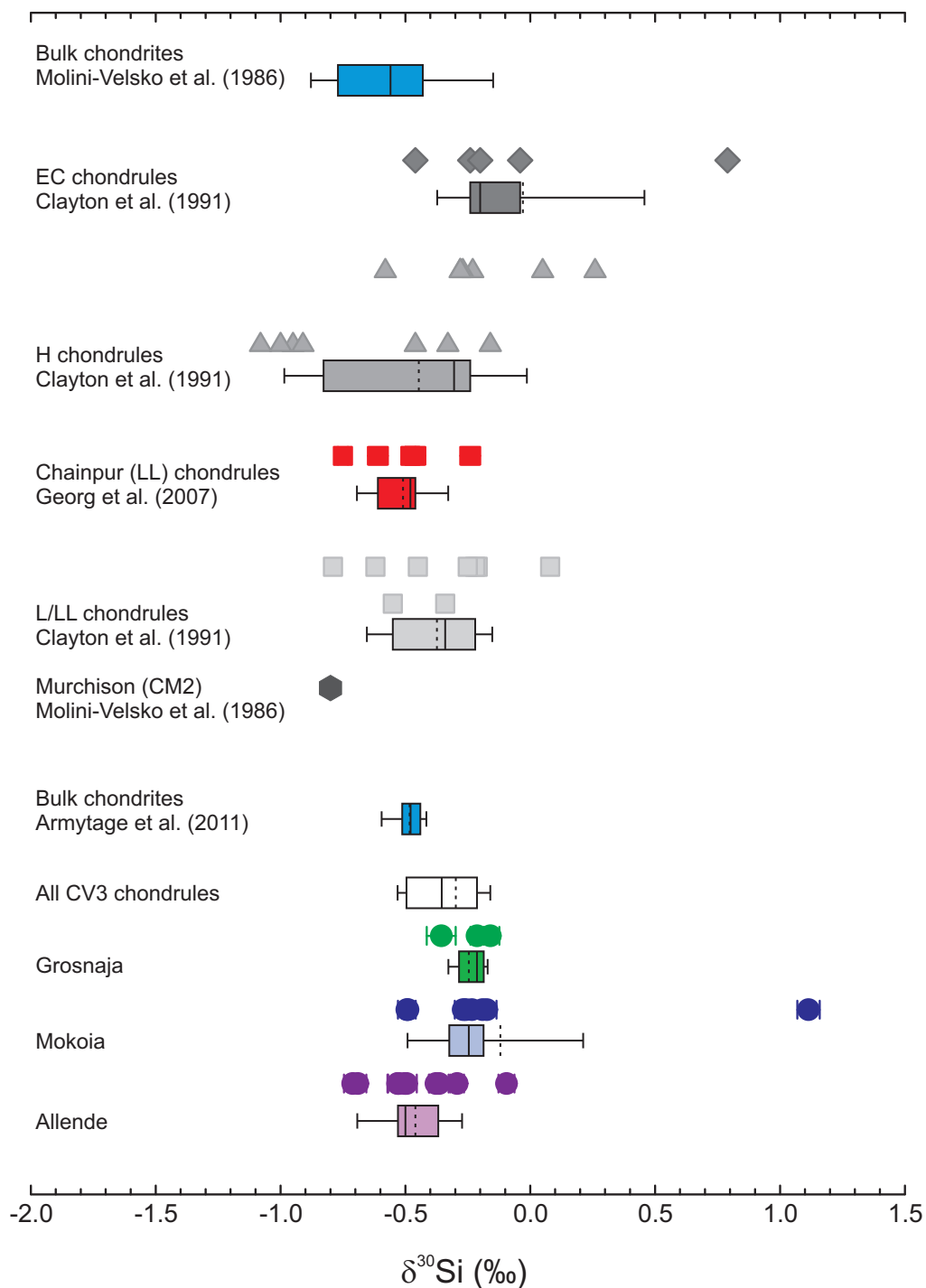


Figure (7.3): Variation in $\delta^{30}\text{Si}$ of the chondrules for both high and low precision datasets. The box limits are 1st and 3rd quartiles with the internal line showing the median of the data. The dashed line shows the mean where it is different from the median. The error bars are the 10th and 90th percentiles. The greyscale data indicates data from GS-MS studies where the external precision was a factor of two greater than current MC-ICPMS limits.

drules span a range from 16-22wt%, while the Mokoia chondrules have a slightly greater range of 16-26wt%. The sole Grosnaja chondrule contains ~ 19.5 wt% Si. As with Mg, the Si concentrations of the bulk CV3 chondrites are lower than the average Si of the chondrules from the meteorites.

Iron concentrations show the greatest offset between the average chondrule Fe abundances and those of the bulk meteorites (Figure 7.4). The concentrations of the bulk samples of Grosnaja, Mokoia and Allende are in the range 21 to 25wt% Fe, whereas the ranges for the Allende and Mokoia chondrules are 3-12wt%. In terms of their Al and Ca concentrations, the chondrules from Mokoia and Allende span ranges between 0.5-14wt% Al and 3-22wt% Ca. Within those ranges lie the bulk compositions of the CV3 meteorites.

The different petrologic types of chondrule do not appear to correlate with different regions on any of the $\delta^{30}\text{Si}$ vs element plots. 04a and 05o, the two porphyritic olivine and pyroxene chondrules do have identical $\delta^{30}\text{Si}$ and very similar elemental concentrations (Table 7.1) but that is the only group of chondrules where it is observed and the sample population is very small. On the whole, these data are consistent with the observations of Clayton et al. (1991) that there is no correlation in individual chondrules between Si isotopic abundance and chondrule texture or mineralogy.

The outlier chondrule for Mokoia VI, which appears almost CAI-like in its Si isotopic composition, is hard to explain. Hezel et al. (2010) raised the outlier status of this chondrule (#2 Mokoia in that study) but the only petrologic difference they could find was a dominance of pyroxene. This is unlikely to be the cause, as a dominance of pyroxene, if anything, would drive it towards lighter values due to the light $\delta^{30}\text{Si}$ composition of pyroxene relative to olivine (Savage et al., 2011). However, lunar mineral separate $\delta^{30}\text{Si}$ data suggests that this direction of fractionation may not be universal (Chapter 6). We do not have the full range of elemental data for VI, only the photospectrometer Si data. Si concentration of VI does plot in the chondrule field

7.3. Results

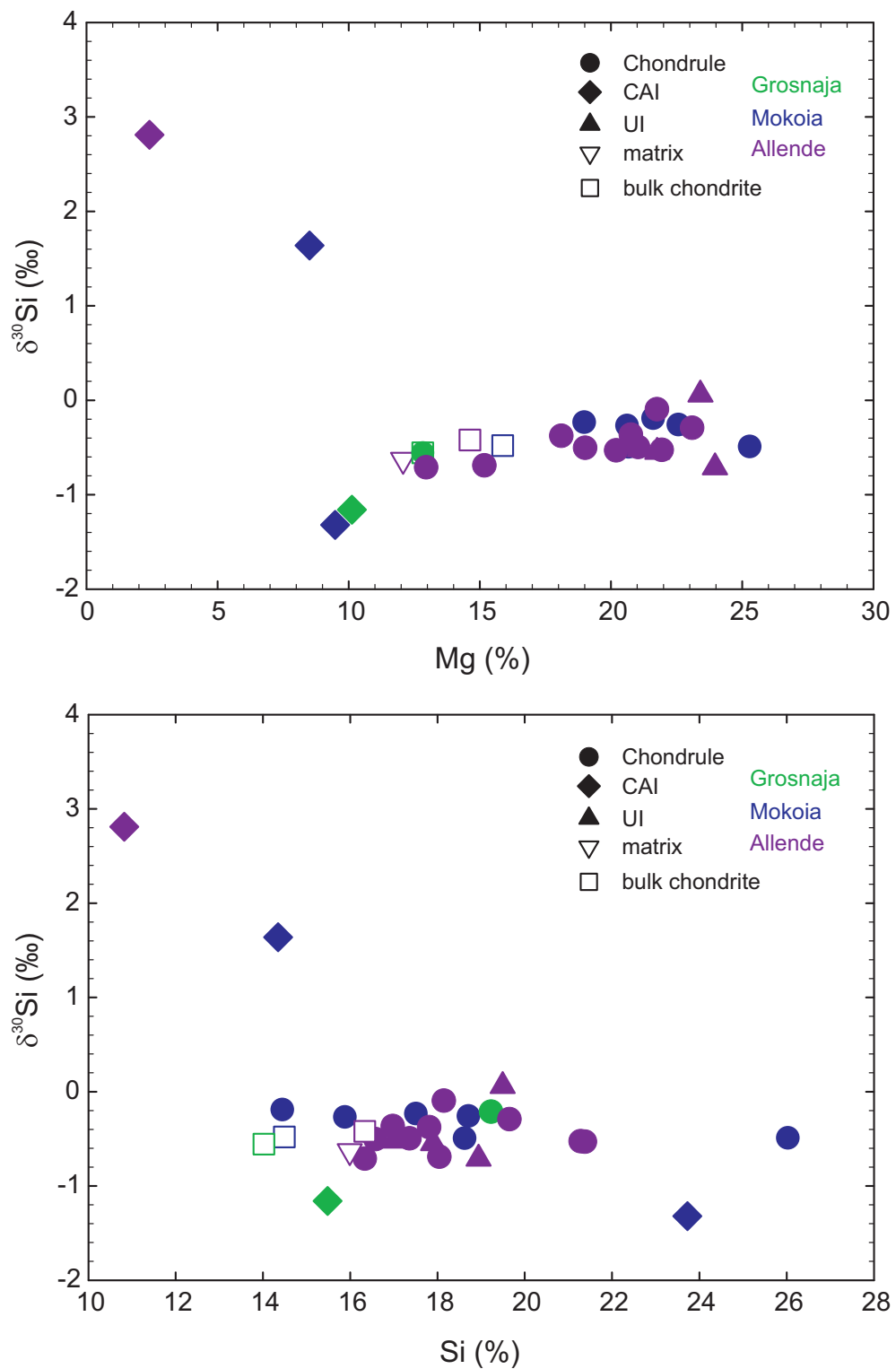
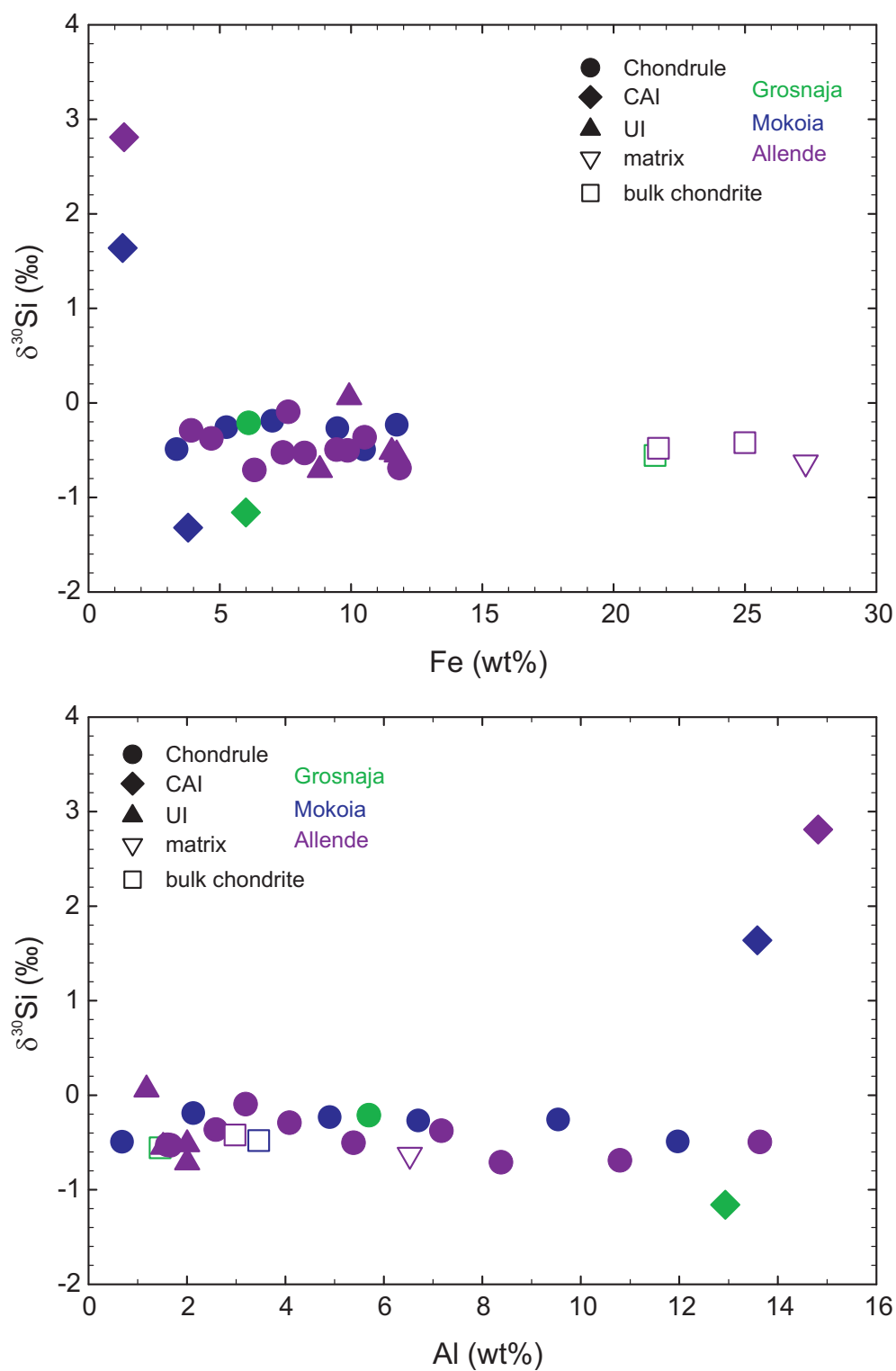


Figure (7.4): $\delta^{30}\text{Si}$ versus the concentrations of Mg and Si in the components and bulk samples of three CV3 chondrites. All the uncertainty bars on the data are within the symbol size



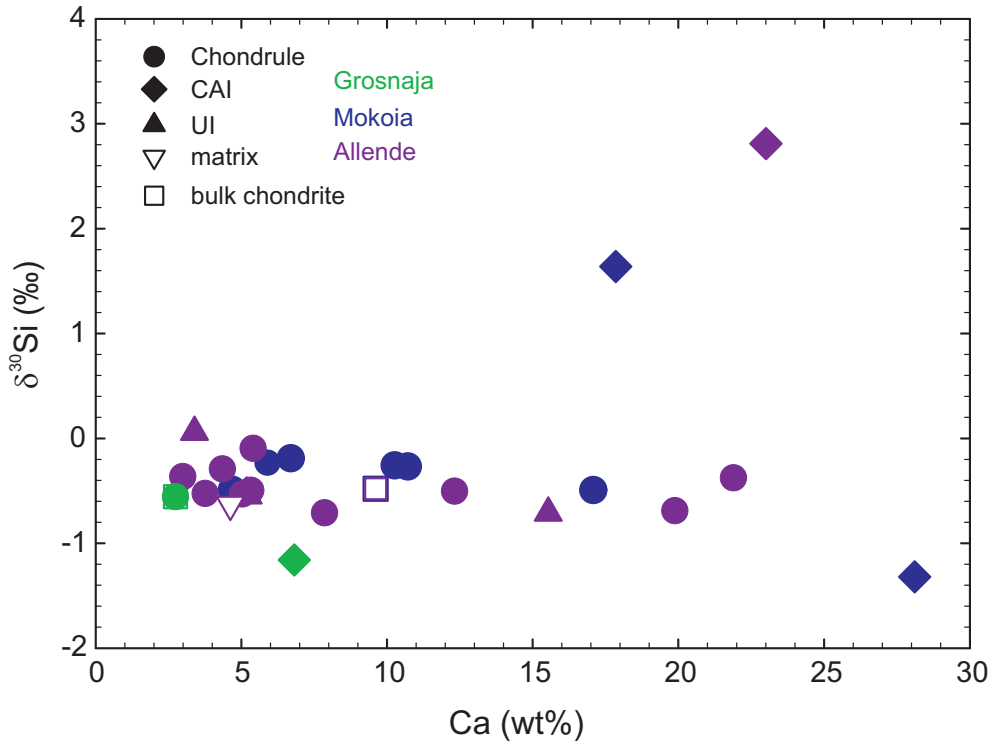


Figure (7.4): $\delta^{30}\text{Si}$ versus the concentrations of Ca in the components and bulk samples of three CV3 chondrites.

rather than with CAIs but a more thorough investigation is required for this sample.

7.3.3 Refractory inclusions

7.3.3.1 Calcium aluminium inclusions

Silicon isotopic analysis of refractory CAIs (calcium aluminium inclusions) is more prevalent in the literature than for chondrules (e.g. Yeh and Epstein, 1978; Clayton et al., 1988; Becker and Epstein, 1981), due in part to the early search for Si mass independent anomalies. Yeh and Epstein (1978) found a range in $\delta^{30}\text{Si}$ for Allende inclusions between $+1.4\text{‰}$ and -3.1‰ . Only one inclusion, EK 1-4-1, showed a significant mass independent anomaly ($\delta^{30}\text{Si} = 12.5\text{‰}$, $\delta^{29}\text{Si} = 7.54\text{‰}$, $\delta^{29}\text{Si}_{\text{calc.}} = 6.41\text{‰}$) that correlated with a large nuclear anomaly in $\delta^{26}\text{Mg}$. One other inclusion also exhibited mass independent behaviour (Figure 7.5). Clayton et al. (1988) reported data from a whole series of CAIs, with only 1 (the same EK 1-4-1) out of 32 in-

clusions demonstrating any mass independent behaviour. Most of the fractionations were heavy, indicating an evaporation origin (mostly coarse grained CAIs), but some of the refractory inclusions (mostly fine grained CAIs) had light $\delta^{30}\text{Si}$ compositions (Clayton et al., 1988)

Most of the recent work on refractory inclusions have been in-situ studies of igneous CAIs. In-situ studies allow for the measurement of internal fractionations, which may give additional constraints on formation mechanisms. Shahar et al. (2009) carried out a LA MC-ICPMS (laser ablation multi-collector inductively-coupled-plasma mass spectrometer) study of a type-A CAI from Leoville (CV3) which had an average mass dependent fractionation of $\delta^{29}\text{Si} = 3.4 \pm 0.3\%$ relative to San Carlos Olivine. Correcting to NBS-28 based on the composition of San Carlos Olivine in Chapter 4 and Savage et al. (2010), this would give a Si isotopic composition of $\delta^{30}\text{Si} = 6.3 \pm 0.6$. SIMS (secondary ionisation mass spectrometer) studies of type-B CAIs also found isotopically heavy Si compositions (Sugiura et al., 2004; Knight et al., 2009a). The only recent $\delta^{30}\text{Si}$ data from dissolved samples are three bulk CAIs from CV chondrites (two from Mokoia and one from Grosnaja) that were analysed for their Si isotopic compositions in Oxford using solution chemistry and MC-ICPMS (multi-collector inductively-coupled-plasma mass spectrometer) (Hezel et al., 2009).

Only one calcium aluminium inclusion (CAI) was picked from Allende and analysed (05m). It had the heaviest $\delta^{30}\text{Si}$ of all the Allende components measured ($\delta^{30}\text{Si} = 2.81 \pm 0.03$, $2\sigma_{SEM}$). This is consistent with previous $\delta^{30}\text{Si}$ data (e.g. Shahar et al., 2009; Knight et al., 2009a) for igneous CAIs. The Si isotopic compositions of the samples identified as CAIs from a previous study (Hezel et al., 2009) show considerable variation relative to the Allende datum (Figure 7.1 and 7.5). The CAI from Grosnaja (sample IV) also has quite an extreme Si isotopic composition but in the opposite direction as $\delta^{30}\text{Si} = -1.16 \pm 0.08$ ($2\sigma_{SEM}$). The two CAIs from Mokoia almost span the range of the CAIs from Grosnaja and Allende as one has the isotopic

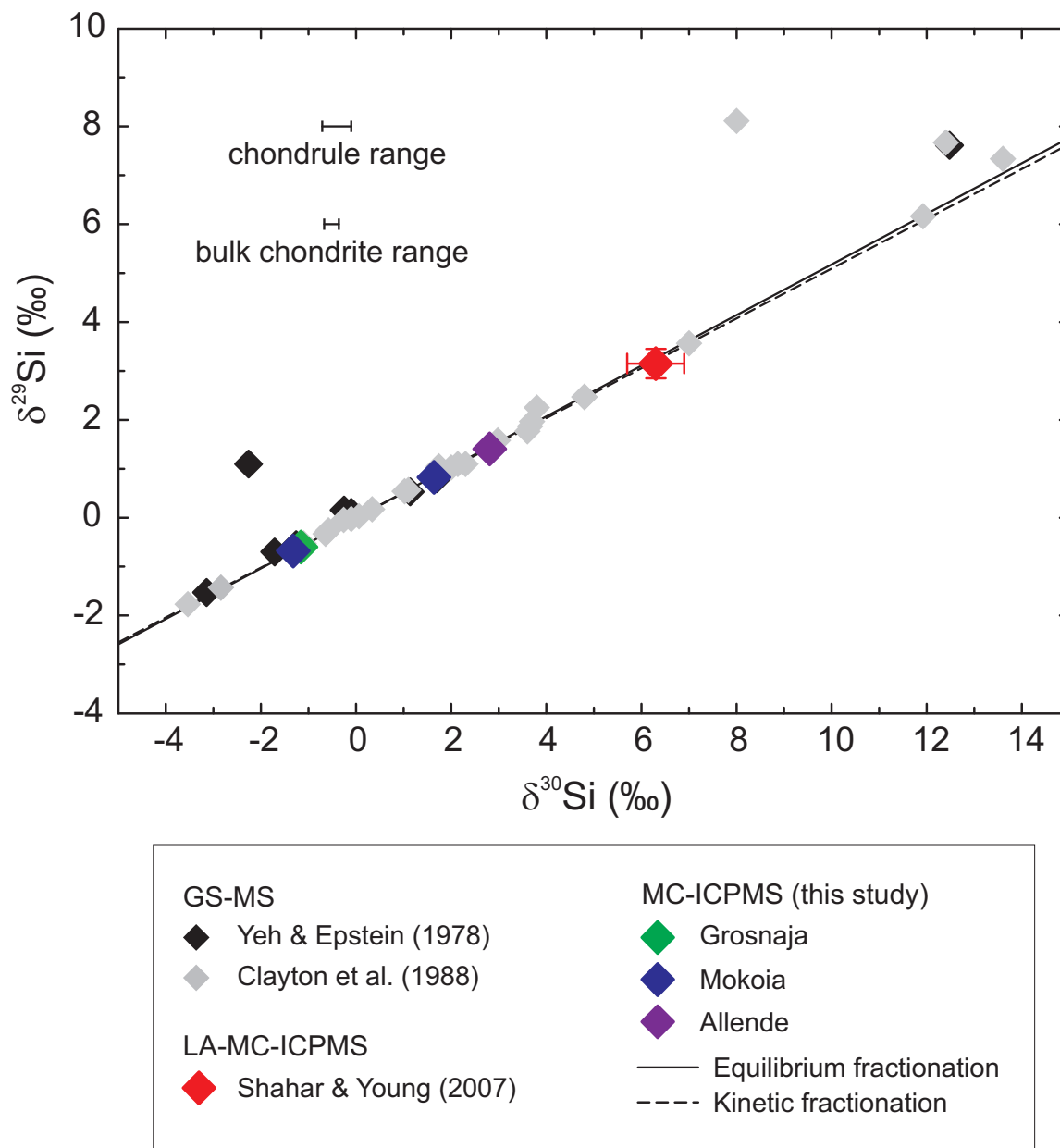


Figure (7.5): $\delta^{30}\text{Si}$ of CAIs. Error bars are not plotted for GS-MS (gas source mass spectrometry) data as they are not explicit in these studies but they are likely to be on the order of $\sim 0.4\text{‰}$; hence would be smaller than the data points. The error bars on the Shahar and Young (2007) CAI are $\pm 2\sigma_{SD}$ of a series of spot analyses. The chondrule and bulk chondrites ranges are from this study. The equilibrium and kinetic fractionation lines are calculated using equation 1.1 & 1.2.

composition $\delta^{30}\text{Si} = 1.64 \pm 0.02$ ($2\sigma_{SEM}$), whereas the other is $\delta^{30}\text{Si} = -1.32 \pm 0.11$ ($2\sigma_{SEM}$). The reproducibility of the CAIs IV and XI is poor in comparison to the other samples analysed, however, as they have such extreme isotopic compositions it does not significantly alter the interpretation of the data. The wide range in CAI $\delta^{30}\text{Si}$ composition is consistent with the early studies of Yeh and Epstein (1978) and the summary of Clayton et al. (1988).

7.3.4 Other components

Only one matrix sample from Allende was analysed (05r). Its Si isotope composition ($\delta^{30}\text{Si} = -0.63 \pm 0.04$, $2\sigma_{SEM}$) is approximately 0.2‰ lighter than the bulk composition of Allende or the Allende chondrule average, $\delta^{30}\text{Si} = -0.46 \pm 0.36$ ($2\sigma_{SD}$), though clearly it is within the range of the latter. Across the elements analysed for their concentrations, there is no consistent relationship pattern between the chondrules, the matrix and the bulk.

Another, though minor, component of chondrites are AOAs. These are irregularly shaped objects with grain sizes of $520\mu\text{m}$ that usually only make up a few percent of a chondrite (e.g. Scott, 2007). It has been suggested that AOAs have a genetic relationship to CAIs despite having mineralogies closer to chondrules (Itoh et al., 2002).

The UIs or “undefined inclusions” analysed from Allende have an average $\delta^{30}\text{Si}$ composition of -0.43 ± 0.67 ($2\sigma_{SD}$). This is a mean composition that is close to the bulk $\delta^{30}\text{Si}$ for Allende -0.42 ± 0.04 ($2\sigma_{SEM}$), and similar to the mean for the Allende chondrules (-0.43 ± 0.67 , $2\sigma_{SD}$) but with greater variation. Looking in more detail, however, it is interesting to note that the most AOA-like (amoeboid olivine aggregate) inclusion, 04j, is offset from the other UIs by $\sim 0.6\text{‰}$ towards heavier $\delta^{30}\text{Si}$ compositions. This is the sample primarily responsible for the large $2\sigma_{SD}$ of the UIs as the mean Si composition for 04h, 05k and 05l is $\delta^{30}\text{Si} = -0.59 \pm 0.20$ ($2\sigma_{SD}$). Even

so, the range seen in all of the UI is not as great as the range in Si composition of CAIs from Allende, Grosnaja and Mokoia.

The bulk measured elemental compositions for the UIs, on the whole, fall within the ranges defined by the Allende chondrules. The Mg concentrations of the UIs are occasionally higher than those of the chondrules but still within 1wt%. With the exception of the Ca concentrations, the elemental abundances for these objects have a relatively limited range of a few weight percent.

7.4 Discussion

7.4.1 Si isotopic composition of CAIs

The heavy $\delta^{30}\text{Si}$ isotopic composition of the Allende CAI is consistent with an evaporative origin as has been observed in previous carbonaceous chondrite CAIs (Sugiura et al., 2004; Shahaar et al., 2009; Knight et al., 2009a). These large offsets are also consistent with the laboratory evaporative experiments of Davis et al. (1990) and Wang et al. (2001).

Of the previously analysed samples from Grosnaja and Mokoia, the isotopically heavy CAI was a “fluffy” type A CAI, whereas the two isotopically light CAIs were both fine grained and rather altered (Sara Russell pers. comm.). Fluffy type CAIs are thought to have formed as condensates from the solar nebula (MacPherson and Grossman, 1984), and the $\delta^{30}\text{Si}$ of Mokoia X is consistent with this interpretation. The light $\delta^{30}\text{Si}$ compositions for the fine-grained CAIs concurs with the observations by Clayton et al. (1988). However, the sample population for bulk high precision $\delta^{30}\text{Si}$ compositions of chondrules is still relatively limited.

All the Fe isotopic data from the CAIs from Mokoia and Gronaja were light with $\delta^{56}\text{Fe}$ compositions of -0.3 to -1.3‰ (Hezel et al., 2009). However Mokoia X, the fluffy CAI has a heavy $\delta^{30}\text{Si}$ composition (1.64 ± 0.02 , $2\sigma_{SEM}$). Metasomatic processes

have been invoked to explain light $\delta^{56}\text{Fe}$ compositions for CAIs from Mokoia, Grosnaja (Hezel et al., 2008) and Allende (Mullane et al., 2005), which may explain the discrepancy in direction of fractionation between the Si and Fe isotopic compositions for this CAI.

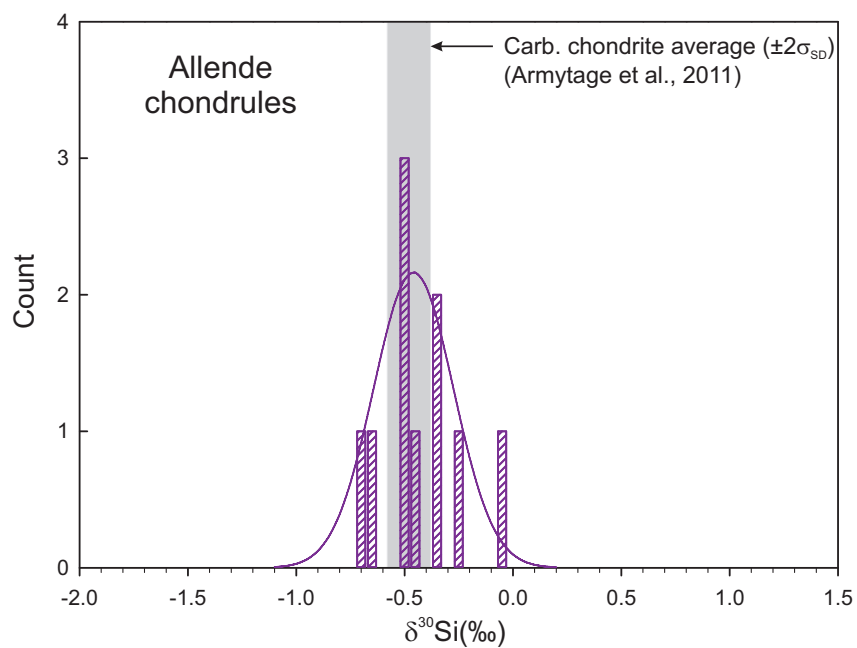
7.4.2 Cause of variation in $\delta^{30}\text{Si}$ of chondrules

The key observation of the $\delta^{30}\text{Si}$ chondrule data is that they scatter over a much larger range than the bulk chondrites. There are three primary situations that could give rise to the observed fractionation, one or all of which could affect an individual chondrule's history. These mechanisms are: (i) chondrule formation from variable dust reservoirs that were heterogeneous in $\delta^{30}\text{Si}$; (ii) the initial formation processes of chondrules leading to different degrees of fractionation; (iii) subsequent perturbation of the isotopic compositions of the chondrules due to alteration processes on the chondrite parent body.

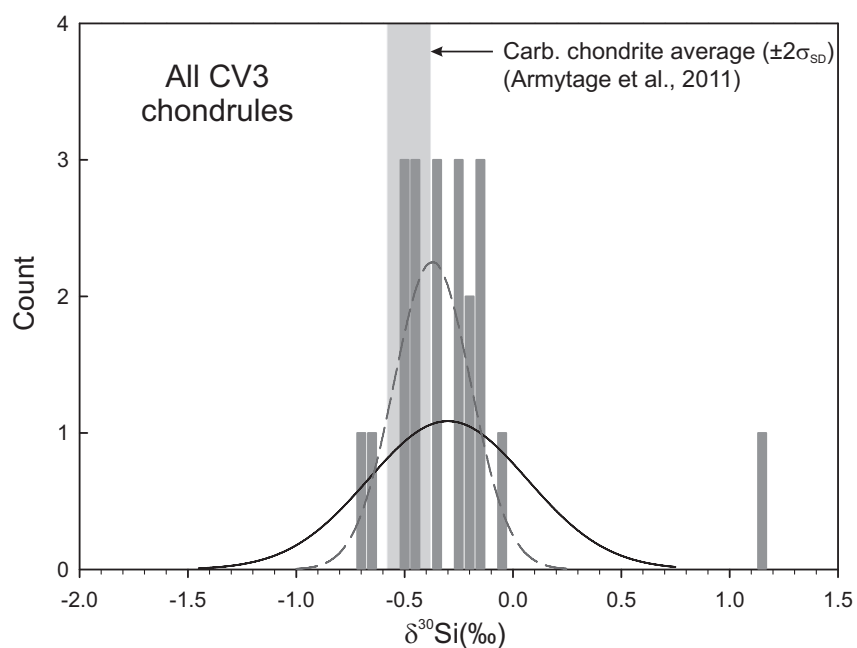
7.4.2.1 Heterogeneity in $\delta^{30}\text{Si}$ of source reservoirs

One mechanism to generate limited non-systematic isotope variations in chondrules is for chondrules to be closed system objects that inherited their compositions from precursor materials (e.g. Larimer and Anders, 1970; Grossman and Wasson, 1982; Jones, 1990). For this mechanism to be the cause of the $\delta^{30}\text{Si}$ variation seen in the chondrules, a nebular rather than planetary origin for chondrule formation is more likely, as the bulk $\delta^{30}\text{Si}$ compositions of all the planets and asteroids analysed to date show a much more limited range than the chondrules from Allende.

The constraints that exist on the nature of chondrules precursors are minimal despite information from relict grains preserved in some chondrules (Connolly Jr and Hewins, 1996). Some kind of “dustballs” with micron-scale grains that are aggregates of even smaller components are almost universally assumed to be the precursors to



(a)



(b)

Figure (7.6): Histogram of Si isotopic composition of chondrules and calculated normal distribution curves. The solid line is the normal distribution for all the CV3 chondrules including the Mokoia outlier, whereas the dashed line is the calculated normal distribution with this removed.

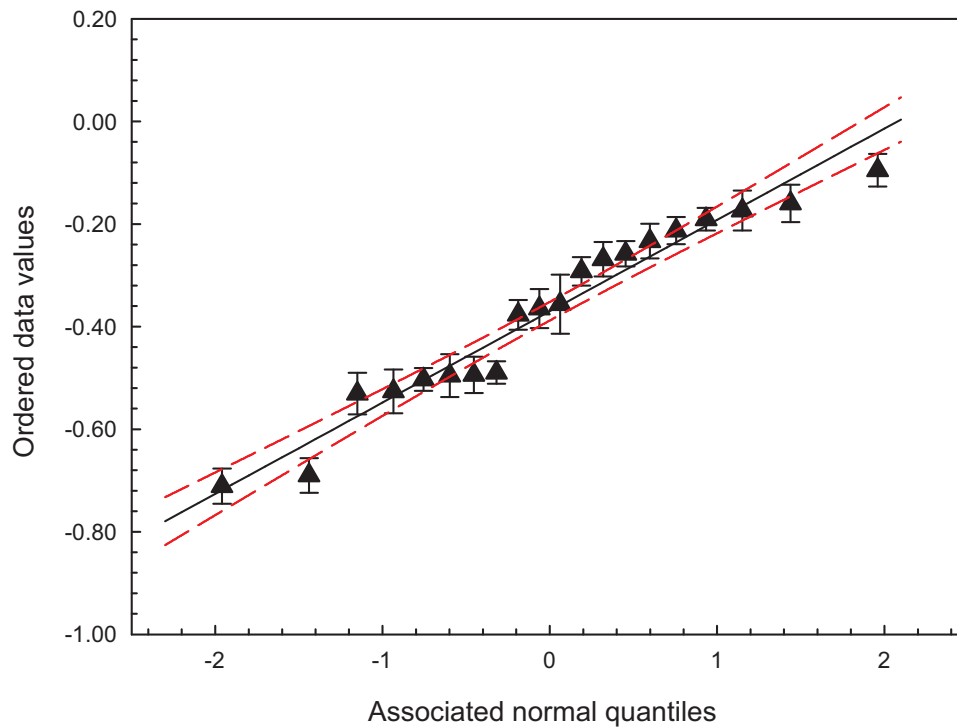


Figure (7.7): Normal probability plot. Black solid line is a weighted regression line through the data and the red dashed lines defined the 95% confidence interval on this regression

chondrule formation in the solar nebula. However, there are significant gaps in our understanding of how such dustballs may arise (Wood, 1996).

One way to assess the viability of different source $\delta^{30}\text{Si}$ reservoirs giving rise to Si isotopic variations in chondrules, would be to look at the distribution of the $\delta^{30}\text{Si}$ chondrule data. If the data show a multi-modal distribution, this could be evidence for chondrule precursor reservoirs with different $\delta^{30}\text{Si}$ compositions. The presence of the Mokoia outlier, VI, could reflect another reservoir but for the moment it will be excluded from the discussion. A visual inspection of the CV3 chondrule data both from the individual meteorites and all of them combined is somewhat ambiguous as to whether it follows a normal distribution (Figure 7.6). Another way to visually assess the distribution of the data is a normal probability plot. Figure 7.7 does show

some scatter about the regressed line, but not with any significant departure from linearity, and all the data are within uncertainty of the 95% confidence interval.

A perhaps more rigorous assessment would be a Chi-squared test. The results from the Chi-squared test for all the CV3 chondrules at the appropriate degree of freedom gives, $\chi^2 \geq \chi_{\text{observed}}^2$ at percentage probability of 9.1%. Therefore at the $\sim 90\%$ confidence level the data are normally distributed but not at the 99% level. There is the caveat that the sample size is so small it was almost always going to pass the test. The only evidence for a multi-modal distribution comes from the one sample Mokoia VI. As it is only sample it cannot be taken as hard evidence for retaining heterogeneities from precursor materials as the primary cause of the variation in $\delta^{30}\text{Si}$ in chondrules. There is also always the possibility that the variable populations would also be normally distributed with respect to their $\delta^{30}\text{Si}$ compositions.

The source of any $\delta^{30}\text{Si}$ isotopic heterogeneities in the solar nebula is not immediate obvious. Pre-solar grains are known to have extreme isotopic compositions ($\sim 400\%$) but mostly show mass independent anomalies (see Figure 1.5 and references therein). As no mass independent variation is observed in the chondrule data (Table 7.1), this is unlikely to be the cause of the heterogeneity. The CAIs do show a large, and on the whole mass dependent, range in $\delta^{30}\text{Si}$ (Figure 7.5) which has been linked to evaporative processes in the solar nebula (see previous section). As CAIs are thought, in general, to predate chondrules (e.g. Amelin et al., 2010), the fractionating processes associated with CAI formation could introduce the $\delta^{30}\text{Si}$ heterogeneities into the nebula. If precursor heterogeneity were the source of the $\delta^{30}\text{Si}$ variation in chondrules, it would make a planetary volcanism or impact origin for chondrules very unlikely as the range in $\delta^{30}\text{Si}$ composition for all the planets and parent bodies analysed to date is much more limited than the $\delta^{30}\text{Si}$ range observed in chondrules

Evidence from other properties of chondrules such as the correlation seen between chondrule mineralogy and redox state, and the relationship between oxygen isotopic

composition and chondrule size are hard to explain in terms of closed system behaviour for chondrules (Sears, 2004). The consensus seems to be moving towards open system behaviour, but it is a far from settled question (e.g. Wood, 1996; Krot et al., 2009) and does not exclude the possibility that part of the range in the $\delta^{30}\text{Si}$ composition of the chondrules result from variable precursor material.

7.4.2.2 Formation mechanisms of chondrules as cause of $\delta^{30}\text{Si}$ variations

The results from this study does not support any straightforward correlation between chondrule texture or mineralogy and the $\delta^{30}\text{Si}$ composition, which is consistent with the earlier study of Clayton et al. (1991). As with Si and Fe (Zhu et al., 2001), the Mg isotopic composition of chondrules shows a much greater range, $\sim 0.4\text{‰}$ (e.g. Galy et al., 2000), than that of bulk meteorites $\sim 0.2\text{‰}$ (Wiechert and Halliday, 2007; Teng et al., 2010). The exact values are not quoted as the $\delta^{25}\text{Mg}$ were defined relative to different Mg isotopic standards. In the chondrules from Allende, $\delta^{25}\text{Mg}$ shows an inverse relationship with size and Mg/Al ratio (Galy et al., 2000). This is taken to be consistent with evaporation during formation, though at high gas pressures ($P_{\text{H}_2} \sim 100\text{Pa}$) to suppress isotopic fractionation. Alexander (2004) suggest however, that these pressures are too high to be plausible and explain the data through re-equilibration between the chondrules and the gas.

It might be expected that Si isotopes would also show the effects of limited evaporation, and perhaps to a greater extent as Si is marginally more volatile than Mg with a 50% condensation temperature of 1310K rather than 1336K (Lodders, 2003). However, unlike for the Mg isotopic study of Galy et al. (2000), the sizes of the chondrules, estimated from Figure 7.2, do not correlate with the $\delta^{30}\text{Si}$ compositions for the Allende chondrules. Also there is no correlation between $\delta^{30}\text{Si}$ and the Si/Al ratio, which one might expect if there was a strong evaporation control. This potential discrepancy between Mg and Si isotopic data is at odds with what has been

observed for CAIs (Clayton et al., 1988). However, the lack of correlation in individual chondrules between $\delta^{30}\text{Si}$ and chondrule size has been previously observed by Clayton et al. (1991), though they did find a small effect of increasing $\delta^{30}\text{Si}$ with decreasing chondrule size for composite size-sorted chondrules in the H3 chondrite, Dhajala. One caveat that must be considered when interpreting any of our size data for chondrules from Allende is that there was a definite bias during picking towards the largest chondrules, because of the splitting of the samples. It may be that there is some inverse size to $\delta^{30}\text{Si}$ correlation but we are not sampling enough of the spectrum. If this were the case however, one might expect the range in $\delta^{30}\text{Si}$ to be even greater than the $\sim 0.6\text{‰}$ observed currently, and it still does not explain the variation in $\delta^{30}\text{Si}$ among these large chondrules.

One of the reasons for the lack of consistency between the Mg and Si data could potentially be due to any differences in diffusion rates in molten forsterite. The diffusivity (D) of Si in molten forsterite is on the order of $3.9 - 5 \times 10^{-9} \text{m}^2 \text{s}^{-1}$ (Young et al., 1998). In conjunction with the characteristic diffusive length scale, $\lambda = (Dt)^{1/2}$, calculated for $\lambda = 0.6 \text{mm}$ (the average radius of the Allende chondrules analysed in this study), this gives times on the order of $72 - 92$ seconds. The diffusivity of Mg calculated in a similar way to the Si diffusivity, based on model calculations for diffusion limited kinetic isotope fractionation, is $2.5 - 3.2 \times 10^{-9} \text{m}^2 \text{s}^{-1}$. For the same length scale as Si, the times would be $113 - 144$ s. In other words, one would not expect significant departures in behaviour between Mg and Si isotopes for chondrule crystallisation timescales that are on the order of minutes to hours (e.g. Cohen et al., 2000; Desch and Connelly, 2002).

It is hard to prevent the evaporation of K during chondrule formation (50% condensation temperature 1006K, Lodders, 2003), hence the best explanation for the observed limited K isotopic fractionation is exchange with a “normal” isotopic reservoir (Alexander et al., 2000). This reservoir is likely to have been the evaporated gas

unless all the chondrules analysed in Bishunpur remained open systems after formation and were able to exchange with the matrix. If the Allende chondrules were able to react with the evaporated phase, this could be an attractive explanation for the variable, yet limited, fractionation observed in the $\delta^{30}\text{Si}$ compositions. Why the Si isotopic composition of the chondrules should be the result of condensative as well as evaporative processes, where as $\delta^{25}\text{Mg}$ could potentially be explained evaporation with suppressed isotopic fractionation is not clear. Unfortunately there do not exist condensation coefficients for Mg and Si for condensation of silicates and silicate melts (Davis et al., 2005). In the meantime one future aim would be to get Mg and Si isotopic data on the same chondrules.

7.4.2.3 Alteration of chondrules post formation

Post formation alteration is another potential cause of variation in the isotopic composition of chondrules (e.g. Young et al., 2002a). None of the CV3 chondrites examined here are “true” CV3 meteorites. Bonal et al. (2006) determined the petrographic grade of Allende to be ≥ 3.6 and Mokoia and Grosnaja to be ~ 3.6 . The temperature estimates for the thermal metamorphism undergone by these meteorites is 400–500°C for Mokoia and up to $\sim 1800^\circ\text{C}$ for Allende (Keil, 2000). The diffusion rates for Si in olivine and pyroxene are so slow that with cooling rates on the order of 1-3000°C (Hewins et al., 2005) for chondrules, the closure temperatures on the mm scale are in the order of 2700K to 4200K for olivine and $> 12700\text{K}$ for diopside (See Chapter 6 for further details). Therefore it is unlikely that thermal metamorphism would lead to substantial post-formation exchange of Si isotopes between different $\delta^{30}\text{Si}$ reservoirs (e.g. CAIs, matrix) and the chondrules.

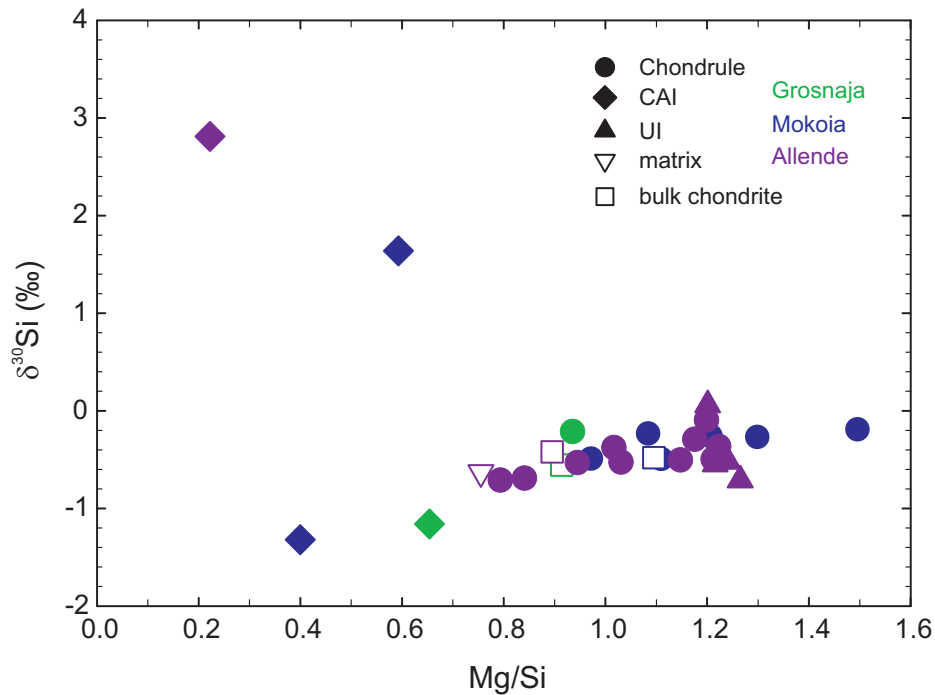
If aqueous alteration was the cause for the limited variation in $\delta^{30}\text{Si}$, the primary mechanism of substantially changing the Si isotopic compositions of the fluids is through formation of clays. There is some evidence of phyllosilicate minerals in the

CV3 chondrites (e.g. Krot et al., 1995) but the main problem would be separating the fluid and minerals post clay formation, otherwise there would be no observable isotopic variation.

7.4.3 Relationship between chondrules and bulk chondrite

According to the $\delta^{30}\text{Si}$ data from Allende (this study) and Chainpur (Georg et al., 2007a), the mean Si isotopic composition of chondrules is more or less identical to that of bulk chondrites. This would be consistent with a generally homogeneous inner solar system with respect to Si isotopes, with the chondrule variability perhaps reflecting re-equilibration with the evaporated phase (Alexander, 2004) or the averaging out of very small scale heterogeneities. However for both Grosnaja and Mokoia the chondrule averages are rather heavier (-0.24 ± 0.20 , -0.32 ± 0.27) than the bulk chondrite average (-0.49 ± 0.15). This either reflects some kind of sampling bias or may be an indication of $\delta^{30}\text{Si}$ complementarity between chondrules and the matrix.

The matrix of chondrites is observed to be more FeO and volatile rich (e.g. Scott and Krot, 2007) than chondrules. One of the key questions is whether chondrules and matrix formed from the same chemical reservoir (e.g. Hezel and Palme, 2010), i.e. whether a complementarity exists, or whether there were completely separate reservoirs for the chondrules and matrix (e.g. Zanda et al., 2006). The former is consistent with shock-wave models for heating of chondrules such as those of Desch and Connelly (2002), but not the X-wind type models that require the formation of matrix and chondrules in separate regions of the solar nebula (e.g. Shu et al., 1996, 2001). Complementary relationships in carbonaceous chondrites have been reported for a number of element ratios, for example Fe/Cr (Palme et al., 1992), Mg/Si (Hezel and Palme, 2010) and a number of volatile trace elements (Bland et al., 2005). The Si composition of the matrix sample from Allende, $\delta^{30}\text{Si} = -0.63 \pm 0.04$ ($2\sigma_{SEM}$), is somewhat lighter than the average $\delta^{30}\text{Si}$ composition of the Allende chondrules ($\delta^{30}\text{Si}$

Figure (7.8): $\delta^{30}\text{Si}$ versus Mg/Si for CV3 components

$= -0.46 \pm 0.36, 2\sigma_{SD}$). This could be consistent with the matrix representing an evaporated, re-condensed complement to the chondrule forming reservoir as was suggested for Mg/Si ratios (Hezel and Palme, 2010). For a complementary relationship one would expect the bulk $\delta^{30}\text{Si}$ composition of Allende would have lie in between these two compositions. Examining the range of all the aliquots of Allende analysed (-0.45 to -0.37% , Chapter 4), this does not appear to be the case. However there are a number of explanation for this. Firstly, the sampling was biased against the smaller chondrules, which might be expected to have heavier compositions due to evaporation; therefore the chondrule reservoir might appear artificially light. Secondly, CAIs have very heavy Si isotopic compositions, such that a few volume percent is enough to perturb the bulk composition of Allende. If 3 vol% with a $\delta^{30}\text{Si}$ of 2.8% , is removed from the bulk composition of Allende ($-0.42 \pm 0.07, 2\sigma_{SD}$), the bulk value becomes -0.50% , which is between the matrix and chondrule Si isotopic compositions for Allende. Unfortunately as there is not the $\delta^{30}\text{Si}$ data for the matrices of Mokoia,

Grosnaja or Chainpur it is hard to assess whether this is truly a complementary relationship, or merely reflects mechanical mixing between two sources.

The Mg/Si compositions of CV chondrules and matrix reflect a complementary relationship (Hezel and Palme, 2010), with the matrix being enriched in Si. There is a suggestion of this in our data (Figure 7.8), therefore it is not unlikely that the Si isotope compositions might be as well. If so, this would lend weight to the idea that the $\delta^{30}\text{Si}$ fractionations in chondrules are as a result of evaporation followed by chondrule/gas re-equilibration (Alexander et al., 2008)

7.5 Conclusion

The high precision Si data produced in this study are consistent with previous work on chondrules that did not find any simple correlations between $\delta^{30}\text{Si}$ and any other bulk properties of chondrules (Clayton et al., 1991). The fractionation observed in the chondrules, though greater than the range observed in bulk meteorites, are still too limited to be consistent with a simple evaporative mechanism as observed for CAIs (Clayton et al., 1988; Shahar et al., 2009; Davis et al., 1990; Richter et al., 2002). A precursor origin for the variation cannot be ruled out, though the primary problem is sustaining small scale heterogeneities in a solar nebula that is thought to be quite well mixed with respect to Si isotopes (Georg et al., 2007a; Chakrabarti and Jacobsen, 2010b; Armytage et al., 2011).

The $\delta^{30}\text{Si}$ chondrule data do not show a strong evaporation control as there is no strong inverse correlation with size or Si/refractory element ratio. Due to the slow rates of Si diffusion in solids (see Chapter 6), there is no convincing argument for post-formation perturbation of the $\delta^{30}\text{Si}$ chondrule compositions. The most likely cause of the $\delta^{30}\text{Si}$ variation is evaporation and re-condensation in the solar nebula (Alexander, 2004).

Summary and Outlook

The aim of this thesis was to apply high precision Si isotopic measurement methods (external precision $\leq 0.15\text{‰}$, $2\sigma_{SD}$) to a variety of extra-terrestrial materials in order to further our understanding about the degree of heterogeneity of Si in the inner solar system and the nature of early differentiation of planetary bodies.

At the beginning of the study there existed considerably controversy over the $\delta^{30}\text{Si}$ composition of meteorites, bulk silicate Earth (BSE) and the difference between them, with the attendant implications for the amount of Si in the core. Georg et al. (2007a) measured an offset of $\Delta^{30}\text{Si}_{\text{BSE-chondrites}}$ of 0.2‰ with $\delta^{30}\text{Si}_{\text{BSE}} = -0.38 \pm 0.06$ ($1\sigma_{SD}$) and $\delta^{30}\text{Si}_{\text{chondrites}} = -0.58 \pm 0.05$ ($1\sigma_{SD}$). Fitoussi et al. (2009) using the exact same mass spectrometer measured $\delta^{30}\text{Si}_{\text{BSE}} = -0.28 \pm 0.03$ ($1\sigma_{SD}$) and $\Delta^{30}\text{Si}_{\text{BSE-carb. chondrites}} = -0.08 \pm 0.04\text{‰}$ ($1\sigma_{SD}$). Both these studies used the method developed by Georg et al. (2006a), and therefore the initial focus was to carry out a series of tests on this method to try and identify a cause of the variation in $\delta^{30}\text{Si}$ of individual samples and also $\Delta^{30}\text{Si}_{\text{BSE-chondrites}}$. No systematic differences in $\delta^{30}\text{Si}$ could be identified during re-analysis of the sample solutions from Georg et al. (2007a). Through tests on various aliquots of Allende, it was demonstrated that sample heterogeneity, filtration, and running acid did not impart any systematic shifts in the measured Si isotopic composition. Tests on the USGS standard, BHVO-2, rules out variations in pH being the cause of the discrepancies between Georg et al. (2007a) and Fitoussi et al. (2009). Sample addition tests on Allende doped with the Si standard IRMM-018 did not

reveal any systematic matrix effects inherent in the method of Georg et al. (2006a).

In addition to these tests, the Si isotopic composition of forty-two bulk meteorite and terrestrial mantle samples were measured. The terrestrial mantle samples had a $\delta^{30}\text{Si}$ composition of $-0.32 \pm 0.09\text{‰}$ ($2\sigma_{SD}$) in contrast to the meteorite average of $\delta^{30}\text{Si} = -0.48 \pm 0.13\text{‰}$ ($2\sigma_{SD}$). Although these populations are the same within $2\sigma_{SD}$ uncertainty, a student *t*-test confirms the difference of the means of BSE and meteorites of 0.16‰ at the 99.9% confidence level. Within the meteorites, no resolvable difference was observed in $\delta^{30}\text{Si}$ between achondrites and chondrites. The achondrites analysed included both wholly differentiated samples from Mars and Vesta, as well as the more primitive achondrite group the ureilites. The only meteorite group that showed variation from this fairly homogeneous population was the enstatite chondrites with a mean $\delta^{30}\text{Si}$ of $-0.63 \pm 0.07\text{‰}$ ($2\sigma_{SD}$). The cause for the deviation from this otherwise quite homogeneous inner solar system (excluding the Earth-Moon system) is still unclear. The BSE $\delta^{30}\text{Si}$ compositions were closer to Fitoussi et al. (2009) and Savage et al. (2010), than Georg et al. (2007a) or Chakrabarti and Jacobsen (2010b), whereas the meteorite $\delta^{30}\text{Si}$ compositions lay in between Fitoussi et al. (2009) and Georg et al. (2007a).

The measured offset $\Delta^{30}\text{Si}_{\text{BSE-meteorite}}$ was used, in conjunction with the metal-silicate fractionation factor from Shahar et al. (2009), to calculate the amount of Si in the core by fixing the temperature to the peridotite liquidus. The $\delta^{30}\text{Si}$ data is consistent with $\sim 9\text{wt}\%$ of Si in the core, which concurs with some experimental work (e.g. Gessmann et al., 2001), but is an overestimate relative to some models of the Earth's core (e.g. Tuff et al., 2010).

Analysis of 24 bulk lunar samples confirmed that the Moon is the only body measured so far in the inner solar system that has a Si isotopic composition like that of the bulk silicate Earth. The similarity is striking with average composition of the bulk Moon $\delta^{30}\text{Si} = -0.29 \pm 0.08\text{‰}$ ($2\sigma_{SD}$) being identical to that of bulk silicate

Earth $\delta^{30}\text{Si} = -0.29 \pm 0.08\text{‰}$ ($2\sigma_{SD}$) as constrained by Savage et al. (2011). The BSE Si isotopic composition is thought to result from Si partitioning into the metal phase during high-temperature high-pressure core formation, which would not have happened on bodies the size of Mars or the impactor without invoking extremely low oxygen fugacities. As it is thought the Moon is mostly derived from material from the impactor (e.g. Canup and Asphaug, 2001), this implies that Si isotopes, like oxygen isotopes, were homogenised in a vapour cloud in the aftermath of the giant Moon-forming impact (Pahlevan and Stevenson, 2007). It also means that any processes in the vapour cloud such as rainout (e.g. Pahlevan et al., 2011), did not operate to a degree to measurably fractionate Si isotopes. The homogeneity of the Si isotope composition of lunar rocks means that there is no evidence for different Si isotope reservoirs in the lunar mantle.

The Si isotopic composition of mineral separates from five lunar basalts were analysed. Plagioclase was found to be consistently the heaviest phase and show the most consistent composition between the samples. The mafic minerals were always light relative to plagioclase but were less consistent in $\delta^{30}\text{Si}$. As with the bulk lunar samples, the mineral separates $\delta^{30}\text{Si}$ compositions did not show any systematic differences between the low-Ti and high-Ti mare basalts. The inter-mineral Si isotope fractionation factors measured in lunar basalts were not consistent with those from the Skaergaard intrusion (Savage et al., 2011), in particular the direction of the olivine-pyroxene fractionation. Cooling rate and crystallisation history effects could not generate the observed $\delta^{30}\text{Si}$ patterns; hence it was concluded that mineral-melt Si isotopic fractionation factors are different in lunar and terrestrial settings. The lack of fractionation between bulk anorthosites and mare basalts, despite significant differentiation during the lunar magma ocean, was shown to be consistent with the measured mineral-melt fractionation factors.

Various components of the Allende meteorite including chondrules, one CAI (cal-

cium aluminium inclusion) and one matrix sample were separated and analysed both for their $\delta^{30}\text{Si}$ and major element bulk composition. The CAI showed mass-dependent behaviour and had the heaviest $\delta^{30}\text{Si}$ composition of any sample analysed in this thesis ($\delta^{30}\text{Si} = 2.81 \pm 0.03$, $2\sigma_{SEM}$), consistent with an evaporative origin (Davis et al., 1990; Wang et al., 2001). The $\delta^{30}\text{Si}$ composition of Allende chondrules showed a greater range in $\delta^{30}\text{Si}$ ($\sim 0.6\%$) than that of bulk meteorites ($\sim 0.3\%$), as observed in previous studies on chondrules from other meteorites (Molini-Velsko et al., 1986; Clayton et al., 1991; Georg et al., 2007a). The range in $\delta^{30}\text{Si}$ of the chondrules is still smaller than what is expected however, if the variation was purely the result of evaporation processes in the solar nebula (e.g. Davis et al., 2005). The $\delta^{30}\text{Si}$ of the chondrules also did not show any correlations with size, bulk chemical composition or Si/refractory element ratio, ruling out limited isotopic fractionation during evaporation into a high P_{H_2} environment. There was also no conclusive evidence that the variation was a result of precursor heterogeneity in $\delta^{30}\text{Si}$ or that the post-formation thermal or aqueous alteration caused the range in $\delta^{30}\text{Si}$. The most likely explanation is therefore that the $\delta^{30}\text{Si}$ variation was caused by evaporation and variable degrees of re-equilibration with the evaporated gas in the solar nebula (Alexander, 2004). The Si isotopic compositions of a matrix sample and chondrules from Allende are consistent with a complementary relationship between chondrules and matrix. However, more $\delta^{30}\text{Si}$ analyses on matrix and chondrules samples from other meteorites are needed to confirm this.

Fusion chemistry coupled with MC-ICPMS measurements have been shown to be a powerful tool to analyse a range of solar system materials for their Si isotopic composition. There is still the issue of a certain amount of inter laboratory discrepancy which will likely persist until there is a large-scale sample exchange programme with meteorite and rock standards not just pure Si standards. However, despite this, a non-zero $\Delta^{30}\text{Si}_{\text{BSE-meteorite}}$ appears to be relatively robust (Georg et al., 2007a; Fitoussi

et al., 2009; Ziegler et al., 2010; Armytage et al., 2011). Future avenues for the application of Si isotopes to cosmochemical questions should include experimental work on mineral $\delta^{30}\text{Si}$ fractionation factors in lunar basalts and a more detailed examination of the $\delta^{30}\text{Si}$ composition of enstatite chondrites and their components. Another useful direction, particularly for understanding the source of $\delta^{30}\text{Si}$ variation in chondrules, would be to combine Si isotopic analyses with Mg isotopic measurements on the same sample components.

References

- Abraham, K., Opfergelt, S., Fripiat, F., Cavagna, A. J., de Jong, J. T. M., Foley, S. F., André, L. and Cardinal, D. (2008). $\delta^{30}\text{Si}$ and $\delta^{29}\text{Si}$ determinations on USGS BHVO-1 and BHVO-2 reference materials with a new configuration on a Nu Plasma Multi-Collector ICP-MS, *Geostandards and Geoanalytical Research* **32**(2): 193–202.
- Ahrens, L. H., Von Michaelis, H. and Fesq, H. W. (1969). The composition of the stony meteorites (IV) some analytical data on Orgueil, Nogoya, Ornans and Ngawi, *Earth and Planetary Science Letters* **6**(4): 285–288.
- Alexander, C. (2004). Chemical equilibrium and kinetic constraints for chondrule and CAI formation conditions, *Geochimica et Cosmochimica Acta* **68**(19): 3943 – 3969.
- Alexander, C. M. O., Grossman, J. N., Ebel, D. S. and Ciesla, F. J. (2008). The formation conditions of chondrules and chondrites, *Science* **320**(5883): 1617–1619.
- Alexander, C. M. O., Grossman, J. N., Wang, J., Zanda, B., Bourot-Denise, M. and Hewins, R. H. (2000). The lack of potassium-isotopic fractionation in Bishunpur chondrules, *Meteoritics & Planetary Science* **35**(4): 859–868.
- Allègre, C. J., Poirier, J.-P., Humler, E. and Hofmann, A. W. (1995). The chemical composition of the Earth, *Earth and Planetary Science Letters* **134**(3-4): 515–526.
- Allenby, R. (1954). Determination of the isotopic ratios of silicon in rocks, *Geochimica et Cosmochimica Acta* **5**(1): 40 – 48.
- Amelin, Y., Kaltenbach, A., Iizuka, T., Stirling, C. H., Ireland, T. R., Petaev, M. and Jacobsen, S. B. (2010). U-Pb chronology of the solar system’s oldest solids with variable $^{238}\text{U}/^{235}\text{U}$, *Earth and Planetary Science Letters* **300**(3-4): 343–350.
- Amelin, Y., Krot, A. N., Hutcheon, I. D. and Ulyanov, A. A. (2002). Lead isotopic ages of chondrules and calcium-aluminum-rich inclusions, *Science* **297**(5587): 1678–1683.

- Anders, E. and Ebihara, M. (1982). Solar-system abundances of the elements, *Geochimica et Cosmochimica Acta* **46**(11): 2363–2380.
- André, L., Cardinal, D., Alleman, L. Y. and Moorbath, S. (2006). Silicon isotopes in ~3.8Ga West Greenland rocks as clues to the Eoarchaeon supracrustal Si cycle, *Earth and Planetary Science Letters* **245**(1-2): 162–173.
- Andreasen, R. and Sharma, M. (2006). Solar nebula heterogeneity in p-process samarium and neodymium isotopes, *Science* **314**(5800): 806–809.
- Apollo 16 Preliminary Examination, T. (1973). The Apollo 16 lunar samples: Petrographic and chemical description, *Science* **179**(4068): 23–34.
- Armytage, R., Georg, R., Savage, P., Williams, H. and Halliday, A. (2011). Silicon isotopes in meteorites and planetary core formation, *Geochimica et Cosmochimica Acta* **75**(13): 3662 – 3676.
- Asphaug, E., Jutzi, M. and Movshovitz, N. (2011). Chondrule formation during planetesimal accretion, *Earth and Planetary Science Letters* **308**(3-4): 369 – 379.
- Audi, G. and Wapstra, A. H. (1993). The 1993 atomic mass evaluation : (i) atomic mass table, *Nuclear Physics A* **565**(1): 1–65.
- Basile-Doelsch, I., Meunier, J. D. and Parron, C. (2005). Another continental pool in the terrestrial silicon cycle, *Nature* **433**(7024): 399–402.
- Beaty, D. W. and Albee, A. L. (1978). Comparative petrology and possible genetic relations among the Apollo 11 basalts, *Lunar and Planetary Science Conference Proceedings* **9**: 359–463.
- Becker, J. S. (2007). *Inorganic mass spectrometry: principles and applications*, John Wiley & Sons Ltd, Chichester, England.
- Becker, R. H. and Epstein, S. (1981). Silicon and oxygen isotopes in some selected Allende inclusions, *Lunar and Planetary Institute Science Conference Abstracts*, Vol. 12, pp. 56–58.
- Béjina, F. and Jaoul, O. (1996). Silicon self-diffusion in quartz and diopside measured by nuclear micro-analysis methods, *Physics of The Earth and Planetary Interiors* **97**(1-4): 145–162.

- Beucher, C. P., Brzezinski, M. A. and Jones, J. L. (2008). Sources and biological fractionation of silicon isotopes in the Eastern Equatorial Pacific, *Geochimica et Cosmochimica Acta* **72**(13): 3063 – 3073.
- Bianco, A. S. and Taylor, L. A. (1977). Applications of dynamic crystallization studies - lunar olivine-normative basalts, *Lunar and Planetary Science Conference Proceedings*, Vol. 8, pp. 1593–1610.
- Bigeleisen, J. and Mayer, M. G. (1947). Calculation of equilibrium constants for isotopic exchange reactions, *The Journal of Chemical Physics* **15**(5): 261–267.
- Birch, F. (1964). Density and composition of mantle and core, *J. Geophys. Res.* **69**: 4377–4388.
- Bland, P. A., Alard, O., Benedix, G. K., Kearsley, A. T., Menzies, O. N., Watt, L. E. and Rogers, N. W. (2005). Volatile fractionation in the early solar system and chondrule/matrix complementarity, **102**(39): 13755–13760.
- Bland, P. A., Lee, M. R., Sexton, A. S., Franchi, I. A., Fallick, A. E. T., Miller, M. F., Cadogan, J. M., Berry, F. J. and Pillinger, C. T. (2000). Aqueous alteration without a pronounced oxygen-isotopic shift: Implications for the asteroidal processing of chondritic materials, *Meteoritics & Planetary Science* **35**(6): 1387–1395.
- Bonal, L., Quirico, E., Bourot-Denise, M. and Montagnac, G. (2006). Determination of the petrologic type of CV3 chondrites by Raman spectroscopy of included organic matter, *Geochimica et Cosmochimica Acta* **70**(7): 1849 – 1863.
- Boss, A. (1996). A concise guide to chondrule formation mechanisms, *in* R. Hewins, R. Jones and E. Scott (eds), *Chondrules and Protoplanetary disk*, Cambridge University Press, pp. 257–264.
- Boss, A. (2007). The solar nebula, *in* H. D. Holland and K. K. Turekian (eds), *Treatise on Geochemistry*, Pergamon, Oxford, pp. 1 – 23.
- Bourdon, B., Tipper, E. T., Fitoussi, C. and Stracke, A. (2010). Chondritic Mg isotope composition of the earth, *Geochimica et Cosmochimica Acta* **74**(17): 5069–5083.
- Brandon, A. D., Humayun, M., Puchtel, I. S., Leya, I. and Zolensky, M. (2005). Osmium isotope evidence for an s-process carrier in primitive chondrites, *Science* **309**(5738): 1233–1236.

- Brearley, A. J. (2003). Nebular versus parent-body processing, in D. H. Heinrich and K. T. Karl (eds), *Treatise on Geochemistry*, Pergamon, Oxford, pp. 247–268.
- Brearley, A. J. and Jones, R. H. (1998). Chondritic meteorites, *Reviews in Mineralogy* **36**.
- Brown, G. M., Peckett, A., Emeleus, C. H., Phillips, R. and Pinsent, R. H. (1975). Petrology and mineralogy of Apollo 17 mare basalts, *Lunar and Planetary Science Conference Proceedings*, Vol. 6, pp. 1–13.
- Brzezinski, M. A., Jones, J. L., Beucher, C. P., Demarest, M. S. and Berg, H. L. (2006). Automated determination of silicon isotope natural abundance by the acid decomposition of cesium hexafluosilicate, *Analytical Chemistry* **78**(17): 6109–6114.
- Bunch, T. E. and Reid, A. M. (1975). The Nakhilites. I - petrography and mineral chemistry, *Meteoritics* **10**: 303–315.
- Cameron, A. (2000). High resolution simulations of the giant impact, in K. Righter and R. M. Canup (eds), *Origin of the Earth and Moon*, University of Arizona Press, Tuscon, AZ, pp. 133–144.
- Canup, R. M. and Asphaug, E. (2001). Origin of the Moon in a giant impact near the end of the Earth's formation, *Nature* **412**(6848): 708–712.
- Cardinal, D., Alleman, L. Y., de Jong, J., Ziegler, K. and André, L. (2003). Isotopic composition of silicon measured by multi collector plasma source mass spectrometry in dry plasma mode, *Journal of Analytical Atomic Spectrometry* **18**(3): 213–218.
- Chakrabarti, R. and Jacobsen, S. B. (2009). A combined silicon and magnesium isotopic study of bulk meteorites and the earth, *Lunar and Planetary Science Conference*, Vol. 40, p. 2089.
- Chakrabarti, R. and Jacobsen, S. B. (2010a). The isotopic composition of magnesium in the inner solar system, *Earth and Planetary Science Letters* **293**(3-4): 349–358.
- Chakrabarti, R. and Jacobsen, S. B. (2010b). Silicon isotopes in the inner solar system: Implications for core formation, solar nebular processes and partial melting, *Geochimica et Cosmochimica Acta* **74**(23): 6921–6933.
- Chakraborty, S. (2010). Diffusion coefficients in olivine, wadsleyite and ringwoodite, *Reviews in Mineralogy and Geochemistry* **72**(1): 603–639.

-
- Chambers, J. (2007). Planet formation, *in* H. D. Holland and K. K. Turekian (eds), *Treatise on Geochemistry*, Pergamon, Oxford, pp. 1 – 17.
- Chen, J. H., Papanastassiou, D. A. and Wasserburg, G. J. (2010). Ruthenium endemic isotope effects in chondrites and differentiated meteorites, *Geochimica et Cosmochimica Acta* **74**(13): 3851–3862.
- Cherniak, D. J. (2003). Silicon self-diffusion in single-crystal natural quartz and feldspar, *Earth and Planetary Science Letters* **214**(3-4): 655–668.
- Chmeleff, J., Horn, I., Steinhofel, G. and von Blanckenburg, F. (2008). In situ determination of precise stable Si isotope ratios by UV-femtosecond laser ablation high-resolution multi-collector ICP-MS, *Chemical Geology* **249**(1-2): 155–166.
- Ciesla, F. J. and Hood, L. L. (2002). The nebular shock wave model for chondrule formation: Shock processing in a particle-gas suspension, *Icarus* **158**(2): 281 – 293.
- Clayton, D. D. (2003a). *Handbook of Isotopes in the Cosmos: Hydrogen to Gallium*, Cambridge University Press, Cambridge.
- Clayton, R. N. (2003b). Oxygen isotopes in meteorites, *in* D. H. Heinrich and K. T. Karl (eds), *Treatise on Geochemistry*, Pergamon, Oxford, pp. 129–142.
- Clayton, R. N., Hinton, R. W. and Davis, A. M. (1988). Isotopic variations in the rock-forming elements in meteorites, *Philosophical Transactions of the Royal Society of London Series a-Mathematical Physical and Engineering Sciences* **325**(1587): 483–501.
- Clayton, R. N. and Mayeda, T. K. (1996). Oxygen isotope studies of achondrites, *Geochimica et Cosmochimica Acta* **60**(11): 1999–2017.
- Clayton, R. N. and Mayeda, T. K. (1999). Oxygen isotope studies of carbonaceous chondrites, *Geochimica et Cosmochimica Acta* **63**(13-14): 2089 – 2104.
- Clayton, R. N., Mayeda, T. K., Goswami, J. N. and Olsen, E. J. (1991). Oxygen isotope studies of ordinary chondrites, *Geochimica et Cosmochimica Acta* **55**(8): 2317–2337.
- Clayton, R. N., Mayeda, T. K. and Rubin, A. E. (1984). Oxygen isotopic compositions of enstatite chondrites and aubrites, *J. Geophys. Res.* **89**(S1): C245–C249.

- Clayton, R. N., Onuma, N. and Mayeda, T. K. (1976). A classification of meteorites based on oxygen isotopes, *Earth and Planetary Science Letters* **30**(1): 10 – 18.
- Cohen, B. A., Hewins, R. H. and Yu, Y. (2000). Evaporation in the young solar nebula as the origin of ‘just-right’ melting of chondrules, *Nature* **406**(6796): 600–602.
- Connolly Jr, H. and Hewins, R. (1996). Constraints on chondrule precursors from experimental data, in R. Hewins, R. Jones and E. Scott (eds), *Chondrules and Protoplanetary disk*, Cambridge University Press, pp. 129–135.
- Cornbleet, P. and Gochman, N. (1979). Incorrect least-squares regression coefficients in method-comparison analysis, *Clin Chem* **25**(3): 432–438.
- Cuzzi, J. N. and Alexander, C. M. O. (2006). Chondrule formation in particle-rich nebular regions at least hundreds of kilometres across, *Nature* **441**(7092): 483–485.
- Dauphas, N., Marty, B. and Reisberg, L. (2002). Molybdenum evidence for inherited planetary scale isotope heterogeneity of the protosolar nebula, *The Astrophysical Journal* **565**(1): 640–644.
- Davis, A. M., Alexander, C. M. O., Nagahara, H. and Richter, F. M. (2005). Evaporation and condensation during CAI and chondrule formation, in A. N. Krot, E. R. D. Scott, & B. Reipurth (ed.), *Chondrites and the Protoplanetary Disk*, Vol. 341 of *Astronomical Society of the Pacific Conference Series*, pp. 432–455.
- Davis, A. M., Hashimoto, A., Clayton, R. N. and Mayeda, T. K. (1990). Isotope mass fractionation during evaporation of Mg_2SiO_4 , *Nature* **347**(6294): 655–658.
- Day, J. M. D., Pearson, D. G. and Taylor, L. A. (2007). Highly siderophile element constraints on accretion and differentiation of the Earth-Moon system, *Science* **315**(5809): 217–219.
- Day, J. M. D., Walker, R. J., James, O. B. and Puchtel, I. S. (2010). Osmium isotope and highly siderophile element systematics of the lunar crust, *Earth and Planetary Science Letters* **289**(3-4): 595–605.
- de Hoffmann, E. and Stroobant, V. (2007). *Mass spectrometry: principles and applications*, 3rd edn, John Wiley & Sons Ltd, Chichester, England.
- De La Rocha, C. (2002). Measurement of silicon stable isotope natural abundances via multicollector inductively coupled plasma mass spectrometry (MC-ICP-MS), *Geochemistry, Geophysics, Geosystems* p. 1045.

- De La Rocha, C. L., Brzezinski, M. A. and DeNiro, M. J. (1996). Purification, recovery, and laser-driven fluorination of silicon from dissolved and particulate silica for the measurement of natural stable isotope abundances, *Analytical Chemistry* **68**(21): 3746–3750.
- De La Rocha, C. L., Brzezinski, M. A. and DeNiro, M. J. (2000). A first look at the distribution of the stable isotopes of silicon in natural waters, *Geochimica et Cosmochimica Acta* **64**(14): 2467–2477.
- Delstanche, S., Opfergelt, S., Cardinal, D., Elsass, F., André, L. and Delvaux, B. (2009). Silicon isotopic fractionation during adsorption of aqueous monosilicic acid onto iron oxide, *Geochimica et Cosmochimica Acta* **73**(4): 923–934.
- Desch, S. J. and Connelly, H. C. (2002). A model of the thermal processing of particles in solar nebula shocks: Application to the cooling rates of chondrules, *Meteoritics & Planetary Science* **37**(2): 183–207.
- Ding, T., Jiang, S., Wan, D., Li, Y., Li, J., Song, H., Liu, Z. and Yao, X. (1996). *Silicon Isotope Geochemistry*, Geological Publishing House, Beijing, China.
- Ding, T. P., Tian, S. H., Sun, L., Wu, L. H., Zhou, J. X. and Chen, Z. Y. (2008). Silicon isotope fractionation between rice plants and nutrient solution and its significance to the study of the silicon cycle, *Geochimica et Cosmochimica Acta* **72**(23): 5600–5615.
- Dodson, M. (1963). A theoretical study of the use of internal standards for precise isotopic analysis by the surface ionization technique: Part I - general first-order algebraic solutions, *Journal of Scientific Instruments* **40**(6): 289.
- Dodson, M. H. (1973). Closure temperature in cooling geochronological and petrological systems, *Contributions to Mineralogy and Petrology* **40**(3): 259–274. 0010-7999.
- Dohmen, R., Chakraborty, S. and Becker, H.-W. (2002). Si and O diffusion in olivine and implications for characterizing plastic flow in the mantle, *Geophys. Res. Lett.* **29**(21): 2030.
- Douthitt, C. B. (1982). The geochemistry of the stable isotopes of silicon, *Geochimica et Cosmochimica Acta* **46**(8): 1449–1458.
- Drake, M. J. and Righter, K. (2002). Determining the composition of the earth, *Nature* **416**(6876): 39–44.

- Dreibus, G., Palme, H., Spettel, B., Zipfel, J. and Wanke, H. (1995). Sulfur and selenium in chondritic meteorites, *Meteoritics* **30**: 439–445.
- Dreibus, G., Spettel, B., Haubold, R., P., J. K., Palme, H., D., W., Zipfel, J. and Wanke, H. (2000). Chemistry of a new shergottite: Sayh al Uhaymir 005, *Meteorit. Planet. Sci.* **35**: A49.
- Dymek, R. F., Albee, A. L. and Chodos, A. A. (1975). Comparative mineralogy and petrology of Apollo 17 mare basalts - Samples 70215, 71055, 74255, and 75055, *Lunar and Planetary Science Conference Proceedings*, Vol. 6, pp. 49–77.
- Easton, A. J. (1985a). E-chondrites - significance of the partition of elements between ‘silicate’ and ‘sulphide’, *Meteoritics* **20**: 89–101.
- Easton, A. J. (1985b). Seven new bulk chemical analyses of aubrites, *Meteoritics* **20**: 571–573.
- Engström, E., Rodushkin, I., Baxter, D. C. and Ohlander, B. (2006). Chromatographic purification for the determination of dissolved silicon isotopic compositions in natural waters by high-resolution multicollector inductively coupled plasma mass spectrometry, *Analytical Chemistry* **78**(1): 250–257.
- Epstein, S. and Taylor Jr., H. P. (1970a). $^{18}\text{O}/^{16}\text{O}$, $^{30}\text{Si}/^{28}\text{Si}$, D/H, and $^{13}\text{C}/^{12}\text{C}$ studies of lunar rocks and minerals, *Science* **167**(3918): 533–535.
- Epstein, S. and Taylor Jr., H. P. (1970b). The concentration and isotopic composition of hydrogen, carbon and silicon in Apollo 11 lunar rocks and minerals, *Proc. Apollo 11 Lunar Science Conf.*, Vol. 2, Pergamon, New York, pp. 1085–1096.
- Epstein, S. and Taylor Jr., H. P. (1971). $^{18}\text{O}/^{16}\text{O}$, $^{30}\text{Si}/^{28}\text{Si}$, D/H and $^{13}\text{C}/^{12}\text{C}$ ratios in lunar samples, *Lunar and Planetary Science Conference Proceedings* **2**: 1421.
- Epstein, S. and Taylor Jr., H. P. (1972). $^{18}\text{O}/^{16}\text{O}$, $^{30}\text{Si}/^{28}\text{Si}$, $^{13}\text{C}/^{12}\text{C}$ and D/H studies of Apollo 14 and 15 samples, *Lunar and Planetary Science Conference Proceedings* **3**: 1429.
- ESO (1997). New detailed image of the disk around Beta Pictoris. Accessed 22 Jun 2011.
URL: <http://www.eso.org/public/news/eso9714/>

- Fantle, M. S. and Bullen, T. D. (2009). Essentials of iron, chromium, and calcium isotope analysis of natural materials by thermal ionization mass spectrometry, *Chemical Geology* **258**(1-2): 50–64.
- Fehr, M., Rehkämper, M., Halliday, A. N., Schönbächler, M., Hattendorf, B. and Günther, D. (2006). Search for nucleosynthetic and radiogenic tellurium isotope anomalies in carbonaceous chondrites, *Geochimica et Cosmochimica Acta* **70**(13): 3436 – 3448.
- Fitoussi, C., Bourdon, B., Kleine, T., Oberli, F. and Reynolds, B. C. (2008). Si isotopic composition of the Earth’s mantle and meteorites, *Geochimica et Cosmochimica Acta* **72**(12, Supplement 1): A273.
- Fitoussi, C., Bourdon, B., Kleine, T., Oberli, F. and Reynolds, B. C. (2009). Si isotope systematics of meteorites and terrestrial peridotites: implications for Mg/Si fractionation in the solar nebula and for Si in the Earth’s core, *Earth and Planetary Science Letters* **287**(1-2): 77–85.
- Fitoussi, C., Bourdon, B., Pahlevan, K. and Wieler, R. (2010). Si isotope constraints on the moon-forming impact, *Lunar and Planetary Science Conference*, Vol. 41, p. 2653.
- Fulton, C. R. and Rhodes, J. M. (1984). The chemistry and origin of the ordinary chondrites: implications from refractory-lithophile and siderophile elements, *J. Geophys. Res.* **89**: 543.
- Galer, S. J. G. and O’Nions, R. K. (1989). Chemical and isotopic studies of ultramafic inclusions from the San Carlos Volcanic Field, Arizona: a bearing on their petrogenesis, *Journal of Petrology* **30**(4): 1033–1064.
- Galy, A., Young, E. D., Ash, R. D. and O’Nions, R. K. (2000). The formation of chondrules at high gas pressures in the solar nebula, *Science* **290**(5497): 1751–1753.
- Gancarz, A., Albee, A. and Chodos, A. (1971). Petrologic and mineralogic investigation of some crystalline rocks returned by the Apollo 14 mission, *Earth and Planetary Science Letters* **12**(1): 1 – 18.
- Ganguly, J. and Domeneghetti, M. C. (1996). Cation ordering of orthopyroxenes from the skaergaard intrusion: implications for the subsolidus cooling rates and permeabilities, *Contributions to Mineralogy and Petrology* **122**(4): 359–367. 0010-7999.

- Georg, R. B. (2006). *Geochemistry of Stable silicon isotopes measured by High-resolution multi-collector inductively-coupled-plasma mass-spectrometry (HR-MC-ICP-MS)*, PhD thesis, ETH Zürich.
- Georg, R. B., Halliday, A. N., Schauble, E. A. and Reynolds, B. C. (2007a). Silicon in the earth's core, *Nature* **447**(7148): 1102–1106.
- Georg, R. B., Reynolds, B. C., Frank, M. and Halliday, A. N. (2006a). New sample preparation techniques for the determination of Si isotopic compositions using MC-ICPMS, *Chemical Geology* **235**(1-2): 95–104.
- Georg, R. B., Zhu, C., Reynolds, B. C. and Halliday, A. N. (2009a). Stable silicon isotopes of groundwater, feldspars, and clay coatings in the Navajo Sandstone aquifer, Black Mesa, Arizona, USA, *Geochimica et Cosmochimica Acta* **73**(8): 2229–2241.
- Georg, R., Reynolds, B., Frank, M. and Halliday, A. (2006b). Mechanisms controlling the silicon isotopic compositions of river waters, *Earth and Planetary Science Letters* **249**(3-4): 290 – 306.
- Georg, R., Reynolds, B., West, A., Burton, K. and Halliday, A. (2007b). Silicon isotope variations accompanying basalt weathering in Iceland, *Earth and Planetary Science Letters* **261**(3-4): 476 – 490.
- Georg, R., West, A., Basu, A. and Halliday, A. (2009b). Silicon fluxes and isotope composition of direct groundwater discharge into the Bay of Bengal and the effect on the global ocean silicon isotope budget, *Earth and Planetary Science Letters* **283**(1-4): 67 – 74.
- Gessmann, C. K. and Rubie, D. C. (2000). The origin of the depletions of V, Cr and Mn in the mantles of the Earth and Moon, *Earth and Planetary Science Letters* **184**(1): 95–107.
- Gessmann, C. K., Wood, B. J., Rubie, D. C. and Kilburn, M. R. (2001). Solubility of silicon in liquid metal at high pressure: implications for the composition of the earth's core, *Earth and Planetary Science Letters* **184**(2): 367–376.
- Gibson, E. K. and Moore, C. B. (1983). Sulfur in achondritic meteorites, *Lunar and Planetary Science Conference*, Vol. 14, pp. 247–248.
- Goodrich, C. (1992). Ureilites: A critical review, *Meteoritics* **27**: 327–352.

-
- Grady, M. (2000). *Catalogue of Meteorites*, 5th edn, Cambridge University Press, Cambridge.
- Graham, A. L., Easton, A. J., Hutchison, R. and Jérôme, D. Y. (1976). The Bovedy meteorite; mineral chemistry and origin of its Ca-rich glass inclusions, *Geochimica et Cosmochimica Acta* **40**(5): 529–530, IN3, 531–535.
- Greenwood, R. C., Franchi, I. A., Jambon, A. and Buchanan, P. C. (2005). Widespread magma oceans on asteroidal bodies in the early solar system, *Nature* **435**(7044): 916–918.
- Grossman, J. N. and Wasson, J. T. (1982). Evidence for primitive nebular components in chondrules from the Chainpur chondrite, *Geochimica et Cosmochimica Acta* **46**(6): 1081 – 1099.
- Grove, T. L. and Krawczynski, M. J. (2009). Lunar mare volcanism: Where did the magmas come from?, *ELEMENTS* **5**(1): 29–34.
- Hallis, L. J., Anand, M., Greenwood, R. C., Miller, M. F., Franchi, I. A. and Russell, S. S. (2010). The oxygen isotope composition, petrology and geochemistry of mare basalts: Evidence for large-scale compositional variation in the lunar mantle, *Geochimica et Cosmochimica Acta* **74**(23): 6885–6899.
- Hartmann, W. K. and Davis, D. R. (1975). Satellite-sized planetesimals and lunar origin, *Icarus* **24**(4): 504–515.
- Head, J. W. and Wilson, L. (1992). Lunar mare volcanism: Stratigraphy, eruption conditions, and the evolution of secondary crusts, *Geochimica et Cosmochimica Acta* **56**(6): 2155–2175.
- Hendry, K. R., Georg, R. B., Rickaby, R. E., Robinson, L. F. and Halliday, A. N. (2010). Deep ocean nutrients during the Last Glacial Maximum deduced from sponge silicon isotopic compositions, *Earth and Planetary Science Letters* **292**(3–4): 290 – 300.
- Herbert, C. G. and Johnstone, R. A. W. (2003). *Mass spectrometry basics*, CRC Press LLC, Boca Raton, Florida.
- Heuer, A. H., Nord Jr., G. L., Radcliffe, S. V., Fisher, R. M., Lally, J. S., Christie, J. M. and Griggs, D. T. (1972). High-voltage (HVEM) electron petrographic study of Apollo 15 rocks., *The Apollo 15 Lunar Samples*, pp. 98–102.

- Hewins, R., Connolly Jr., H., Lofgren, G. E. and Libourel, G. (2005). Experimental constraints on chondrule formation, *in* A. N. Krot, E. R. D. Scott, & B. Reipurth (ed.), *Chondrites and the Protoplanetary Disk*, Vol. 341 of *Astronomical Society of the Pacific Conference Series*, p. 286.
- Hezel, D. C., Armytage, R. M. G., Georg, R. B., Keren, E. and Russell, S. S. (2009). Combined Fe- and Si-isotope measurements of CV chondrite chondrules and CAIs, *Lunar and Planetary Science Conference*, Vol. 40.
- Hezel, D. C., Needham, A. W., Armytage, R., Georg, B., Abel, R. L., Kurahashi, E., Coles, B. J., Rehkämper, M. and Russell, S. S. (2010). A nebula setting as the origin for bulk chondrule Fe isotope variations in CV chondrites, *Earth and Planetary Science Letters* **296**(3-4): 423 – 433.
- Hezel, D. C., Needham, A. W. and Russell, S. S. (2008). Fe-isotopic composition of chondrules, CAIs, matrix and bulk meteorite in Mokoia and Grosnaja CV-chondrites, *Lunar and Planetary Institute Science Conference Abstracts*, Vol. 39, p. 1603.
- Hezel, D. C. and Palme, H. (2010). The chemical relationship between chondrules and matrix and the chondrule matrix complementarity, *Earth and Planetary Science Letters* **294**(1-2): 85 – 93.
- Hoppe, P., Amari, S., Zinner, E., Ireland, T. and Lewis, R. S. (1994). Carbon, nitrogen, magnesium, silicon, and titanium isotopic compositions of single interstellar silicon carbide grains from the Murchison carbonaceous chondrite, *The Astrophysical Journal* **430**: 870–890.
- Hoppe, P., Amari, S., Zinner, E. and Lewis, R. S. (1995). Isotopic compositions of C, N, O, Mg, and Si, trace element abundances, and morphologies of single circumstellar graphite grains in four density fractions from the Murchison meteorite, *Geochimica et Cosmochimica Acta* **59**(19): 4029 – 4056.
- Hoppe, P., Annen, P., Strebel, R., Eberhardt, P., Gallino, R., Lugaro, M., Amari, S. and Lewis, R. S. (1997). Meteoritic silicon carbide grains with unusual Si-isotopic compositions: Evidence for an origin in low-mass, low-metallicity asymptotic giant branch stars, *The Astrophysical Journal Letters* **487**(1): L101.
- Hoppe, P., Strebel, R., Eberhardt, P., Amari, S. and Lewis, R. S. (1996). Small SiC grains and a nitride grain of circumstellar origin from the Murchison meteorite:

- Implications for stellar evolution and nucleosynthesis, *Geochimica et Cosmochimica Acta* **60**(5): 883 – 907.
- Horan, M. F., Walker, R. J., Morgan, J. W., Grossman, J. N. and Rubin, A. E. (2003). Highly siderophile elements in chondrites, *Chemical Geology* **196**(1-4): 27–42.
- Huss, G. R. and Hutcheon, Ian D. and Wasserburg, G. J. (1997). Isotopic systematics of presolar silicon carbide from the Orgueil (CI) chondrite: Implications for solar system formation and stellar nucleosynthesis, *Geochimica et Cosmochimica Acta* **61**(23): 5117 – 5148.
- Hutchison, R. (2006). *Meteorites: a petrologic, chemical and isotopic synthesis*, Cambridge University Press.
- Ito, E., Morooka, K., Ujike, O. and Katsura, T. (1995). Reactions between molten iron and silicate melts at high-pressure - implications for the chemical evolution of earths core, *Journal of Geophysical Research-Solid Earth* **100**(B4): 5901–5910.
- Itoh, S., Rubin, A. E., Kojima, H., Wasson, J. T. and Yurimoto, H. (2002). Amoeboid olivine aggregates and AOA-bearing chondrule from Y-81020 CO3.0 chondrite: Distribution of oxygen and magnesium isotopes, *Lunar and Planetary Institute Science Conference Abstracts*, Vol. 33, p. 1490.
- Jarosewich, E. (1967). Chemical analyses of seven stony meteorites and one iron with silicate inclusions, *Geochimica et Cosmochimica Acta* **31**(6): 1103–1106.
- Jarosewich, E. (1990). Chemical analyses of meteorites: A compilation of stony and iron meteorite analyses, *Meteoritics* **25**: 323–337.
- Jarosewich, E., Clarke, R. S. and Barrows, J. N. (1987). The Allende Meteorite Reference Sample, *Smithsonian Contributions to the Earth Sciences* **27**: 1–49.
- Jarosewich, E. and Mason, B. (1969). Chemical analyses with notes on one mesosiderite and seven chondrites, *Geochimica et Cosmochimica Acta* **33**(3): 411 – 416.
- Javoy, M., Kaminski, E., Guyot, F., Andrault, D., Sanloup, C., Moreira, M., Labrosse, S., Jambon, A., Agrinier, P., Davaille, A. and Jaupart, C. (2010). The chemical composition of the Earth: Enstatite chondrite models, *Earth and Planetary Science Letters* **293**(3-4): 259–268.

- Jochum, K., Grais, K. and Hintenberger, H. (1980). Chemical composition and classification of 19 Yamato meteorites, *Meteoritics* **15**: 31–39.
- Jolliff, B. L., Gillis, J. J., Haskin, L. A., Korotev, R. L. and Wieczorek, M. A. (2000). Major lunar crustal terranes: Surface expressions and crust-mantle origins, *J. Geophys. Res.* **105**(E2): 4197–4216.
- Jones, R. H. (1990). Petrology and mineralogy of Type II, FeO-rich chondrules in Semarkona (LL3.0): Origin by closed-system fractional crystallization, with evidence for supercooling, *Geochimica et Cosmochimica Acta* **54**(6): 1785 – 1802.
- Keil, K. (2000). Thermal alteration of asteroids: evidence from meteorites, *Planetary and Space Science* **48**(10): 887 – 903.
- Keil, K. (2010). Enstatite achondrite meteorites (aubrites) and the histories of their asteroidal parent bodies, *Chemie der Erde - Geochemistry* **70**(4): 295–317.
- Kilburn, M. R. and Wood, B. J. (1997). Metal-silicate partitioning and the incompatibility of S and Si during core formation, *Earth and Planetary Science Letters* **152**(1-4): 139–148.
- Kitts, K. and Lodders, K. (1998). Survey and evaluation of eucrite bulk compositions, *Meteoritics & Planetary Science* **33**(S4): A197–A213. 1945-5100.
- Kleine, T., Mezger, K., Palme, H., Scherer, E. and Münker, C. (2005). Early core formation in asteroids and late accretion of chondrite parent bodies: Evidence from ^{182}Hf - ^{182}W in CAIs, metal-rich chondrites, and iron meteorites, *Geochimica et Cosmochimica Acta* **69**(24): 5805–5818.
- Knight, K. B., Kita, N. T., Davis, A. M., Richter, F. M. and Mendybaev, R. A. (2009a). Mg and Si isotope fractionation within three Type B Ca-Al-rich inclusions, *Lunar and Planetary Institute Science Conference Abstracts*, Vol. 40, p. 2360.
- Knight, K. B., Kita, N. T., Mendybaev, R. A., Richter, F. M., Davis, A. M. and Valley, J. W. (2009b). Silicon isotopic fractionation of CAI-like vacuum evaporation residues, *Geochimica et Cosmochimica Acta* **73**(20): 6390–6401.
- Kong, P., Ebihara, M. and Palme, H. (1999). Siderophile elements in martian meteorites and implications for core formation in Mars, *Geochimica et Cosmochimica Acta* **63**(11-12): 1865–1875.

- Krot, A., Amelin, Y., Bland, P., Ciesla, F., Connelly, J., Davis, A., Huss, G., Hutcheon, I., Makide, K., Nagashima, K., Nyquist, L., Russell, S., Scott, E., Thrane, K., Yurimoto, H. and Yin, Q.-Z. (2009). Origin and chronology of chondritic components: A review, *Geochimica et Cosmochimica Acta* **73**(17): 4963 – 4997.
- Krot, A. N., Keil, K., Scott, E. R. D., Goodrich, C. A. and Weisberg, M. K. (2007). Classification of meteorites, in D. H. Heinrich and K. T. Karl (eds), *Treatise on Geochemistry*, Pergamon, Oxford, pp. 1–52.
- Krot, A. N., Scott, E. R. D. and Zolensky, M. E. (1995). Mineralogical and chemical modification of components in CV3 chondrites: Nebular or asteroidal processing?, *Meteoritics* **30**: 748–775.
- Kubota, R. (2009). Simultaneous determination of total carbon, nitrogen, hydrogen and sulfur in twenty-seven geological reference materials by elemental analyser, *Geostandards and Geoanalytical Research* **33**(2): 271–283.
- Lagrange, A.-M., Bonnefoy, M., Chauvin, G., Apai, D., Ehrenreich, D., Boccaletti, A., Gratadour, D., Rouan, D., Mouillet, D., Lacour, S. and Kasper, M. (2010). A giant planet imaged in the disk of the young star β Pictoris, *Science* **329**(5987): 57–59.
- Larimer, J. and Anders, E. (1970). Chemical fractionations in meteorites -III. Major element fractionations in chondrites, *Geochimica et Cosmochimica Acta* **34**(3): 367 – 387.
- Laul, J. C. and Schmitt, R. A. (1973). Chemical composition of Apollo 15, 16, and 17 samples, *Proceedings of the Fourth Lunar Science Conference*, Vol. 4, p. 1349.
- Lee, D. C. and Halliday, A. N. (2000). Accretion of primitive planetesimals: Hf-W isotopic evidence from enstatite chondrites, *Science* **288**(5471): 1629–1631.
- Lee, D.-C., Halliday, A. N., Singletary, S. J. and Grove, T. L. (2009). ^{182}Hf - ^{182}W chronometry and early differentiation of the ureilite parent body, *Earth and Planetary Science Letters* **288**(3-4): 611–618.
- Lee, D.-C., Halliday, A. N., Snyder, G. A. and Taylor, L. A. (1997). Age and origin of the moon, *Science* **278**(5340): 1098–1103.
- Leng, M. J. and Sloane, H. J. (2008). Combined oxygen and silicon isotope analysis of biogenic silica, *Journal of Quaternary Science* **23**(4): 313–319.

- Leya, I., Graf, T., Nishiizumi, K. and Wieler, R. (2001). Cosmic-ray production rates of He-, Ne- and Ar-isotopes in H-chondrites based on ^{36}Cl - ^{36}Ar -ages, *Meteoritics & Planetary Science* **36**: 963–973.
- Leya, I., Schönbächler, M., Wiechert, U., Krahenbuhl, U. and Halliday, A. N. (2008). Titanium isotopes and the radial heterogeneity of the solar system, *Earth and Planetary Science Letters* **266**(3-4): 233–244.
- Lindstrom, M. M. and Lindstrom, D. J. (1986). Lunar granulites and their precursor anorthositic norites of the early lunar crust, *Lunar and Planetary Science Conference Proceedings*, Vol. 16, p. 263.
- Liu, Y., Spicuzza, M. J., Craddock, P. R., Day, J. M. D., Valley, J. W., Dauphas, N. and Taylor, L. A. (2010). Oxygen and iron isotope constraints on near-surface fractionation effects and the composition of lunar mare basalt source regions, *Geochimica et Cosmochimica Acta* **74**(21): 6249–6262.
- Lodders, K. (1998). A survey of shergottite, nakhlite and chassigny meteorites whole-rock compositions, *Meteorit. Planet. Sci.* **33**: A183–A190.
- Lodders, K. (2003). Solar system abundances and condensation temperatures of the elements, *Astrophysical Journal* **591**(2 I): 1220–1247.
- Longhi, J., Walker, D., Stolper, E. N., Grove, T. L. and Hays, J. F. (1972). Petrology of mare/rille basalts 15555 and 15065., *The Apollo 15 Lunar Samples*, pp. 131–134.
- LSPET (1973). Preliminary Examination of lunar samples, *Apollo 17 Preliminary Science Rpt.*, Vol. NASA SP-330, pp. 7–1 7–46.
- MacPherson, G. (2003). Calcium-aluminum-rich inclusions in chondritic meteorites, in H. D. Holland and K. K. Turekian (eds), *Treatise on Geochemistry*, Pergamon, Oxford, pp. 1 – 47.
- MacPherson, G. J. and Grossman, L. (1984). “Fluffy” type A Ca-, Al-rich inclusions in the Allende meteorite, *Geochimica et Cosmochimica Acta* **48**(1): 29 – 46.
- Magna, T., Wiechert, U. and Halliday, A. N. (2006). New constraints on the lithium isotope compositions of the moon and terrestrial planets, *Earth and Planetary Science Letters* **243**(3-4): 336–353.

- Makishima, A. and Nakamura, E. (2001). Determination of total sulfur at microgram per gram levels in geological materials by oxidation of sulfur into sulfate with in situ generation of bromine using isotope dilution high-resolution ICPMS, *Analytical Chemistry* **73**(11): 2547–2553.
- Marin-Carbonne, J., Chaussidon, M., Boiron, M.-C. and Robert, F. (2011). A combined in situ oxygen, silicon isotopic and fluid inclusion study of a chert sample from Onverwacht Group (3.35Ga, South Africa): New constraints on fluid circulation, *Chemical Geology* **286**(3-4): 59 – 71.
- Markowski, A., Leya, I., Quitté, G., Ammon, K., Halliday, A. and Wieler, R. (2006). Correlated helium-3 and tungsten isotopes in iron meteorites: Quantitative cosmogenic corrections and planetesimal formation times, *Earth and Planetary Science Letters* **250**(1-2): 104 – 115.
- Marti, K., Kim, J., Thakur, A., McCoy, T. and Keil, K. (1995). Signatures of the martian atmosphere in glass of the Zagami meteorite, *Science* **267**(5206): 1981–1984.
- Marvin, U. B. (1992). The meteorite of Ensisheim - 1492 to 1992, *Meteoritics* **27**: 28–72.
- Mason, B. (1963). The carbonaceous chondrites, *Space Science Reviews* **1**(4): 621–646.
- Mason, B. H. and Wiik, H. (1966a). The composition of the Barrata, Carraweena, Kapoeta, Mooresfort, and Ngawi meteorites., *American Museum Novitates* **2273**.
- Mason, B. H. and Wiik, H. (1966b). The composition of the Bath, Frankfort, Rose City, and Tadjera meteorites, *American Museum Novitates* **2272**.
- Mason, B. H. and Wiik, H. (1967). The composition of the Belly River, Bluff, Bremervörde, and Modoc meteorites, *American Museum novitates* **2280**.
- McCord, T. B., Adams, J. B. and Johnson, T. V. (1970). Asteroid Vesta: Spectral reflectivity and compositional implications, *Science* **168**(3938): 1445–1447.
- McDonough, W. F. (2003). Compositional model for the Earth’s core, in D. H. Heinrich and K. T. Karl (eds), *Treatise on Geochemistry*, Pergamon, Oxford, pp. 547–568.

- McGee, P. E., Warner, J. L. and Simonds, C. H. (1977). Introduction to the Apollo collections. Part 1: Lunar igneous rocks, *NASA STI/Recon Technical Report N 772*: 22034.
- McKeegan, K. D., Kallio, A. P. A., Heber, V. S., Jarzebinski, G., Mao, P. H., Coath, C. D., Kunihiro, T., Wiens, R. C., Nordholt, J. E., Moses, R. W., Reisenfeld, D. B., Jurewicz, A. J. G. and Burnett, D. S. (2011). The oxygen isotopic composition of the Sun inferred from captured solar wind, *Science* **332**(6037): 1528–1532.
- McKeegan, K. and Davis, A. (2007). Early solar system chronology, in H. D. Holland and K. K. Turekian (eds), *Treatise on Geochemistry*, Pergamon, Oxford, pp. 1 – 38.
- McSween Jr, H. Y. and Treiman, A. (1998). Martian meteorites, *Reviews in Mineralogy* **36**.
- Méheut, M., Lazzeri, M., Balan, E. and Mauri, F. (2009). Structural control over equilibrium silicon and oxygen isotopic fractionation: A first-principles density-functional theory study, *Chemical Geology* **258**(1-2): 28–37.
- Messenger, S., Sandford, S. and Brownlee, D. (2006). The population of starting materials available for solar system construction, in D. Lauretta and H. Y. McSween Jr (eds), *Meteorites and the Early Solar System II*, University of Arizona Press, Tucson, pp. 187–208.
- Meyer, C., J., McKay, D. S., Anderson, D. H. and Butler, P., J. (1975). The source of sublimates on the Apollo 15 green and Apollo 17 orange glass samples, *Lunar and Planetary Science Conference Proceedings*, Vol. 6, pp. 1673–1699.
- Mittlefehldt, D. W., McCoy, T. J., Goodrich, C. A. and Kracher, A. (1998). Non-chondritic meteorites from asteroidal bodies, *Reviews in Mineralogy* **36**.
- Molini-Velsko, C., Mayeda, T. K. and Clayton, R. N. (1986). Isotopic composition of silicon in meteorites, *Geochimica et Cosmochimica Acta* **50**(12): 2719–2726.
- Moynier, F., Agranier, A., Hezel, D. C. and Bouvier, A. (2010). Sr stable isotope composition of Earth, the Moon, Mars, Vesta and meteorites, *Earth and Planetary Science Letters* **300**(3-4): 359–366.
- Moynier, F., Albarède, F. and Herzog, G. F. (2006). Isotopic composition of zinc, copper, and iron in lunar samples, *Geochimica et Cosmochimica Acta* **70**(24): 6103–6117.

-
- Moynier, F., Blichert-Toft, J., Telouk, P., Luck, J.-M. and Albarède, F. (2007). Comparative stable isotope geochemistry of Ni, Cu, Zn, and Fe in chondrites and iron meteorites, *Geochimica et Cosmochimica Acta* **71**(17): 4365–4379.
- Moynier, F., Yin, Q.-Z. and Schauble, E. (2011). Isotopic evidence of Cr partitioning into Earth’s core, *Science* **331**(6023): 1417–1420.
- Mullane, E., Russell, S. and Gounelle, M. (2005). Nebular and asteroidal modification of the iron isotope composition of chondritic components, *Earth and Planetary Science Letters* **239**(3-4): 203 – 218.
- Nord Jr., G. L., Lally, J. S., Heuer, A. H., Christie, J. M., Radcliffe, S. V., Griggs, D. T. and Fisher, R. M. (1973). Petrologic study of igneous and metaigneous rocks from Apollo 15 and 16 using high voltage transmission electron microscopy, *Lunar and Planetary Science Conference Proceedings*, Vol. 4 of *Lunar and Planetary Science Conference Proceedings*, p. 953.
- Norman, M. D., Borg, L. E., Nyquist, L. E. and Bogard, D. D. (2003). Chronology, geochemistry, and petrology of a ferroan noritic anorthosite clast from Descartes breccia 67215: Clues to the age, origin, structure, and impact history of the lunar crust, *Meteoritics & Planetary Science* **38**(4): 645–661.
- Norman, M. D., Shih, C. Y., Nyquist, L. E., Bogard, D. D. and Taylor, L. A. (2007). Early impacts on the moon: Crystallization ages of apollo 16 melt breccias, *Lunar and Planetary Institute Science Conference Abstracts* **38**: 1991.
- Nyquist, L., Bogard, D., Shih, C.-Y., Greshake, A., Stffler, D. and Eugster, O. (2001). Ages and geologic histories of martian meteorites, *Space Science Reviews* **96**: 105–164.
- Opfergelt, S., Cardinal, D., André, L., Delvigne, C., Bremond, L. and Delvaux, B. (2010). Variations of $\delta^{30}\text{Si}$ and Ge/Si with weathering and biogenic input in tropical basaltic ash soils under monoculture, *Geochimica et Cosmochimica Acta* **74**(1): 225–240.
- Ott, U. (2007). Presolar grains in meteorites and their compositions, *Space Science Reviews* **130**(1-4): 87–95.
- Pack, A., Vogel, I., Rollion-Bard, C., Luais, B. and Palme, H. (2011). Silicon in iron meteorite metal, *Meteoritics & Planetary Science* **46**(10): 1470–1483.

- Pahlevan, K. and Stevenson, D. J. (2007). Equilibration in the aftermath of the lunar-forming giant impact, *Earth and Planetary Science Letters* **262**(3-4): 438–449.
- Pahlevan, K., Stevenson, D. J. and Eiler, J. M. (2011). Chemical fractionation in the silicate vapor atmosphere of the earth, *Earth and Planetary Science Letters* **301**(3-4): 433–443.
- Palme, H. and O'Neill, H. S. C. (2003). Cosmochemical estimates of mantle composition, in D. H. Heinrich and K. T. Karl (eds), *Treatise on Geochemistry*, Pergamon, Oxford, pp. 1–38.
- Palme, H., Spettel, B., Kural, G. and Zinner, E. (1992). Origin of Allende Chondrules, *Lunar and Planetary Institute Science Conference Abstracts*, Vol. 23, p. 1021.
- Papanastassiou, D. and Wasserburg, G. (1973). Rb–Sr ages and initial strontium in basalts from Apollo 15, *Earth and Planetary Science Letters* **17**(2): 324 – 337.
- Papike, J. J., Hodges, F. N., Bence, A. E., Cameron, M. and Rhodes, J. M. (1976). Mare basalts: Crystal chemistry, mineralogy, and petrology, *Rev. Geophys.* **14**(4): 475–540. 8755-1209.
- Papike, J. J., Ryder, G. and Shearer, C. K. (1998). Lunar samples, *Reviews in Mineralogy* **36**.
- Papike, J., Karner, J. and Shearer, C. (2005). Comparative planetary mineralogy: Valence state partitioning of Cr, Fe, Ti, and V among crystallographic sites in olivine, pyroxene, and spinel from planetary basalts, *American Mineralogist* **90**(2-3): 277–290.
- Patchen, A. P. and Taylor, L. A. (2004). The most reduced rock from the Moon – Apollo 14 basalt 14053: Extreme reduction entirely from a re-heating event, *Lunar and Planetary Institute Science Conference Abstracts*, Vol. 35, p. 1762.
- Pogge von Strandmann, P. A., Elliott, T., Marschall, H. R., Coath, C., Lai, Y.-J., Jeffcoate, A. B. and Ionov, D. A. (2011). Variations of Li and Mg isotope ratios in bulk chondrites and mantle xenoliths, *Geochimica et Cosmochimica Acta* **75**(18): 5247 – 5268.
- Poirier, J.-P. (1994). Light elements in the Earth's outer core: A critical review, *Physics of The Earth and Planetary Interiors* **85**(3-4): 319–337.

- Poitrasson, F., Halliday, A. N., Lee, D. C., Levasseur, S. and Teutsch, N. (2004). Iron isotope differences between Earth, Moon, Mars and Vesta as possible records of contrasted accretion mechanisms, *Earth and Planetary Science Letters* **223**(3-4): 253–266.
- Potts, P. J. (1987). *A Handbook of Silicate Rock Analysis*, Chapman & Hall, London.
- Prytulak, J., Nielsen, S. G. and Halliday, A. N. (2011). Determination of precise and accurate $^{51}\text{V}/^{50}\text{V}$ isotope ratios by Multi-Collector ICP-MS, part 2: Isotopic composition of six reference materials plus the Allende chondrite and verification tests, **35**: 307–318.
- Regelous, M., Elliott, T. and Coath, C. D. (2008). Nickel isotope heterogeneity in the early solar system, *Earth and Planetary Science Letters* **272**(1-2): 330–338.
- Reynolds, B. C., Aggarwal, J., André, L., Baxter, D., Beucher, C., Brzezinski, M. A., Engstrom, E., Georg, R. B., Land, M., Leng, M. J., Opfergelt, S., Rodushkin, I., Sloane, H. J., van den Boorn, S. H. J. M., Vroon, P. Z. and Cardinal, D. (2007). An inter-laboratory comparison of Si isotope reference materials, *J. Anal. At. Spectrom.* **22**(5): 561–568.
- Reynolds, B. C., Frank, M. and Halliday, A. N. (2006). Silicon isotope fractionation during nutrient utilization in the north pacific, *Earth and Planetary Science Letters* **244**(1-2): 431–443.
- Reynolds, J. H. and Verhoogen, J. (1953). Natural variations in the isotopic constitution of silicon, *Geochimica et Cosmochimica Acta* **3**(5): 224 – 234.
- Rhodes, J. M., Brannon, J. C., Rodgers, K. V., Blanchard, D. P. and Dungan, M. A. (1977). Chemistry of Apollo 12 mare basalts - magma types and fractionation processes, *Lunar Science Conference Proceedings*, Vol. 8, pp. 1305–1338.
- Rhodes, J. M. and Hubbard, N. J. (1973). Chemistry, classification, and petrogenesis of Apollo 15 mare basalts, *Lunar and Planetary Science Conference Proceedings*, Vol. 4, p. 1127.
- Rhodes, J. M., Wiesmann, H., Rodgers, K. V., Brannon, J. C., Bansal, B. M. and Hubbard, N. J. (1976). Chemistry, classification, and petrogenesis of Apollo 17 mare basalts, *Lunar and Planetary Science Conference Proceedings*, Vol. 7, pp. 1467–1489.

- Richter, F. M., Davis, A. M., Ebel, D. S. and Hashimoto, A. (2002). Elemental and isotopic fractionation of Type B calcium-, aluminum-rich inclusions: experiments, theoretical considerations, and constraints on their thermal evolution, *Geochimica et Cosmochimica Acta* **66**(3): 521 – 540.
- Richter, K., Drake, M. J. and Scott, E. (2006). Compositional relationships between meteorites and terrestrial planets, *in* D. S. Laretta and H. Y. McSween Jr (eds), *Meteorites and the Early Solar System II*, University of Arizona Press, pp. 803–828.
- Ringwood, A. E. (1959). On the chemical evolution and densities of the planets, *Geochimica et Cosmochimica Acta* **15**(4): 257–283.
- Ringwood, A. E. (1986). Terrestrial origin of the Moon, *Nature* **322**(6077): 323–328.
- Robert, F. and Chaussidon, M. (2006). A palaeotemperature curve for the precambrian oceans based on silicon isotopes in cherts, *Nature* **443**(7114): 969–972.
- Roedder, E. and Weiblen, P. W. (1975). Anomalous low-K silicate melt inclusions in ilmenite from Apollo 17 basalts, *Lunar and Planetary Science Conference Proceedings*, Vol. 6, pp. 147–164.
- Rosman, K. and Taylor, P. (1998). Isotopic compositions of the elements 1997, *Pure and Applied Chemistry* **70**(1): 217–235.
- Ryder, G. and Schuraytz, B. C. (2001). Chemical variation of the large Apollo 15 olivine-normative mare basalt rock samples, *J. Geophys. Res.* **106**(E1): 1435–1451.
- Savage, P., Georg, R. B., Armytage, R. G., Williams, H. and Halliday, A. N. (2010). Silicon isotope homogeneity in the mantle, *Earth and Planetary Science Letters* **295**(1-2): 139–146.
- Savage, P. S., Georg, R. B., Williams, H. M., Burton, K. W. and Halliday, A. N. (2011). Silicon isotope fractionation during magmatic differentiation, *Geochimica et Cosmochimica Acta* **75**(20): 6124 – 6139.
- Schauble, E. A. (2004). Applying stable isotope fractionation theory to new systems, *Reviews in Mineralogy and Geochemistry* **55**: 65–111.
- Schauble, E. A., Georg, R. and Halliday, A. N. (2007). Silicate metal fractionation of silicon isotopes at high pressure and temperature, *Eos Trans. AGU* **88**(52): Fall Meet. Suppl., Abstract V42A–07.

- Scherstén, A., Elliott, T., Hawkesworth, C., Russell, S. and Masarik, J. (2006). Hf-W evidence for rapid differentiation of iron meteorite parent bodies, *Earth and Planetary Science Letters* **241**(3-4): 530 – 542.
- Schoenberg, R. and von Blanckenburg, F. (2006). Modes of planetary-scale Fe isotope fractionation, *Earth and Planetary Science Letters* **252**(3-4): 342–359.
- Schönbächler, M., Lee, D.-C., Rehkämper, M., Halliday, A. N., Hattendorf, B. and Günther, D. (2005a). Nb/Zr fractionation on the moon and the search for extinct ^{92}Nb , *Geochimica et Cosmochimica Acta* **69**(3): 775–785.
- Schönbächler, M., Rehkämper, M., Fehr, M., Halliday, M. A., Hattendorf, B. and Günther, D. (2005b). Nucleosynthetic zirconium isotope anomalies in acid leachates of carbonaceous chondrites, *Geochimica et Cosmochimica Acta* **69**(21): 5113 – 5122.
- Scott, E. R. D. (2007). Chondrites and the protoplanetary disk, *Annual Review of Earth and Planetary Sciences* **35**: 577–620.
- Scott, E. R. D. and Krot, A. N. (2007). Chondrites and their components, *in* D. H. Heinrich and K. T. Karl (eds), *Treatise on Geochemistry*, Pergamon, Oxford, pp. 1–72.
- Sears, D. W. G. (2004). *The Origin of Chondrules and Chondrites*, Cambridge University Press, Cambridge.
- Seitz, H.-M., Brey, G. P., Zipfel, J., Ott, U., Weyer, S., Durali, S. and Weinbruch, S. (2007). Lithium isotope composition of ordinary and carbonaceous chondrites, and differentiated planetary bodies: Bulk solar system and solar reservoirs, *Earth and Planetary Science Letters* **260**(3-4): 582–596.
- Shahar, A. and Young, E. D. (2007). Astrophysics of CAI formation as revealed by silicon isotope LA-MC-ICPMS of an igneous CAI, *Earth and Planetary Science Letters* **257**(3-4): 497–510.
- Shahar, A., Ziegler, K., Young, E. D., Ricolleau, A., Schauble, E. A. and Fei, Y. (2009). Experimentally determined Si isotope fractionation between silicate and Fe metal and implications for earth’s core formation, *Earth and Planetary Science Letters* **288**(1-2): 228–234.
- Shearer, C. K., Hess, P., Wieczorek, M. A., Pritchard, M. E., Parmentier, E., Borg, L., Longhi, J., Elkins-Tanton, L., Neal, C. R., Antonenko, I., Canup, R. M., Halliday,

- A. N., Grove, T. L., Hager, B. H., Lee, D. C. and Wiechert, U. (2006). Thermal and magmatic evolution of the moon, *Reviews in Mineralogy & Geochemistry* **60**: 365–518.
- Shu, F. H., Shang, H., Gounelle, M., Glassgold, A. E. and Lee, T. (2001). The origin of chondrules and refractory inclusions in chondritic meteorites, *The Astrophysical Journal* **548**(2): 1029.
- Shu, F. H., Shang, H. and Lee, T. (1996). Toward an astrophysical theory of chondrites, *Science* **271**(5255): 1545–1552.
- Siebert, C., Nögler, T. F. and Kramers, J. D. (2001). Determination of molybdenum isotope fractionation by double-spike multicollector inductively coupled plasma mass spectrometry, *Geochem. Geophys. Geosyst.* **2**: 1032.
- Simon, J. I. and DePaolo, D. J. (2010). Stable calcium isotopic composition of meteorites and rocky planets, *Earth and Planetary Science Letters* **289**(3-4): 457–466.
- Smith, J. V., Anderson, A. T., Newton, R. C., Olsen, E. J., Crewe, A. V., Isaacson, M. S., Johnson, D. and Wyllie, P. J. (1970). Petrologic history of the moon inferred from petrography, mineralogy and petrogenesis of Apollo 11 rocks, *Proceedings of the Apollo 11 Lunar Science Conference*, Vol. 1, pp. 897–925.
- Snyder, G. A., Taylor, L. A. and Neal, C. R. (1992). A chemical model for generating the sources of mare basalts: Combined equilibrium and fractional crystallization of the lunar magmasphere, *Geochimica et Cosmochimica Acta* **56**(10): 3809 – 3823.
- Spicuzza, M. J., Day, J. M. D., Taylor, L. A. and Valley, J. W. (2007). Oxygen isotope constraints on the origin and differentiation of the moon, *Earth and Planetary Science Letters* **253**(1-2): 254–265.
- Steinboefel, G., von Blanckenburg, F., Horn, I., Konhauser, K. O., Beukes, N. J. and Gutzmer, J. (2010). Deciphering formation processes of banded iron formations from the Transvaal and the Hamersley successions by combined Si and Fe isotope analysis using UV femtosecond laser ablation, *Geochimica et Cosmochimica Acta* **74**(9): 2677 – 2696.
- Sugiura, N., Mizuno, T., Ushikubo, T. and Hiyagon, H. (2004). Si and Mg isotope fractionations in melilite in coarse-grained CAIs measured by SIMS, *Geochemical Journal* **38**(5): 405–415.

- Takafuji, N., Hirose, K., Mitome, M. and Bando, Y. (2005). Solubilities of O and Si in liquid iron in equilibrium with (Mg,Fe)SiO₃ perovskite and the light elements in the core, *Geophysical Research Letters* **32**(6).
- Taylor, J. R. (1997). *An Introduction to Error Analysis: The Study of Uncertainties in Physical Measurements*, 2nd edn, University Science Books, Sausalito.
- Taylor Jr., H. P. and Epstein, S. (1970). Oxygen and silicon isotope ratios of lunar rock 12013, *Earth and Planetary Science Letters* **9**(2): 208–210.
- Taylor Jr., H. P. and Epstein, S. (1973a). ¹⁸O/¹⁶O and ³⁰Si/²⁸Si studies of some Apollo 15,16, and 17 samples, *Lunar and Planetary Science Conference Proceedings* **4**: 1657–1679.
- Taylor Jr., H. P. and Epstein, S. (1973b). Oxygen and silicon isotope ratios of the Luna 20 soil, *Geochimica et Cosmochimica Acta* **37**(4): 1107–1109.
- Taylor, S. (1982). *Planetary Science: A lunar perspective*, Lunar Planetary Institute, Houston.
- Taylor, S. R., Taylor, G. J. and Taylor, L. A. (2006). The Moon: A Taylor perspective, *Geochimica et Cosmochimica Acta* **70**(24): 5904–5918.
- Teng, F.-Z., Dauphas, N. and Helz, R. T. (2008). Iron isotope fractionation during magmatic differentiation in Kilauea Iki lava lake, *Earth and Planetary Science Letters* **320**(5883): 1620–1622.
- Teng, F.-Z., Li, W.-Y., Ke, S., Marty, B., Dauphas, N., Huang, S., Wu, F.-Y. and Pourmand, A. (2010). Magnesium isotopic composition of the Earth and chondrites, *Geochimica et Cosmochimica Acta* **74**(14): 4150–4166.
- Teng, F.-Z., Wadhwa, M. and Helz, R. T. (2007). Investigation of magnesium isotope fractionation during basalt differentiation: Implications for a chondritic composition of the terrestrial mantle, *Earth and Planetary Science Letters* **261**(1-2): 84–92.
- Thiemens, M. H. (2006). History and applications of mass-independent isotope effects, *Annual Review of Earth and Planetary Science* **34**: 217–262.
- Thy, P., Tegner, C. and Leshner, C. E. (2009). Liquidus temperatures of the Skaergaard magma, *American Mineralogist* **94**(10): 1371–1376.
- Tilles, D. (1961). Natural variations in isotopic abundances of silicon, *Journal of Geophysical Research* **66**(1-2): 3003–3013.

- Tipper, E. T., Louvat, P., Capmas, F., Galy, A. and Gaillardet, J. (2008). Accuracy of stable Mg and Ca isotope data obtained by MC-ICP-MS using the standard addition method, *Chemical Geology* **257**(1-2): 65–75.
- Treiman, A. H. (2005). The nakhlite meteorites: augite-rich igneous rocks from Mars, *Chemie der Erde - Geochemistry* **65**(3): 203–270.
- Trinquier, A., Elliott, T., Ulfbeck, D., Coath, C., Krot, A. N. and Bizzarro, M. (2009). Origin of nucleosynthetic isotope heterogeneity in the solar protoplanetary disk, *Science* **324**(5925): 374–376.
- Tuff, J., Wood, B. J. and Wade, J. (2010). The effect of Si on metal-silicate partitioning of siderophile elements and implications for the conditions of core formation, *Geochimica et Cosmochimica Acta* **75**(2): 673–690.
- Unruh, D. M., Stille, P., Patchett, P. J. and Tatsumoto, M. (1984). Lu-Hf and Sm-Nd evolution in lunar mare basalts, *Lunar and Planetary Science Conference Proceedings*, Vol. 14, p. 459.
- Usselman, T. M., Lofgren, G. E., Williams, R. J. and Donaldson, C. H. (1975). Experimentally reproduced textures and mineral chemistries of high-titanium mare basalts, *Lunar and Planetary Science Conference Proceedings* **6**: 997–1020.
- van den Boorn, S. H. J. M., Vroon, P. Z., van Belle, C. C., van der Wagt, B., Schwieters, J. and van Bergen, M. J. (2006). Determination of silicon isotope ratios in silicate materials by high-resolution MC-ICP-MS using a sodium hydroxide sample digestion method, *Journal of Analytical Atomic Spectrometry* **21**(8): 734–742.
- van den Boorn, S. H. J. M., Vroon, P. Z. and van Bergen, M. J. (2009). Sulfur-induced offsets in MC-ICP-MS silicon-isotope measurements, *Journal of Analytical Atomic Spectrometry* **24**(8): 1111–1114.
- van den Boorn, S. H., van Bergen, M. J., Nijman, W. and Vroon, P. Z. (2007). Dual role of seawater and hydrothermal fluids in Early Archean chert formation: Evidence from silicon isotopes, *Geology* **35**(10): 939–942.
- Von Michaelis, H., Ahrens, L. H. and Willis, J. P. (1968). The composition of stony meteorites ii. the analytical data and an assessment of their quality, *Earth and Planetary Science Letters* **5**: 387–394.

-
- Wade, J. and Wood, B. J. (2005). Core formation and the oxidation state of the earth, *Earth and Planetary Science Letters* **236**(1-2): 78–95.
- Wager, L. R. (1960). The major element variation of the layered series of the Skaergaard intrusion and a re-estimation of the average composition of the hidden layered series and of the successive residual magmas, *J. Petrology* **1**(3): 364–398.
- Walker, D., Lasaga, A. C., Stolper, E. M., Hays, J. F., Longhi, J. and Grove, T. L. (1977). Slowly cooled microgabbros 15555 and 15065, *Lunar and Planetary Science Conference Proceedings*, Vol. 8, pp. 1521–1547.
- Wang, J., Davis, A. M., Clayton, R. N., Mayeda, T. K. and Hashimoto, A. (2001). Chemical and isotopic fractionation during the evaporation of the FeO-MgO-SiO₂-CaO-Al₂O₃-TiO₂ rare earth element melt system, *Geochimica et Cosmochimica Acta* **65**(3): 479 – 494.
- Warren, P. H. (1985). The magma ocean concept and lunar evolution, *Annual Reviews in Earth and Planetary Science* **13**(1): 201–240.
- Warren, P. H. (2005). “New” lunar meteorites: Implications for composition of the global lunar surface, lunar crust, and the bulk moon, *Meteoritics & Planetary Science* **40**(3): 477–506.
- Warren, P. H. and Wasson, J. T. (1977). Pristine nonmare rocks and the nature of the lunar crust, *Lunar and Planetary Science Conference Proceedings*, Vol. 8, pp. 2215–2235.
- Weigand, P. (1973). Petrology of a coarse-grained Apollo 17 ilmenite basalt (abs.), *EOS Trans. Amer. Geophys. Union*, Vol. 54, pp. 621–622.
- Weisburg, M., McCoy, T. and Krot, A. (2006). Systematics and evaluation of meteorite classification, in L. S. Dante and H. Y. McSween Jr (eds), *Meteorites and the Early Solar System II*, The University of Arizona Press, pp. 19–52.
- Wetherill, G. W. and Stewart, G. R. (1989). Accumulation of a swarm of small planetesimals, *Icarus* **77**(2): 330 – 357.
- Weyer, S., Anbar, A. D., Brey, G. P., Munker, C., Mezger, K. and Woodland, A. B. (2005). Iron isotope fractionation during planetary differentiation, *Earth and Planetary Science Letters* **240**(2): 251–264.

- Wiechert, U. H., Halliday, A. N., Palme, H. and Rumble, D. (2004). Oxygen isotope evidence for rapid mixing of the HED meteorite parent body, *Earth and Planetary Science Letters* **221**(1-4): 373–382.
- Wiechert, U. and Halliday, A. N. (2007). Non-chondritic magnesium and the origins of the inner terrestrial planets, *Earth and Planetary Science Letters* **256**(3-4): 360–371.
- Wiechert, U., Halliday, A. N., Lee, D. C., Snyder, G. A., Taylor, L. A. and Rumble, D. (2001). Oxygen isotopes and the moon-forming giant impact, *Science* **294**(5541): 345–348.
- Williams, H. M., Peslier, A. H., McCammon, C., Halliday, A. N., Levasseur, S., Teutsch, N. and Burg, J. P. (2005). Systematic iron isotope variations in mantle rocks and minerals: The effects of partial melting and oxygen fugacity, *Earth and Planetary Science Letters* **235**(1-2): 435–452.
- Willis, J. P., Erlank, A. J., Gurney, J. J., Theil, R. H. and Ahrens, L. H. (1972). Major, minor, and trace element data for some Apollo 11, 12, 14 and 15 samples, *Lunar and Planetary Science Conference Proceedings*, Vol. 3, p. 1269.
- Wilson, S. (1997). Data compilation for USGS reference material BHVO-2, Hawaiian Basalt, U.S. Geological Survey Open-File Report xxxxx.
- Wombacher, F., Rehkamper, M., Mezger, K., Bischoff, A. and Munker, C. (2008). Cadmium stable isotope cosmochemistry, *Geochimica et Cosmochimica Acta* **72**(2): 646–667.
- Wood, J. (1996). Unresolved issues in the formation of chondrules and chondrites, in R. Hewins, R. Jones and E. Scott (eds), *Chondrules and Protoplanetary disk*, Cambridge University Press, pp. 55–69.
- Wood, J. A., Dickey, Jr., J. S., Marvin, U. B. and Powell, B. N. (1970). Lunar anorthosites and a geophysical model of the moon, *Proceedings of the Apollo 11 Lunar Science Conference*, pp. 965–988.
- Yeh, H. W. and Epstein, S. (1978). $^{29}\text{Si}/^{28}\text{Si}$ and $^{30}\text{Si}/^{28}\text{Si}$ of meteorites and Allende inclusions, *Lunar and Planetary Institute Science Conference Abstracts*, Vol. 9, pp. 1289–1291.

- Young, E. D., Ash, R. D., Galy, A. and Belshaw, N. S. (2002a). Mg isotope heterogeneity in the Allende meteorite measured by UV laser ablation-MC-ICPMS and comparisons with O isotopes, *Geochimica et Cosmochimica Acta* **66**(4): 683 – 698.
- Young, E. D., Galy, A. and Nagahara, H. (2002b). Kinetic and equilibrium mass-dependent isotope fractionation laws in nature and their geochemical and cosmochemical significance, *Geochimica et Cosmochimica Acta* **66**(6): 1095–1104.
- Young, E. D., Nagahara, H., Mysen, B. O. and Audet, D. M. (1998). Non-Rayleigh oxygen isotope fractionation by mineral evaporation: theory and experiments in the system SiO₂, *Geochimica et Cosmochimica Acta* **62**(18): 3109 – 3116.
- Young, E. D., Tonui, E., Manning, C. E., Schauble, E. and Macris, C. A. (2009). Spinel-olivine magnesium isotope thermometry in the mantle and implications for the Mg isotopic composition of Earth, *Earth and Planetary Science Letters* **288**(3-4): 524–533.
- Zambardi, T. and Poitrasson, F. (2010). Precise determination of silicon isotopes in silicate rock reference materials by MC-ICP-MS, *Geostandards and Geoanalytical Research* **35**: 89–99.
- Zanda, B., Hewins, R. H., Bourot-Denise, M., Bland, P. A. and Albarède, F. (2006). Formation of solar nebula reservoirs by mixing chondritic components, *Earth and Planetary Science Letters* **248**(3-4): 650 – 660.
- Zhu, X. K., Guo, Y., O’Nions, R. K., Young, E. D. and Ash, R. D. (2001). Isotopic homogeneity of iron in the early solar nebula, *Nature* **412**(6844): 311–313.
- Ziegler, K., Chadwick, O. A., White, A. F. and Brzezinski, M. A. (2005). $\delta^{30}\text{Si}$ systematics in a granitic saprolite, Puerto Rico, *Geology* **33**(10): 817–820.
- Ziegler, K., Young, E. D., Schauble, E. A. and Wasson, J. T. (2010). Metal-silicate silicon isotope fractionation in enstatite meteorites and constraints on Earth’s core formation, *Earth and Planetary Science Letters* **295**(3-4): 487–496.